Structure-property relationships of sodium carboxymethyl cellulose (Na CMC) in pure water and formulated solutions

Juliette Sylviane Behra

Submitted in accordance with the requirements
for the degree of Doctor of Philosophy

The University of Leeds

School of Chemical and Process Engineering
&
School of Physics and Astronomy

September 2018

The candidate confirms that the work submitted is their own, except where work which has formed part of jointly authored publications has been included. The contribution of the candidate and the other authors to this work has been explicitly indicated below. The candidate confirms that appropriate credit has been given within the thesis where reference has been made to the work of others.

The work in Chapter 3 of the thesis is under review for publication as follows:

Behra, J. S.; Mattsson, J.; Cayre, O. J.; Robles, E. S. J.; Tang, H.; Hunter, T. N. Characterization of Sodium Carboxymethyl Cellulose (Na CMC) Aqueous Solutions to Support Complex Product Formulation – a Rheology and Light Scattering Study. Submitted to *ACS Applied Polymer Materials* (Manuscript ID: ap-2018-00110q.R2).

The work in Chapter 4 of the thesis is in preparation for publication as follows:

Behra, J. S.; Mattsson, J.; Cayre, O. J.; Robles, E. S. J.; Tang, H.; Hunter, T. N. Ultrasonication-induced changes in Sodium Carboxymethyl Cellulose (Na CMC) solutions characterised with rheology, Size Exclusion Chromatography (SEC) and Light Scattering (LS). In preparation.

For both publications, I was responsible for designing and performing the experiments, analysing the data and writing the publications.

The contribution of the other authors was to discuss the experimental design and the results, as well as to assist during writing-up.

Acknowledgements

Thank you, Tim, for your immense kindness, strong support and availability throughout this both great and extremely tough adventure. I miss words to express my gratefulness. Many thanks, Johan, for having made Physics, which I have always been frightened of, more accessible to me and having shared your passion for it. Thanks for having taken the time to read some of the fundamental papers about the physics of polyelectrolytes to make sure I had understood them properly. Thanks also for all our great scientific discussions; please give my apologies to your wife for all the evenings you left Uni much later than you had promised because of me. *Merci à toi aussi*, Olivier, for your help and advice, as well as for having offered me the opportunity to co-supervise the medical-related project. It has been such a formidable and enriching experience! Thanks, finally, to the three of you, for your patience, and for having put up with my lack of self-confidence and my perfectionism.

I would like to thank the University of Leeds for having awarded me one of its 110 Anniversary Research Scholarships, as well as Procter & Gamble (P&G) for having co-founded this project. Thanks, Haico and Eric, for your patience when results were so long to come, for your faith in me and for having offered me the possibility to spend another year working on my PhD.

Thank you, Dan, for your amazing management of the Physics labs. Thanks for having kept an eye on me during my late night and weekend light scattering experiments. Without you, it would not have been possible to collect all the data for this thesis and the papers to come. Thanks, Susanne, Ben and Peter, for your technical support in the School of Chemical and Process Engineering labs. Thanks, Nick and Sam, for having allowed me to use your size exclusion chromatograph and helped me performing my experiments. Thanks, Sarah, for having given me the chance to perform neutron scattering experiments during my PhD. The results are not part of the thesis, but this great experience is definitely part of my PhD and I will not forget it. Thanks, Elaine, for having allowed me to perform out-of-hours work, especially during the time the size exclusion chromatograph was set-up for my experiments, as well as for the preparation of the neutron scattering experiments. Thanks to both the Colloid and Polymer Engineering Group and the Soft Matter Physics Group.

I wish to thank the NHS and its brilliant staff for the great care provided during my PhD. Many thanks to you too, Gemma and James, for your attentive listening and your support over the last couple of years.

As much as my PhD has been a long and lonely journey full of personal, practical and scientific challenges, it has also allowed me to meet some wonderful people, and made me cherish even more the time spent with you, my friends. Thanks Laura, Mike and Shafeeq for your moral support, especially during writing-up. Thank you, EJ and Belle, for your immense support, especially in the toughest moments. You are both crazy in your own ways, and it has been great to get to share a bit of this craziness together, and to laugh about so many things. Thanks to my beloved 'English grandparents', Jillian and Chris, for your kindness, for your help in so many circumstances, and for having allowed me to join you to play some early music. Thanks, Barbarba, for your amazing baroque dance classes. They have been perfect escapes from the lab and my PhD, giving me my energy and motivation back. *Merci*, Cécile, for your always warm hospitality and these great London breaks. Sharing PhD and personal experiences together has been very helpful. Many thanks to both of you, Fiona and Marietta, for having so well looked after me, and made sure I was having proper breaks from my PhD at the hardest times. *Un grand merci* to my Parisian friends, and especially to Anna, Thierry, Benoît, Maxime and Rémi, for having believed in me and supported me, in your own ways and despite the distance. Moments shared with you have been much needed fresh air and rays of sunshine in the middle of the storm. *Merci infiniment*, Pauline, for your continuous and so precious support during my PhD marathon and the final sprint. I am looking forward to being free again and sharing many more things than a quick Saturday lunch between morning and afternoon writing-up sessions! Last but not least, I would like to thank my family for its support. *Merci* for your visits, Werner, and for having followed me when I suggested to organise what ended up being a fabulous sibling weekend in Vienna. Thanks, Elsa, for your sense of humour and your drawings, which have accompanied me during my PhD. I could not resist to have the chemist character you kindly drew for my Postgraduate Research Show poster. Last but not least, *merci*, Maman & Papa, for having allowed me to do this PhD, hence realising the dream of a little fourteen year-old girl.

Abstract

Sodium Carboxymethyl Cellulose (Na CMC) is used for its thickening and swelling properties in a wide range of applications including pharmaceutical, food, home and personal care products, as well as in paper, water treatment and mineral processing industries. Despite its broad industrial use, Na CMC structure-property relationships in solution are known to be highly complex and influenced by a number of parameters. The focus of this thesis was to expand fundamental understanding of its solution characteristics.

The behaviour of salt-free semi-dilute aqueous Na CMC solutions was investigated over a wide range of concentrations using rheology as well as Light Scattering (LS). The concentration dependence of the solution specific viscosities could be described using an approach which interpolates between two power law regimes and introduces one characteristic crossover concentration. This behaviour was interpreted as a transition from the semi-dilute non-entangled to the entangled concentration regimes, and was not observed in the solution structure, as determined using Static Light Scattering (SLS). Dynamic Light Scattering (DLS) revealed three relaxation modes. The two faster relaxations were assigned as the ‘fast’ and ‘slow’ relaxation modes typically observed in salt-free polyelectrolyte solutions within the semi-dilute concentration range. The third, typically weak mode, was attributed to the presence of a small amount of poorly dissolved cellulose residuals. Since filtration altered the solution behaviour, without sufficiently removing the residuals, data collection and processing were adapted to account for this, which facilitated a detailed light scattering investigation of the original solutions. The relaxation time of the slow mode demonstrated a similar crossover behaviour as observed for the specific viscosity, further demonstrating the crossover dynamic nature.

Sonication led to a decrease in the solution shear-thinning behaviour and viscosity. The relaxation time of the slow relaxation was also found to decrease, consistent with the previously established correlation between solution viscosity and the slow relaxation mode. SLS did not probe any change in the structure. Additional LS and Size Exclusion Chromatography (SEC) suggested that there was no significant Na CMC chain breakage, if any, and that the proportion of Na CMC chains involved in the domains decreased. Hence, it was proposed that the shear forces applied during sonication were strong enough

to remove some Na CMC chains from the domains, while the domain sizes remained constant. These looser domains would be more deformable under flow, leading to the observed decrease in the viscosity and shear-thinning behaviour. A partial or full recovery of the slow relaxation mode was also observed after a month, supporting the hypothesis that domains could correspond to a metastable equilibrium, while sonication had no effect on the solutions with added salt, suggesting that electrostatic forces could be responsible for the cohesion of the domains.

Table of Contents

Table of Figures

Table of Tables

Chapter 1: Introduction

Sodium Carboxymethyl Cellulose (Na CMC) is a linear semi-flexible negatively charged polyelectrolyte. It is made from cellulose, which is the most abundant biopolymer on Earth.[1,2] Because of its high availability as well as its thickening and swelling properties, Na CMC is widely used in numerous industries.[1-3] Application fields are shown in Figure 1-1 and include food, pharmaceutical, home and personal-care products, as well paper industry, paint, water treatment and mineral processing.[1-5] The Na CMC global market represented 1.2 billion USD in 2016[6] and is expected to exceed 1.7 billion USD by 2024.[7]

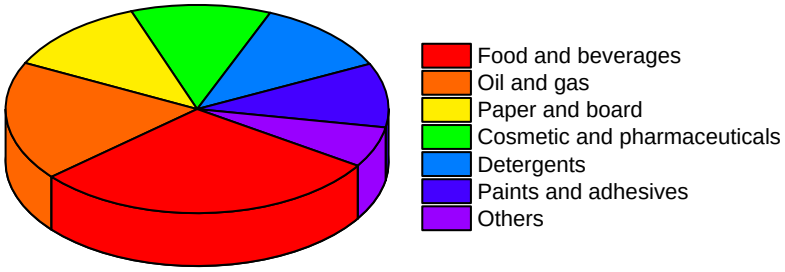

Figure 1-1: Global Na CMC market by application in 2016 (%). Data from Grand View Research.[6]

The market of formulated products (*i.e.* food & beverages, cosmetic & pharmaceuticals, and detergents) represents more than half of the global Na CMC market. Such products contain a large number of compounds as illustrated in Table 1-1. The nature of these compounds is broad: solid particles (*e.g.* silica), polymers (*e.g.* Na CMC), oils (*e.g.* fragrance and flavouring oils), surfactants, salts or proteins are a few examples. As seen in Table 1-1, each of them fulfil a specific role in the formulated product. The active ingredients allow the product to fulfil its purpose, while other ingredients are incorporated to manage the product structure, taste, appearance or shelf-life. A general challenge in formulating such complex systems is to understand the interactions between all the components and their effects on the efficacy and the stability of the product over its full shelf-life.

Table 1-1: Examples of compositions of formulated products.

Ingredient type[8-11]	Purpose[8-11]	Toothpaste[8] (%)	Hand-washing liquid[10] (%)	High-protein soy desserts[11] (%)
Abrasives	Clean and polish	Xerogel silica (14)	*n/a*	*n/a*
Binders (or thickeners)	Prevent separation of ingredients, control the rheological properties	Precipitated silica (8), Na CMC (0.3)	Na CMC (0.05)	Na CMC (0.9-3)
Colouring agents	Attractive appearance	Colour solution (1.5)	Fluorescent whitening agent (0.1)	Colouring (0.026)
Surfactants (or detergents or emulsifiers)	Foaming action, stabilisation of emulsions and foams	SLS (1.5)	Alkylbenzenesul-fonate (6.5), potassium soap (1.5), non-ionic surfactants (2.5)	
Flavouring/ fragrance agents	Pleasant taste, lingering aftertaste	Flavour (1)	Perfume (1)	Citrus flavour (0.026)
Preservatives	Prevent growth of bacteria and mould	Na benzoate (0.1)		
Sweeteners	Pleasant flavour	96% glycerine (25), Na saccharin (0.2)	*n/a*	Sucrose (4)
Humectants	Maintain moisture and consistency	70% sorbitol solution (46.02)		
Fluoride source		Na_2PO_3F (0.78)	*n/a*	*n/a*
Water softening agents		*n/a*	STP (30), Na silicate (2)	*n/a*
Proteins		*n/a*	*n/a*	SPI (6-8)
Water		Water (24.12)	Water (balance)	Water (balance)

SLS: Sodium Lauryl Sulfate; STP: Na triphosphate; SPI: Soy Protein Isolate; *n/a*: not appropriate (*i.e.* not expected to enter the composition of this type of product, even if the formulation was different). Figures in brackets correspond to the proportion of each compound.

Na CMC is often used in formulated products to control their rheological properties. For example, in the case of toothpaste, Na CMC is responsible for toothpaste performances, including toothpaste stability in its container, dispensing, in-mouth behaviour and rinsing of the sink after use.[8] Despite its broad use in industry, Na CMC behaviour in solution is still relatively poorly understood and is the subject of research from both fundamental[1,12-15] and applied perspectives.[11,16-19] The polyelectrolyte nature of Na CMC is, in itself, a reason for this poor understanding. Indeed, many questions remain about the behaviour of charged polymers in solution,[15,20] and especially in salt-free solutions, such as the origin of the slow relaxation mode observed with Light Scattering (LS) whose presence is not predicted by the theory.[21-23] Furthermore, because of Na CMC biological origin, there is a broad diversity between batches as well as within individual batches. This diversity can come from the typically high polydispersity of the chain length distribution,[1,3,24,25] the crystallinity of the cellulose raw material,[24,26,27] and/or the amount and the distribution of the carboxymethyl groups along the chains.[18,26,28-30] These charged carboxymethyl groups are key to the behaviour of Na CMC in solution as they confer its water-solubility to Na CMC. If there are not enough of these groups and/or if they are not homogeneously distributed along Na CMC chains, Na CMC chains or chain sections are not fully solubilised in water.[26,28,29] These inter- and intra-batch variabilities make it harder to investigate and understand the behaviour of Na CMC in solution.

Light Scattering (LS) has been widely used to study other charged polymers[31-34] and/or polysaccharides.[35-38] Static Light Scattering (SLS) allows to study the conformation and the organisation of the polymer chains in solution, while Dynamic Light Scattering (DLS) studies their dynamics.[39,40] Such information, combined with rheological investigations, would allow establishing structure-properties relationships, which could then be used to understand the rheological behaviour of Na CMC formulations and help formulating products. Surprisingly, to my knowledge, no extensive LS investigation of the behaviour of Na CMC in solution across a wide range of concentrations has been performed. The possible presence of poorly dissolved Na CMC fractions which would scatter the light strongly, thus adding another contribution to the scattering and possibly hiding the scattering contribution of the properly dissolved Na CMC chains, as well as the typically high viscosity of Na CMC solutions as used in the industry, are two of the few obstacles that need overcoming to investigate the behaviour of Na CMC in solution with LS.

A decrease in Na CMC solution viscosity has been observed over time[12,41,42] and attributed to the breakage of Na CMC chains.[1] Meanwhile, sonication has been widely used to break polymer chains,[43,44] including Na CMC chains.[45,46] Studying the effect of sonication on Na CMC solution may thus provide some information about ageing phenomena occurring in Na CMC formulations, which would be of interest for industrial applications as shelf-life is a major concern for formulated products.

The aim of this thesis is to investigate structure-property relationships of Na CMC in solutions with and without added salt using both rheology and light scattering. The objectives are:

1. To assess the current knowledge about polyelectrolyte behaviour in solution, and especially, about how rheology and light scattering measurements can help understanding their behaviour in solution.
2. To identify Na CMC characteristics and understand how they influence its behaviour in pure water and in presence of salt, especially in terms of rheological and scattering behaviour.
3. To study the behaviour of Na CMC in salt-free water using both rheology and light scattering.
4. To investigate the influence of sonication on Na CMC formulated solution structure-property relationships.

To answer the first two objectives, a literature review has been completed and its main outcomes are presented in Chapter 2. Then, rheological and light scattering methods have been developed and subsequently used to study the behaviour of salt-free Na CMC solutions as reported in Chapter 3. The developed methods have also been used to investigate the influence of sonication on Na CMC formulated solutions, in combination with Size Exclusion Chromatography (SEC), and these investigations are detailed in Chapter 4.

Chapter 2: Literature review

2-1. Outline

In this Chapter, the behaviour of polyelectrolytes in solution is reviewed first. The conformation and dynamics of polymer chains in solution is described, and it is shown how rheology and light scattering typically help assessing them. Then, Na CMC and its characteristics are introduced, before the main outcomes of the already performed scattering and rheological studies about salt-free Na CMC solutions are presented and compared to the ones of polyelectrolytes. Finally, the influence of Na CMC characteristics, salt addition and sonication on Na CMC behaviour in solution as studied by scattering and rheology are discussed.

2-2. Polyelectrolytes

2-2.1. Polymers in good solvents: overall picture

In this Section, the behaviour of polyelectrolytes in pure water is described, as well as the one of neutral polymers in good solvents. Polyelectrolytes are described here in absence of added salt.

2-2.1.1. Three main regimes to describe polyelectrolyte conformation as a function of concentration

The conformation of the polymer chains in solution depends on polymer concentration. Three different regimes can thus generally be observed. They are called (i) dilute regime, (ii) semi-dilute regime and (iii) concentrated regime. The scaling model, established by de Gennes in the 1970s, describes these three regimes for neutral and charged polymers.[47,48] It consists in the definition of characteristic length scales, which are appropriate to describe the conformation of the polymer chains in solution.

(i) Dilute regime

In the dilute regime, neutral polymer chains are far from each other. They can be described by chains of thermal 'blobs' of diameter ξ_T as illustrated in Figure 2-1.A. This length-scale corresponds to the length-scale at which the excluded volume interactions

equal k_BT (k_B: Boltzman constant; T: temperature).[49] Below this length-scale (*i.e.* inside the thermal blobs), thermal energy dominates over excluded volume interactions and the polymer chains follow a random walk. Above this length-scale, however, the energy related with excluded volume interactions is higher than k_BT and the chains can be described as a sequence of thermal blobs undergoing a self-avoiding walk.[49]

Regarding polyelectrolytes in the dilute regime, one first needs to understand how the counterions behave. An important length-scale in this regard is the so-called Bjerrum length (Eq. 2-1),[1] l_B, which corresponds to the distance at which the electrostatic (or Coulomb) energy of two elementary charges e equals the thermal energy k_BT.

$$l_B = \frac{e^2}{4\pi\varepsilon\varepsilon_0 k_B T} \tag{2-1}$$

where ε and ε_0 are the relative dielectric constant and the permittivity of vacuum, respectively. For example, water Bjerrum length equals 7.1 Å at 25°C.[1,50] According to Manning counterion condensation theory, if the distance between two charges on the polymer chain is above the Bjerrum length, all the counterions are free in solution and the polymer chains are stretched to reduce the repulsive interactions.[50,51] Otherwise, counterions condense on the chains to lower the repulsion until the distance between effective charges equals the Bjerrum length,[50,51] and the chains can be divided into 'electrostatic blobs' of diameter $\xi_e = l_B$.[20,48] Consequently, polymer chains can be represented by chains of electrostatic blobs of diameter ξ_e as depicted in Figure 2-1.B. On scales larger than ξ_e, repulsive electrostatic interactions dominate: the chains of electrostatic blobs form a stretched directed random walk chain (*i.e.* they are stretched along the chain axis while the statistics they follow into the two other directions are random walks).[1,50] Within an electrostatic blob, there is no electrostatic interaction: in good solvents, the statistics of the chain follows a self-avoiding random walk.[1,50]

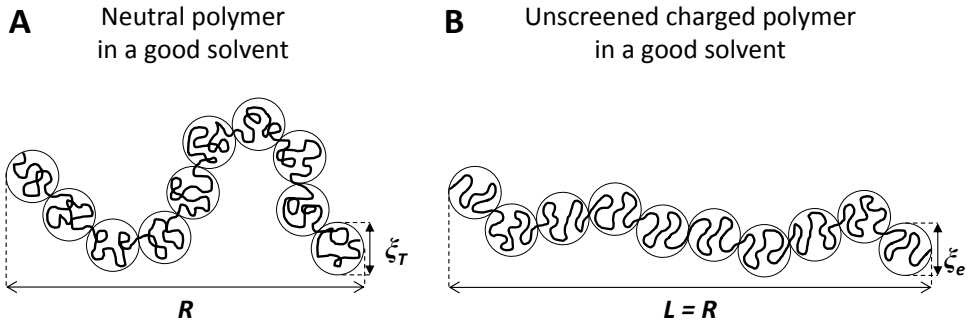

Figure 2-1: Neutral (**A**) and unscreened charged (**B**) polymers in dilute solutions. ξ_T: diameter of the thermal blob; ξ_e: diameter of the electrostatic blob; L: polymer chain length; R: end-to-end polymer chain distance.

One may wonder what happens to the counterions which are not condensed on polymer chains. As for small electrolytes, charged species tend to be surrounded by oppositely charged species to maintain electroneutrality. The free counterions therefore form clouds around polymer chains, thus screening the electrostatic interactions at large distances.[51] The distance at which the screening of the electrostatic interactions occurs is the Debye screening length r_D[20,51] given by Eq. 2-2.[52]

$$r_D = (4\pi l_B \sum_s c_s {q_s}^2)^{-1/2} \quad (2\text{-}2)$$

where c_s is the concentration of small ions and q_s their valence. As illustrated in Figure 2-2, the Debye screening length can be viewed as a sphere of equivalent radius r_D containing the cloud counterions.

As shown in Figure 2-2.A, when the counterion concentration is very low in dilute solutions, the Debye screening length r_D is large compared with the distance between the chain centres of mass R_{cm}.[20] Hence, as previously explained, the effective charges on polyions interact with each other. When the polyelectrolyte concentration increases, the counterion concentration increases too, leading to a decrease in the Debye screening length which eventually equals the distance between the chains R_{cm} (note that R_{cm} decreases too when the polyelectrolyte concentration increases).[47] The concentration at which the Debye screening length r_D equals the distance between chains R_{cm} is referred as c_{int}. Below this concentration, chains interact strongly with each other, and $c_{int} \approx 4 \times 10^{-8}$ M was found for a 690,000 g/mol poly(styrene sulfonate) sample in water.[47] As shown in Figure 2-2.B, when $r_D < R_{cm}$, there would be counterion-free spaces in solution, leading to a large entropy penalty. Dobrynin *et al.*[47] thus proposed that, above c_{int}, the screening length r_{sc} is the inter-chain distance R_{cm} as illustrated in Figure 2-2.C. It is worth noting that the previous explanations about the Debye screening length are valid for temperatures below the θ temperature; which is the most common case.[47]

From the description of the conformation of both neutral and charged polymers in good solvents, it can easily be deduced that the size of unscreened charged chains is larger than neutral chains of similar structure and molecular weight M_w. As electrostatic repulsion decreases when polyelectrolyte concentration increases, the size of the polyelectrolyte chains decreases across the dilute regime.

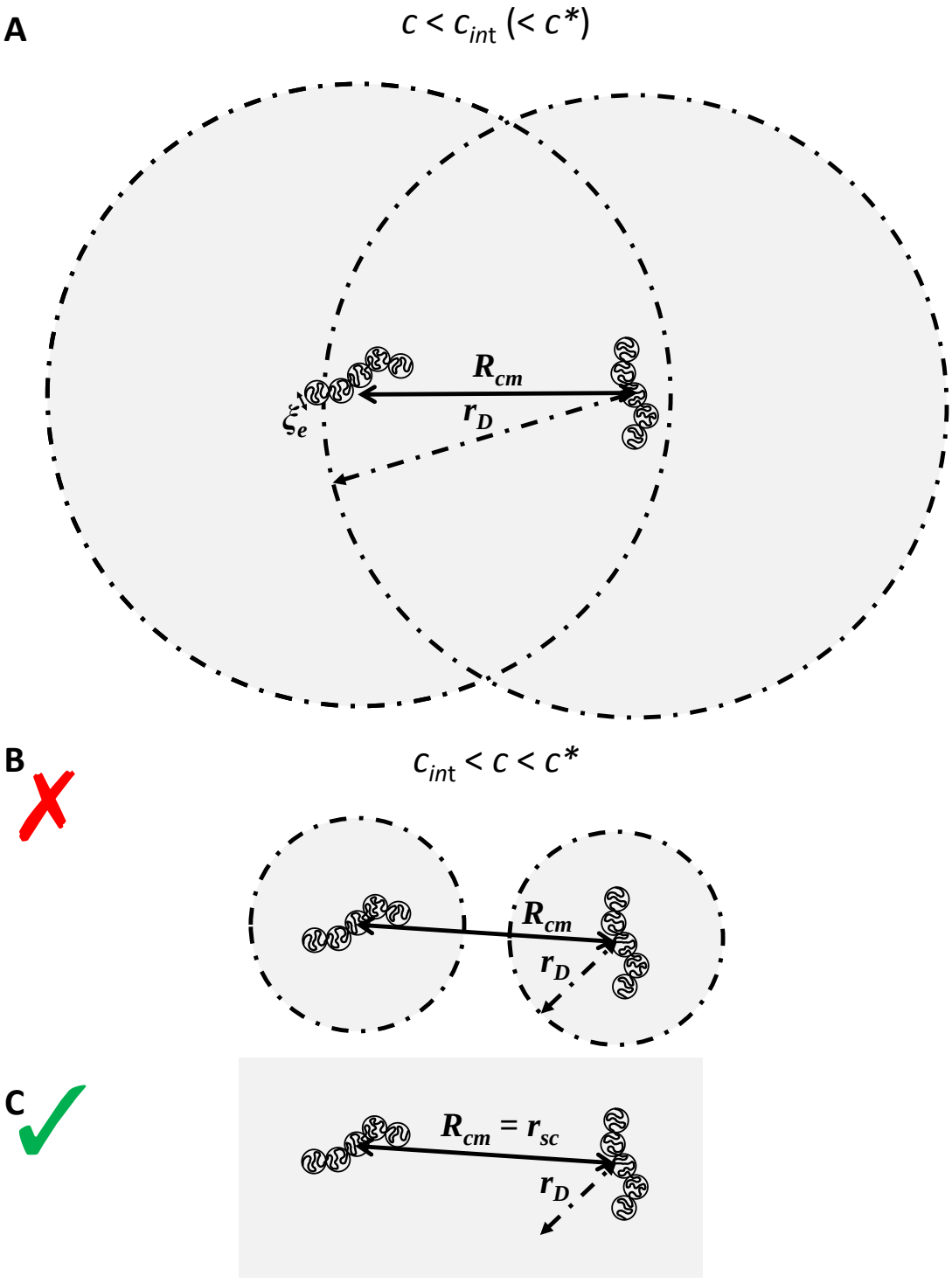

Figure 2-2: Illustration of the Debye screening length r_D as a function of polyelectrolyte concentration c when $c_{int} < c^*$. c_{int}: concentration below which chains interact strongly; c^*: overlap concentration; R_{cm}: distance between chain mass centres; r_{sc}: screening distance; ξ_e: electrostatic blob diameter. **A.** $c < c_{int} < c^*$. **B & C.** $c_{int} < c < c^*$. B corresponds to the case where Debye-Hückel theory is violated, while C is the alternative model proposed by Dobrynin *et al.*[47] to solve the violation. The grey areas represent the counterion clouds. *N.B*: The reduction in polyion size upon increasing polyelectrolyte concentration is not depicted in the Figure.

(ii) Semi-dilute regime

As the polymer concentration increases, polymer chains, whether neutral or charged, start to interpenetrate, which defines the beginning of the semi-dilute regime. In the semi-dilute concentration regime, both neutral and charged polymer chains can be depicted by chains of correlation blobs of diameter ξ as shown in Figure 2-3. The correlation length ξ represents the typical distance between two chains (also called mesh size). As illustrated in Figure 2-4, the characteristic concentration at which the semi-dilute regime starts is called the overlap concentration c^* and corresponds to the concentration at which the distance between two polymer chains is on the order of their size. The correlation volumes defined by ξ are space-filling and are at overlap with each other.[49] The overlap concentration also corresponds to the concentration at which the local polymer concentration is identical to the one of the overall solution. A correlation blob (*i.e.* length-scales smaller than ξ) mainly contains monomers from a single monomer chain.[49]

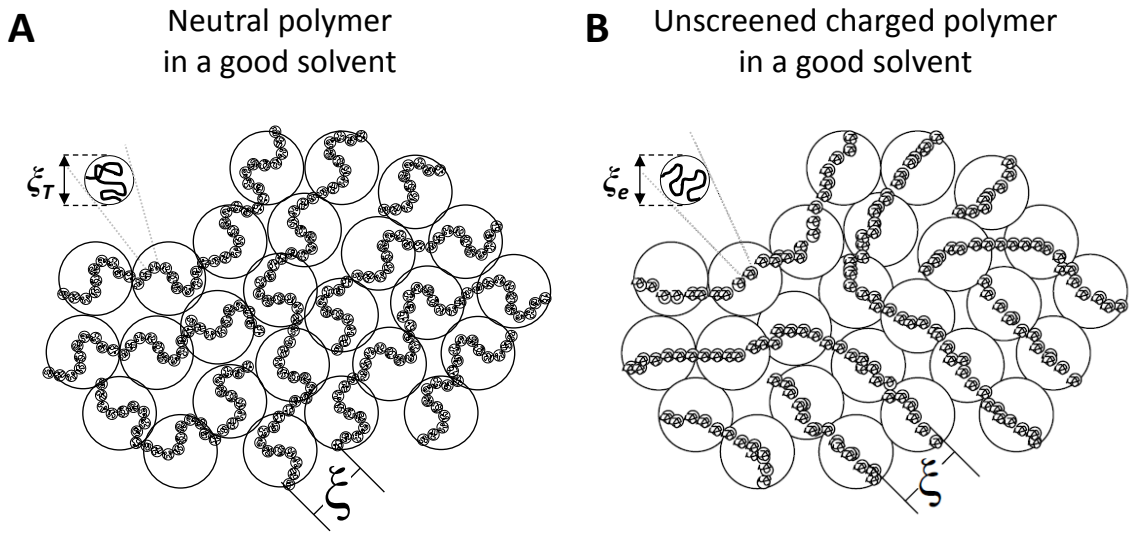

Figure 2-3: Neutral (**A**) and unscreened charged (**B**) polymers in semi-dilute solutions. ξ: correlation length (*i.e.* diameter of the correlation blobs); ξ_T: diameter of the thermal blob; ξ_e: diameter of the electrostatic blobs. B adapted by permission from Springer Nature, *Rheology Acta*, Colby,[48] Copyright © Springer-Verlag 2009.

For neutral polymers, ξ sets the range of the excluded volume interactions. On scales larger than ξ, the excluded volume interactions are screened by the neighbouring (and overlapping) chains, and the chains of correlation blobs follow a random walk. On scales between ξ and ξ_T, excluded volume interactions are significant, and the chains of thermal blobs follow a self-avoiding random walk like in the dilute regime (see previous sub-

section). Likewise, on scales smaller than ξ_T, the chain conformation is identical to that in the dilute regime.[49]

For charged polymers, ξ sets the range of the electrostatic interactions.[20,50,53] On scales larger than ξ, electrostatic interactions are screened by the other polymer chains (and their associated counterions), and the polymer chains can be viewed as random walks of correlation blobs. Within a correlation blob, the local conformation of the monomer chain is a directed random walk of electrostatic blobs as in the dilute regime (see previous sub-section).

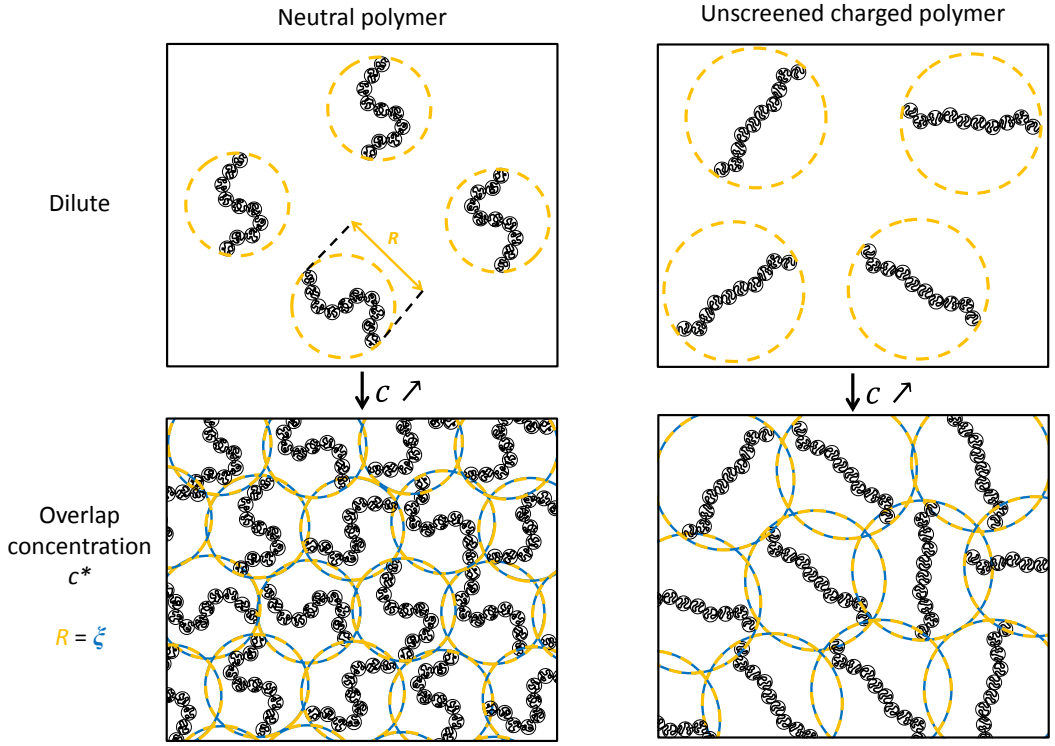

Figure 2-4: Illustration of the overlap concentration c^* for both neutral and charged polymers. R: end-to-end chain distance (yellow dashed circles); ξ: correlation length (blue circles); c: polymer concentration.

Because of the more extended conformation of the charged polymer chains compared to the neutral ones, the overlap concentration of a charged polymer is lower than the one of a neutral polymer of identical M_w.

(iii) Concentrated regime

As the polymer concentration increases, the distance between the polymer chains (*i.e.* the correlation length ξ) decreases, while the smallest characteristic length-scales (*i.e.* thermal blob ξ_T or electrostatic blob ξ_e for neutral or charged polymers, respectively)

does not change. Thus, there is a characteristic concentration c^{**} where both length-scale equal each other (*i.e.* $\xi = \xi_T$ or $\xi = \xi_e$ for neutral or charged polymers, respectively).

For neutral polymers above c^{**}, the correlation length ξ becomes smaller than the diameter of the thermal blobs ξ_T. Hence, the excluded volume interactions are screened at all length-scales and the polymer chains behave like ideal chains, thus following a random walk.[49] It is worth noting that non-fully flexible polymer chains would only follow a random walk at large length-scales. [49]

For charged polymers above c^{**}, the correlation length ξ becomes smaller than the diameter of the electrostatic blobs ξ_e. The electrostatic interactions are screened at all length-scales and the polymer chains behave like neutral polymer chains.[47,50,54]

Although these three regimes can be identified by experiments, they are not enough for explaining all the experimental outcomes. The next Section thus provides the required information to complete the picture.

2-2.1.2. Additional information to complete the picture

Experiments show that the semi-dilute regime may be divided into two sub-regimes: the non-entangled semi-dilute regime and the entangled semi-dilute regime (although, this may not be the case for all polymers as the polymer chains need to be long enough to get entangled[50]). To understand the distinction between these two regimes, one needs to look at the dynamics of the chains in the different concentration regimes.

Dilute regime

When a segment of a polymer chain moves, it drags the surrounding solvent molecules and makes the other segments of the polymer chain move in a similar way.[49,51] This phenomenon is called hydrodynamic coupling. Consequently, the motion of a polymer chain can be seen as the motion of a single object constituted by the polymer chain and the surrounding solvent molecules.[49,51] The radius of a sphere having the same volume as this object is called hydrodynamic radius (see Eq. 2-19).[55] The description of the polymer chain motion in the dilute regime, where hydrodynamic coupling is important, can be well described using the so-called Zimm model. The time required for a chain to diffuse a distance of order of its own size is called the Zimm relaxation time τ_z.[49]

Non-entangled semi-dilute regime

As depicted in Figure 2-5, according to Rouse model, the chains of correlation blobs can be viewed as beads connected by springs.[20,49,51] The beads only interact with each other through the connecting springs while solvent molecules freely drain through the chains as the chains move, *i.e.* there are no hydrodynamic interactions. The motion of such chains in solution is diffusive. The time required for a chain to diffuse a distance of order of its own size is called the Rouse relaxation time τ_R.[49] Within a correlation blob, polyelectrolyte chain conformations look like the conformation in the dilute regime. At this scale, the dynamics of the chains thus follow the dynamics of polymer chains in the dilute regime (*i.e.* Zimm dynamics; see previous paragraph).[20,49]

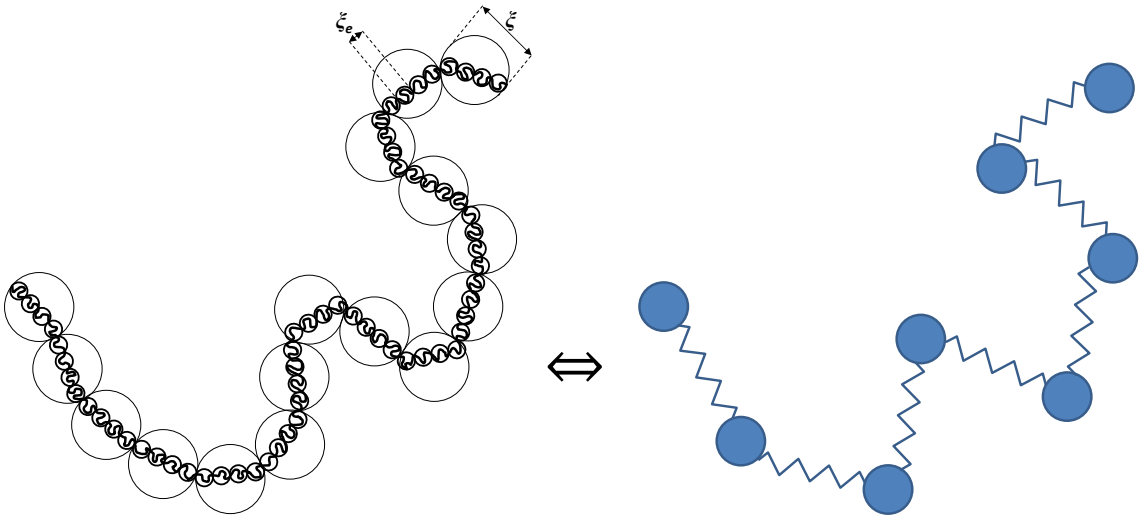

Figure 2-5: Spring and bead representation of polyelectrolyte chains in the Rousse model. On the left: a polyelectrolyte chain in the semi-dilute regime. ξ: correlation length; ξ_e: of the electrostatic blobs. On the right: spring (∿) and bead (●) representation of the same polyelectrolyte chain. *N.B:* the spring and bead model is also valid for neutral polymers; the 'blob representation' of such polymer chains is depicted in Figure 2-3.

Entangled semi-dilute regime

Entanglements are the consequence of the fact that polymer chains cannot cross each other.[49] Another length-scale has to be introduced to describe the polymer conformation: the Edwards tube diameter *a*, which is directly related to the length-scale between entanglements.[20,47,48] Each polymer chain can be depicted as a random walk of correlation blobs diffusing along an effective tube of diameter *a* formed by the surrounding chains, as illustrated in Figure 2-6. *a* is much larger than the correlation length ξ.

Regarding hydrodynamics, on length-scales larger than the tube diameter *a*, polymer chains reptate in tubes of diameter *a*. The reptation relaxation time τ_{rep} corresponds to the

time needed by the polymer chains to go out of the tube they are initially contained in. On length-scales smaller than *a* but larger than the correlation length ξ, polymer chain conformation and dynamics are similar to those of the non-entangled semi-dilute regime (*i.e.* chains of correlation blobs following Rouse dynamics), while on length-scales lower than the correlation length ξ, polymer chain conformation and dynamics are similar to the ones of the dilute regime (*i.e.* chains of electrostatic blobs following Zimm dynamics).[20,49]

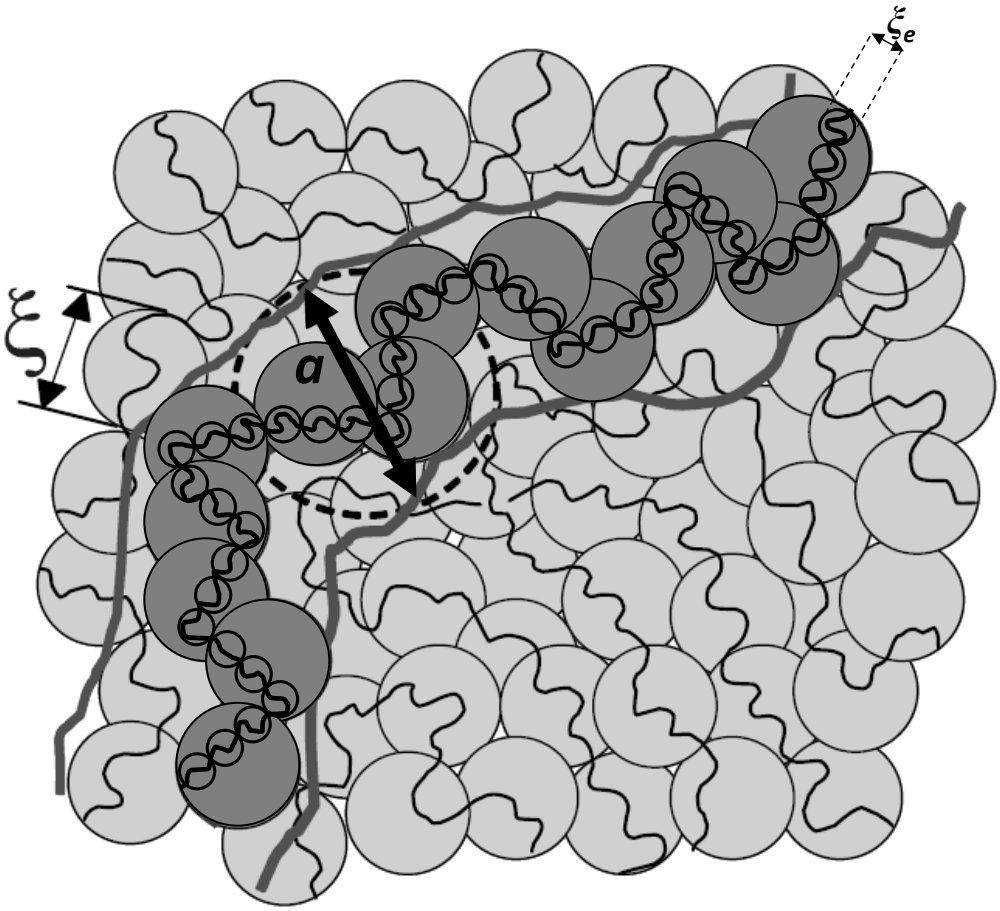

Figure 2-6: Polyelectrolyte chain conformation in a semi-dilute entangled solution. ξ: correlation length; ξ_e: electrostatic blobs; *a*: diameter of the Edwards tube. *N.B:* To avoid overloading the picture, the electrostatic blobs are only represented for the chain whose Edwards tube is depicted. Moreover, a schematic showing a similar polymer chain conformation at length-scales above ξ, and where the polymer chain conformation inside the correlation blobs (*i.e.* below ξ) would be similar to the one depicted in Figure 2-3.A, would describe neutral polymer chain conformation in a semi-dilute entangled solution. Adapted from Dobrynin and Rubinstein,[20] Copyright © 2005 Elsevier Ltd, with permission from Elsevier.

2-2.2. Concentration-dependence of polymer solution viscosity and scaling laws of neutral and charged polymers in good solvents

Both neutral and charged polymer conformations and dynamics in good solvents have just been described. Hence, it has been shown that, depending on the polymer chain ability

to form entanglements, they are three to four concentration regimes and that each of them can be described using one or several characteristic length-scales. DeGennes has established scaling laws which quantitatively describe these concentration regimes[20,48] and thus allow their identification. These scaling laws consist of power law relationships where one quantity changes as the power of another, *i.e.* $Y \sim X^{\nu}$, where Y could, for example, be a rheological parameter, X could be the polymer concentration, and ν is the power law exponent and has a distinct value for each concentration regime and (X,Y) variables.[49] It is shown hereafter how viscosity measurements can be used to determine the concentration regimes. The typical flow behaviour of polymer solutions is first described. Here too, polyelectrolytes are described in the absence of added salt.

Figure 2-7.A shows the flow curves of a 17% quaternized poly(2-vinyl pyridine) at different concentrations in ethylene glycol, which is a good solvent for the investigated polymer. At low shear-rates, the solution viscosity is shear-rate independent, while it decreases as the shear-rate increases at high shear-rates. Such a decrease in viscosity upon an increase in shear-rate is called shear-thinning and is explained by the alignment of the initially interpenetrated or entangled polymer chains along the direction of flow.[56] This behaviour can be described by the Carreau model[1,14,50] (Eq. 2-3) defined as:

$$\eta(\dot{\gamma}) = \frac{\eta_0}{(1+(\tau\dot{\gamma})^2)^p} \quad (2\text{-}3)$$

where the zero-shear viscosity η_0 describes the viscosity plateau at low shear-rates, the time constant τ corresponds to the inverse of the shear-rate characterising the onset of the shear-thinning behaviour, and the exponent p describes the behaviour of the viscosity as a function of the shear-rate in the shear-thinning region.

As the polymer concentration increases, the solution viscosity increases. Though not shown on the graph, the authors say that the viscosity of dilute solutions is shear-rate independent.[50] Such a behaviour is called Newtonian behaviour.[1,57]

It is worth noting that similar behaviours are found for neutral polymers in good solvents, apart from the fact that the onset of the shear-thinning region exhibits a different behaviour.[56,58,59] Indeed, the data displayed in Figure 2-7.A corresponding to a charged polymer shows that the shear-rate from which the shear-thinning behaviour starts increases as the polymer concentration increases,[50,56,60] while it is the opposite for a neutral polymer.[56,58,59] The shear-rate from which the shear-thinning behaviour starts corresponds to the reciprocal of the longest Rousse relaxation time τ_R, defined in

Section 2-2.1.1.[56] τ_R has been shown to scale as $\tau_R \sim c^{0.31} \sim \dot{\gamma}^{-1}$ and $\tau_R \sim c^{-0.5} \sim \dot{\gamma}^{-1}$ for neutral and charged polymers, respectively.[48] This is due to the fact that, above c^*, for the same increase in polymer concentration, the reduction in polymer chain size for polyelectrolytes is much more significant than for neutral polymers.[48]

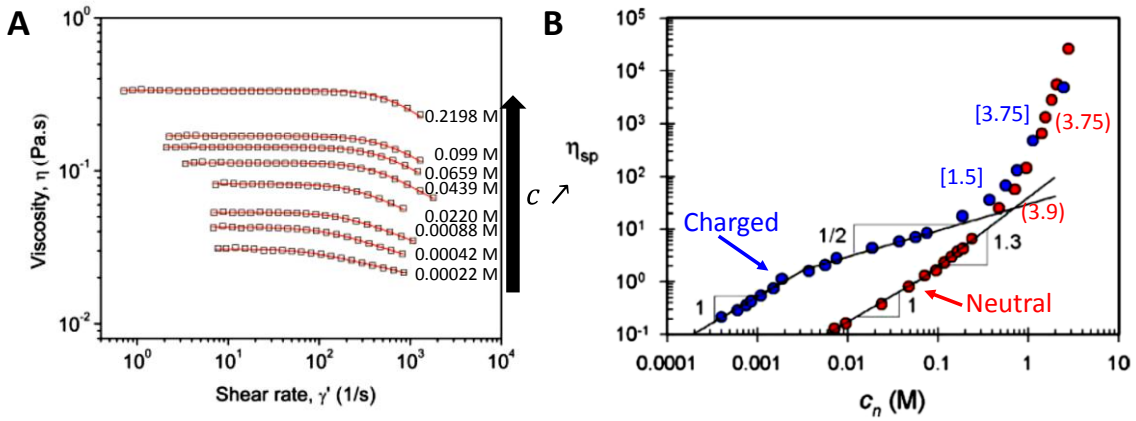

Figure 2-7: Example of polymer flow behaviour (**A**) and concentration-dependence of the specific viscosity η_{sp} for both neutral and charged polymers in good solvents (**B**). **A.** Flow curves of 17% quaternized poly(2-vinyl pyridine) solutions in ethylene glycol. Solution concentrations are indicated on the right-hand side. Red lines represent fits to the Carreau model. From Dou and Colby,[50] Copyright © 2006 Wiley Periodicals, Inc, adapted by permission from John Wiley and Sons, Inc. **B.** Specific viscosity η_{sp} as a function of the monomer concentration c_n. Black lines: fits to power laws. Power law exponents are provided in black. Exponents expected for the regimes at higher concentrations are provided into red brackets and blue crochets for the neutral and the charged polymers, respectively. Blue: 55% quaternized poly(2-vinyl pyridine) in ethylene glycol; red: poly(2-vinyl pyridine) in ethylene glycol. Adapted by permission from Springer Nature, *Rheology Acta*, Colby,[48] Copyright © Springer-Verlag 2009. Both quaternized polymers presented in this Figure come from the poly(2-vinyl pyridine) sample shown in B. Its characteristics are the following: M_w = 364,000 g/mol; M_w/M_n = 1.06; degree of polymerisation N: 3,230; supplier: Polymer Source.

From the shear-rate independent viscosity of dilute solutions or the zero-shear viscosity η_0 of more concentrated solutions determined using the Carreau model (Eq. 2-3), the specific viscosity η_{sp} (Eq. 2-4) can be calculated as:[1,14,15,48,50]

$$\eta_{sp} = (\eta_{sp} - \eta_s)/\eta_s \qquad (2\text{-}4)$$

where η_s is the solvent viscosity. Figure 2-7.B shows the concentration dependence of the specific viscosity for a non-quaternized (neutral) and a 55% quaternized (charged) poly(2-vinyl pyridine) polymer in a good solvent. The charged polymer was derived from the neutral polymer and thus has the same polymerisation degree (*i.e.* the same number of monomers per chain).[48] Hence, for proper comparison of the behaviour of both polymers, the specific viscosity was plotted as a function of the monomer concentration.

At low monomer concentrations, the specific viscosity of the charged polymer solution is higher than the one of the neutral polymer solution. This is due to the fact that charged polymer chains are more extended in solution than neutral polymer chains in solution (see Section 2-2.1). At high concentrations, the behaviour of both polymer solutions is identical. Indeed, charges are screened on polyelectrolyte chains and they behave like neutral chains.[15,48] As illustrated by the black lines, the data can be described by power laws $\eta_{sp} \sim c^{v}$ where the exponent *v* depends on the concentration region. Each of these regions has a characteristic power law exponent (displayed above and below the data of the charged and the neutral polymers, respectively), and corresponds to a different concentration regime, *i.e.* (i) dilute, (ii) semi-dilute non-entangled, (iii) semi-dilute entangled and (iv) entangled. The exponent values are also provided in Table 2-1.

Table 2-1: Power law exponents[15,48,61] *v* predicted by the scaling laws for both neutral and charged polymers in good solvents.

Concentration regime	*v(neutral polymer)*	*v(charged polymer)*
Dilute	1	1
Semi-dilute non-entangled	1.3	0.5
Semi-dilute entangled	3.9	1.5
Concentrated	3.75	3.75

Variations from the power law exponents predicted by the scaling laws have been reported in the literature. For example, values of 0.35 and 0.68 ± 0.02 were found for sodium poly(styrene sulfonate) and Na CMC, respectively.[1] Hypotheses to explain the higher value obtained for Na CMC included its polydispersity and its semi-flexible nature.[1] The scaling laws have indeed been established for flexible polymers.

Figure 2-7.B also shows that the overlap concentration *c** characterising the transition between the dilute regime (*v* = 1) and the semi-dilute regime (*v(charged polymer)* = 0.5 and *v(neutral polymer)* = 1.3) is lower for neutral polymers than charged polymers, as already mentioned when *c** was introduced in Section 2-2.1.1. *c** is reached for a value of the specific viscosity of 1.[1,48] For two polymers of identical polymerisation degree, it is found that *c*(neutral polymer)* ≈ 10 *c*(charged polymer)*.[48] It is worth noting that the concentration-dependence of the specific viscosity η_{sp} of fully screened polyelectrolyte solutions is identical to the one described above for neutral polymer solutions.[15] When

the added salt concentration is not high enough to screen all the charges along the chains, intermediate behaviours are observed.[15]

2-2.3. Light Scattering (LS) of polyelectrolyte solutions

Polyelectrolytes have been widely characterised using Light Scattering (LS), which is a powerful technique to study the conformation of polymer chains in solution as well as the dynamics. Before going through the typical outcomes of LS measurements on polyelectrolyte solutions, the principle of LS measurements is first explained, where Dynamic Light Scattering (DLS) and Static Light Scattering (SLS) are introduced. The findings reported for both types of LS measurements for polyelectrolyte solutions are then summarised. Finally, more details are given about the slow relaxation mode observed with DLS and which is not predicted by the theory.

2-2.3.1. The principle of Light Scattering (LS) measurements

In LS experiments, a laser beam goes through a sample. The light of the laser is a plane electromagnetic wave and induces an electric field. When the 'objects' present in the solution (*e.g.* molecules, particles, aggregates) are subjected to this electric field, their charges experience a force, are accelerated and scatter the light.[62] The total scattered electric field corresponds to the sum of the electric fields coming from all the scatterers illuminated by the laser beam. It thus depends on the relative arrangement of the scatterers in the sample. The 'objects' in the solution are constantly moving because of thermally driven fluctuations. The position of the scatterers thus changes over time. This also makes the scattered electric field fluctuate over time.[62] Such fluctuations contain information related to both solution structure and dynamics. The present Section aims to show how the information related to the electric field is obtained from the experiments.

Description of a Light Scattering (LS) spectrometer

Figure 2-8 shows a schematic of a LS spectrometer. The sample, contained in a glass vial, is inserted in the measurement cell. The outer part of the measurement cell is filled in with decalin. The refraction index of decalin is indeed very close to the one of the glass to reduce stray light.[63]

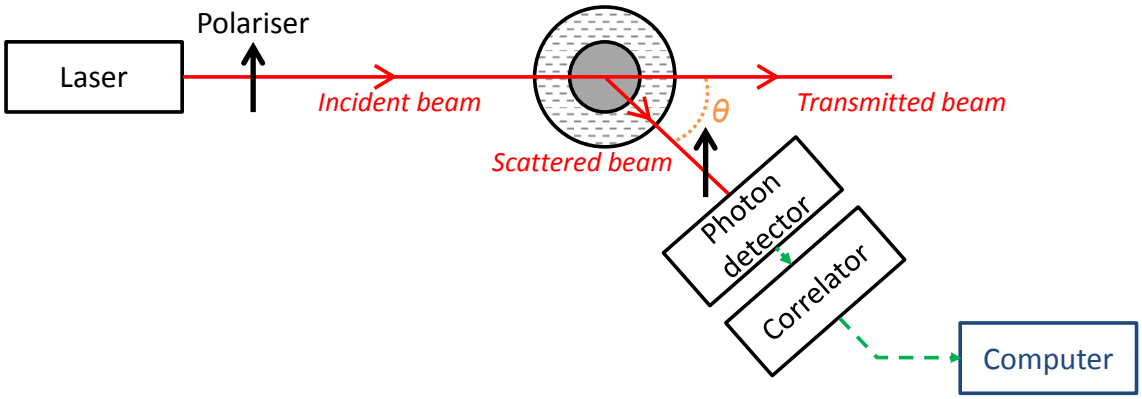

Figure 2-8: Schematic of a LS spectrometer. Black elements: belong to the LS spectrometer; Blue element: computer; —: laser beam; - -: signal; ■: sample; - -: glass index matching liquid; θ: scattering angle.

The laser beam goes through the sample. A fraction of the laser beam is scattered by the sample in all directions and gives rise to scattered light, while the rest of the laser beam simply goes through the sample and gives rise to the transmitted beam. The scattered light at angle θ reaches the photon detector. If a screen would be placed in front of the photon detector, a speckle pattern would be seen (see left-hand side of Figure 2-9).[63,64] As the 'objects' move in the sample, this speckle pattern would change: some previously dark speckles would become bright while some previously bright speckles would become dark.[63,64] Depending on the LS spectrometers, the photon detector records the fluctuations over time of the intensity of either one speckle or several speckles. The instrument used for the experiments reported in Chapters 3 and 4 records the intensity fluctuations of a single speckle as illustrated in Figure 2-9. The curve of the intensity of the light *I(t)* over time is commonly called count trace (right-hand side of Figure 2-9).

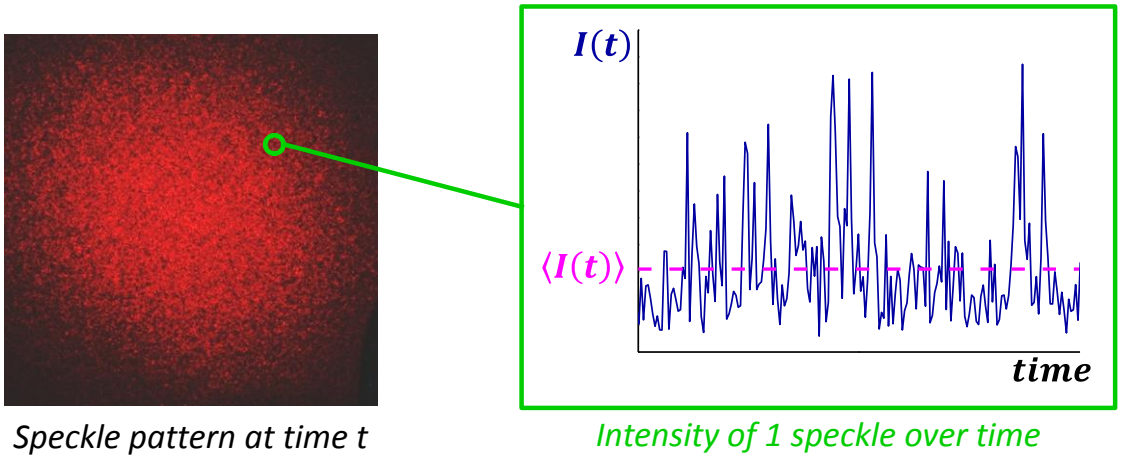

Figure 2-9: Example of a speckle pattern (left-hand side) and time-evolution of the intensity of one speckle (right-hand side; data collected with the instrument used to collect the LS data for this thesis). *I(t)*: scattering intensity at time *t*; $\langle I(t) \rangle$: scattering intensity averaged over time.

As seen from Figure 2-9, the count trace looks like a noisy signal.[62] Indeed, as the motion of the 'objects' present in solution is erratic, the signal collected by the detector varies randomly over time. This noisy signal can be analysed using two approaches: (i) looking at the fluctuations of the scattering intensity over time (Dynamic Light Scattering), or (ii) looking at the time-average intensity (Static Light Scattering)

Dynamic Light Scattering (DLS)

To be able to analyse the data, a mathematical function called 'intensity auto-correlation function' needs to be computed. It is a way to measure the characteristic time(s) of the fluctuations of the signal.[62] The intensity auto-correlation function is defined by Eq. 2-5:[64]

$$\langle I(t)I(t+\tau)\rangle = \lim_{T\to\infty} \frac{1}{T}\int_0^T I(t)I(t+\tau)\,dt \qquad (2\text{-}5)$$

It can be approximated by Eq. 2-6:[62,64]

$$\langle I(t)I(t+\tau)\rangle \approx \lim_{N\to\infty} \frac{1}{N}\sum_{i=1}^{\infty} I(t_i)I(t_i+\tau) \qquad (2\text{-}6)$$

Figure 2-10 illustrates the way the intensity auto-correlation function is computed. When τ approaches 0 ($\tau = \tau'$ in Figure 2-10), $I(t)$ and $I(t+\tau)$ are very close to each other: they are correlated.[62] From a mathematical point-of-view, $\langle I(t)I(t+\tau)\rangle$ tends towards $\langle I(t)^2\rangle$.[64] When τ is very long compared to the characteristic time scale of the motions ($\tau = \tau''$ in Figure 2-10), $I(t)$ and $I(t+\tau)$ are uncorrelated,[62] and $\langle I(t)I(t+\tau)\rangle = \langle I(t)\rangle^2$.[64]

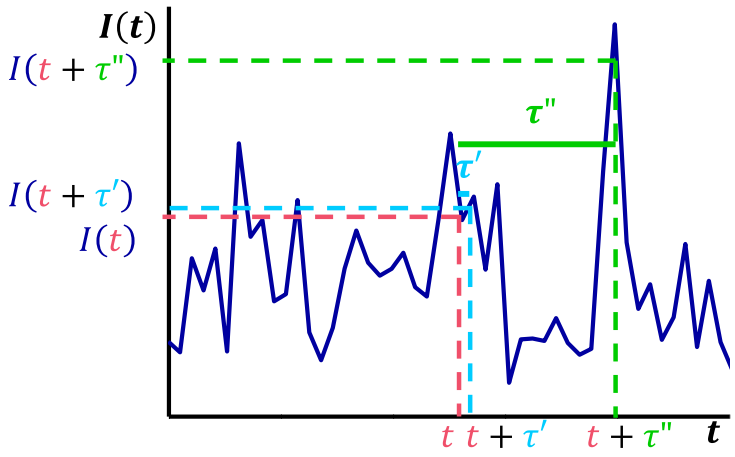

Figure 2-10: Illustration of the process used to compute the intensity auto-correlation function. τ short ($\tau = \tau'$): the values of *I(t)* (pink) and *I(t+τ')* (light blue) are very close to each other: they are correlated; τ long ($\tau = \tau''$): the values of *I(t)* (pink) and *I(t+τ'')* (green) are very different from each other: they are uncorrelated.

Figure 2-11 shows different representations of the Intensity Auto-Correlation (IAC) function. The IAC function has its maximum value $\langle I(t)^2 \rangle$ for $\tau = 0$, and decreases over time towards $\langle I(t) \rangle^2$ as shown in Figures 2-11.A and B.[62,64] In the simplest cases (*e.g.* a particle undergoing Brownian diffusion), the intensity auto-correlation function decays in an exponential way. It is thus often represented on a semi-log graph as illustrated in Figure 2-11.B.[64]

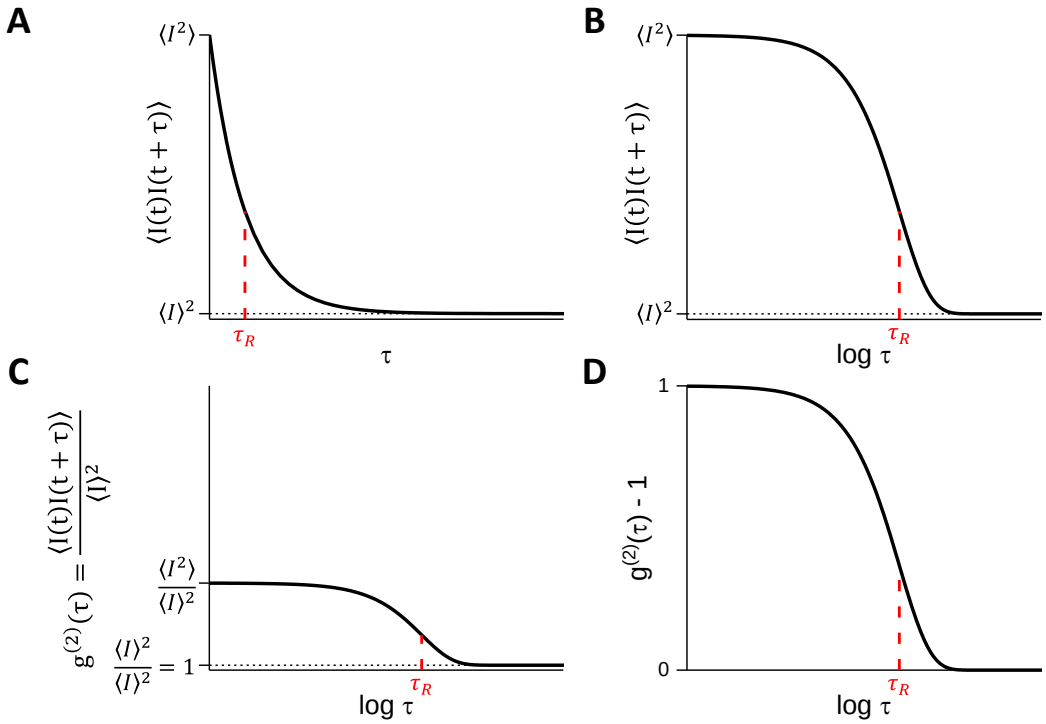

Figure 2-11: Intensity Auto-Correlation (IAC) function decaying in an exponential way with a relaxation time τ_R. **A.** Lin-lin representation of the IAC function. **B.** Semi-log representation of the IAC function. **C.** Semi-log representation of the normalised IAC function $g^{(2)}(\tau)$. **D.** Typical representation of the normalised IAC function $g^{(2)}(\tau) - 1$.

The time at which the decay occurs is the relaxation time τ_R.[62] It is the characteristic time of the fluctuations of the signal. When the IAC function exhibits several decays, the characteristic times are called correlation times and noted τ_c.[62] The intensity auto-correlation function is then normalised by $<I>^2$ (see Eq. 2-7).[62-64] It can be demonstrated that the normalised IAC functions $g^{(2)}(\tau)$ ranges from a value above 1 as illustrated in Figure 2-11.C. Figure 2-11.D shows a more common way of representing the normalised IAC, where 1 is subtracted from the previously described normalised IAC $g^{(2)}(\tau)$.

$$g^{(2)}(\tau) = \frac{\langle I(t)I(t+\tau) \rangle}{\langle I(t) \rangle^2} \quad (2\text{-}7)$$

It is now possible to access the field correlation function $g^{(1)}(\tau)$ with the help of Siegert equation (Eq. 2-8; valid if the scattered light follows a Gaussian distribution and only

comes from the sample), where σ is a coherence length and relates to the number of speckles that are detected.[62-64] For instruments performing LS measurements over one speckle, σ should be close to 1, while σ is smaller than 1 for instruments performing LS measurements across several speckles.

$$g^{(2)}(\tau) = 1 + \sigma\left[g^{(1)}(\tau)\right]^2 \quad (2\text{-}8)$$

As previously mentioned, in the simplest cases, the decay is exponential. The field correlation function $g^{(1)}(\tau)$ can therefore be fitted by Eq. 2-9.[64]

$$g^{(1)}(\tau) = e^{-\tau/\tau_R} \quad (2\text{-}9)$$

Eq. 2-10 combines Eqs 2-8 and 2-9. The parameter σ can thus be easily determined from the intercept of the curve $\ln[g^{(2)}(\tau) - 1] = f(\tau)$ as shown in Figure 2-12.[64]

$$ln[g^{(2)}(\tau) - 1] = ln\sigma - \frac{2\tau}{\tau_R} \quad (2\text{-}10)$$

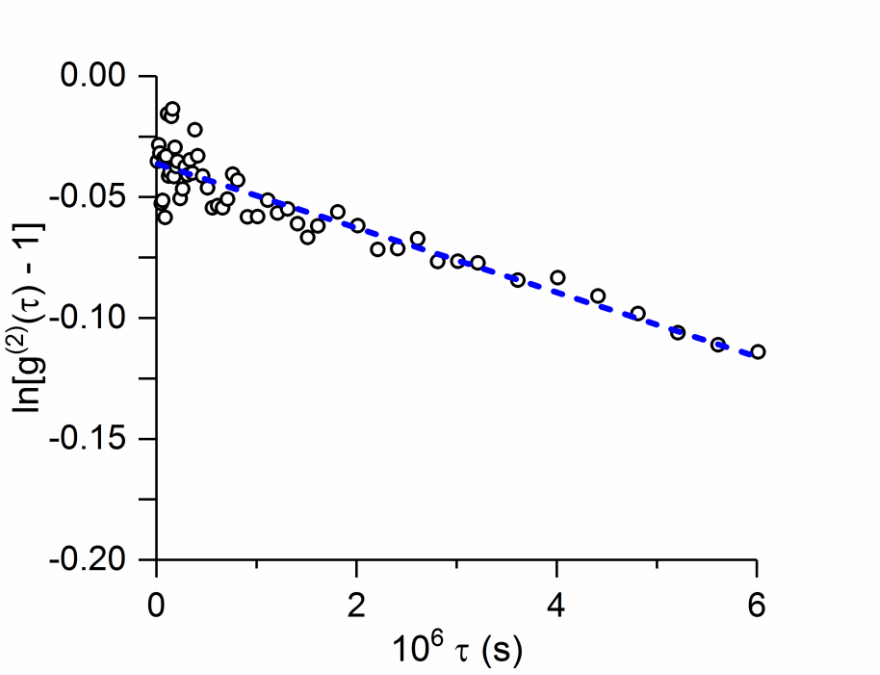

Figure 2-12: Determination of the instrumental parameter σ. The data shown here was collected with the instrument used to collect the LS data for this thesis.

Figure 2-13 illustrates a couple of more complex cases, where the experimental data cannot be fitted by an exponential decay as discussed hereafter.

The IAC data are sometimes fitted by a stretched exponential function (Eq. 2-11) as illustrated in Figure 2-13.A, β is the stretching parameter.[64]

$$g^{(1)}(\tau) = e^{-(\frac{\tau}{\tau_c})^{\beta}} \quad (2\text{-}11)$$

These cases corresponds to cases where there is not a single relaxation time τ_R but a distribution of relaxation times. The lower the stretching exponent β, the broader the

distribution of relaxation times. The average relaxation time $\langle\tau\rangle$ of the distribution is given by Eq. 2-12.[13,38] In the rest of the thesis, the $\langle\ \rangle$ notation will be omitted.

$$\langle\tau\rangle = \frac{\tau_c}{\beta}\Gamma\left(\frac{1}{\beta}\right) \quad (2\text{-}12)$$

where Γ is the gamma function.

The IAC data can exhibit several decays as shown in (see Figure 2-13.B. In such a case, the data are fitted by a sum of *i* exponentials (Eq. 2-13).[64]

$$g^{(1)}(\tau) = \sum A_i\, e^{-\tau/\tau_{c,i}} \quad (2\text{-}13)$$

where *i* corresponds to the number of relaxation modes, A_i and $\tau_{c,i}$ are the amplitude and the correlation time of the mode *i*, respectively. Such cases correspond, for example, to samples containing particles whose distribution size is multimodal where *i* would be the number of populations in the sample.

The IAC data can exhibit both trends. In such a case, they are fitted by a sum of stretched exponentials (Eq. 2-14).[64]

$$g^{(1)}(\tau) = \sum A_i\, e^{-\left(\frac{\tau}{\tau_{c,i}}\right)^{\beta_i}} \quad (2\text{-}14)$$

where β_i is the stretching exponent associated with the mode *i*.

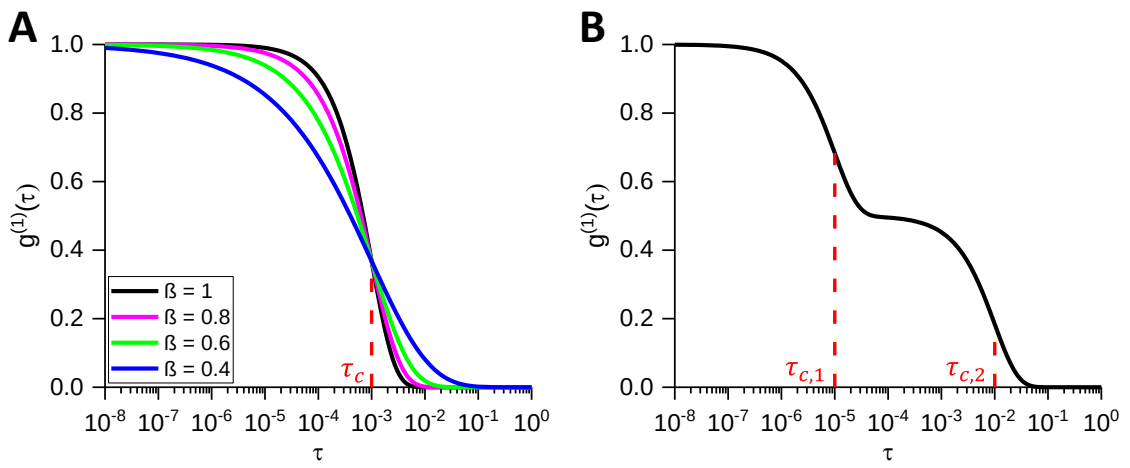

Figure 2-13: Examples of different shapes of field correlation functions $g^{(1)}(\tau)$. **A.** Examples correlation functions described by stretched exponentials having different values of the stretching exponent β. The example with $\beta = 1$ (black curve) corresponds to a single non-stretched exponential. **B.** Example of a field correlation function described by a sum of two single exponentials.

The field correlation function is then used to obtain information about the dynamics of the studied solution, as shown in Section 2-2.3.2 for polyelectrolyte solutions.

It can be deduced from the explanations above that the duration of the measurements has to be long enough to obtain reliable data. Furthermore, the longer the relaxation (or

correlation) times, the longer the measurements should be.[63] From a practical point-of-view, DLS measurements are very sensitive to dust and bubbles. As dust and bubbles scatter a lot, the count trace exhibits high intensity peaks when they enter the scattering volume and the intercept of the intensity auto-correlation functions becomes very high.[63] Such data have to be discarded. It is worth noting that these last statements are valid for both SLS and DLS measurements.

Static Light Scattering (SLS)

Contrary to DLS which considers the fluctuations of the scattering intensity over time, SLS considers the time-averaged scattering intensity, as represented by the pink dashed line on the right-hand side of Figure 2-9. This time-averaged scattering intensity, provided by the LS device as a count rate, is normalised according to Eq. 2-15:

$$I_{norm} = \frac{measured\ count\ rate \times sin(\theta)}{laser\ intensity} \quad (2\text{-}15)$$

with I_{norm} the normalised scattering intensity and θ the scattering angle. The term $sin(\theta)$ corrects for the angular dependence of the scattering volume. The normalised intensity I_{norm} is then used to calculate the excess Rayleigh ratio ΔR (Eq. 2-16),[65] where the scattering contribution of the solvent is subtracted from the one of the solution, and normalised to the scattering of a reference solvent (*e.g.* toluene, benzene).

$$\Delta R(\theta) = \frac{I_{norm,sample}(\theta) - I_{norm,water}(\theta)}{I_{norm,ref}(\theta)} \left(\frac{n_c}{n_{ref}}\right)^2 R_{ref} \quad (2\text{-}16)$$

where n_c and n_{ref} are the continuous phase refractive index and the toluene refractive index respectively, and R_{ref} is the Rayleigh ratio of the reference solvent at the laser excitation wavelength λ. The angular-dependence of the excess Rayleigh ratio ΔR can then be used to determine the size and the shape of the scatterers in solution. Section 2-2.3.3 summarises the information that can be obtained from ΔR to understand the behaviour of polyelectrolytes in solution.

2-2.3.2. Dynamic Light Scattering (DLS) of polyelectrolyte solutions

For low polyelectrolyte concentrations in the dilute regime, polyelectrolyte chains interact with one another throughout their counterion clouds, and in absence of added salt, chains are extended to minimise intra-chain repulsion between similarly charged chain sections (see Section 2-2.1.1); thus occupying a much larger volume than a non-charged polymer chain of similar length.[32,33]

DLS performed in such solutions probes a single relaxation mode.[32,66,67] This is illustrated by the field correlation data of the 0.01 g.L^{-1} quaternized poly(vinyl pyridine) solution seen in Figure 2-14, showing field correlation data for quaternized poly(vinyl pyridine) solutions at different concentrations.

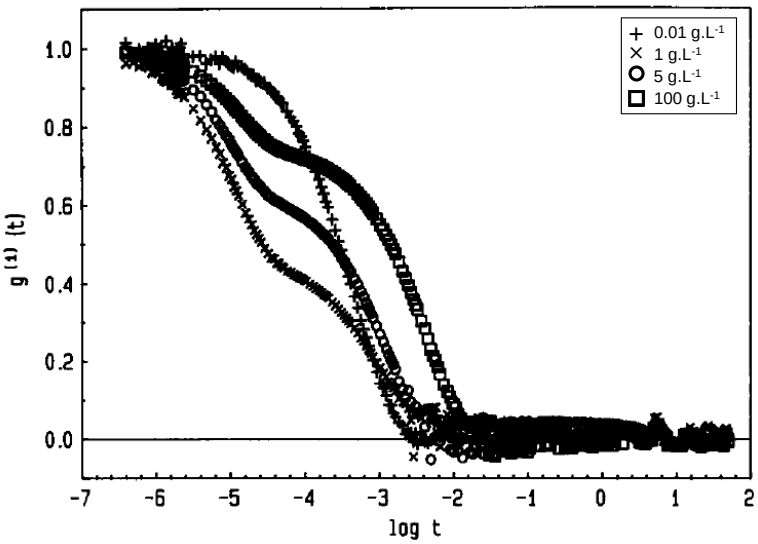

Figure 2-14: Field correlation data collected at 90° scattering angle for salt-free solutions at different concentrations of 65% quaternized poly(vinyl pyridine) in water. Polymer characteristics: M_w = 109,000 g/mol; M_w/M_n = 1.04. Adapted from Förster *et al*,[32] Copyright © 1990 Elsevier Ltd, with permission from Elsevier.

The relaxation time τ of this single relaxation mode is obtained by fitting the field correlation data to Eq. 2-11. β is typically found to be around 1; meaning that Eq 2-10 can actually be used to determine the relaxation time of this mode.[21,32] The obtained relaxation time follows a q^2-dependence, characteristic for diffusive behaviour.[32,66,67] q (Eq. 2-17) is the scattering vector defined as:

$$q = \frac{4\pi n \sin(\theta/2)}{\lambda} \tag{2-17}$$

with λ the laser excitation wavelength, n the refractive index, and θ the scattering angle.

The diffusion coefficient D (Eq. 2-18) associated with the relaxation time τ is defined as:[33,66,67]

$$\tau^{-1} = Dq^2 \tag{2-18}$$

D characterises the coupled diffusion between polyions and counterions.[33,66,67] Counterions form clouds around the polyions to screen the charges. Due to their small size, they diffuse quickly in solution, dragging the polyions with them.[33,66,67] At low polyelectrolyte concentrations, D is independent of polyelectrolyte M_w and concentration,[32] as seen in Figure 2-15.A for polyelectrolyte concentrations below c_a.

When salt is added, the charges on the polyions get screened. Intra-chain repulsion decreases and the polymer chains coil.[32] Moreover, the coupling between the less charged polyions and the counterions thus weakens, generally leading to a decrease in D,[32,67] as shown in Figure 2-15.B for polyelectrolyte concentrations below c_b. Exceptions to this behaviour have been reported for polyelectrolytes such as hyaluronan, whose diffusion coefficient remains constant when small amounts of salt are added; no explanation has yet been found to explain this behaviour.[67]

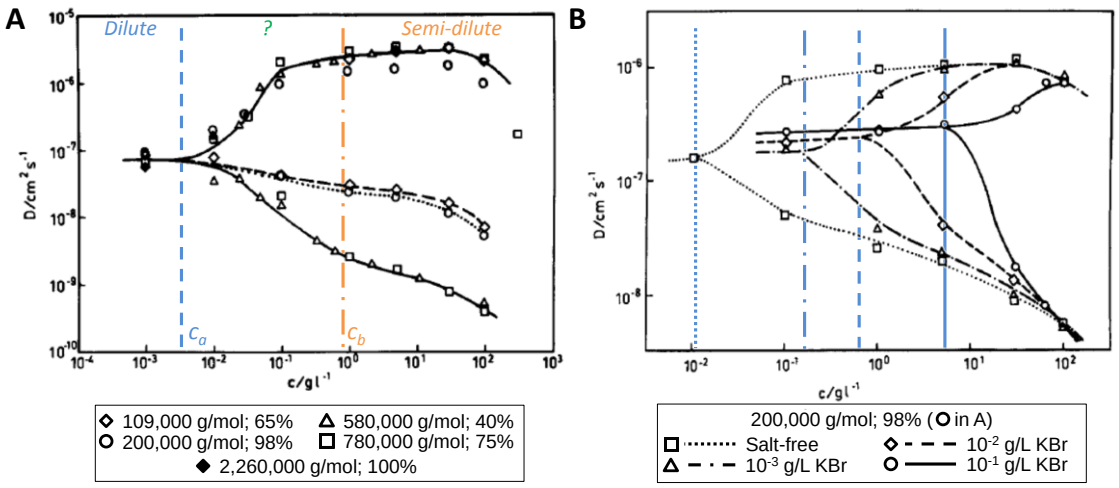

Figure 2-15: Influence of polyelectrolyte concentration c, molecular weight M_w and added salt concentration on the diffusion coefficients D observed by DLS in quaternized poly(vinyl pyridine) solutions. Adapted from Förster *et al*,[32] Copyright © 1990 Elsevier Ltd, with permission from Elsevier. Coloured elements were added by the present author to the original Figures. **A.** Influence of polyelectrolyte concentration and molecular weight on D. M_w values are given below the graph together with the degree of quaternization (in %). Blue dashed line: crossover concentration c_a between the dilute regime and a transition regime marked with a green question mark as it has not been fully assigned yet and could either correspond to the beginning of the semi-dilute regime or the end of the dilute regime. Orange dashed-and-dotted line: crossover concentration c_b between the transition regime and the semi-dilute regime. The notations c_a and c_b for both crossover concentrations were added by the present author to facilitate discussion. **B.** Influence of salt and polyelectrolyte concentrations on D. The blue vertical lines correspond to c_a for each salt concentration. The polyelectrolyte used to collect this series of data has a molecular weight of 200,000 g/mol and a quaternization degree of 98%.

When the added salt concentration is high enough to screen all the charges along the polyions, polymer chains behave like neutral polymers, and the single relaxation mode probed by DLS corresponds to the diffusion of the screened polyion chains in solutions.[32] Their hydrodynamic radius R_H can be determined using the Stokes-Einstein equation[35,37] (Eq. 2-19) defined as:

$$R_H = \frac{kT}{6\pi\eta_c D} \tag{2-19}$$

where k is the Boltzmann constant, T is the temperature, and η_c the viscosity of the continuous phase. As the salt concentration increases, D becomes dependent on M_w.[32,68] and when full screening is achieved, it follows an $M_w^{-\upsilon}$-dependence (υ = 0.5-0.6) like neutral polymers.[32]

When the polymer concentration reaches a characteristic value, here called c_a and highlighted by the dashed blue line in Figure 2-15.A, inter-chain interactions start to become stronger. Counterions get closer to the polyions to screen charges and minimise repulsive interactions. They also have less space to diffuse away from polyions. All these phenomena induce an increase in coupled diffusion between polyions and counterions; leading to an increase in D (see upper curve in Figure 2-15.A). The variation of D with polyelectrolyte concentration is M_w-independent.[32,33,68] Meanwhile, a second relaxation mode is probed with DLS, as seen from the field correlation data shown in Figure 2-14 for polyelectrolyte concentrations of 1 g/L and above, as well as from Figure 2-15.A where the lower curves correspond to the diffusion coefficient of this second mode. Because its relaxation time is about two orders of magnitude larger than the other relaxation time, this relaxation mode is here called 'slow relaxation mode' while the previously discussed relaxation mode is called 'fast relaxation mode'; subscripts 's' and 'f' are used to differentiate them.

The relaxation times of both modes are obtained from fitting the field correlation data to Eq. 2-14 with the number of exponential functions i equal to 2. The stretching exponent β_f of the fast relaxation mode is typically found to be 1 as for the single relaxation mode observed below c_a, and is thus usually set to 1 for fitting. The stretching exponent β_s of the slow mode has been found to be 1 for systems such as salt-free sodium poly(styrene sulfonate)[33] and quaternized poly(vinyl pyridine)[32] solutions, as well as chitosan[35] solutions with added salt. For systems such as salt-free dextran solutions, as well as Na CMC, hyaluronan and xanthan solutions in presence of a background electrolyte, β_s has been found to be around 0.7; its value decreasing as the scattering angle θ (or scattering vector q) increases.[13,37,38] In such cases, the mean value of the distribution of relaxation times is obtained using Eq. 2-12 as explained in Section 2-2.3.1.

This slow relaxation mode is typically attributed to the formation of polyion clusters called 'domains' and is not predicted by polyelectrolyte theories. At very low polyelectrolyte concentrations, polyions are far from each other and each of them has its own counterion cloud.[32] The formation and the existence of these domains is still subject

to hypotheses. One of them is that, at higher polyelectrolyte concentrations, counterion clouds start overlapping, and that this mechanism of sharing counterions would provide the cohesive interactions required for the domains to exist.[32,36] The domains are thought to be temporal.[32,36] As seen in Figure 2-15.A, D_s depends on the molecular weight of the polyectrolyte: the higher M_w, the lower D_s.[32,33,68] Addition of salt delays the appearance of the slow mode as seen in Figure 2-16 showing the field correation data obtained for quaternized poly(vinyl pyridine) solutions with and without added salt, as well as in Figure 2-15.B. Indeed, more oppositely charged ions surround each polyion[32] so that higher polyelectrolyte concentrations are needed for polyions to be close enough to each other to form domains.

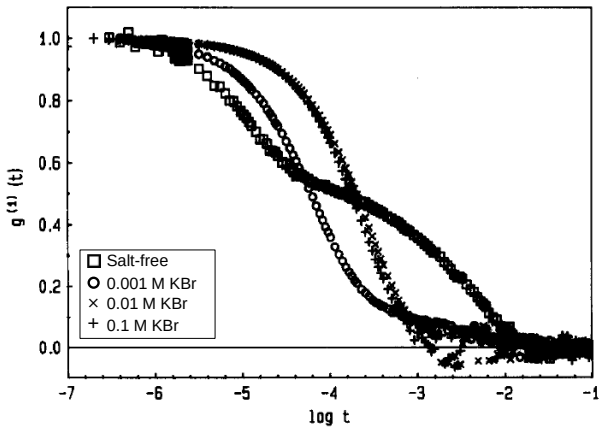

Figure 2-16: Field correlation data collected at 90° scattering angle for 0.03 g.L^{-1} 75% quaternized poly(vinyl pyridine) solutions with and without added KBr. Polymer characteristics: M_w = 780,000 g/mol; M_w/M_n = 1.10. Adapted from Förster *et al*,[32] Copyright © 1990 Elsevier Ltd, with permission from Elsevier.

When the polyelectrolyte concentration is further increased, the fast relaxation mode no longer varies with the polyelectrolyte concentration[32,33,66,68] and remains M_w-independent (see Figure 2-15.A).[32,33,68] As above c_a, the fast relaxation mode is associated with coupled diffusion between the counterions and the polyions or segments of the polyions for low and high M_w polyelectrolyte, respectively.[32] Meanwhile, when the polyelectrolyte concentration is increased, D_s keeps decreasing[32,33,66,68] and is M_w-dependent (see Figure 2-15.A).[33] It is worth noting that, for high M_w polyelectrolytes, its dependence upon polyelectrolyte concentration changes for the same concentration as the one where D_f plateaus.[32,33,66] It is not clear whether it is this crossover concentration, noted c_b here, or the one associated with the appearance of the slow relaxation-mode previously noted c_a, which corresponds to the beginning of the semi-dilute regime. Förster *et al.*[32] assigned the beginning of the semi-dilute to c_b while Tanahatoe and Kuil[68] assigned it to c_a after

showing that D_f followed a $c^{0.72}$-dependence between c_a and c_b, comparable to the $c^{0.75}$-dependence predicted by Odijk for the concentration-dependence of the polyelectrolyte diffusion coefficient in the semi-dilute regime. Odijk's theory did however not predict the presence of a second relaxation mode. It is worth noting that Förster *et al.*[32] questioned the appropriateness of a power law to describe the behaviour of D_f, highlighting that the increase in D_f between c_a and c_b resembles more a sigmoid than a power law. Interestingly, the theory predicts that the overlap concentration c^* marking the transition between the dilute and the semi-dilute regimes (see Sections 2-2.1 and 2-2.2) is M_w-dependent while neither c_a nor c_b seems to be M_w-dependent. Hence, c^* may even be different from both c_a and c_b. It would be interesting to combine both viscosity and LS measurements on such systems to determine c^* with the help of the polyelectrolyte scaling laws (see Section 2-2.2), and compare it with c_a and c_b.

When salt is added, coupling is weakened and D_f decreases,[32,35] while D_s remains constant[23] or increases,[23,32] and may eventually disappear (see Figures 2-15.B and 2.16).[23,32] For polyelectrolytes such as hyaluronan (M_w = 8.5 × 10^4 – 2 × 10 g/mol),[37] xanthan (4.2 × 10^6 g/mol),[37] sodium poly(styrene sulfonate) (M_w = 7.8 × 10^5 – 1.2 × 10^6 g/mol)[23] and chitosan (1.9 × 10^5 g/mol),[35] the slow relaxation mode does not disappear, even when the amount of added salt is expected to screen all the charges. Sedlák's investigations[23] showed that the slow relaxation mode is less likely to disappear when both the polyelectrolyte concentration and M_w are high. The disappearance of the slow mode upon salt addition could be due to the fact that adding salt brings the solution back to the dilute regime. Indeed, as explained at the end of Section 2-2.2, the overlap concentration c^* is shifted towards higher polyelectrolyte concentrations as the charges on polyelectrolyte chains are screened by added salts. Similarly, c_a, which corresponds to the appearance of the slow mode, is also shifted towards higher polyelectrolyte concentrations upon salt addition (see previous discussion and Figure 2-15.B). If the polyelectrolyte concentration is high enough so that the solution remains above c_a when salt has been added, the slow mode should still be observed. Also, as seen in Figure 2-17, where the influence of M_w on the polyelectrolyte concentration dependence of the diffusion coefficients is shown for sodium poly(styrene sulfonate) solutions in a low background electrolyte solutions, c_a is M_w-dependent in presence of added-salt, and is lower for higher M_w polyelectrolytes. So, following a similar reasoning as for the polyelectrolyte concentration, in presence of salt, the concentration from which the slow

mode would be observed would be lower for high M_w polyelectrolytes than for low M_w ones. Here too, a combined viscosity/LS study would help understanding this behaviour.

It is worth noting that the slow relaxation mode is not always purely diffusive. Indeed, sizes associated with the domains can be as large as a few hundreds of nanometers,[33,37,68] in which cases internal relaxation modes are probed too. More explanations are given in Section 2-2.3.4, which provides more details about the characteristics of the slow relaxation mode.

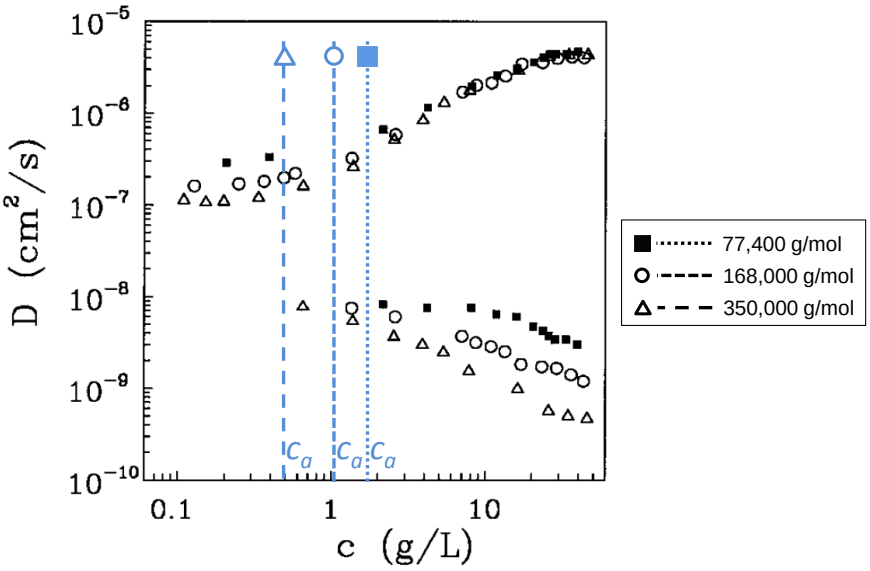

Figure 2-17: Influence of the polyelectrolyte concentration and M_w on the diffusion coefficients observed using DLS for poly(styrene sulfonate) solutions in 0.01 M NaCl. Adapted with permission from Tanahatoe and Kuil,[68] Copyright © 1997 American Chemical Society. The crossover concentration c_a was added by the present author.

Another change in the concentration-dependence of the slow mode relaxation, yet unexplained, has been observed for high M_w polyelectrolytes such as sodium poly(styrene sulfonate).[66] A low and high M_w sodium poly(styrene sulfonate) samples are compared in Figures 2-18.A and 2-18.B, respectively. The additional concentration crossover is highlighted using a grey dashed-dotted-dotted line and noted c_c.

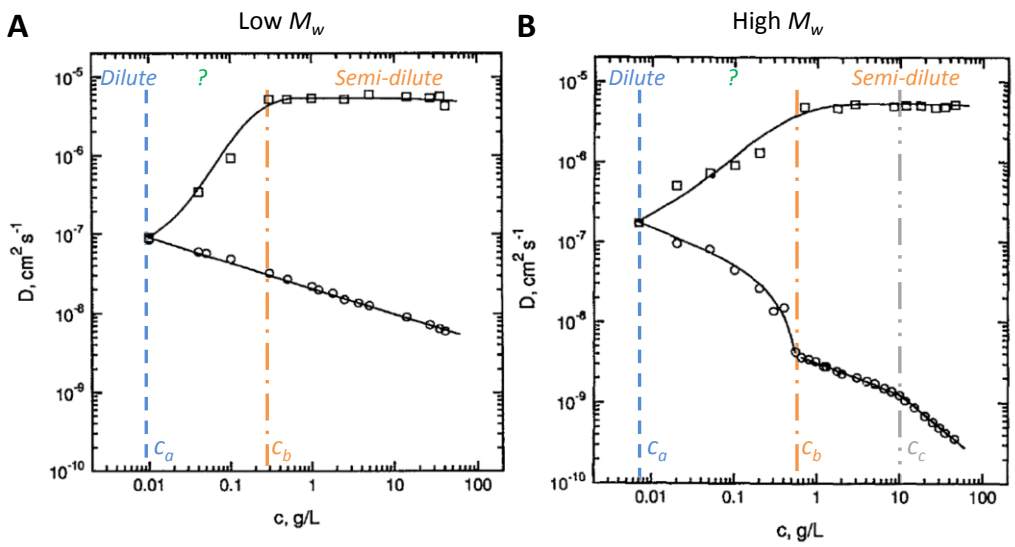

Figure 2-18: Diffusion coefficients observed using DLS for both a 5,000 g/mol (**A**) and a 1,200,000 g/mol (**B**) sodium poly(styrene sulfonate) sample in salt-free water. Squares and circles represent the fast and the slow mode diffusion coefficients, respectively. Coloured (see caption of Figure 2-15 for explanations) and grey elements were added by the present author to the original Figures. The grey dashed-dotted-dotted line represents the third crossover concentration, noted c_c, observed for high M_w polyelectrolytes. Adapted from from Sedlák and Amis,[66] with the permission of AIP Publishing, Copyright © 1992 American Institute of Physics.

At even higher polyelectrolyte concentrations, the value of D_f may decrease as local friction is high due to the high viscosity of the solution (see Figure 2-15).[32]

A third mode has been observed for some polyelectrolyte solutions. Its relaxation time is either between the one of the fast and the slow modes,[69-71] or longer than the slow mode.[72,73] Examples are given in Table 2-2, where the origins of the third mode suggested by the authors of the studies are also provided.

Table 2-2: Examples of polyelectrolyte systems where a 3rd relaxation mode is observed.

τ_3	Suggested origin	Polyelectrolyte system	Comment(s)	Ref
$\tau_f < \tau_3 < \tau_s$	Motion of the polyion chain segments which are not in the domains	PDADMAC in aqueous or aqueous alcoholic solutions with added NaCl or Na_2SO_4		69
$\tau_f < \tau_3 < \tau_s$	*n/a*	Na PSS in water	The author says that he does not have enough information to determine whether the 3rd mode was real or came from an artefact.	70
$\tau_f < \tau_3 < \tau_s$	Caused by intramolecular hydrophobic regions	Quaternized P2VP in KBr aqueous solutions		71
$\tau_s < \tau_3$	'Loose aggregates of DNA globules'	DNA in salt-free water or in 1 M NaCl aqueous solutions	The 3rd mode amplitude can represent up to 70% of the total amplitude.	72
$\tau_s < \tau_3$	*n/a*	Na PSS in NaN_3 or NaCl aqueous solutions	Only observed for a few solutions at low ionic strengths. Measurement durations were not long enough to investigate this mode.	73

τ_f, τ_s and τ_3: relaxation times of the fast, slow and 3rd mode, respectively. PDADMAC: poly(diallyl-*N*,*N*-dimethylammonium chloride); P2VP: poly(2-vinyl pyridine) ; Na PSS: sodium poly(styrene sulfonate). Ref: reference.

To conclude this Section, at low polyelectrolyte concentrations, a single relaxation mode, diffusive, is typically observed and corresponds either to the coupled diffusion between counterions and polyions, or to the diffusion of screened polyion chains when the amount of added salt is high enough to screen all the charges along polyion chains. From a characteristic concentration, here termed c_a, a second relaxation mode with a slower relaxation time appears while the diffusion coefficient associated with the other relaxation mode, referred as fast mode, increases as the hydrodynamic coupling between counterions and polyions becomes stronger. Above another characteristic concentration c_b, the fast relaxation mode coefficient remains constant while the slow relaxation mode

keeps decreasing. A third crossover concentration c_c, where the concentration dependence of the slow relaxation mode changes, is observed for high M_w polyelectrolytes only. Though it has been suggested that either c_a or c_b could correspond to the overlap concentration c^* predicted by the polyelectrolyte scaling laws, such an assignment has not been confirmed. The physical meaning of c_c also has yet to be understood. It is worth noting that all these characteristic concentrations seem to be below c^{**}, characteristic for the transition between the semi-dilute and the concentrated regimes, thus where the polyelectrolyte scaling laws only predict two crossover concentrations. It would be interesting to combine both rheology and DLS measurements to understand what these crossover concentrations corresponds to, and possibly assign them.

2-2.3.3. Static Light Scattering (SLS) of polyelectrolytes solutions

As discussed in Section 2-2.3.2 just above, DLS allows the investigation of polyelectrolyte solution dynamics. SLS measurements are complementary and provide information about the polyelectrolyte solution structure as well as about the interactions occurring between the scatterers present in such solutions. Figure 2-19 shows the concentration-dependence of the excess Rayleigh ratio ΔR as a function of the polyelectrolyte concentration for two different M_w sodium poly(styrene sulfonate) sample in salt-free solution (see Figure 2-19.A) as well as for a sodium poly(styrene sulfonate) samples in 0.05 M NaCl (see Figure 2-19.B). As seen in Figure 2-19, the excess Rayleigh ratio increases with polyelectrolyte concentration, and the two transition concentrations c_a and c_b determined with DLS measurements are observed,[33,34,68] while the transition concentration c_c observed in DLS for high M_w polyelectrolytes is not observed;[33] suggesting that this transition concentration is linked to changes in solution dynamics rather than in solution structure. Owing to the facts that this transition at c_c (i) corresponds to a dynamical rather than a structural transition and (ii) is only probed for high M_w polyelectrolytes, I suggest that it could be related to the entanglement concentration c_e (see Section 2-2.1 where both the solution structure and dynamics are described).

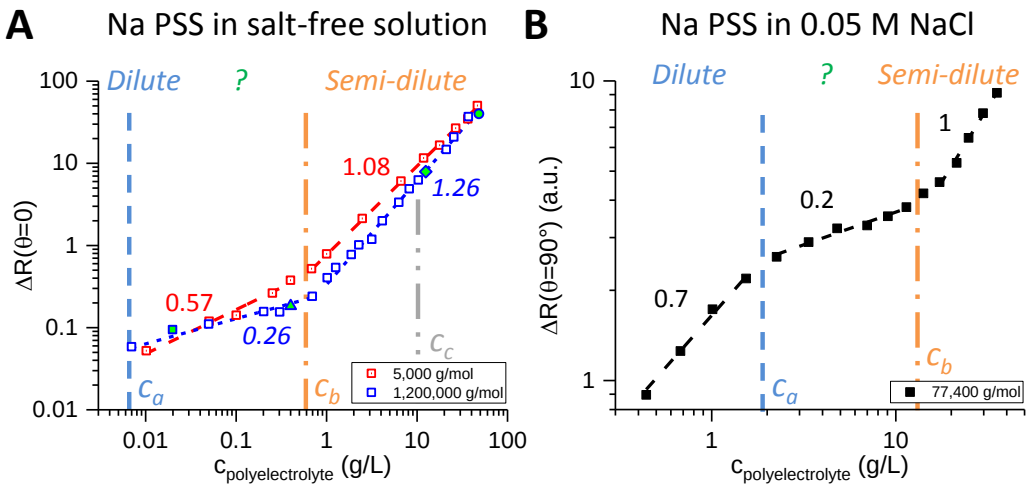

Figure 2-19: Excess Rayleigh ratio ΔR as a function of the polyelectrolyte concentration for different M_w sodium poly(styrene sulfonate) (Na PSS) samples with and without added salt. **A** and **B** were replotted by the present author from Sedlák and Amis,[66] and Tanahatoe and Kuil,[34] respectively. Numbers are exponents of the power law models describing the different regions. The exponent values provided in A are the ones given by Sedlák and Amis[66], while the ones provided in B were calculated by the present author. In A, regular red numbers correspond to the 5,000 g/mol sample, whereas italic blue numbers correspond to the 1,200,000 g/mol sample. Vertical lines correspond to the same concentration transitions as the ones shown in Figure 2-17 were more details are provided. c_c is only shown in A for the 1,200,000 g/mol sample because it has not been observed for the 5,000 g/mol sample shown in A and no information is available to determine whether it would be observed for the 77,400 g/mol sample shown in B. In A, the meaning of the data green-filled data points having a symbol with a different shape is related to Figure 2-20 and explained in its caption. It is of no importance for the present Figure.

As seen in Figure 2-19, the excess Rayleigh ratio ΔR is only slightly M_w-dependent above c_b where the exponent of the power law describing this region is around 1[33,68] and increases with M_w.[66] Sedlák and Amis[66] say that such an exponent is expected for scatterers which do not interact with each other. Moreover, DLS results suggest that, in salt-free solutions above c_b, large domains are present in solution (Section 2-2.3.2) and are most likely to be responsible for most of the scattering (this is further discussed in Section 2-2.3.4 dedicated to the slow mode). Therefore, Sedlák and Amis[66] conclude that the domains can be viewed as non-interacting scatterers. It may not be that straightforward, though, as the linear concentration dependence of ΔR has been established for the polyelectrolyte concentration rather than the domain concentration which is not known. As seen in Figure 2-19.B, the linear relationship between ΔR and the polyelectrolyte is also valid in presence of added salt.

In salt-free solutions, the excess Rayleigh ratio ΔR is more M_w-dependent between c_a and c_b (compared to solutions containing added salt; see Figure 2-19), where the power law exponent describing $\Delta R = f(c_{polyelectrolyte})$ varies from 0.26 to 0.57 for sodium poly(styrene

sulfonate) with M_w varying from 5,000 g/mol to 1,200,000 g/mol. Sedlák and Amis[66] suggest that power law exponents significantly below 1 are characteristic for strong repulsive interactions between scatterers. However, as seen from the field correlation data in Figure 2-14, as the polyelectrolyte concentration decreases, the amplitude of the slow mode decreases and the one of the fast mode increases. It is thus likely that, in this concentration range, neither the slow relaxation mode nor the fast relaxation mode dominates the total excess Rayleigh ratio, and it would most probably be better to examine the contributions of each mode to conclude on the presence of possible interactions between scatterers (Section 2-2.3.4 provides details about how to determine such contributions). As shown in Figure 2-19.B, the power law exponent found for this region when salt is added to the solution is similar to the ones found for salt-free solutions.

I have not found any study investigating ΔR below c_a for salt-free polyelectrolyte solutions. This is most probably due to the fact that the low scattering from such solutions is too low to collect reliable data. Indeed, polyelectrolyte concentrations are very low, meaning that there are only a few scatterers in solution (see Section 2-2.1.1). These scatterers are also expected to have an extended conformation (see Section 2-2.1.1), and would thus scatter less than coiled polymer chains. In presence of excess salt, polymer chains are expected to behave like neutral polymer chains, as explained at the end of Section 2-2.2. In this dilute regime of concentrations, for neutral or screened polymer chains, Eq. 2-20 applies.[40,74]

$$\frac{Kc}{\Delta R(\theta)} = \frac{1}{M_w P(q)} + 2A_2 c + \ldots \qquad (2\text{-}20)$$

where K is an optical constant (see Eq. AI-3), c the polymer concentration, q the scattering vector related to the scattering angle θ through Eq. 2-17, $P(q)$ the particle form factor given approximated by $P(q) = 1 - \frac{1}{3}{R_g}^2 q^2 + \ldots$ at low q values, R_g is the radius of gyration of the polymer chains, and A_2 is the second virial coefficient. Eq. 2-20 shows that the scattering intensity is proportional to the polymer concentration. An exponent of 1 would thus be expected for this concentration regime. The value calculated from the data published by Tanahatoe and Kuil[34] is slightly lower than 1. This could come from the fact that the amount of added salt is not high enough to screen all the charges along the chains. It can also be deduced from Eq. 2-20 that the scattering intensity increases with M_w.

The q^2-dependence of $\Delta R(q=0)/\Delta R(q)$ obtained for salt-free sodium poly(styrene sulfonate and quaternized poly(vinyl pyridine) solutions with added KBr shown in Figure 2-20 provides information about the solution structure. In absence of added salt, at low polyelectrolyte concentrations, the initial slope of $\Delta R(q=0)/\Delta R(q) = f(q^2)$ is negative and a minimum is observed as seen in Figure 2-20.A for the lowest polyelectrolyte concentration.[32,33] This behaviour is characteristic for systems where repulsive interactions occur between scatterers[32,33] and supports the previous description of these systems at these low concentrations. When $c_{polyelectrolyte}$ increases and is around c_b, $\Delta R(q=0)/\Delta R(q)$ becomes independent from q^2. Finally, at concentrations above c_b, $\Delta R(q=0)/\Delta R(q)$ varies linearly with q^2, and the apparent radius of gyration $R_{g,app}$ can be calculated[32,33,66] using Eq. 2-21.[33,34] The obtained sizes are much larger than the ones expected for single polymer chains and are attributed to the domains.[31-33,66]

$$\frac{\Delta R(0)}{\Delta R(\theta)} \cong 1 + \frac{1}{3} {R_{g,app}}^2 q^2 \qquad (2\text{-}21)$$

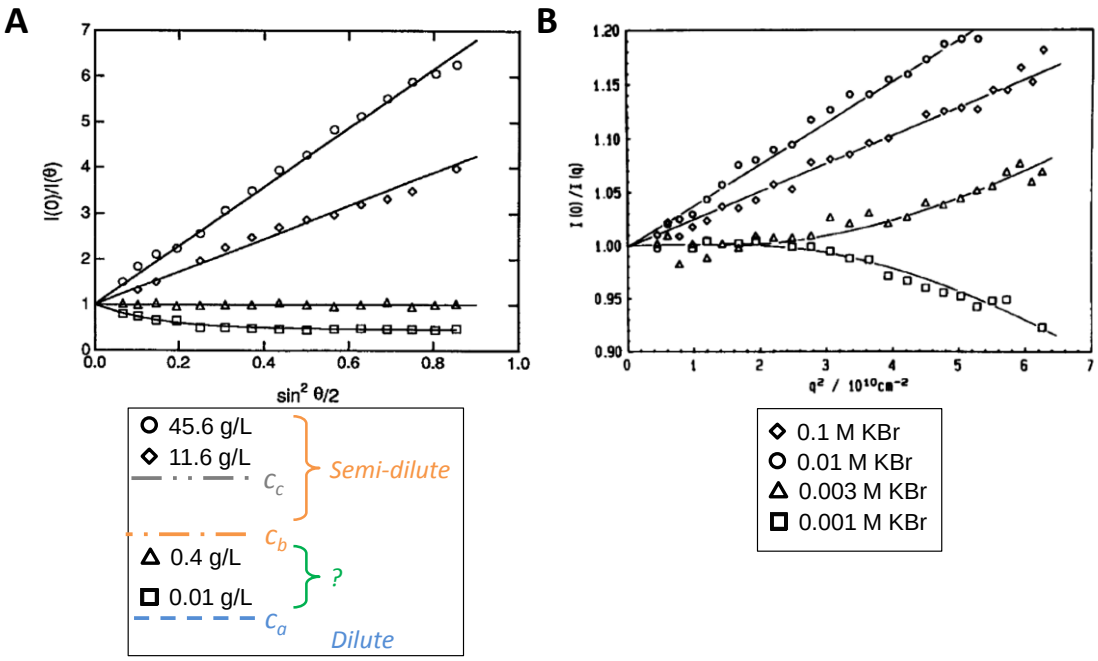

Figure 2-20: q^2- (or $\sin^2\theta/2$-) dependence of the scattering intensity of salt-free sodium poly(styrene sulfonate) solutions (**A**) and quaternized poly(vinyl pyridine) solutions in KBr (**B**). *I(0)* and *I(θ)* correspond to the excess Rayleigh ratio at $\theta = 0$ scattering angle and θ, respectively. **A.** Polyelectrolyte concentrations correspond to the green data points in Figure 2-19.A. M_w*(polyelectrolyte)* = 1,200,000 g/mol. Adapted from from Sedlák and Amis,[66] with the permission of AIP Publishing, Copyright © 1992 American Institute of Physics. **B.** Polyelectrolyte concentration is 0.33 g/L. Polyelectrolyte M_w, M_w/M_n and quaternization degrees are 780,000 g/mol, 1.10 and 75%, respectively. Adapted from Förster *et al*,[32] Copyright © 1990 Elsevier Ltd, with permission from Elsevier.

The influence of the polyelectrolyte concentration on $R_{g,app}$ seems to vary from one study to another. Indeed, in salt-free solutions, Sedlák and Amis[66] showed that $R_{g,app}$ increases with $c_{polyelectrolyte}$ for sodium poly(styrene sulfonate), while Ermi and Amis[75] showed that it does not for poly(*N*-methyl-2-vinylpyridinium chloride) and suggested that the number of polyelectrolyte chains in the domains increases with $c_{polyelectrolyte}$ while the domain size remains constant. $R_{g,app}$ is found to be M_w-independent for low M_w polyelectrolytes[33] and M_w-dependent for high M_w polyelectrolytes.[32,33] Sedlák and Amis[66] investigations suggest that the molecular weight from which $R_{g,app}$ becomes M_w-dependent is similar to the one from which the transition at c_c is probed by DLS (see Section 2-2.3.2). They suggested that polyions would belong to one domain only below the critical M_w, while they would belong to several domains above it.[66]

Upon salt addition, the excess Rayleigh ratio typically increases[23,74] apart for the low M_w sodium poly(stryrene sulfonate) sample (*i.e.* M_w = 5,000 g/mol) studied by Sedlák.[23] As shown in Figure 2-20.B, the q^2-dependence is modified. At low $c_{polyelectrolyte}$ and as the salt concentration is increased, the behaviour characteristic for repulsive interactions disappears and is replaced by a linear q^2-dependence (see Figure 2-20.B).[32] If enough salt is added to screen all the charges, the value of $R_{g,app}$ corresponds to the radius of gyration of the screened polyions.[32] *E.g.* Förster *et al.*[32] showed that the value they calculated for their fully screened quaternized poly(2-vinylpyridine) sample matched the same unquaternized (*i.e.* neutral) poly(2-vinylpyridine) in tetrahydrofuran (THF).[32] At high $c_{polyelectrolyte}$, the slope of $\Delta R(q=0)/\Delta R(q) = f(q^2)$ decreases upon salt addition, meaning that the size of the domains, characterised by $R_{g,app}$, decreases (see Figure 2-20.B).[32,68]

In conclusion of this Section, SLS measurements probe the same characteristic crossover concentrations c_a and c_b as DLS measurements, but not the third crossover concentration c_c probed by DLS. This suggests that c_c is related to dynamical rather than structural changes. As it is only observed for high M_w polyelectrolytes, which can get entangled contrary to low M_w polyelectrolytes, it is suggested that this crossover concentration c_c corresponds to the entanglement concentration c_e. Here too, rheology measurements would help confirming this suggested assignment of c_c.

2-2.3.4. Slow mode

Though the origin of the slow mode and its nature have still not been fully elucidated yet, its characteristics and properties have been extensively studied in both salt-free and

background electrolyte solutions by varying the polyelectrolyte intrinsic properties (*e.g.* M_w,[32,33,37,66,68] degree of ionisation[32,71,76,77]), the environmental conditions (*e.g.* polyelectrolyte concentration,[22,31,33,34,37,66,68] addition of salt,[23,32,34-36,76,78] pH,[13,76] solvent allowing better solvation of the polyelectrolyte backbone[71,75,78]), the solution preparation process (*e.g.* filtration,[76,79,80] centrifugation,[36,69,80] dialysis[73,76,79]), and ageing.[70] They are reviewed in this Section to provide a better picture of what the domains, thought to be responsible for the slow relaxation mode, are.

Polyelectrolyte molecular weight M_w

For a polyelectrolyte concentration above c_b (*i.e.* well in the semi-dilute regime), Sedlák and Amis[33] have shown that the apparent radius of gyration $R_{g,app}$ of the domains determined with SLS (see Section 2-2.3.3) for salt-free poly(styrene sulfonate) solutions is not M_w-dependent below a value of about 70,000 g/mol and increases slightly with M_w above this value as seen in Figure 2-21, where Sedlák and Amis' data were plotted together with the data reported for other polymers in the literature in presence or in absence of added salt. The three other data sets show that $R_{g,app}$*(domains)* increases with M_w.[32,37,68] It is worth noting that all the M_w investigated in the other studies were above the critical value of 70,000 g/mol found by Sedlák and Amis.

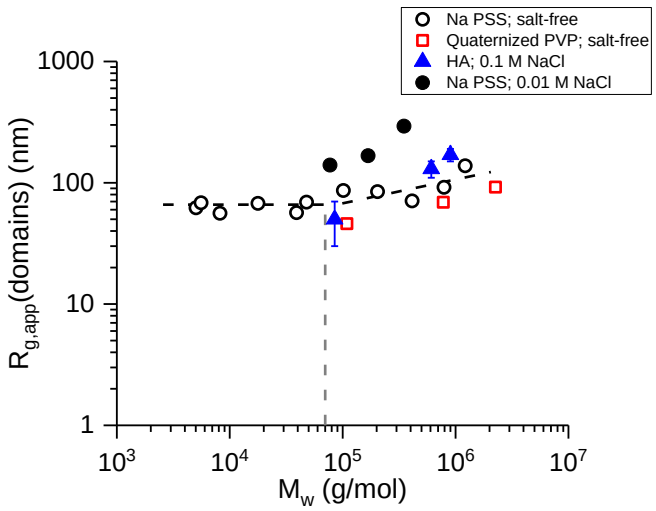

Figure 2-21: Influence of polyelectrolyte M_w on the apparent radius of gyration of the domains $R_{g,app}$. Empty black circles: sodium poly(styrene sulfonate) (Na PSS); $c_{polyelectrolyte}$ = 45.6 g/L; black dashed lines are from the original Figure; from Sedlák and Amis.[33] Empty red squares: quaternized poly(vinyl pyridine) (PVP); $c_{polyelectrolyte}$ = 100 g/L; quaternization degrees (for increasing values of M_w): 65%, 75% and 100%; from Förster *et al.*[32] Blue triangles: hyaluronan (HA); $c_{polyelectrolyte}$ unknown; from Esquenet and Buhler.[37] Full black circles: Na PSS; $c_{polyelectrolyte}$ = 16 g/L; from Tanahatoe and Kuil.[68] Vertical grey dashed line: crossover M_w determined by Sedlák and Amis.[33] $R_{g,app}$ values were calculated from the scattering intensity from the solutions for all data sets apart for Esquenet and Buhler's[37] who calculated $R_{g,app}$ values from the contribution of the slow relaxation mode only as explained in the main text.

The values of $R_{g,app}$ were calculated from the total scattering intensity for all data sets apart from the one of Esquenet and Buhler[37] who calculated $R_{g,app}$ from the contribution of the slow relaxation mode to the total scattering intensity. Indeed, when fitting the field correlation data to Eqs. 2-13 or 2-14, the relative amplitudes of both the fast and the slow modes, A_f and A_s respectively, are obtained and can be used to calculate the contribution of each relaxation mode to the total scattering of the solution defined as:[23,37,70]

$$\Delta R_i = \frac{A_i}{\sum_{j=1}^{N} A_j} \Delta R \tag{2-22}$$

where N the number of relaxation modes in the field correlation data, A_i and A_j are the relative amplitudes of the modes i and j obtained from Eqs. 2-13 or 2-14, and ΔR_i is the contribution of the mode i to the total excess Rayleigh ratio ΔR. At high polyelectrolyte concentrations, the domains are mainly responsible for the scattering of the polyelectrolyte solutions as $A_s/A_f >> 1$.[33,37,66] Hence, the contribution of the fast mode to the total excess Rayleigh ratio ΔR_f is negligible, and the error on $R_{g,app}$*(domains)* when calculated from ΔR rather than ΔR_s is small. When the polyelectrolyte concentration is smaller, the error on $R_{g,app}$*(domains)* becomes larger (see further evidence for this in the up-coming Section about the influence of the polyelectrolyte concentration and in Figure 2-23). The fact that the values of $R_{g,app}$*(domains)* provided by Tanahatoe and Kuil[68] are larger than the ones obtained by Sedlák and Amis[33] could, for example, come from differences in their sodium poly(styrene sulfonate) samples or the way they have prepared their solutions, but also from the fact that the polyelectrolyte at which Tanahatoe and Kuil[68] measured $R_{g,app}$*(domains)* (*i.e.* 16 g/L) was below c_b as seen from Figure 2-17. In such a case, the size of the domains, calculated from the total scattering intensity of the solutions, has been overestimated.

Using optical microscopy, Tanahatoe and Kuil[68] observed the presence of some structures in their sodium poly(styrene sulfonate) solutions. The diameter of these structures was about twice the value of $R_{g,app}$*(domains)* reported above. They thus assigned these structures to the domains. Most of these structures were immobile, but a few of them were moving.

Regarding DLS measurements, it has been previously mentioned (see Section 2-2.3.2) that the q-dependence of the slow relaxation mode is not always q^2. Indeed, for sodium poly(styrene sulfonate),[33] hyaluronan,[37] xanthan,[37] dextran[35] and Na CMC[13] solutions, either salt-free or with added salt, deviations from this behaviour have been observed.

They are reported in Table 2-3. Such deviations are attributed to the large size of the domains. Indeed, when $q.R_g(scatterers) > 1$, internal relaxation modes (*i.e.* relaxation modes corresponding to dynamics inside the scatterers) are also probed.[33,37] It is worth noting that a q^2-dependence of the relaxation time of the slow mode was observed for the lower M_w hyaluronan samples investigated;[37] suggesting that deviations from purely q^2-dependence is more likely to happen for higher M_w polyelectrolytes. This is consistent with the larger size of the domains reported for higher M_w polyelectrolytes (see above discussion and Figure 2-21).

Table 2-3: Examples of polyelectrolyte systems where the slow relaxation mode is not q^2-dependent.

q-dependence	System	M_w(*polyelectrolyte*) (g/mol)	Ref
$\tau_s^{-1} \sim q^{2.5}$	Dextran in 0.3 M CH_3COOH and various amounts of CH_3COONa	194,000 ± 5,000	35
$\tau_s^{-1} \sim q^3$	Hyaluronan in 0.1 M NaCl	2,000,000	37
$\tau_s^{-1} \sim q^3$	Xanthan in 0.1 M NaCl	4,200,000	37
$\tau_s^{-1} \sim q^3$	Na CMC in .0.1 M NaCl/HCl	90,000	13
$\tau_s^{-1} = aq^2 + bq^4$	Salt-free sodium poly(styrene sulfonate)	It is not clear whether this applies to all the investigated M_w in the article. It applies at least for the 1,200,000 g/mol sample.	33

At a given polyelectrolyte concentration around or above c_b, the diffusion coefficient of the slow mode D_s has been found to decrease with M_w[33,68] as illustrated in Figures 2-15 and 2-22 for salt-free poly(styrene sulfonate) solutions. When M_w increases, the decrease in D_s as the polyelectrolyte concentration increases is stronger (see Figure 2-32).[33]

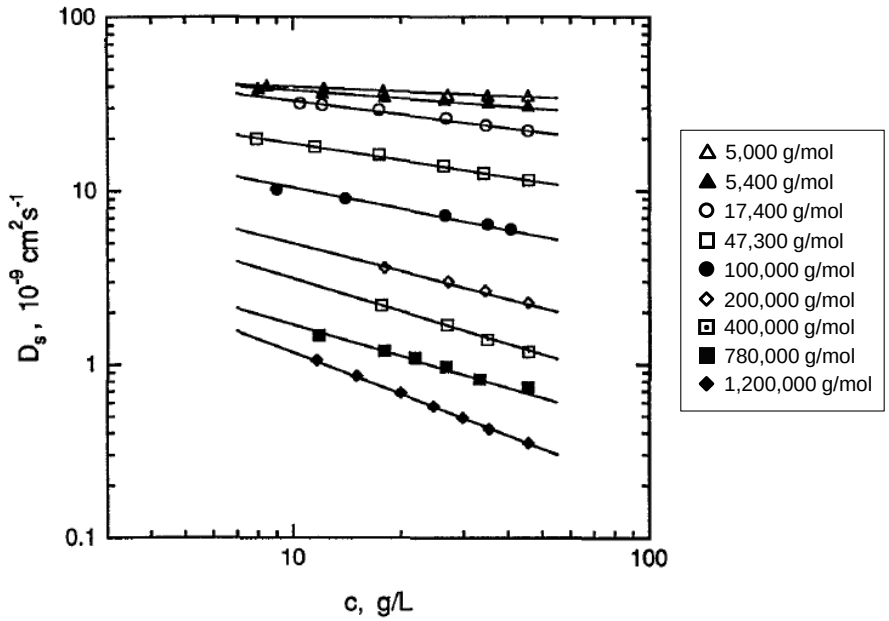

Figure 2-22: Influence of M_w on the concentration dependence of the slow relaxation mode of the diffusion coefficient D_s. The investigated polyelectrolyte systems are salt-free sodium poly(styrene sulfonate) solutions. Adapted from Sedlák and Amis,[33] with the permission of AIP Publishing, Copyright © 1992 American Institute of Physics.

Polyelectrolyte degree of ionisation

The ionisation degree has been varied using different methods: (i) addition of NaOH or HCl for polyelectrolytes whose charges are born by acid or basic groups,[13,76] (ii) control of the degree of quaternization when neutral poly(vinyl pyridine) is quaternized,[71] and (iii) synthesis of new polymers that can be triggered to switch from their neutral to their charged forms.[77] This list does not pretend to be exhaustive.

When polymer chains are ionised, the following changes are observed: an increase in D_f[76,77] (or a decrease in τ_f[13]) as the coupled diffusion between counterions and polyions appears and becomes stronger when polymer chains get charged (see Section 2-2.3.2), a decrease in D_s as the slow mode appears,[76,77] and a decrease in the total scattering intensity of the solutions.[13,76,77]

Sedlák[76] observed that the formation of the domains upon addition of NaOH in poly(acrylic acid) solutions was not instantaneous. Indeed, both D_f and ΔR_f increased immediately after the addition of each NaOH drop, while the domains could only be observed after 72 h when some small domains were already present in the initial solution, and after several months when the initial solution was domain-free. Sedlák[76] suggested that some critical conditions should be met for the formation of the domains to start such as achieving a certain arrangement of polyelectrolyte chains. Owing to the abrupt

appearance of the domains in solution, Sedlák[76] concluded that they should be due to 'real associates of macroions', by opposition to the domains being long-range concentration fluctuations in solution, as it would be unlikely that these fluctuations suddenly appear in solution.

Method (ii) allows the synthesis of polyelectrolytes with ionisation degrees as low as 9%.[71] At low ionisation degrees, only one relaxation mode is observed. At higher ionisation degrees, the fast and slow relaxation modes typically reported for polyelectrolytes are observed. At high enough ionisation degrees to observe both relaxation modes, but low enough ionisation degrees so that there are at least 12 carbon atoms between two carbon atoms bearing a charged group, a third relaxation mode was observed for quaternized poly(2-vinyl pyridine) in KBr aqueous solutions.[71] The relaxation of this third relaxation time is between the one of the slow and the fast modes. Combining these results with viscosity and surface tension measurements, the authors suggest that this third mode, diffusive, is related to the diffusion of the uncharged, hydrophobic, chain segments.[71] At higher ionisation degrees, the third relaxation mode disappears and only the fast and the slow modes are observed.[71]

Polyelectrolyte concentration

The influence of polyelectrolyte concentration on the outcomes of LS measurements is discussed in Sections 2-2.3.2 and 2-2.3.3, where it is shown that results depend on the studies. Indeed, upon increasing the polyelectrolyte concentration, $R_{g,app}(domains)$ has either been found to remain constant for quaternized poly(vinyl pyridine) in D_2O[31] and chitosan in 0.3 M CH_3COOH + 0.05 M CH_3COONa,[35] or to increase for sodium poly(styrene sulfonate) in H_2O[22] and in 0.01 M NaCl.[68] In the study about quaternized poly(vinyl pyridine) in D_2O, the authors suggested that the number of chains in the domains was increasing while the size of the domains remained unchanged. In the study about chitosan, the authors provided a relationship (Eq. 2-23) linking the real radius of gyration $R_{g,real}(domains)$ of the domains to the apparent one $R_{g,app}(domains)$:[35]

$$[R_{g,app}(domains)]^2 = \frac{3\partial\left[\frac{\Delta R_S(q=0,c_{domains})}{\Delta R_S(0,c_{domains})}\right]}{\partial q^2} = \frac{[R_{g,real}(domains)]^2}{1+A_2 M_{w,domains} c_{domains}} \quad (2\text{-}23)$$

where A_2 is the second virial coefficient. For the apparent radius of gyration of the domains to be equal to the real one, $A_2 M_{w,domains} c_{domains}$ should be significantly smaller than 1. As they had previously determined that A_2 was not negligible, they

concluded that despite $R_{g,app}(domains)$ being constant when the polyelectrolyte concentration increases, the size of the domains actually increases.

Moreover, as mentioned in the above Section about the influence of polyelectrolyte M_w, care must to be exercised when calculating $R_{g,app}(domains)$ from the total excess scattering of the solution ΔR. Indeed, the relative amplitudes of the fast and the slow mode vary with the polyelectrolyte concentration as already seen from the field correlation data in Figure 2-14, as well as from the ratio of both amplitudes shown in Figure 2-23.A for dextran solutions with added salts. Just above c_a, the amplitude of the fast mode is not negligible, so that both relaxation modes contribute to the total excess Rayleigh ratio to a similar extent as illustrated in Figure 2-23.B. Hence, at these polyelectrolyte concentrations, $R_{g,app}(domains)$ calculated from the total excess Rayleigh ratio ΔR would be overestimated, and should be calculated from the contribution of the slow relaxation mode to the total excess Rayleigh ratio ΔR_s using Eq. 2-22 instead.

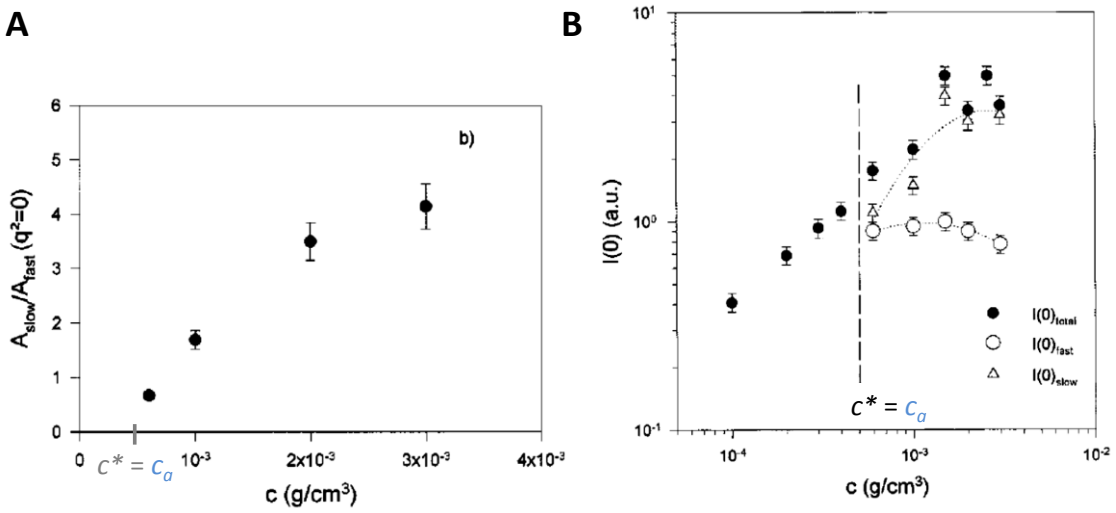

Figure 2-23: Polyelectrolyte-concentration dependence of the ratio A_{slow}/A_{fast} between the amplitudes of the slow and the fast mode at zero scattering vector (**A**) and of contributions of the whole solution, the fast relaxation mode and the slow relaxation mode to the excess Rayleigh ratio at zero scattering vector (**B**). The studied system is dextran in 0.3 M CH_3COOH + 0.05 M CH_3COONa. The concentration c^*, defined as the overlap concentration by the authors, corresponds to the previously defined concentration c_a which has been defined as the concentration from which the slow relaxation mode is observed. c_a was added to the Figure by the present author as well as c^* in A. Adapted with permission from Buhler and Rinaudo,[35] Copyright © 1997 American Chemical Society.

Salt addition

The influence of salt addition has already been lengthily discussed in the previous sections about DLS and SLS (see Sections 2-2.3.2 and 2-2.3.3, respectively). Additional elements are added here to complete the pictures.

Sedlák[23] performed an extensive combined DLS and SLS study about the influence of salt addition on sodium poly(styrene sulfonate) solutions. Figure 2-24 shows some of his findings for both a low and a high M_w sample. As seen from Figures 2-24.A and B and explained in Section 2-2.3.2, the decrease in the fast mode coefficient D_f upon salt addition can be attributed to the weakening of the coupled diffusion between counterions and polyions as charges on polyions get screened by the added electrolyte ions. D_s does not vary upon salt addition for the low M_w sample while it increases slightly for the high M_w sample. Sedlák[23] suggested that this could be due to the presence of entanglements in the high M_w solution as the M_w of the polymer is high enough for entanglements to be present (if the polymer concentration is high enough, of course). Considering the relative amplitudes of the fast and the slow modes obtained from fitting the correlation data and the excess Rayleigh ratio ΔR of the solutions (the ratio of the both relative amplitudes and ΔR are plotted in Figures 2-24.C and D), Sedlák[23] calculated their contribution to the excess Rayleigh ratio using Eq. 2-22 as described in the previous Section about the influence of polyelectrolyte M_w. These contributions are displayed in Figures 2-24.E and F.

For the low M_w sample, when the added salt concentration is above 10^{-3} M, ΔR_s decreases upon salt addition, and eventually disappears. Indeed, below 10^{-3} M, the amount of added ions would be too small to have an influence on the solution behaviour. The decrease in ΔR_s is, according to Sedlák,[23] the proof that the slow mode disappears upon salt addition and that electrostatic interactions are responsible for the existence of the domains. This was confirmed by the calculation of $R_{g,app}$*(domains)* from ΔR_s, which was found to decrease upon salt addition. Such a result was also found for poly(diallyl-*N*,*N*-dimethylammonium chloride) in presence of NaCl.[69] It is worth noting that, here too, it is important to use ΔR_s rather than ΔR to estimate $R_{g,app}$*(domains)* as the ratio of the relative amplitudes of both relaxation modes changes upon salt addition (see Figures 2-24.C and D), and the contribution of the fast mode to the excess Rayleigh ratio becomes significant.

The increase in ΔR_s for the high M_w sample is explained by the competing effects of the disappearance of the domains leading to a decrease in ΔR_s, and the greater flexibility of the chains as the charges are getting screened, which allows them to get more coiled and to scatter more.[23] When the added salt concentration is low, it seems that the second effect is stronger than the first one. As discussed in Section 2-2.3.2, there are cases where the slow relaxation mode does not disappear. The increase in ΔR_f, though not visible at low

salt concentrations because of the log scale, starts as soon as salt is added to the polyelectrolyte solution.

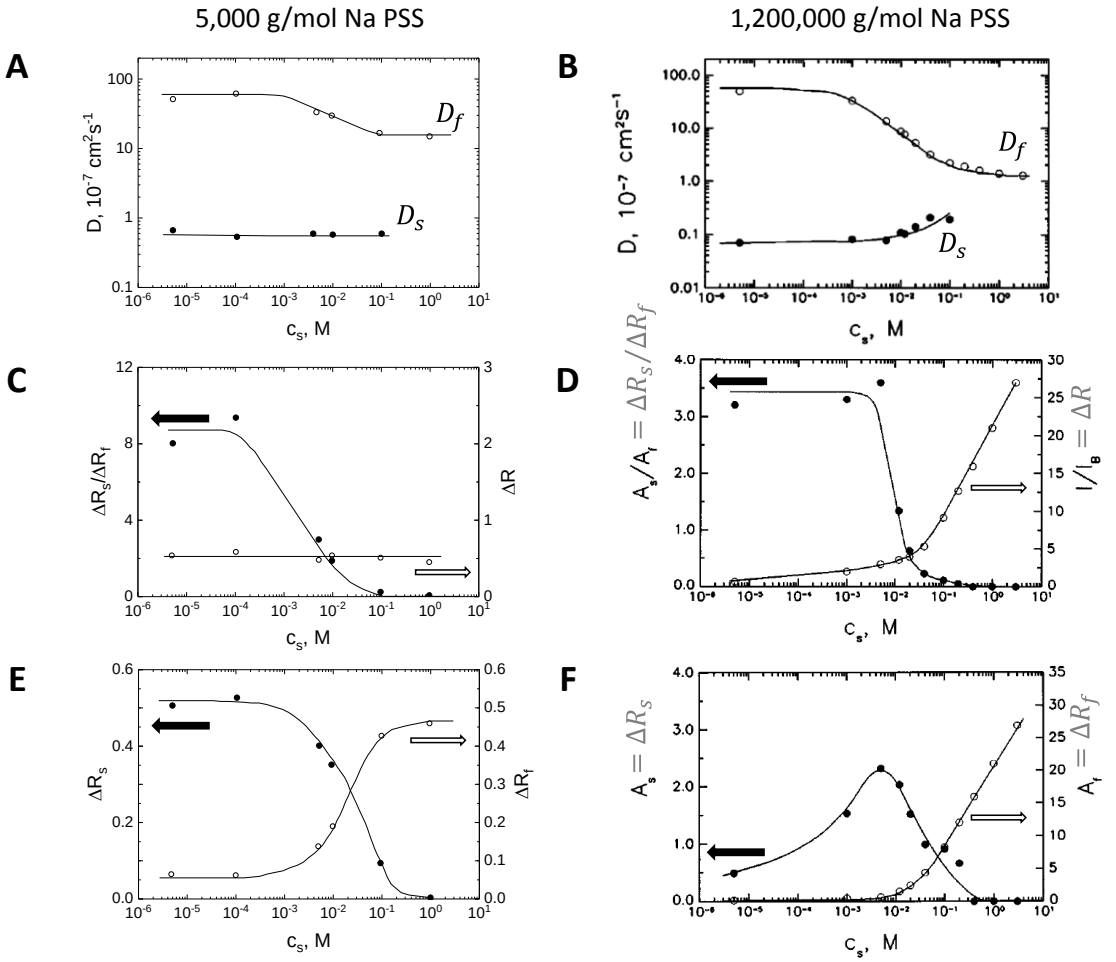

Figure 2-24: Influence of salt addition on the behaviour probed with both DLS and SLS measurements. Grey elements were added by the present author to harmonise notations with the ones adopted in the present thesis. Arrows as well as D_f and Ds notations were also added by the present author. c_s: NaCl concentration; *f* and *s* refer to the fast and the slow mode, respectively; Na PSS: sodium poly(styrene sulfonate). Na PSS concentration was 5 g/L for both polymers. Data were collected at 90° scattering angle. The graphs on the left have been replotted using data from Sedlák,[23] while those on the right have been adapted from Sedlák,[23] with the permission of AIP Publishing, Copyright © 1996 American Institute of Physics.

Nierling and Nordmeier[69] compared the influence of the addition of a monovalent salt (Na^+; Cl^-) to the one of a divalent salt (2 Na^+; SO_4^{2-}) on solutions of positively charged poly(diallyl-*N*,*N*-dimethylammonium chloride). When the salts were added to aqueous solutions, they observed that the diffusion coefficients of both the fast and the slow mode were smaller for the divalent salt compared to the monovalent salt. They explained this by the fact that the diffusion coefficient of SO_4^{2-} which is larger than Cl^-, is smaller than the one of Cl^-; hence the coupled diffusion mechanism would be slower when the divalent

salt would be added.[69] This observed difference could also come from the fact that the effective charge of the polyions is lower in presence of SO_4^{2-} compared to Cl^-, which would also weaken the coupled diffusion mechanism as the polyions would be effectively less charged in presence of SO_4^{2-}.[69] As it has been previously shown that electrostatic interactions control the formation of the domains, polyions which are less charged in presence of SO_4^{2-} would thus form smaller domains than in presence of Cl^-.

Interestingly, when Nierling and Nordmeier[69] repeated the experiments in a 25% methanol/75% water solvent, they found that the domains were larger in presence of SO_4^{2-} compared to Cl^-, and explained this by the ability of SO_4^{2-} to form bridges between polyions because of its divalent nature. 25% methanol/75% water is a poor solvent for the investigated polyelectrolyte.[69] Polyions would thus be closer to each other than in a good solvent so that the chains would be close enough for the suggesting bridging mechanism to occur compared to water where the chains would be too far from each other.

pH

Changes in pH lead to a change in the polyelectrolyte behaviour if they bear acid or basic function groups. For example, upon HCl addition, the $–CH_3COO^-$ groups born by Na CMC chains would adopt their acid form $–CH_3COOH$ which is no longer charged. In other words, for such polyelectrolytes, a change in pH leads to a change in their ionisation degree.[13,76] The effect of changes in the polyelectrolyte ionisation degree have been described in the corresponding Section above. For some polymers such as Na CMC, whose solubility in water is due to the presence of its charged groups, the polymer is no longer soluble in the solvent when too many of the charges are neutralised (see discussion about Na CMC substitution in Section 2-3.1).[13,29,81-83] In the case of Na CMC, the behaviour of H-CMC then resembles the one of cellulose in water, which is in a swollen state rather than a dissolved one.[13,81]

Solvation of the polyelectrolyte backbone

As mentioned for Na CMC in the previous Section about the influence of the pH on the behaviour of polyelectrolytes in solution, the backbone of most polyelectrolytes is poorly or non-soluble in water, and it is the presence of charges on the polymer chains that makes them solubilise in water.[29,82-84] It has thus been suggested that the slow relaxation mode could come from the poor solubility of polyelectrolyte backbones.[84] To investigate this

matter, Sehgal and Seery[78] studied the behaviour of sodium poly(styrene sulfonate) in *N*-methylformamide, while Ermi and Amis[84] studied the behaviour two quaternized poly(vinyl pyridine) polymers in ethylene glycol. In both cases, the selected solvent was a good solvent for both the neutral polymer (*i.e.* the backbone) and the charged polymer.[78,84] The results obtained from LS measurements were identical to the ones typically obtained for polyelectrolytes in water: (i) two diffusive relaxation modes were observed, and (ii) the slow relaxation mode faded upon salt addition.[78,84] Interestingly, the results obtained by Ermi and Amis[84] showed that the neutral poly(vinyl pyridine) also exhibited two relaxation modes in ethylene glycol, suggesting that the slow relaxation mode, often defined as a polyelectrolyte specificity, is more common.

Topp *et al.*'s[71] study of the influence of the ionisation degree of quaternized poly(vinyl pyridine) in KBr solutions, already mentioned in the above Section related to the polyelectrolyte ionisation degree, showed that the two typically reported relaxation modes were observed for an ionisation degree as low as 9%. At such a low ionisation degree, a third relaxation mode was also observed and attributed to the hydrophobicity of the polymer chain backbone.

Filtration

Filtration is widely used prior to LS measurements to remove dust or large particles, as they scatter significantly and bring an additional contribution to the scattering of the investigated samples.[39] For polyelectrolytes, filtration has not only been used to remove dust or particles, but also to remove the slow relaxation mode contribution, especially at low polyelectrolyte concentrations, or to study the nature of this relaxation mode.

Ghosh *et al.*[79] used a wide range of filters with different membranes and pore sizes ranging from 0.1 μm to 0.45 μm on polyelectrolyte solutions prepared with different polyelectrolytes. For each of them, they found a filter with a pore size and a membrane that could remove the slow relaxation mode. After a week, the slow relaxation mode had not reappeared in the solutions. It is worth noting that it could be that the domains have not disappeared but that their size is too small to be probed by LS.[85]

Sedlák[80] performed extensive studies to investigate the influence of filtration on the slow relaxation mode. He found that it was not always possible to remove the slow relaxation mode. Figure 2-25 displays some DLS and SLS results from two of his studies of poly(styrene sulfonate) solutions. Figure 2-25.A shows that the diffusion coefficient of

the slow mode increases upon filtration. Figure 2-25.B shows that filtration usually leads to a lower value and a less pronounced angular dependence of ΔR_s; suggesting that the size of the domains decreases upon filtration. This is confirmed by the decrease in the values of $R_{g,app}$*(domains)*. The 0.8-µm pore size filter however shows the reverse trend. It is thought that the size of the 0.8-µm pores is just about right to allow the domains to coalesce during filtration. Meanwhile, ΔR_f was not modified upon filtration.

ΔR_s of the sample filtered through the 0.1-µm pore size filter was monitored during 24 h after filtration. It was observed that ΔR_s increased over time, but the angular-dependence remained the same as the one observed just after filtration; suggesting that the size of the domains remained constant after filtration. It was thus proposed that the domains had been loosened by filtration and they would become denser afterwards as the number of polyions they contain would increase.[80]

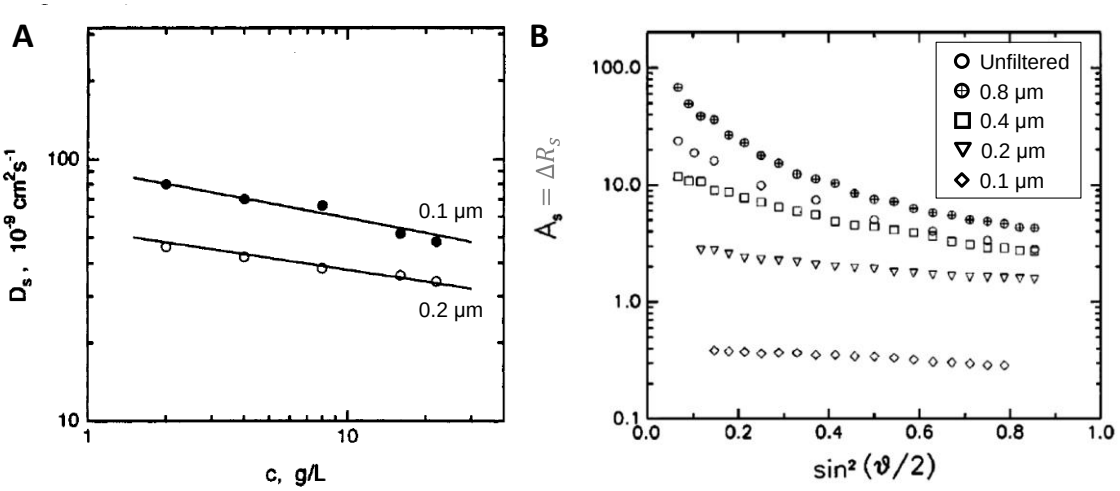

Figure 2-25: Influence of filtration on the slow relaxation mode. **A.** Influence of filtration on the slow mode diffusion coefficient. The investigated polymer was a 5,000 g/mol sodium poly(styrene sulfonate). Adapted with permission from Sedlák,[22] Copyright © 1993 American Chemical Society. **B.** Influence of filtration on the contribution of the slow mode to the excess Rayleigh ratio and its angular dependence. The investigated sample was a 710,000 g/mol sodium poly(styrene sulfonate) solution at 5 g/L. The non-filtered solution was centrifuged to remove dust and possible impurities. Adapted from Sedlák,[80] with the permission of AIP Publishing, Copyright © 1992 American Institute of Physics.

To determine whether the filtration process is based on size-exclusion (*i.e.* domains retained by the membrane filter because of their size being larger than the pores) or strength-exclusion (*i.e.* domains not strong enough to resist filtration and getting broken during the process), both resulting in the disappearance of the larger domains, Sedlák[80] compared the behaviour of solutions filtered several times through the same filter to solutions filtered several times through different filters. He found that the size of the

obtained domains was smaller when new filters were used every time; leading to the conclusion that the main mechanism occurring during filtration is strength-exclusion. Indeed, if it had been size-exclusion, the re-used filter would have become clogged and the size of the domains would have been smaller at the end of the successive filtrations than when new filters are used. The proposed mechanism is that the filter membrane is getting wetter and wetter when re-used so that the forces applied on the domains are becoming weaker and the domains have a larger size at the end than when new filters are used as they always apply the same and stronger force on the domains.[80]

Relatively concentrated solutions of high M_w polyelectrolytes have proved to be difficult to filter because of the high viscosity of the solutions. Larger pore sizes were thus used such as 1.2-µm and 3-µm pore size filters for hyaluronan and xanthan solutions,[37] or even 5-µm pore size filters for dextran solutions.[38] For hyaluronan and xanthan solutions, the authors said that no ageing effect was observed after filtration.[37]

Centrifugation

Centrifugation is another technique that allows removal of dust and impurities. Under mild conditions (*i.e.* relatively low centrifugal forces, low acceleration and deceleration rates, short durations), centrifugation has been shown to help preparing solutions that are suitable for LS without modifying them, as shown in Figure 2-26, where contribution of the slow relaxation mode to the excess Rayleigh ratio was measured after centrifugation at different centrifugation speeds for salt-free poly(styrene sulfonate solutions).[80] Sedlák[80] said that stronger centrifugation conditions significantly affected the slow mode relaxation. Such a behaviour was also found by Nierling and Nordmeier,[69] who found that the slow relaxation mode temporarily disappeared from their solution of poly(diallyl-*N*,*N*-dimethylammonium chloride) in a 25% *n*-propanol/75% water solvent. The recovery of the slow relaxation mode was noticeable after 4 days but took about 21 days to be completed.[69] Cao and Zhang[36] showed that the unique relaxation time they observed during their ultracentrifugation experiments was similar to the fast mode relaxation time probed by DLS and that the slow relaxation mode was absent. Hence, they also concluded that centrifugal forces could be strong enough to overcome the interactions responsible for the cohesion of the domains.[36]

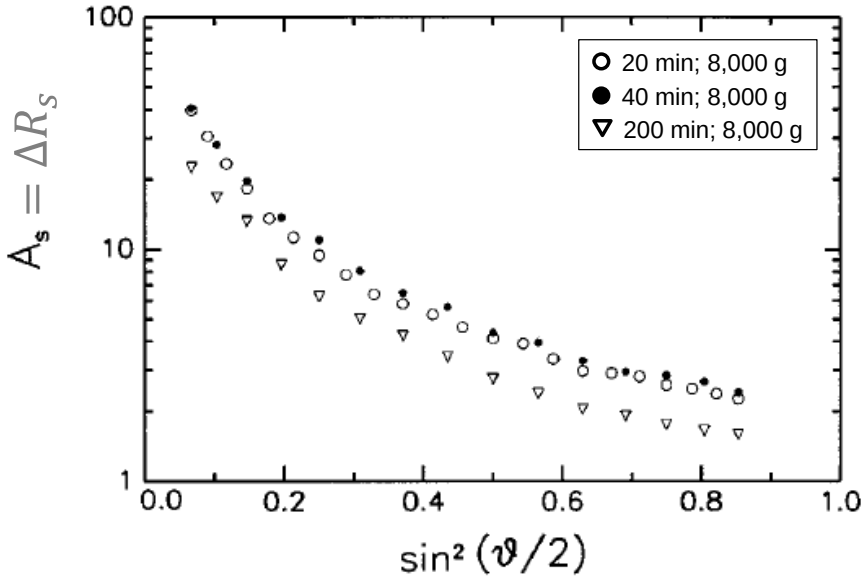

Figure 2-26: Influence of centrifugation on the slow relaxation mode. Centrifugation duration and speed are indicated in the legend directly in the Figure. The investigated sample is a 50,000 g/mol sodium poly(styrene sulfonate) solution at 5 g/L. Adapted from Sedlák,[80] with the permission of AIP Publishing, Copyright © 1992 American Institute of Physics.

Dialysis

Dialyses of either salt-free polyelectrolyte solutions against salt solutions or polyelectrolyte solutions in presence of salts against water were performed to investigate the appearance and the disappearance of the slow relaxation mode.[73,76,79] It has been reported that the slow relaxation mode disappeared from salt-free polyelectrolyte solutions dialysed against salt solutions and reappeared when the obtained solutions were dialysed against pure water,[73,76,79] as illustrated in Figure 2-27.A, which shows the evolution of the slow mode diffusion coefficient across successive dialysis cycles for poly(styrene sulfonate) solutions. In early studies such as the one Ghosh *et al.*,[79] these experiments allowed checking that the slow relaxation mode was real and was not coming from impurities present in the initial solutions.

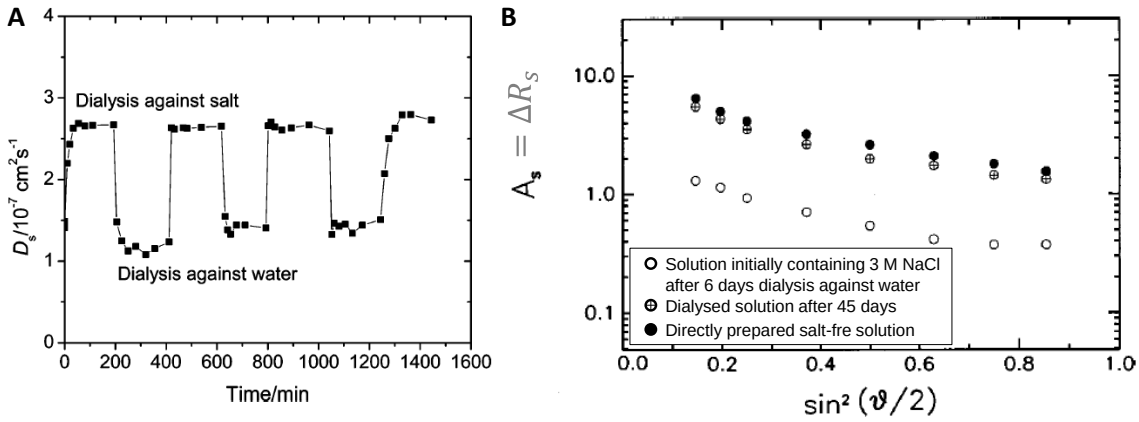

Figure 2-27: Influence dialysis on polyelectrolyte solutions. **A.** Evolution of the slow mode diffusion coefficient over time under successive dialysis cycles. The sample was a 70,000 g/mol fluoresceinamine-labelled sodium poly(styrene sulfonate) at 1.54 mg/mL. Reprinted with permission from Cong *et al*,[73] Copyright © 2006 American Chemical Society. **B.** Evolution of the slow relaxation mode to the excess Rayleigh ratio of a sodium poly(styrene sulfonate) solution in 3 M NaCl after dialysis and comparison with a directly prepared salt-free solution. Studied samples were 50,000 g/mol sodium poly(styrene sulfonate) solution at 5 g/L. Adapted from Sedlák,[76] with the permission of AIP Publishing, Copyright © 2002 American Institute of Physics.

As seen in Figure 2-27.B, Sedlák[76] showed that the recovery of the slow relaxation mode after dialysis may require long periods of time to be complete in poly(styrene sulfonate) solutions. Indeed, the slow mode contribution to the excess Rayleigh ratio after 6 days of dialysis needed 45 days to reach the same level as the one observed for a directly prepared salt-free solution.

Ageing

Some ageing effects have already been reported in the three previous sections such as the possible reappearance of the slow relaxation mode or its strengthening after filtration,[80] centrifugation[69] or salt removal using dialysis.[76] Time-scales depend on the studied systems. Some studies have explicitly reported the absence of ageing.[35,37,79] However, Sedlák's[70] investigations of polyelectrolyte solution ageing showed that ageing may only be detectable using LS after tens of days. Figure 2-26 shows the time evolution of ΔR_s for a salt-free sodium poly(styrene sulfonate) solution. It can be seen in Figure 2-26.A that ΔR_s decreases over time until it reaches a plateau. The angular-dependence of ΔR_s does however not vary over time; suggesting that $R_{g,app}$*(domains)* does not vary upon ageing. Using DLS data collected on the same solutions and the Stokes-Einstein equation (Eq. 2-19), Sedlák[70] found that the apparent hydrodynamic radius of the domains $R_{H,app}$*(domains)* decreased upon ageing. Combining both results, he suggested that polyion chains would escape the domains over time. Their arrangement in the domains

would be such that the domain size would not vary. The fact that there would be fewer polymer chains in the domains would allow water molecules to go through the domains more easily and lead to the observed decrease in $R_{H,app}$*(domains)*, corresponding to a facilitated draining process. The small increase in the local viscosity due to the higher concentration of polyions outside of the domains would not be high enough to compete against draining. Sedlák[70] showed that the fast relaxation mode was not modified upon ageing. Ageing was different from one investigated system to another.

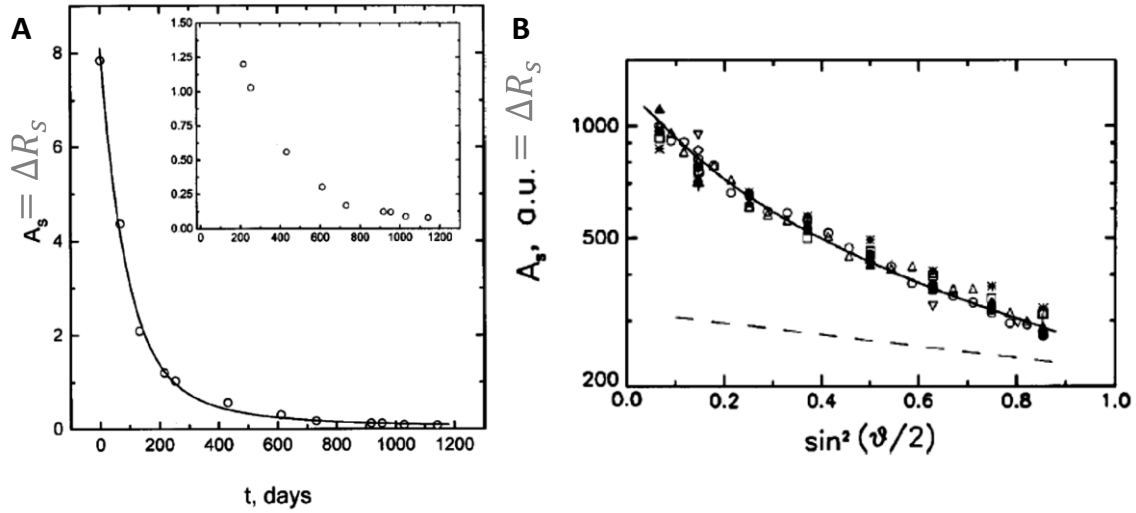

Figure 2-28: Influence of ageing on the slow relaxation mode contribution to the excess Rayleigh ratio ΔR_s. **A.** Time-dependence of ΔR_s. **B.** Angular-dependence of ΔR_s for all the time points shown in A. The dashed-line represents an example of expected angular-dependence if $R_{g,app}$*(domains)* were to decrease over time. The studied sample was a salt-free 710,000 g/mol sodium poly(styrene sulfonate) solution at 10 g/L. Adapted from Sedlák,[70] with the permission of AIP Publishing, Copyright © 2002 American Institute of Physics.

In this Section investigating the current knowledge about the slow relaxation mode, it has been shown that, despite the origin of the domains attributed to the slow relaxation mode still being unknown, and some discrepancies observed between the studied systems, such as whether the size of the domains depends on the polyelectrolyte concentration, whether the domains can be fully removed by filtration or would simply be reduced to a size smaller than what can be probed by LS, and whether the domains always evolve over time until they reach an equilibrium state in all polyelectrolyte systems, some typical properties of the domains can be established. Indeed, it has been established that they are not due to the presence of impurities as they can reform in solutions that have been carefully purified. High forces such as the ones applied during centrifugation and ultracentrifugation seem to be strong enough to break them. They may reappear afterwards; which further supports the fact that they correspond to a metastable

equilibrium in solution. Salt addition leads to a decrease in their size, and domains may even fully disappear for low M_w polyelectrolytes and concentrations. A rheological study allowing the determination of the crossover concentration regimes as defined by the scaling laws would be helpful to assess whether the cases for which the slow mode disappears upon salt addition correspond to cases where salt addition takes the solution from the salt-free semi-dilute concentration regime to the screened dilute concentration regime where only one relaxation mode is expected. Investigating other techniques that could weaken the slow relaxation mode, or even make it disappear, could bring more information about its characteristics; getting closer to understand the origin and the nature of this slow relaxation mode.

2-2.4. Attempts to describe the concentration regimes with M_w-c maps

In 1980, Graessley[86] established M_w-c maps describing the concentration regimes for two neutral polymers in good solvents (*i.e.* polysterene in toluene and polybutadiene in tetrahydrofuran) using viscosity measurements. The map they obtained for polystyrene in toluene is shown in Figure 2-29.A. In 1992, Sedlák and Amis[66] attempted to establish a similar map for polyelectrolyte sodium polystyrene sulfonate in water using their light scattering data. This map is depicted in in Figure 2-29.B. Contrary to the maps established for neutral polymers, it does not cover all the concentration regimes predicted by the scaling theory as solutions of both very low and very high polyelectrolyte concentrations are difficult to investigate using light scattering. Moreover, as already discussed in Section 2-2.3, light scattering allows the definition of more concentration regimes than those predicted by the scaling theory in the low concentration region. On the map displayed in Figure 2-29.B, it even seems that the transition concentrations c_a, c_b and c_d probed by LS (the latter is defined by Sedlák and Amis[66] as the concentration below which a peak is observed in the SLS profile, which would correspond to the form factor) could all be different from the ones both predicted by the scaling theory and determined using viscosity measurements. It is worth noting that the line representing c_c, suggested to be c_e by the present author, is vertical and does not meet the line representing c_e. This is likely to be due to the fact that Sedlák and Amis' experiments[66] seems to include only one polymer exhibiting this behaviour so that the line they have plotted would be an extrapolation. To my knowledge, no other attempt has been made to complete this map

for polyelectrolytes nor to solve the apparent disagreements between the scaling theory and the concentration regimes probed by light scattering.

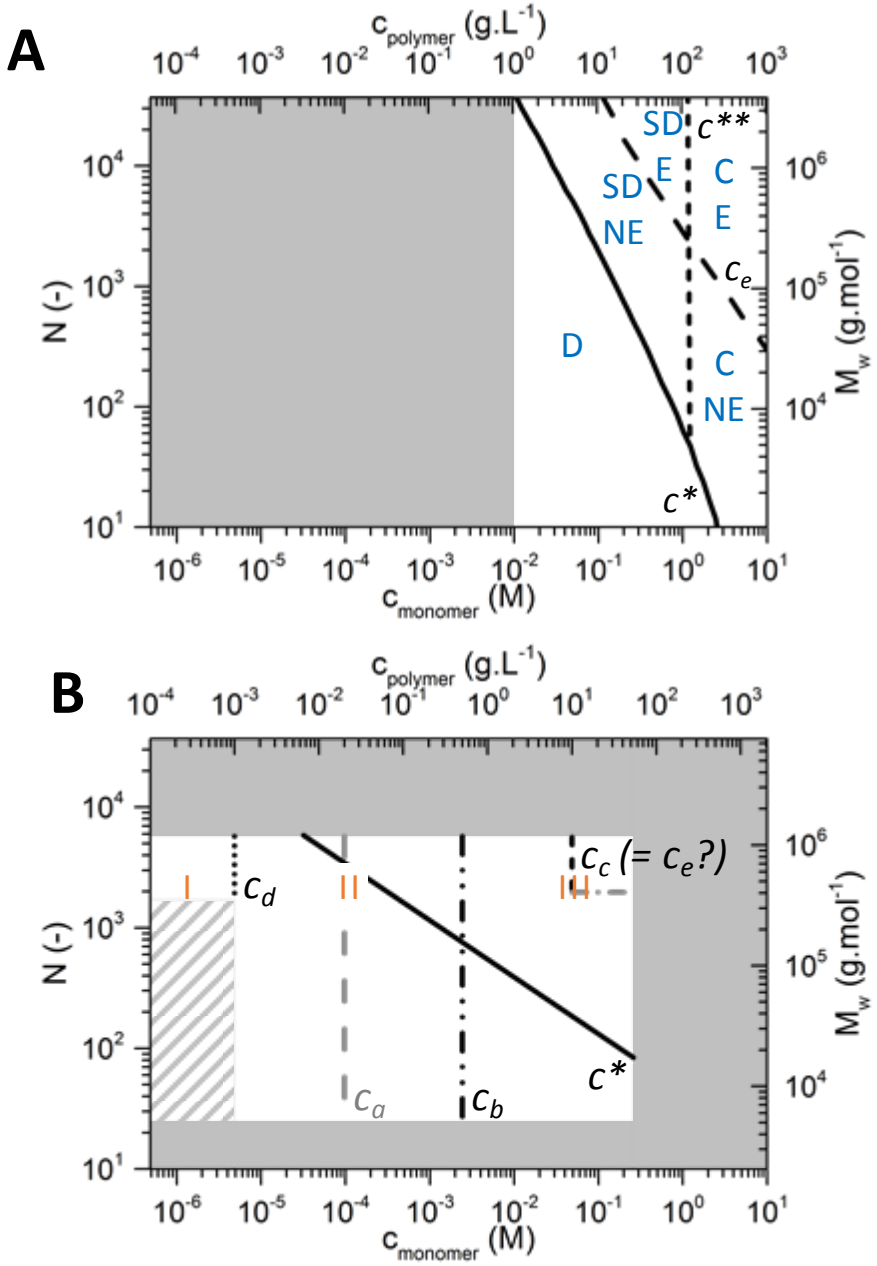

Figure 2-29: M_w-c maps of the concentration regimes for salt-free solutions of a neutral polymer (polystyrene in toluene; **A**) and a polyelectrolyte (sodium polystyrene sulfonate in water; **B**). Both maps, originally presented as $c_{copolymer}$ *vs* $M_{w,polymer}$, have been replotted as $N = f(c_{monomer})$ with N the degree of polymerisation. The original scales are also shown. Black and grey lines correspond to the transition concentrations; they are labelled in italic in the Figure. Grey areas correspond to areas where no experiment was performed, while the dashed area in B corresponds to an area where the original authors have not been able to carry out experiments as the collected data were below the sensitivity of the instrument. A was established with viscosity measurements. The concentration regimes are identified in the Figure as D (dilute), SD NE (Semi-dilute Non-Entangled), SD E (Semi-dilute Entangled), C E (Concentrated Entangled) and C NE (Concentrated Non-Entangled). c^*: overlap concentration; c_e: entanglement concentration; c^{**}: transition concentration between the semi-dilute and the concentrated regimes. B was

established with light scattering measurements. Areas I, II and III correspond to the experimentally determined concentration regions. Area I corresponds to the high concentration region where the fast relaxation mode is concentration-independent. The dashed line represents the concentration c_c which I have suggested to be c_e and was only observed for the highest investigated M_w polyelectrolyte (hence the horizontal dashed-dotted grey line added here compared to the original map). Area II corresponds to the intermediate concentration region between c_d and c_b where the two relaxation modes are probed by DLS and are c-dependent. Below c_d (*i.e.* area III), a peak is observed in the SLS profile. c_a has been added in the Figure by the present author and corresponds to the transition concentration below which only the fast relaxation time is probed by DLS. The overlap concentration c^* plotted by the original authors was calculated rather than experimentally determined, and defines the transition between the dilute and the semi-dilute regimes. A and B have been replotted and adapted from Graessley[86] and Sedlák and Amis, respectively.

2-3. Sodium Carboxymethyl Cellulose (Na CMC)

Now that some general features about the behaviour of polyelectrolytes in solution have been explained, the present Section focuses on Sodium Carboxymethyl Cellulose (Na CMC), which is a linear semi-flexible polyelectrolyte,[1,14,15] and is the subject of this thesis. The main characteristics of Na CMC are first discussed. Then, its overall behaviour in solution is described and compared to the behaviour typically observed for polyelectrolyte solutions as detailed in Section 2-2 above. Finally, the influence of some key Na CMC characteristics as well as some key external parameters is reviewed.

2-3.1. Structure, characteristics and synthesis

Na CMC is a cellulose derivative. As illustrated in Figure 2-30, it consists of cellulose (*i.e. D*-glucose monomers linked by β-1,4 glucosidic bonds) whose hydroxyl groups have been substituted by carboxymethyl groups.[18,26,87-93] From a theoretical point-of-view, all the hydroxyl groups can be substituted, but full substitution is rarely achieved. Commercial Na CMCs usually have an average of 0.4 to 1.4 substituted hydroxyl groups per monomer referred as the absolute degree of substitution (DS).[18] It is worth noting that the term absolute is usually omitted. Na CMC batches of DS around 2.3-2.5 were synthesised for research purposes by some authors like Barba *et al.*,[28] Heinze *et al.*,[94] Käuper *et al.*,[95] and Kulicke *et al.*[96] DSs as high as 2.9 and 2.96 were obtained by Rinaudo *et al.*[97] and Kulicke *et al.*,[30] respectively.

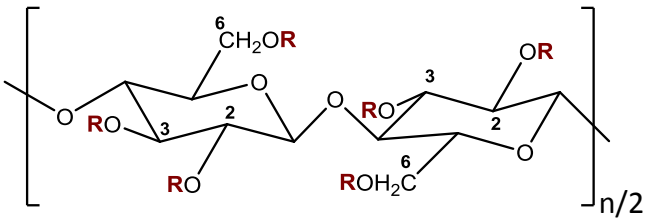

Figure 2-30: Chemical structure of Na CMC. **R** = H or CH_2COO^-, Na^+. *N.B:* **R** = H for cellulose.

Eight different types of monomers can be found depending on the number and the location of the substituted groups they bear.[95,98,99] However, this diversity is not reflected by the absolute DS. To describe more precisely the substitution along Na CMC chains, other parameters have thus been defined, including:

- The partial degrees of substitution: they represent the average number of glucose monomers whose C_2, C_3 and C_6 are substituted.
- The proportion of un-, mono-, di- and tri-substituted glucose monomers.
- The proportion of each of the eight monomers.
- The distribution of the substituted glucose monomers along the polymer chains (*i.e.* are the substituted monomers homogeneously distributed along Na CMC chains?).

The negative charges of the substituted groups allow Na CMC to solubilise in water provided their number is high enough (*N.B:* the insolubility of cellulose in water is discussed at the end of this Section). The lower boundary is around DS 0.5-0.6.[26,28,29] It also depends on the distribution of the substituted monomers along the chains. Indeed, large poorly or non-substituted segments are not water-soluble for the same reason (see Section 2-3.3.2 where more details about these poorly substituted segments and their influence on Na CMC behaviour in water are provided). As Na CMC is a charged polymer, it is a polyelectrolyte.

Na CMC is obtained from cellulose through a two-step reaction, which is depicted in Figure 2-31:

- Mercerisation in presence of NaOH: the cellulose swells and reacts with NaOH to give the alkali cellulose (also called mercerised cellulose)[26];
- Carboxymethylation of the alkali cellulose by reaction with monochloroacetic acid.

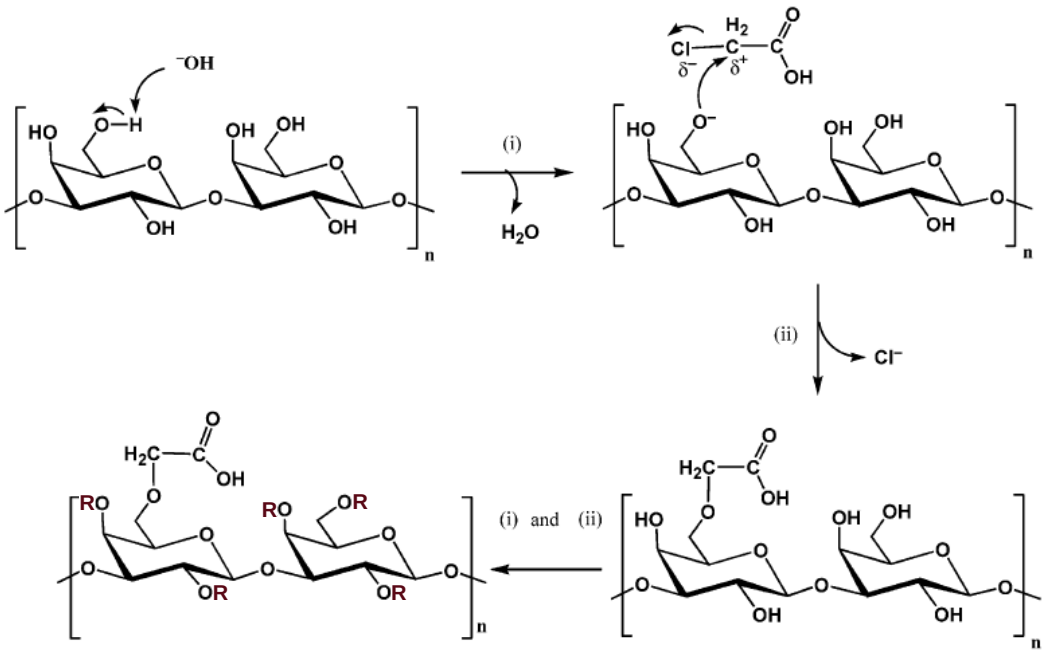

Figure 2-31: Na CMC synthesis. (i): mercerisation with NaOH; (ii) carboxymethylation with monochloroacetic acid. **R** = H or CH_2COO^-, Na^+ as the carboxymethylation (*i.e.* (i) + (ii)) goes ahead. Adapted from Silva *et al*,[100] Copyright © 2004 Elsevier Ltd, with permission from Elsevier.

Traditional cellulose sources used for Na CMC synthesis are cotton linters and wood pulp.[26,27,94,101] The reaction medium is a heterogeneous slurry as the solvent swells but does not dissolve the polymer.[101] To get an homogenous distribution of the components in the reactor, an alcohol is usually used as co-solvent.[26] Heinze et *al.*[94] have synthesised Na CMC under homogeneous reaction conditions using LiCl/*N*,*N*-dimethylaetamide as solvent. Recent studies have been looking at ways of performing greener syntheses such as the use of microwaves as a heating source,[102] the use of water as a solvent,[103] or the extraction of cellulose from waste or by-products from the industry, *e.g.* recycled paper,[103] banana pseudo stem,[104] sugar beet pulp,[105] pomegranate seeds[18] or orange peel.[93]

The substitution pattern along the chains is usually not controlled during the synthesis.[87] However, it has been shown that each absolute DS corresponds to a triplet of partial DSs. Moreover, the most substituted carbon is C2, while the least substituted one is C3.[87,99] Synthesis pathways involving protective groups in non-aqueous solvents have made it possible to get Na CMCs whose substituted groups are on C2 and C3 only.[87,106]

Na CMC is a polymer; its chain length can thus vary. The length of the cellulose raw material used for Na CMC synthesis mostly defines the length of Na CMC chains. They can be shortened by acid hydrolysis,[24] oxidation in presence of H_2O_2[107] or sonication[95]

(see Section 2-3.4.2 for more details about the influence of sonication on polymer solutions in general and Na CMC solutions in particular). Kulicke *et al.*[30] have also reported that obtaining Na CMCs with high DSs leads to shorter polymer chains compared to Na CMCs of lower DS obtained from the same raw material. Both the molecular weight M_w and the degree of polymerisation (*i.e.* number of monomer per polymer chains) reflect the length of the chains; the higher they are, the longer the chains. Na CMCs of very different molecular weights are found in the literature. Most of them are around 10^4-10^5 g/mol, but values as small as 9,000 g/mol[81] or as high as 5,278,000 g/mol[24] can be found. Furthermore, because the cellulose from which Na CMC is produced comes from natural sources, there is a great variability in the molecular weight of the polymer chains in Na CMC batches, as characterised by large polydispersity indices M_w/M_n.[1,3,24,25] Typical values of M_w/M_n are around 1.7-3.6,[1,3,24,25] but higher values such as 8.5 and 8.7 have also been reported.[24]

Cellulose usually contains crystalline fragments.[108] The crystalline structures that can be found in Na CMC are celluloses I and II,[26,27] whose structural differences are illustrated in Figure 2-32. The crystallographic repetitive unit is cellobiose, which consists of two consecutive glucose monomers as shown in Figure 2-32.A.[109,110] It is worth noting that the two ends of a cellulose chain are not identical: the reducing end is in equilibrium with a cyclic hemiacetal, while the non-reducing end is not involved in any equilibrium (see Figure 2-32.A).[110]

Cellulose I is the crystalline structure present in native cellulose, and can be found under two forms: celluloses I_α and I_β.[108,109] Cellulose I_β has a monoclinic structure where consecutive parallel cellobiose units are shifted by a quarter of their size along the *c* axis, while cellulose I_α has a triclinic structure where consecutive cellobiose units are shifted diagonally by the same distance as illustrated at the bottom of Figure 2-32.B.[110] As shown at the top of Figure 2-32.B, both cellulose I_α and I_β chains are aligned towards the same direction, *i.e.* with all reducing end-groups together, and consequently all non-reducing end-groups together, while consecutive cellulose II chains are aligned in opposite directions.[108] Hence, as illustrated in the middle of Figure 2-32.B, the intra- and inter-chain H bonds are different for both cellulose structures.[109]

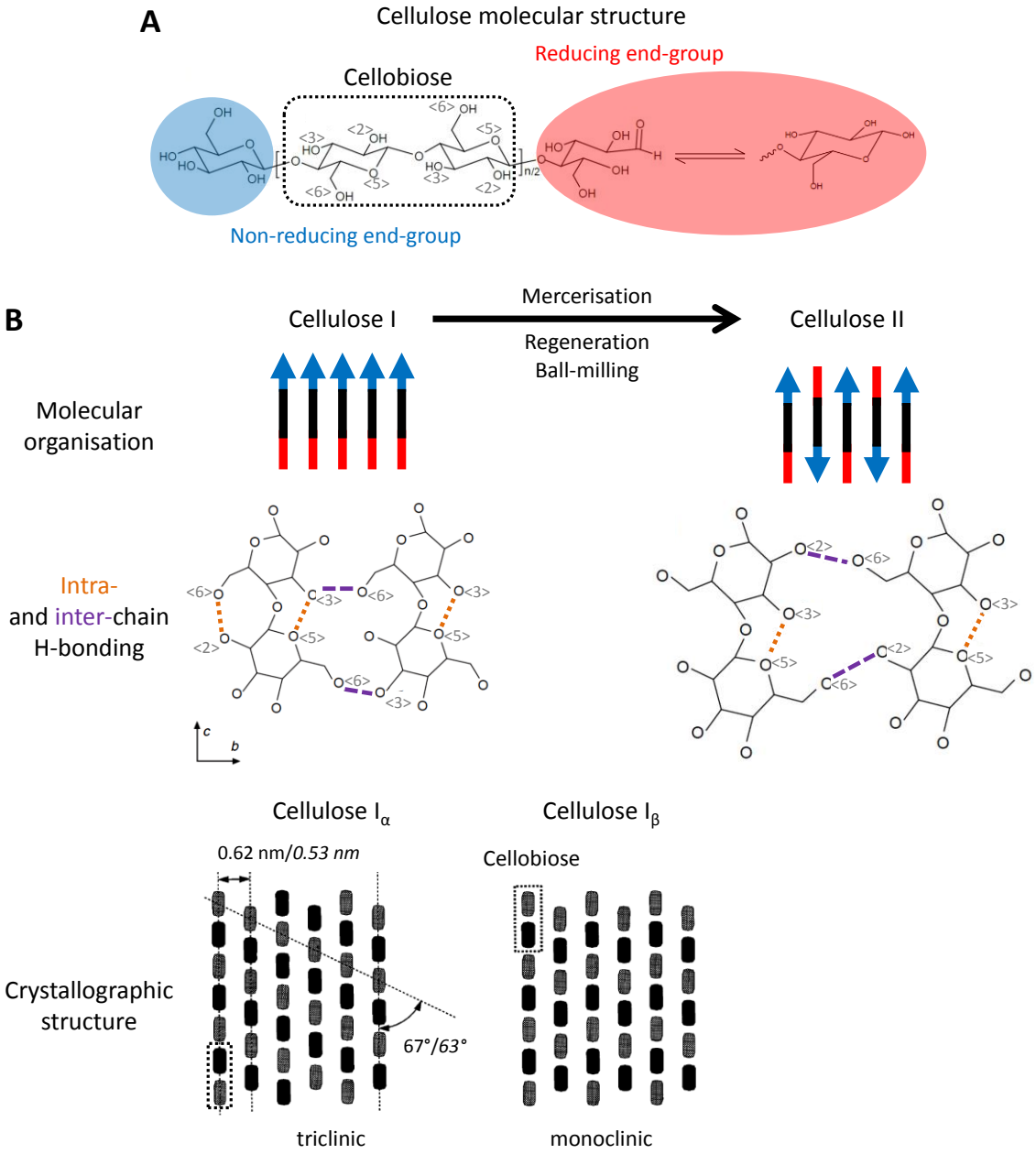

Figure 2-32: Illustration of the differences between celluloses I and II. **A.** Cellulose molecular structure. Blue: non-reducing end-group. Red: reducing end group (*i.e.* in equilibrium with a cyclic hemiacetal). **B.** Structural differences between celluloses I_α & I_β, and II. At the bottom, the distances and angles which are provided refer to faces (100) [normal] and (010) [italic] of the triclinic structure, respectively. The schematics representing the hydrogen interactions and the crystallographic structures were adapted by permission from Springer Nature, *Cellulose*, O'Sullivan,[109] Copyright © Chapman and Hall 1997, and adapted from Baker *et al.*,[110] Copyright © 1997 Academic Press, with permission from Elsevier, respectively.

Cellulose II does not exist in native cellulose and is formed by mercerisation, which is the first step of Na CMC cellulose (see above discussion and Figure 2-31), regeneration (*i.e.* solubilisation and recrystallisation of cellulose) or ball-milling.[108,109] It is more stable than the cellulose I and is therefore less reactive, while the amorphous cellulose is the most reactive cellulose form. It can be easily understood that the crystallinity pattern of

the final Na CMC depends on the cellulose used for the synthesis.[26,27] Kamide *et al.*[27] indicated that the initial crystalline pattern of the cellulose remains visible in the final Na CMC. More recently, Almlöf Ambjörnsson[26] showed that the reaction conditions could also play an important role in controlling the crystalline pattern of the synthesised Na CMC. Kamide *et al.*[27] reported crystallinity values ranging between 0 and 57.8%. Often, X-ray,[27,104,111,112] Raman[26] or Infrared (IR)[82,94,101] spectra, which all allow to differentiate the different crystalline structures, are used to identify the crystalline structure(s) present in the batches and compare them qualitatively.

Na CMC batches can contain different types of impurities such as non-reacted materials from the initial cellulose[29,30,82,83,113] (see Section 2-3.3.2 where more details about these non-reacted materials and their influence on Na CMC solution behaviour are provided), as well as glycolic acid $HOCH_2COOH$ and NaCl produced by a side reaction displayed in Figure 2-33.[26,30]

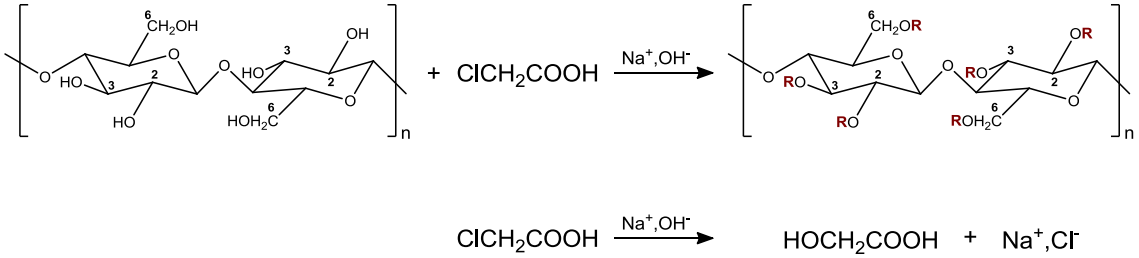

Figure 2-33: Main (top) and side (bottom) reactions occurring during Na CMC synthesis. **R** = H or CH_2COO^-, Na^+. The two products obtained from the side-reaction are glycolic acid $HOCH_2COOH$ and NaCl. After Kulicke et *al.*[30]

Before concluding this Section, and as it is important to important to understand Na CMC aqueous solubility, I would like to discuss the insolubility of cellulose in water. Until very recently, cellulose insolubility in water has mainly been explained by the high number of cellulose-cellulose hydrogen bonds (see Figure 2-32).[114,115] Crystallinity has also sometimes been cited as a factor responsible for cellulose aqueous insolubility.[114,115] Lindman and co-workers[114-117] have however highlighted some striking discrepancies in the reasoning attributing cellulose insolubility to hydrogen bonding. Indeed, water itself contains a high number of H bonds and it is commonly accepted that compounds that can form H bonds should be soluble in water.[114] Hence, glucose, the monomer cellulose is made of, is highly soluble in water.[114,115] Furthermore, other glucose derivatives such as alkylpolyglucosides, dextran (another polyglucose) or cellulose derivatives like methyl and hydroxyethyl cellulose are also water soluble.[114,115] When studying cellulose solubility in water, one should consider all possible H-bonds, *i.e.* carbohydrate-

carbohydrate, water-water and carbohydrate-water. Lindman and co-workers[114-117] have shown that the magnitude of these interactions is very similar and is about 5 kcal/mol. According to all these arguments, cellulose should thus be water-soluble.[114-117] A last yet striking fact is that there does not seem to be any common point between the few solvents capable of solubilising cellulose.[114,115,117]

The new model proposed by Lindman and co-workers[114-117] to explain cellulose aqueous insolubility and overcome these discrepancies is based on cellulose amphiphilicity. Indeed, as illustrated in Figure 2-34, the hydroxyl groups, all located on the equatorial positions of the glucopyranose rings, form the hydrophilic region, while the C-H bonds located on the axial direction of the rings forms the hydrophobic region.[117] Cellulose chains can thus be seen as thick ribbons with two opposite hydrophobic sides; the two other opposite sides being hydrophilic.[117] It is the presence of these hydrophobic regions that would make cellulose water-insoluble.[114-117] Furthermore, Lindman and co-workers[114-117] have suggested that solvents efficient at dissolving cellulose should be amphiphilic like cellulose, and/or have an intermediate polarity so that they reduce or eliminate hydrophobic interactions. Addition of urea facilitates cellulose dissolution in water as it decreases hydrophobic associations.[115,116]

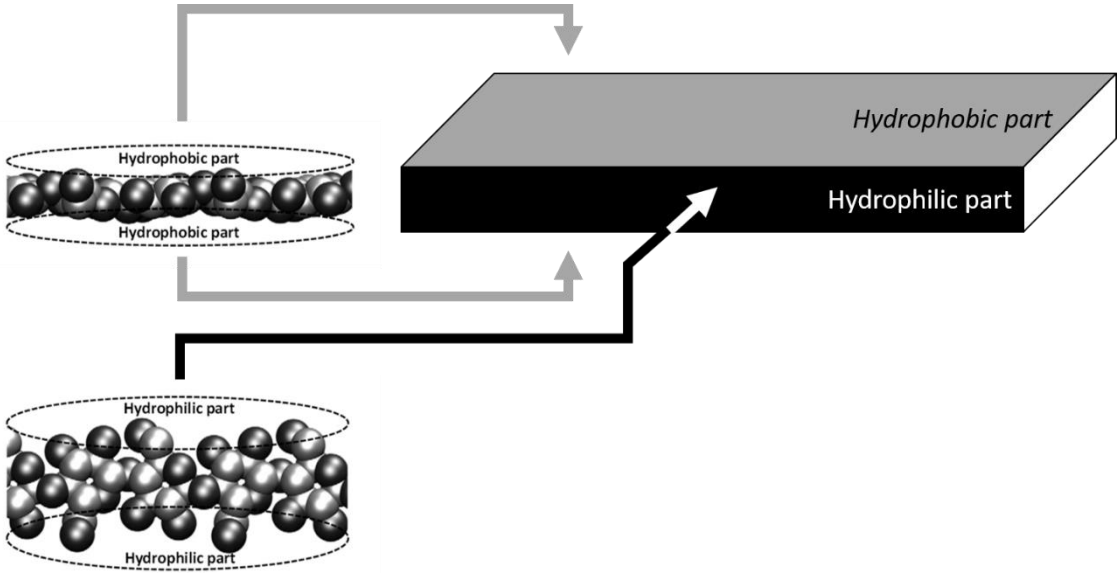

Figure 2-34: Illustration of cellulose amphiphilicity. The molecular structures on the left-hand side (reprinted from Medronho and Lindman,[117] Copyright © 2013 Elsevier Ltd, with permission from Elsevier) are Van der Waals surface representations of a cellulose chain seen from 'above' and from the 'side'. Black and shaded grey atoms are oxygen and non-polar carbon atoms, respectively (*N.B*: the aliphatic protons, all in axial positions and perpendicular to the rings, are not represented for clarity). The hydrophobic and hydrophilic areas are shown by the dashed ellipses. On the right-hand side, a cellulose chain is represented as a flat ribbon to illustrate the model proposed by Medronho and Lindman.[117] Opposite sides of the ribbons exhibit similar hydrophilic/hydrophobic properties.

In conclusion of this Section, despite having a unique name, Na CMC can be very different from one batch to another. Substitution (*i.e.* DS and substitution homogeneity along the polymer chains) and crystallinity are key to determine the solubility of a Na CMC batch in water. Moreover, due to the natural origin of Na CMC, the M_w distribution is expected to be broad. One thus needs to be careful when comparing investigations of Na CMC behaviour with literature about synthetic monodisperse polyelectrolytes.

2-3.2. Measurement techniques to investigate the behaviour of Na CMC in solution

In this Section, scattering and rheological investigations of Na CMC behaviour in salt-free solutions is reviewed as these two techniques are the two main techniques used in the present thesis. When possible, the behaviour reported for Na CMC is compared to the one typically reported for polyelectrolytes and previously discussed in Section 2-2.

2-3.2.1. Scattering

The following scattering techniques have been used to characterise the behaviour of Na CMC in solution: SLS, DLS, Small Angle X-ray Scattering (SAXS) and Small Angle Neutron Scattering (SANS). In LS experiments, a laser beam goes through the sample, which scatters the light, and the resulting scattering intensity collected at different angles is studied. Similarly, in X-ray (or neutron) scattering measurements, an X-ray (or neutron beam) goes through the sample, and the resulting scattering intensity is collected at different angles and studied. X-ray and neutron scattering experiments allow to investigate lower length-scales than LS experiments.[39] Hence, length-scales as small as the correlation length ξ representing the distance between two polymer chains in the semi-dilute concentration regime (see Section 2-2.1) can be studied.[14]

The studies using scattering techniques to investigate the behaviour of Na CMC solutions are compiled in Table 2-4. A couple of straightforward remarks can be made. The number of relevant research papers is very small. Moreover, I have only found three previous studies dealing with measurements performed on Na CMC solutions in pure water: two Small Angle Neutron Scattering (SANS) studies and a SLS study. Indeed, as the polyelectrolyte chains are expended in dilute solutions (see Section 2-2), the scattering intensity is often below the sensitivity of the instruments.[51] The addition of salts brings

additional counterions which screen the charges on the polymer chains. The less charged polymer chains thus adopt a more coiled conformation and, as they are more packed, they scatter light more strongly.[13] However, as the conformation of the polymer chains is modified by the addition of salts, the studied systems cannot be considered as Na CMC in pure water.[51]

Table 2-4: Scattering techniques used to study Na CMC.

Technique(s)	Salt	Variable(s)	Ref
DLS, SLS	DTAB	DTAB concentration	118
DLS, SLS, SAXS	0.1 M electrolyte (NaCl/HCl)	pH (1.6-7.0)	13
LALLS*	0.1 M NH_4NO_3	DS, M_w	97
MALLS*	$NaNO_3$	$NaNO_3$ concentration, DS, M_w	107
SANS	None	Na CMC concentration	1
SANS	None	Na CMC concentration, DS	14
SLS	NaCl	NaCl concentration, M_w	119, 120
SLS	NaCl	Na CMC and NaCl concentrations	121
SLS	None, NaCl	Na CMC and NaCl concentrations	122

*: coupled to a Size Exclusion Chromatograph (SEC); SLS: Static Light Scattering; SAXS: Small Angle X-ray Scattering; DLS: Dynamic Light Scattering; MALLS: Multi-Angle Laser Light Scattering; SANS: Small Angle Neutron Scattering; LALLS: Low Angle Laser Light Scattering. DTAB: dodecyltrimethylammonium bromide; Ref: reference.

For easier comparison with the polyelectrolyte SLS data discussed in Section 2-2.3.3, I have replotted the $Kc/R_{90°} = f(c)$ data collected in water by Trap and Hermans[122] as $\Delta R(90°)/K = f(c)$. Both data sets are shown in Figure 2-35 (K is an optical constant obtained with Eq. AI-3). The excess Rayleigh ratio increases with Na CMC concentration. This increase can be described by a power law of exponent 0.79 in pure water. As discussed for other polyelectrolytes (see Section 2-2.3.3 and Figure 2-19), an exponent below 1 is related to repulsive interactions between scatterers as expected in this low Na CMC concentration range. The data obtained in presence of NaCl are discussed in Section 2-3.4.1.

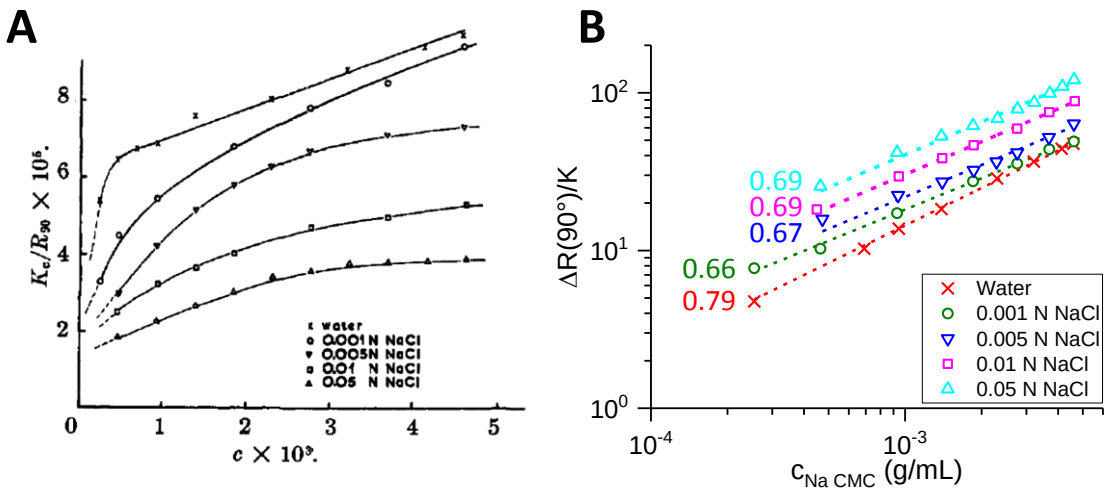

Figure 2-35: SLS data collected on Na CMC solutions of various concentrations with and without added salt. **A.** Original Figure reprinted with permission from Trap and Hermans,[122] Copyright © 1954 American Chemical Society. **B.** SLS data replotted by the present author. Dashed lines are fits of the data to power laws. The power law exponents are provided next to each curve. $R_{90°}$ and $\Delta R(90°)$ are the excess Rayleigh ratio in A and B, respectively. K is an optical constant calculated with Eq. AI-3. The average molecular weight of the studied sample is about 86,000 g/mol.

The Small Angle Neutron Scattering (SANS) measurements performed by Lopez and co-workers on salt-free Na CMC solutions were performed in D_2O to increase the contrast between Na CMC and water as Na CMC scattering is very weak.[1,14] Even in these conditions, it was not possible to collect data at low Na CMC concentrations and the data were collected above the overlap concentration c^*. The curves $I = f(q)$ obtained by Small Angle Neutron Scattering (SANS) at different Na CMC concentrations displayed in Figure 2-36 exhibit a correlation peak whose position q^* is shifted towards higher values with Na CMC concentration, and a characteristic low q upturn, as usually observed for polyelectrolytes.[1,14]

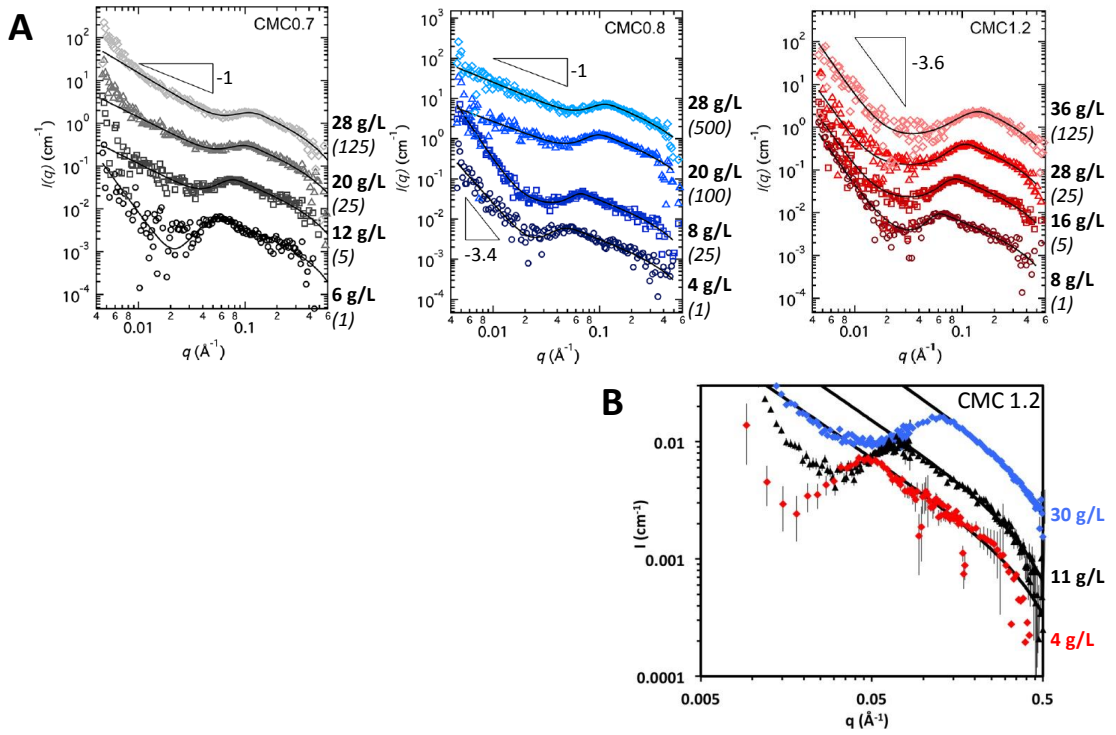

Figure 2-36: SANS profiles of salt-free Na CMC solutions in D_2O at different concentrations (indicated in bold next to each curve) for three Na CMC samples of similar M_w and different DS values. DS values are indicated at the top of each curve. **A.** The values shown into brackets and in italic correspond to the vertical shift factor applied for each data set. The characteristics of the three Na CMC samples can be found in the 2nd, 3rd and 4th columns of Table 2-6. The lines are descriptive fits. See original paper for more details. Adapted from Lopez *et al.*[14] **B.** Non-vertically shifted SANS profiles at large q values collected on the Na CMC sample with DS 1.2. Black lines correspond to the fits of the data at large q values. Adapted from Lopez *et al.*[1]

Figure 2-37 shows the concentration dependence of the value of the scattering vector q^* corresponding to the peak maximum. q^* is proportional to the correlation length ξ ($\xi = 2\pi/q^*$) and follows the expected $q^* \sim c^{0.5} (\sim \xi^{-1})$ relationship predicted by the polyelectrolyte scaling laws.[1,14] As explained in Section 2-2.1 and depicted in the schematic shown in bottom right corner of Figure 2-37, ξ characterises the distance between Na CMC chains. When $c_{Na\ CMC}$ increases, $q^* (\sim \xi^{-1})$ is shifted towards higher q values (see Figures 2-36 and 2-37), indicative of a decrease in the distance between polymer chains.[1,14] Meanwhile, the scattering intensity in the high q region probing length-scales below ξ increases (see Figure 2-36.B), which indicates an increase in the number of chains involved in the network of mesh-size ξ.[1] Furthermore, the determination of the multiplying factor between ξ and $c^{0.5}$ allowed Lopez *et al.*[1,14] to conclude that Na CMC chains adopt a stiff conformation at length-scales below ξ.

The $I(q^*) \sim c^{0.5}$ dependence in the semi-dilute regime is in agreement with the scaling law too (data not shown here).[1] However, the change in the Na CMC concentration

dependence of both q^* and $I(q^*)$ expected at the crossover concentration c^{**} between the semi-dilute and the concentrated regimes was not observed.[1,14] The authors concluded that the electrostatic blob ξ_e and the correlation length ξ concepts (see Section 2-2.1 for the definition of ξ_e and ξ) failed at describing the Na CMC at these high concentrations. This is further discussed in relation to the rheological behaviour of Na CMC solutions in Section 2-3.2.2, while the differences in the scattering behaviour due to the difference in DS are discussed in Section 2-3.3.2.

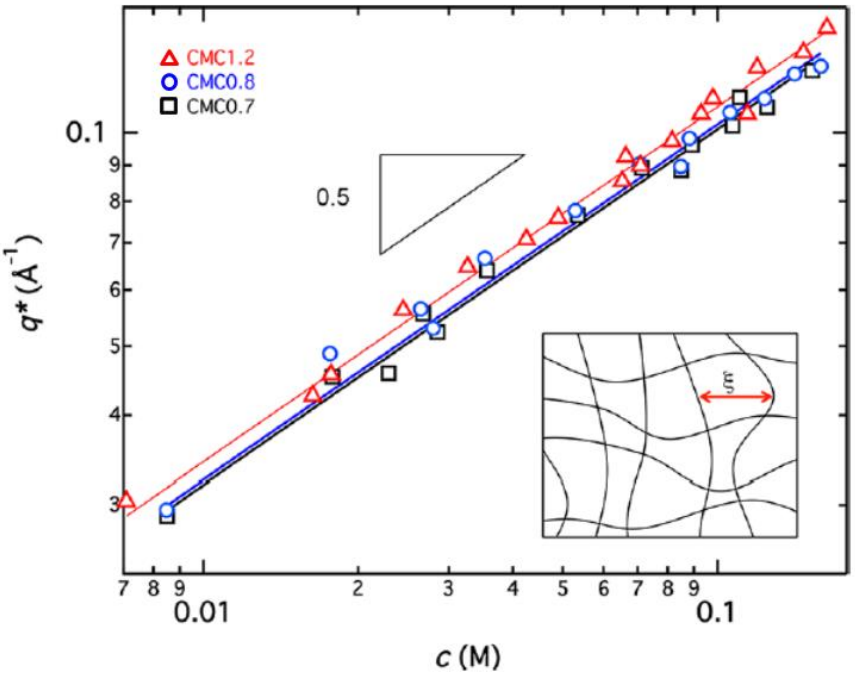

Figure 2-37: Correlation peak position q^* as a function of Na CMC concentration for the same three Na CMC samples as the ones shown in Figure 2-36. The slope obtained for the best fit single power law is indicated on the graph. From Lopez *et al.*[14]

2-3.2.2. Rheology measurements

This Section is divided in two sub-sections. The first sub-section examines the flow behaviour of salt-free Na CMC solutions, while the second one uses the zero-shear viscosity obtained from the flow curves to establish the concentration dependence of the specific viscosity and determine the concentration regimes as defined by the polyelectrolyte scaling laws in Section 2-2.2.

Flow curves

Examples of flow curves collected on Na CMC solutions prepared at different concentrations are shown in Figure 2-38. As for other polyelectrolytes (see Section 2-2.2 and Figure 2-7), a Newtonian and a shear-thinning behaviour are observed at low and

high Na CMC concentration, respectively.[87,123-127] In the example provided, the Newtonian behaviour is however still observed at low concentrations in the semi-dilute regime as all the data shown in Figure 2-38 were collected in the semi-dilute regime (see Figure 2-42). Castelain *et al.*[123] suggested that interpenetrated polymer chains would indeed get aligned along the direction of flow, but that the shear-rate would be low enough to allow other polymer chains to interpenetrate each other at the same time elsewhere in the solution. Hence, simultaneous entanglement and disentanglement of polymer chains would compensate each other. The viscosity of the solution would thus remain the same.

It is worth noting that Castelain *et al.*[123] do not actually talk about interpenetrated chains but about entangled chains instead. Most of the literature about the rheological behaviour of Na CMC solutions has been published in hydrocolloid or food-related journals rather than in polymer physics journals,[123,124,127] and the word 'entanglement' is often used to talk about polymer chains above the overlap concentration c^*, where the polymer chains interpenetrate each other, rather than above the entanglement concentration c_e where the chains are indeed entangled. In this thesis, the word 'entanglement' is used to refer to the entanglements as described by polymer physicists and explained in Sections 2-2.1 and 2-2.2. It is most unlikely that the behaviour of the solutions is Newtonian above c_e.[56] In fact, the authors of Figure 2-38 determined the entanglement concentration c_e (see next sub-section and Table 2-6) and the behaviour of the solutions whose concentration is above c_e is always shear-thinning.[1] This is confirmed by the behaviour of two other Na CMC samples for which both c^* and c_e were determined.[14,15] Other explanations for Na CMC solution shear-thinning behaviour found in Na CMC literature include the breakage of hydrogen bonds between polymer chains by high-shear rates,[126] or the breakage of some polymer aggregates present in solution.[105]

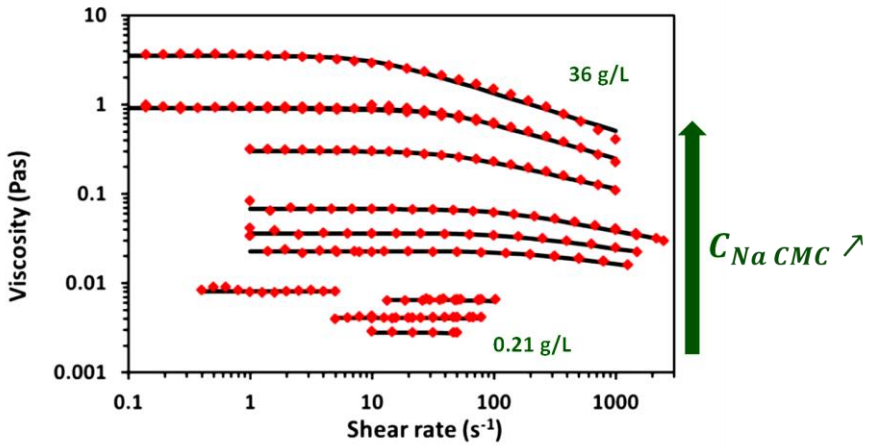

Figure 2-38: Flow curves of salt-free Na CMC solutions at different concentrations. Black lines represent fits to the Carreau model (Eq. 2-3). Na CMC characteristics (from the supplier): M_w = 250,000 g/mol; DS = 1.15-1.45; supplier: Sigma Aldrich. Adapted from Lopez *et al.*[1]

Another difference compared to the typical flow behaviour of polyelectrolytes described in Section 2-2.2 is the fact that the onset of the shear-thinning behaviour decreases with Na CMC concentration, while it has been shown that it usually increases with polyelectrolyte concentration.[50,56] This feature of Na CMC solutions[123,124,126,127] is common for polysaccharide solutions.[57] The onset of the shear-thinning behaviour is indeed not only related to the polyelectrolyte concentration but also to its M_w and M_w distribution.[57,87] When M_w increases, the onset of the shear-thinning behaviour is shifted towards lower values of shear-rates, while an increase in the M_w distribution leads to a broadening of the transition from the Newtonian to the shear-thinning behaviour as well as a decrease in the onset of the shear-thinning behaviour.[57,87] Polysaccharides, including Na CMC, are known to have a broad polydispersity (see Section 2-3.1);[57] which could explain the observed decrease in the onset of shear-thinning as Na CMC concentration is increased.

For high Na CMC concentrations and/or high M_w Na CMC samples, the Newtonian plateau is not always observed as typically investigated shear-rates/shear-stresses are above the shear-rate marking the onset of the shear-thinning behaviour.[57,125,128] This is illustrated in Figure 2-39. Although not commented by the authors,[128] it may be suggested that the end of the Newtonian plateau could be noticeable at low shear-rates for the 5% Na CMC solution.

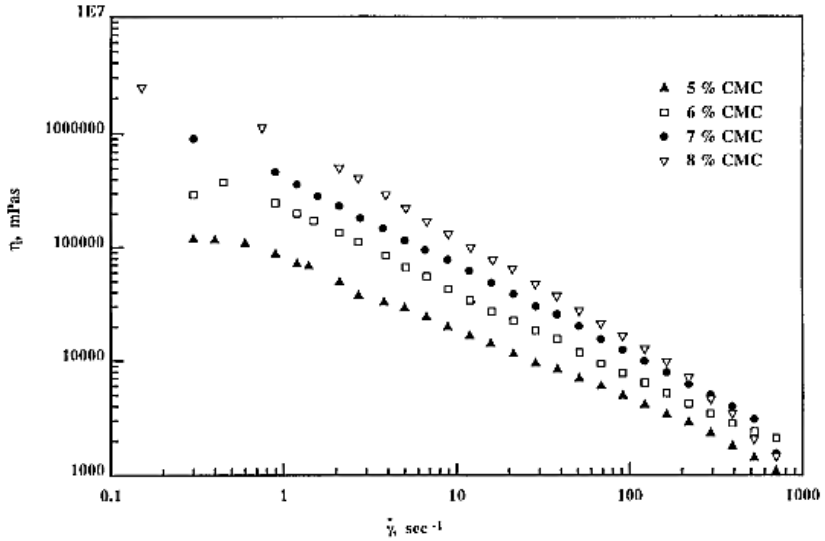

Figure 2-39: Flow curves of salt-free solutions at different Na CMC concentrations. Na CMC characteristics (from the supplier): Medium viscosity (reference: C4888); DS = 0.7; supplier: Sigma Chemical. From Edali *et al*,[128] Copyright © 2001 John Wiley & Sons, Inc. Reprinted by permission of John Wiley & Sons, Inc.

A couple of reported behaviours, though, stand out from the typical behaviour of Na CMC solutions discussed above. Benchabane and Bekkour[127] identified two different behaviours when Na CMC concentration increases: (i) a shear-thinning, Newtonian, shear-thinning behaviour at low Na CMC concentrations, and (ii) a shear-thickening, shear-thinning behaviour at high concentrations, as shown in Figure 2-40. They first identified the concentration at which the change in behaviour occurs (around 1% Na CMC) as the overlap concentration, which seems quite high compared to the other values reported in the literature (see next sub-section and Table 2-6). Their later analysis of this characteristic concentration as the transition between the semi-dilute non-entangled and entangled regimes seems more realistic. They interpret the shear-thickening behaviour of the most concentrated solutions with the building-up of a stiffer structure in the solution as new entanglements and molecular interactions would form at low shear-rates. They do however not provide any explanation about the behaviour observed for the less concentrated solutions.

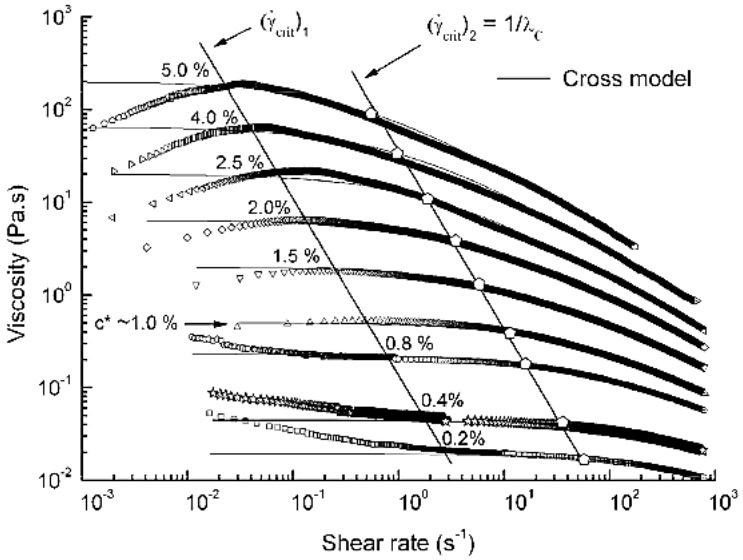

Figure 2-40: Flow curves of salt-free Na CMC solutions at different concentrations collected with a stress ramp. Na CMC characteristics (from the supplier): M_w = 700,000 g/mol; DS = 0.65-0.85; supplier: Sigma Aldrich. Reprinted by permission from Springer Nature, *Colloid and Polymer Science*, Benchabane and Bekkour,[127] Copyright © Springer-Verlag 2008.

It is worth noting, though, that the flow data were collected using a stress ramp rather than the usual sweep. Hence, if a steady-state flow was not achieved instantaneously upon increasing the stress, the presented data do not correspond to steady-state flow data as usually reported. For high M_w and/or concentrations, it has been observed that the viscosity increases over time under constant shear-rate or stress. An example is shown in Figure 2-41.A.

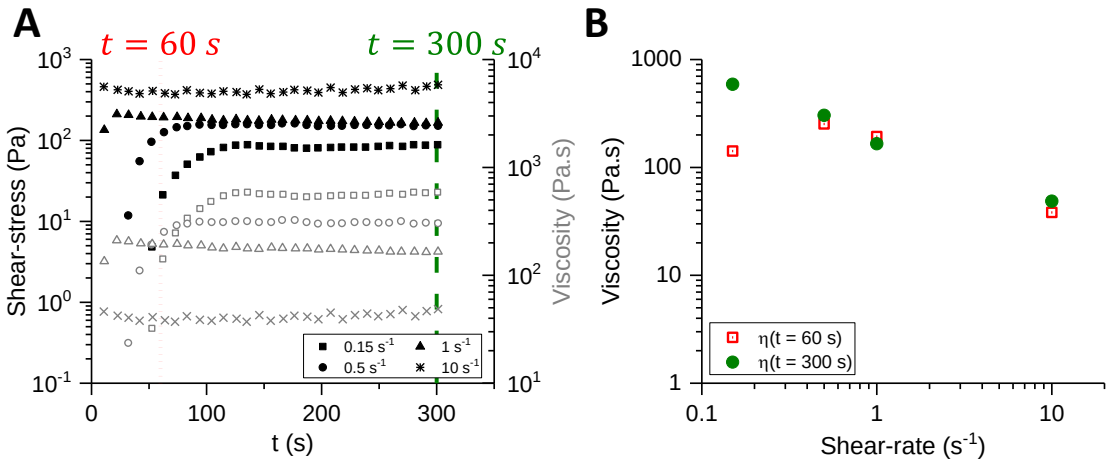

Figure 2-41: Illustration of the viscosity time-dependence of some salt-free Na CMC solutions. **A.** Time-evolution of the shear-stress collected under constant shear-rates. Data are from Edali *et al.*[128] The values of the viscosity were calculated by the present author as explained in the main text. **B.** Flow curves with the values of the viscosity after 60 s and 300 s shearing.

The viscosity η was calculated by the present author as $\eta = \sigma/\dot{\gamma}$ where σ is the shear-stress and $\dot{\gamma}$ the shear-rate. It can be seen from Figure 2-41.A that, at low shear-rates, the viscosity first increases over time, before it reaches a constant value when a steady-state flow has been established in the rheometer. When the shear-rate is increased, the time to achieve a steady-state decreases and becomes very close to 0. The values of the viscosity calculated at early times (*i.e.* 60 s) and after the steady-state flow has been achieved (*i.e.* 300 s) were plotted by the present author as a function of the shear-rate and are displayed in Figure 2-41.B. The flow curve of the steady-state values of the viscosity (*i.e.* $\eta(300\ s)$) exhibits the expected shear-thinning behaviour (see discussion above), while the flow curve of $\eta(60\ s)$ exhibits a shear-thickening behaviour at low shear-rates and a shear-thinning behaviour at high shear-rates, as reported by Benchabane and Bekkour[127] and seen in Figure 2-40. Thus, the hypothesis that the unusual behaviour observed by Benchabane and Bekkour[127] comes from the flow curves representing the instantaneous viscosity rather than the steady-state viscosity seems to be confirmed. This also explains why the overlap concentration c^* is higher than the usually reported values (see next sub-section and Table 2-6). c^* indeed needs to be determined from steady-state flow data.

The results reported by Balmaceda *et al.*[129] show an opposite behaviour to the ones of Benchabane and Bekkour[127] as the shear-thinning behaviour was observed at high Na CMC concentrations while the shear-thickening behaviour was observed at low Na CMC concentrations.

The models used in the literature to fit Na CMC solution flow curves are reported in Table 2-5. The equations of the models have been harmonised with the help of Lapasin and Pricl's book[57] to enable an easier comparison. The reader should therefore not be surprised if the notations and the way the equations are presented in the cited articles vary from the ones given in the Table. The list does not pretend to be exhaustive. In fact, the papers from Lopez and co-workers,[1,14,15] where Na CMC solution flow curves are fitted to the Carreau model as discussed for polyelectrolytes in Section 2-2.2 (Eq. 2-3) and illustrated in Figure 2-38 are not listed in the Table.

It is not very surprising that the use of the Newtonian model is limited as it has previously been shown that most of the Na CMC solutions are shear-thinning. Moreover, the Newtonian model is anyway included in all the models which establish a relationship

between the shear-stress σ and the shear-rate $\dot{\gamma}$. When the models $\sigma = f(\dot{\gamma})$ were compared with each other, the power law was often found to be the most appropriate as the parameter σ_y (yield stress) was very close to 0.

Table 2-5: Models used in the literature to fit Na CMC solution flow curves.

Model	Equation	Ref	Best fit	Selected model
Newtonian	$\sigma = \eta\dot{\gamma}$	105	Power law	Power law
Bingham or linear	$\sigma = \sigma_y + \eta_\infty\dot{\gamma}$	130	Power law (high *c*) Bingham (low *c*)	Power law
		131	Power law (high *c*) Bingham (low *c*)	Power law
		93	Power law	Power law
		105	Power law	Power law
Hershley-Bukley	$\sigma = \sigma_y + K\dot{\gamma}^{\,n}$	131	Power law (high *c*) Bingham (low *c*)	Power law
Casson	$\sigma^{1/2} = \sigma_y^{1/2} + \eta_\infty^{1/2}\dot{\gamma}^{\,1/2}$	131	Power law (high *c*) Bingham (low *c*)	Power law
		93	Power law	Power law
Ostwald de Waele or power law	$\sigma = K\dot{\gamma}^n$	131	Power law (high *c*) Bingham (low *c*)	Power law
		130	Power law (high *c*) Bingham (low *c*)	Power law
		127	Cross	Cross
		132	*n/a*	*n/a*
		124	*n/a*	*n/a*
		128	*n/a*	*n/a*
		125	*n/a*	*n/a*
		133	*n/a*	*n/a*
		92	*n/a*	*n/a*
		93	Power law	Power law
		134	*n/a*	*n/a*
		19	*n/a*	*n/a*
		135	*	*
		105	Power law	Power law
Cross	$\frac{\eta - \eta_\infty}{\eta_0 - \eta_\infty} = \frac{1}{1 + (\lambda\dot{\gamma})^{1-n}}$	127	Cross	Cross
	$\frac{\eta - \eta_\infty}{\eta_0 - \eta_\infty} = \frac{1}{K\dot{\gamma}^{1-n}}$ **	136	**	**
Cross with only 3 parameters	See article	136	**	**
Adapted Cross model	$\frac{\eta}{\eta_0} = \frac{1}{1 + (\lambda\dot{\gamma})^{1-n}}$	123	*n/a*	*n/a*
Carreau-Yasuda	$\frac{\eta - \eta_\infty}{\eta_0 - \eta_\infty} = \frac{1}{(1 + (\lambda\dot{\gamma})^a)^{(1-n)/a}}$	137	*n/a*	*n/a*
Adapted Carreau-Yasuda (cited as	$\frac{\eta}{\eta_0} = \frac{1}{(1 + (\lambda\dot{\gamma})^a)^{(1-n)/a}}$	30	*n/a*	*n/a*

« modified Carreau model »)				
Adapted Carreau (cited as « Carreau model »)	$\frac{\eta}{\eta_0} = \frac{1}{(1+(\lambda\dot{\gamma})^2)^{(1-n)/2}}$	1	*n/a*	*n/a*
		138	*n/a*	*n/a*
Equations derived from the relaxation theory of pseudoplastic fluids	$\sigma = \eta\dot{\gamma} + \frac{1}{b}\sinh^{-1}\frac{\dot{\gamma}}{A}$ $\sigma = \eta\dot{\gamma} + \frac{1}{b}\ln\left(\frac{1}{A_0}\dot{\gamma} + \sqrt{\gamma + e^{\dot{-2b\eta\dot{\gamma}}}}\right)$ $\sigma = \eta\dot{\gamma} + \frac{1}{b}\ln\left(\frac{2}{A_0}\dot{\gamma}\right)$	139	The two first equations fit well the data over the whole range of shear-rates while the third one does not work at low shear-rates.	The two first equations

*Although the authors seem to be satisfied with their fit, it is obvious that their experimental data are not well fitted by the power law. **The equation of the original Cross model is rather unusual. Moreover, although the Cross model with only 3 parameters seems more efficient than the original Cross model as it has one less parameter, the authors precise that their new model requires data over a wide range of shear stresses to be applied. η: viscosity; σ: shear-stress; $\dot{\gamma}$: shear-rate; n: power law exponent; '0' and '∞' subscripts refer to values extrapolated to zero and infinite shear-rates, respectively; Ref: reference.

In a few studies and at low Na CMC concentrations, the Bingham model was more appropriate than the power law,[130,131] which is rather unexpected as solutions at low Na CMC concentrations usually exhibit a Newtonian behaviour. It may be compared with the previously discussed unusual results of Benchabane and Bekkour.[127] Benchabane and Bekkour[127] indeed found a shear-thinning behaviour at low shear-rates, attributed to the fact that the data were collected when the steady-state flow condition was not realised. It means that the viscosity tends to infinity at low shear-rates which could come from the presence of a yield stress; which is unexpected for solutions at such low Na CMC concentrations. However, the authors anyway selected the power law to go further in their analysis as it is a very simple model with only two parameters: the consistency parameter K and the flow behaviour index n. Flow indexes of 1 correspond to a Newtonian behaviour while flow indexes below and above 1 correspond to shear-thinning and shear-thickening behaviours, respectively. It is usually found that the shear-thinning behaviour strengthens when the Na CMC concentration increases, characterised by the decrease in the flow behaviour index with Na CMC concentration.[124,125,128,133,140-142]

The other models are now discussed. Contrary to the power law, they enable the fitting of the Newtonian plateau observed prior to the shear-thinning behaviour with the parameter η_0 (zero-shear viscosity). The shear-rate at which the shear-thinning behaviour starts corresponds to the inverse of the parameter λ (also noted τ and called relaxation time).[1,30] In most cases, the Newtonian plateau at high shear-rates described by the

viscosity at infinite shear-rate η_∞ in the models is not reached at the highest shear-rates used in the experiments. As η_∞ would be very low compared to η_0, it is neglected and leads to the adapted models.[138] In a similar way as for the power law, a flow behaviour index can be defined. The way the equations are presented here leads to the same interpretation of the values of *n* about the shear-thinning behaviour of the solutions as for the flow behaviour index *n* obtained using the power law model. The differences in the power index used in the different models enable to fit diverse shapes of decays in viscosity. Kulicke *et al.*[30] underlines that the coefficient *a* of the Carreau-Yasuda model enables to fit the transition between the Newtonian and the shear-thinning regimes in an appropriate way.

The models are often validated by looking at the value of the squared regression coefficient. However, this coefficient is not always a good indicator of the reliability of the model used to fit the data and it is worth looking at plots showing both experimental data and their fit(s) to the selected model(s) to double-check the reliability of the model. Hence, it is obvious from the graph shown by Yaseen *et al.*[135] (Figure 9 of Yaseen *et al.*'s paper[135]) that the power law model is not well suited. One can also guess from Figure 2-39 that the power law may not be the most appropriate model at the lowest studied concentrations as the flow curves exhibit a Newtonian behaviour at low shear-rates. The authors however unfortunately neither plotted the fitting curves nor provided the squared regression coefficients.

To conclude this Section, Na CMC solution overall flow behaviour is similar to the one reported for polyelectrolyte solutions: at low concentrations, Na CMC solutions exhibit a Newtonian behaviour while they exhibit a shear-thinning behaviour at high concentrations. Contrary to typical polyelectrolyte behaviour, though, the shear-rate characteristic for the onset of the shear-thinning behaviour decreases upon increasing Na CMC concentration. This behaviour, common for polysaccharides, may come from the typically large polydispersity of Na CMC samples.

Concentration-dependence of the zero-shear viscosity

As discussed for polyelectrolytes in Section 2-2.2, the zero-shear viscosity corresponding to the Newtonian plateau of the flow curves can be used to calculate the specific viscosity η_{sp} and plotted as a function of the polyelectrolyte concentration. Such a graph obtained for three Na CMC samples is shown in Figure 2-42. The investigated concentration range

does not cover the dilute regime. The three other regimes typically reported for polyelectrolytes (*i.e.* semi-dilute non-entangled, semi-dilute entangled and concentrated) can be observed. The exponents of the best power law fits to the data as well as the crossover concentrations are shown in Table 2-6, together with the data reported from other studies about salt-free Na CMC solutions. The exponent value obtained for the semi-dilute non-entangled regime is usually around 0.7 instead of the value of 0.5 predicted by the polyelectrolyte scaling laws. Lopez and co-workers[1,15] suggested that this deviation from the predicted behaviour could come from the semi-flexible nature of Na CMC and/or its polydispersity.

The values of the crossover concentrations found using either the exponent values from the scaling laws or from the best fits to the data are usually very close to one another, apart for the overlap concentration c^* for high M_w Na CMC samples. The value of the overlap concentration found by Truzzolillo *et al.*[143] for their 700,000 g/mol Na CMC sample seems anomalously high, especially compared to the values found by Lopez and co-workers.[1,14,15] This could be due to the presence of residual salt in the Na CMC sample, and in the resulting Na CMC solutions, as further explained in Section 2-3.3.4 about the influence of impurities on Na CMC solution behaviour.

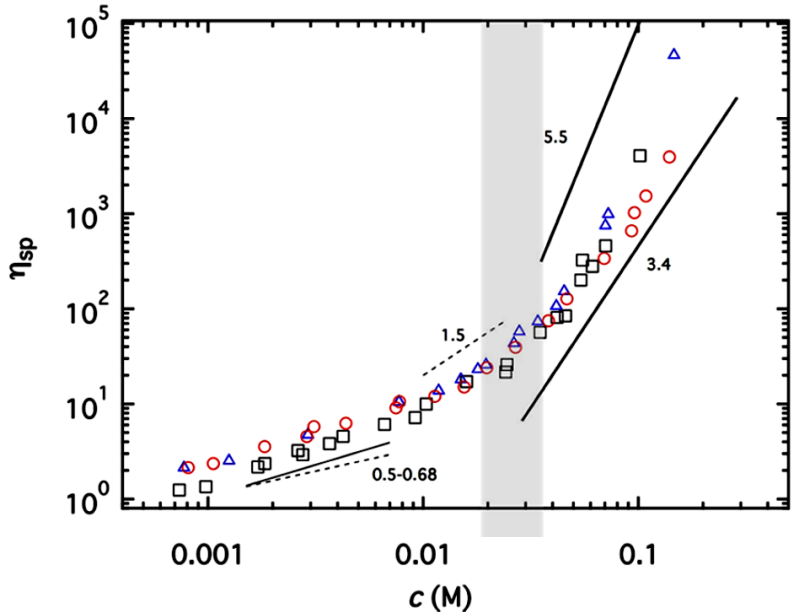

Figure 2-42: Salt-free Na CMC solution concentration-dependence of the specific viscosity η_{sp} for three different Na CMC samples. The characteristics of the Na CMC samples are given in the 2nd (black squares), 3rd (blue triangles) and 4th (red circles) columns of Table 2-6. Dashed and full lines represent the theoretical and best power law fits, respectively. Exponent values are provided next to each line. From Lopez *et al.*[14]

Lopez *et al.*[15] investigated the applicability of the polyelectrolyte scaling laws to Na CMC. For this purpose, they not only studied the power law relationships between the solution specific viscosity and Na CMC concentration, but also compared the power law dependences of the crossover concentrations and the specific viscosity on Na CMC polymerisation degree to the ones predicted by the scaling laws. They found that c^{**} did not follow the behaviour predicted by the scaling laws.[15] Interestingly, the concentration-dependence of the correlation peak observed in the SANS profile (see Section 2-3.2.1 and Figure 2-37) did not follow the expected concentration dependence above c^{**}. Moreover, a study of quaternized poly(vinyl pyridine) carried out by Dou and Colby[50] showed that the concentration dependence of the terminal modulus above c^{**} did not follow the predictions from the scaling laws either. Lopez *et al.*[15] thus concluded that the current description of such polyelectrolyte systems based on the electrostatic blobs and the correlation length is not sufficient to describe them in that concentration range. It is worth reminding here that the polyelectrolyte scaling laws do not predict the presence of the slow relaxation mode observed in DLS above c^* (see Section 2-2.3) and attributed to the presence of some polyelectrolyte chain clusters. Hence, the fact that the electrostatic blobs and the correlation length are not sufficient to describe the polyelectrolyte solutions at concentrations where the unpredicted slow relaxation mode exists may not be that surprising.

Table 2-6: Values of the crossover concentrations and the power law exponents obtained from the polyelectrolyte scaling laws applied to salt-free Na CMC solutions.

Ref	15	14	14	1,14,15	15	118	143	143
M_w (g/mol)	90,000 (70,000)	250,000 (210,000)	250,000 (310,000)	250,000 (320,000)	700,000 (1,200,000)	Blanose 13M31P	90,000	700,000
DS	0.7	0.65-0.9	0.8-0.95	1.15-1.35	0.8-0.95	1.23	0.7	0.8-0.95
Supplier	Sigma	Sigma	Sigma	Sigma	Sigma	Aqualon Hercules	Sigma	Sigma
c_{SL}* (g/L)	*0.73*	0.059	0.036	0.031	*0.00069*		0.6	0.15
c_{BF}* (g/L)	*0.92*			0.07	*0.0061*			
v(SD NE)	0.65	0.68 ± 0.05	0.68 ± 0.05	0.68 ± 0.02	0.74	0.54		
$c_{e,SL}$ (g/L)	*4.0*	1.5	1.7	2.9	*0.95*		5.5	2
$c_{e,BF}$ (g/L)	*4.5*			4	*1.1*			
v(SD E)	1.5	1.5	1.5	1.7 ± 0.2	1.5	1.55		
c_{SL}** (g/L)	*21*	9.8	8.8	14.4	*4.4*		40	15
c_{BF}** (g/L)	*18*			14.3	*3.9*			
v(conc)	3.4	5.5	5.5	3.4 ± 0.3	3.4			

Ref: reference; SD NE: semi-dilute non-entangled; SD E: semi-dilute entangled; conc: concentrated; *v*: exponent of the power law $\eta_{sp} \sim c_{Na\ CMC}{}^{v}$. Subscripts SL and BF refer to crossover concentrations obtained using the power law fits with the Scaling Law exponents (SL) and the Best Fit (BF) exponents, respectively. Crossover concentrations in italic were calculated by the present author from the data provided in the corresponding papers. The values predicted by the scaling laws are: 1, 0.5, 1.5 and 3.75 for the dilute, SD NE, SD E and concentrated regimes, respectively. Values of M_w into brackets are the ones measured by the authors while the other values are the ones provided by the manufacturers. For the data collected by Lopez and co-workers, c^* was obtained by extrapolating the power law describing the SD NE regime to $\eta_{sp}(c^*) = 1$.

After establishing that c^{**} does not follow the predictions of the scaling laws, Lopez *et al.*[15] successfully fitted their $\eta_{sp} = f(c_{Na\ CMC})$ data using Eq. 2-24 which contains only one characteristic concentration within the fitting regime, chosen as the previously determined entanglement concentration c_e. Eq. 2-24[15] is a simple parameterisation of the η_{sp} *vs* $c_{Na\ CMC}$ data above c^*, which uses a single characteristic concentration c_e outside the dilute regime and includes two parameters γ and q to describe the power law exponents

in the non-entangled and entangled regimes. To account for variations in the shape of η_{sp} *vs* $c_{Na\ CMC}$ as the behaviour changes from the low to the high concentration power law behaviour, a last parameter Q is added.

$$\eta_{sp} = \eta_{sp}(c^*) \cdot (c_{Na\ CMC}/c^*)^{\gamma} \cdot (1 + Q(c_{Na\ CMC}/c_e)^q) \quad (2\text{-}24)$$

Kästner *et al.*[81] have reported the presence of another concentration regime that they refer to as 'gel'. Such 'gels' are only observed for high M_w Na CMC samples (*i.e.* above 70,000 g/mol), as lower M_w Na CMC samples become insoluble before Na CMC concentration is high enough to reach this state.[81] It is worth noting that though Kästner *et al.*[81] refer to this state as a 'gel' because of the solid-like macroscopic behaviour of the Na CMC formulations, these formulations could simply be networks of entangled polymer chains which are dense enough to trap and immobilise the water molecules. Indeed, Na^+ ions cannot act as cross-linkers to form physical gels as multivalent ions would be able to, and there has not been any chemical crosslinking to form chemical gels.[57] Another hypothesis to explain the formation of these gel-like structures would be the presence of inter-chain hydrogen bonds as reported when Na CMC films are prepared.[91,144]

2-3.3. Influence of Na CMC characteristics on its behaviour in solution

Now that the behaviour of Na CMC in salt-free solutions has been reported from a general perspective, the influence of Na CMC characteristics defined in Section 2-3.1 on the behaviour of Na CMC solutions is reviewed. Here too, the focus is on scattering and rheological investigations.

2-3.3.1. Molecular weight M_w and M_w distribution

Brown *et al.*[120] used SLS to study the influence of Na CMC molecular weight on the radius of gyration of the chains in the dilute regime in presence of various amounts of NaCl. As illustrated in Figure 2-43 and expected (see Sections 2-2.1 and 2-2.3.3), the radius of gyration increases with Na CMC molecular weight. The influence of the amount of added salt is discussed in Section 2-3.4.1.

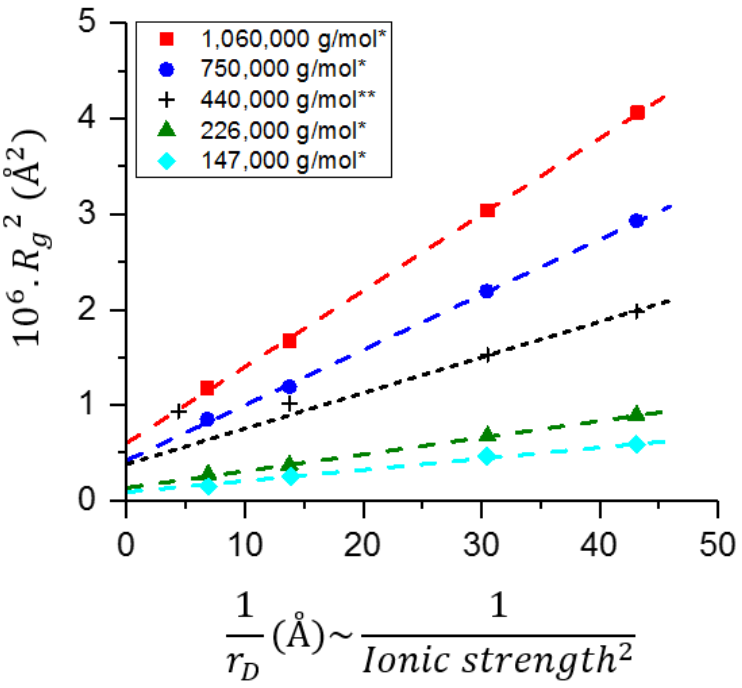

Figure 2-43: Squared end-to-end distance R_g^2 of Na CMC chains as a function of the reciprocal of the Debye screening length r_D (see Eq. 2-2) for Na CMC samples of various M_w (indicated in the legend). Data reported by Brown *et al.*[120], and Schneider and Doty[121] are highlighted with * and **, respectively. Investigated NaCl concentrations are 0.005, 0.01, 0.05 and 0.2 M NaCl. Replotted and adapted from Brown *et al.*[120]

Figure 2-44 illustrates the influence of Na CMC M_w and concentration on both the zero-shear viscosity and the viscosity measured at a shear-rate of 5 s^{-1}. An increase in Na CMC M_w generally leads to an increase in the viscosity of the solution.[30,81,87,94,137,143,145] A strengthening of the shear-thinning behaviour with the molecular weight was also observed by a couple of authors.[123,141] The fact that the difference between the zero-shear viscosity and the viscosity at 5 s^{-1} increases with M_w in Figure 2-44 can be a consequence of this strengthening of the shear-thinning behaviour and/or the smaller shear-rate at which the shear-thinning behaviour is expected to start for higher M_w Na CMC samples.[57,87] The crossover concentrations between the different concentration regimes (see Table 2-6) are shifted towards lower values as the molecular weight increases.[81,143]

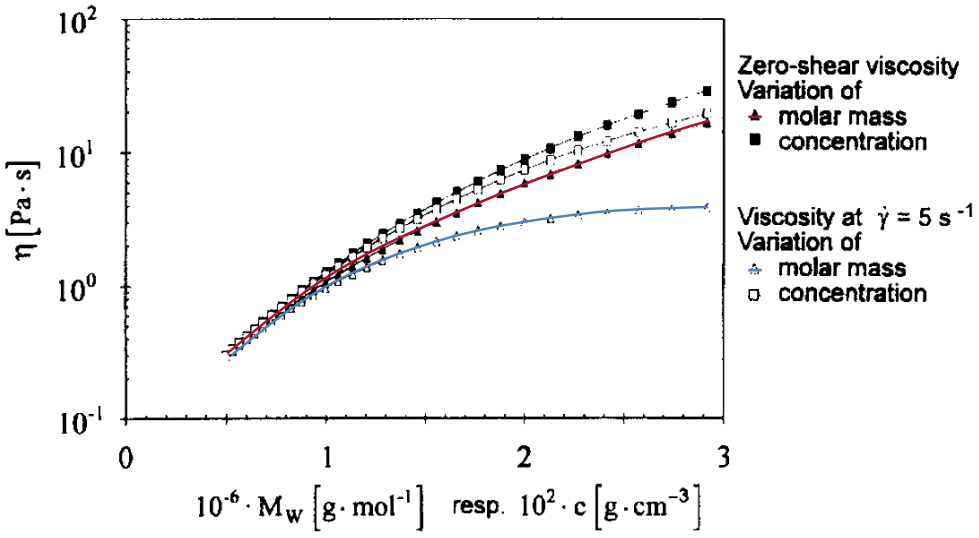

Figure 2-44: Solution viscosity as a function of Na CMC molecular weight. Coloured curves indeed represent the solution viscosity as a function of Na CMC molecular weight. The curve starts at $M_w = 0.5 \times 10^6$ g/mol. The two other curves correspond to the solution viscosity as a function of Na CMC concentration. Temperature: 25°C. Adapted from Kulicke *et al*,[30] Copyright © 1996 Elsevier Ltd, with permission from Elsevier.

As reported at the end of Section 2-3.2.2, Kästner *et al.*[81] found that their low M_w Na CMC samples became insoluble beyond a critical concentration, while their higher M_w Na CMC samples could form gel-like structures at high concentrations. Furthermore, as mentioned in Section 2-3.2.2, a broadening in the M_w distribution (characterised by an increase in the polydispersity index M_w/M_n) leads to a broadening of the shear-rate region where the solution behaviour transitions from the Newtonian to the shear-thinning behaviour.[57,87]

2-3.3.2. Substitution

As shortly mentioned in Section 2-3.1, the DS strongly influences Na CMC solubility in water as the carboxymethyl groups are responsible for Na CMC solubility in water. Non-substituted (*i.e.* cellulose) or poorly-substituted Na CMC fibres are therefore not at all or only partially solubilised. A decrease in the DS is thus often linked with an increase in the amount of undissolved particles.[28,82,124] Several authors have observed these 'objects' with optical microscopes and have shown that they were Na CMC fibres at different swelling stages as described by Stawitz and Kage in 1959,[29,83] whose schematics are displayed in Figure 2-45.A. Höppler[113] already reported the presence of such 'objects' in Na CMC solutions in 1942 as seen in Figure 2-45.B. Other more recent examples of micrographs showing different swelling stages found in a Na CMC solution are displayed in Figure 2-45.C.

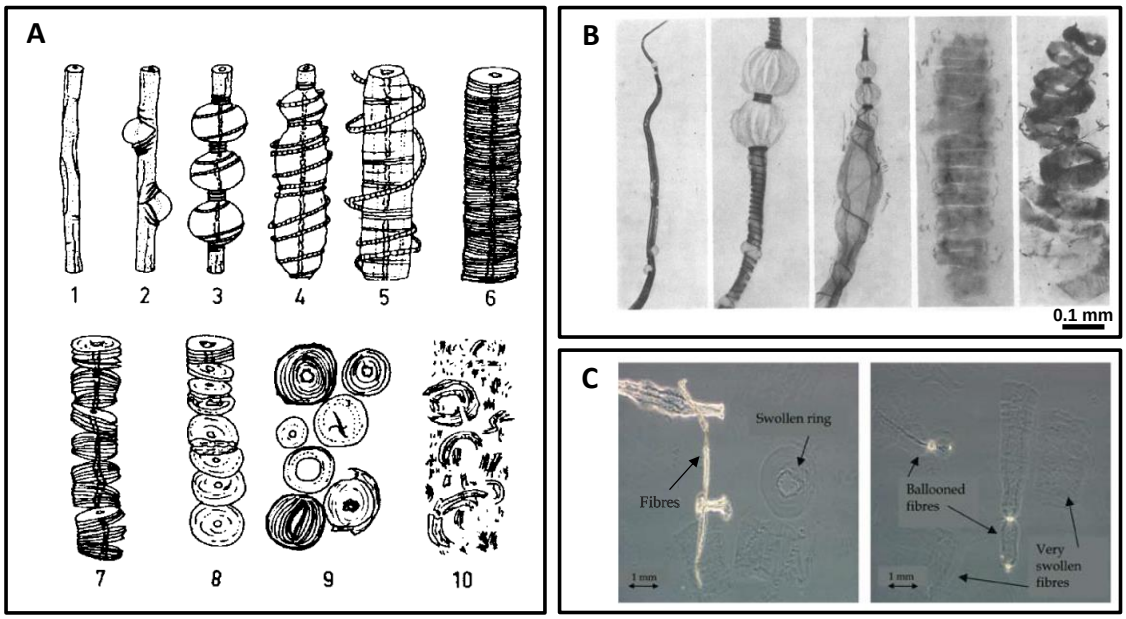

Figure 2-45: Different swelling stages of Na CMC. **A.** Swelling stages described by Stawitz and Kage.[29] Reprinted by permission from Springer Nature, *Cellulose*, Jardeby *et al*,[29] Copyright © Springer 2005. **B.** Micrographs of different swelling stages. From the left to the right: more advanced swollen stages. Reprinted by permission from Springer Nature, *Kolloid-Zeitschrift*, Höppler,[113] Copyright © Verlag von Theodor Steinkopff 1942. **C.** Micrographs of different swelling stages present in a Na CMC solution (obtained with a microscope equipped with phase contrast). Reprinted by permission from Springer Nature, *Cellulose*, Jardeby *et al*,[83] Copyright © Springer 2005.

The first swelling stage corresponds to non-swollen Na CMC fibres. Na CMC fibres are then ballooned (ballooned fibres are defined as 'fibres with an unrolled primary wall and a swollen secondary wall'[29]). At more advanced swelling stages, swollen rings can be seen. According to Stawitz and Kage, these swollen rings would be residuals from the cell walls separated into discs.[29] Jardeby *et al.*[29] rather think that they would come from the ballooned fibres. Then, the fibres become very swollen (see Figure 2-45.C). When fully dissolved (*i.e.* molecularly dispersed), they can no longer be seen by optical microscopy. Fully soluble Na CMC fibres undergo all these stages when put into water, while non-fully soluble fibres (*i.e.* whose DS is too low) are not able to go up to the final stage and remain at some intermediate swelling stage in solution. Jardeby *et al.*[29] gave some rough correspondences between DS values and swelling stages, provided in Figure 2-46.

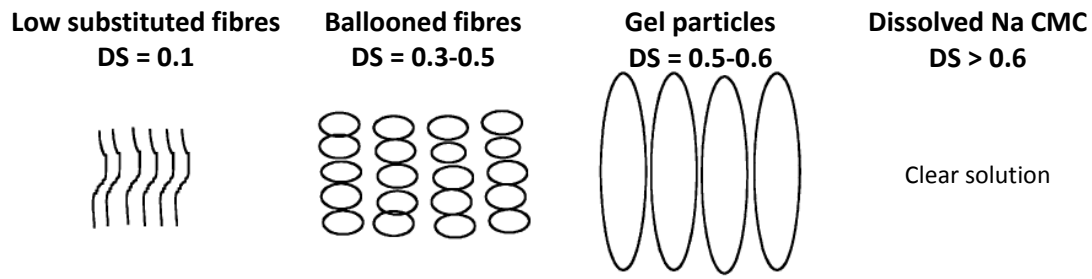

Figure 2-46: Correspondences between the swelling stage of Na CMC fibres and their DS. Adapted by permission from Springer Nature, *Cellulose*, Jardeby *et al*,[29] Copyright © Springer 2005.

It is worth noting that the substitution pattern also influences the dissolution of Na CMC fibres. Indeed, low substituted Na CMC samples which are homogeneously substituted are able to undergo advanced swelling stages as they do not contain long non-substituted segments responsible for poor Na CMC solubility.[1] This explains why the DS value corresponding to the lower solubility boundary varies from one article to another.[26,28,29] Non-fully dissolved fibres can still be found in solutions prepared from Na CMC samples whose DS is as high as 0.95.[28,91] As the substitution becomes more random for DS above 1,[1] such Na CMC samples are expected to be fully soluble. Lopez *et al.*[1] showed with SANS measurements that their DS 1.2 Na CMC sample was fully soluble in water.

It can be expected from the above discussion that solutions containing non-swollen Na CMC fibres, swollen Na CMC fibres or molecularly dispersed Na CMC behave differently. It is indeed generally observed that an increase in the DS first leads to an increase in the solution viscosity,[18,30,112] as seen in Figure 2-47, where the DS-dependence of Na CMC solution viscosity is shown. From DS values around 0.9-1, a further increase in the DS leads to a decrease in the solution viscosity.[30]

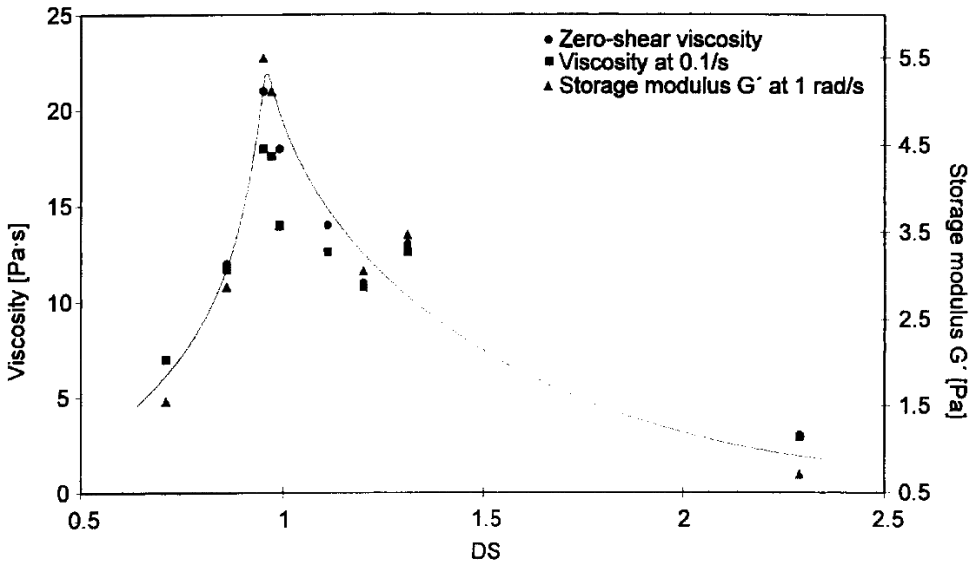

Figure 2-47: Viscosity as a function of DS. The graph also displays the storage modulus at a frequency of 1.0 rad/s as a function of the DS. Characteristics of Na CMC samples: M_w varies from 1,170,000 g/mol to 1,740,000 g/mol. Reprinted from Kulicke *et al*,[30] Copyright © 1996 Elsevier Ltd, with permission from Elsevier.

The evolution of the solution viscosity with the DS can be explained by Na CMC dissolution stages. As the DS increases, Na CMC becomes more and more swollen. The viscosity of the solution, initially driven by insoluble Na CMC particles is then driven by microgel-like particles and the solution viscosity increases.[30,41] The demonstration based on model equations can be found in Francis' article.[41] The decrease in solution viscosity observed at high DS is more complex to explain. It should first be noted that the molecular weight of these samples decreases with DS; which, itself, could explain the decrease in the solution viscosity (see Section 2-3.3.1 about the influence of M_w on Na CMC solution behaviour). Kulicke *et al.*[30] suggested it could also be due to the formation of aggregates. A study involving both flow field flow fractionation and birefringence measurements published a couple of years later seems to support this second hypothesis.[146]

The substitution pattern influences the viscosity of the solution. Enebro *et al.*[88] and Heinze *et al.*[94] showed that solutions made with more heterogeneously substituted Na CMC samples exhibit a higher viscosity than solutions made with more homogeneously substituted Na CMC samples. It is worth noting that low substituted regions or chains are more likely to be crystalline.[27,112,147-149] The influence of crystallinity on Na CMC behaviour in solution is reviewed in Section 2-3.3.3.

As mentioned in Section 2-3.2.1, Lopez *et al.*[14] investigated three Na CMC samples of similar M_w but different DSs using SANS. The SANS profiles in Figure 2-36 show that

the low *q*-upturn depends on DS. For all studied solutions, it can be described by a power law. The power law exponent value is maximum (*i.e.* 3.6) for DS = 1.2, where it is also independent of Na CMC concentration. For DS = 0.7 and DS = 0.8, the power law exponent absolute value is 3.4 at low Na CMC concentrations, similarly to the higher DS sample, and decreases to 1 at high Na CMC concentrations. Lopez *et al.*[14] suggested that the low *q*-upturn could be related to the domains typically reported for DLS measurements on polyelectrolyte solutions (see Section 2-2.3.2). They also suggested that Na CMC solutions whose *q*-upturn is described by a power law exponent of 1 could contain fringed micelle aggregates, which have been reported for other cellulose derivatives. Fringed micelles can be described as a body of aggregated parallel chains with dangling ends.[14] From the Na CMC concentration dependence of q^* shown in Figure 2-37, Lopez *et al.*[14] found that Na CMC chains are more extended when DS = 1.2 than when DS = 0.7 or 0.8. This is consistent with the fact that the chains are expected to be more stretched when their charge density is higher (see Sections 2-2.1 and 2-2.2).[14]

2-3.3.3. Crystallinity

As mentioned at the end of Section 2-3.1, DS and crystallinity are usually correlated; Na CMC samples of low DS also having a higher crystallinity degree.[112] More undissolved matters are typically found in solutions made from Na CMC of higher crystallinity degrees,[104,111,124] though the absence of undissolved fragments in solutions made from crystalline Na CMC was reported by Dürig and Banderet.[111] Na CMC solutions prepared with more crystalline Na CMC samples usually have a higher viscosity.[111,124,147] This higher viscosity is often explained by the fact that crystalline Na CMC could associate in solution *via* hydrogen bonds, thus forming some structure.[111,112] DeButts *et al.*[147] also suggested an association of the crystalline parts in solution but *via* electrostatic or Van der Waals interactions. They observed that the viscosity of the solutions decreased upon shear and that the solution viscosity recovered after a resting period. They thus suggested that shear could break these associations, leading to the observed decrease in the viscosity, and that these associations would reform at rest.

2-3.3.4. Presence of impurities

The influence of the presence of residual salts in Na CMC solutions, such as NaCl from Na CMC synthesis (see Section 2-3.1), has been extensively discussed by Lopez *et al.*[15]

Similarly to Boris and Colby's[60] study of sodium poly(styrene sulfonate), they have shown that the presence of residual salts in Na CMC solutions can lead to an anomalously high value of the power law exponent characteristic for the concentration-dependence of η_{sp} in the semi-dilute non-entangled regime. Indeed, instead of the predicted value of 0.5 for polyelectrolytes (~ 0.7 for Na CMC[1,14,15]; see Section 2-3.2.2), values of the power law exponent close to 1, as predicted for the dilute concentration regime, are found. This may explain why the overlap concentration c^* determined by Truzzolillo *et al.*[143] for their 700,000 g/mol Na CMC sample is significantly higher than the one found by Lopez *et al.*[15] for a similar sample. As a rule of thumb, Lopez *et al.*[15] proposed that Na CMC solutions characterised by a power law exponent of 0.68 ± 0.02 in the semi-dilute non-entangled regime could be considered as salt-free. The behaviour in presence of higher salt concentrations is detailed in Section 2-3.4.1.

2-3.3.5. Simultaneous variation of M_w and substitution

Kästner *et al.*[81] showed that the viscosity of the solution is determined by the molecular weight when both M_w and DS are varied together. However, it is worth paying attention to the DS as the behaviour of Na CMC samples with different DS values and/or substitution patterns can differ from one another as discussed in Section 2-3.3.2.

In this Section, it has been shown that the variability that often exists within Na CMC samples makes the investigation of Na CMC behaviour in solution difficult. Indeed, the variability in terms of substitution and crystallinity may lead to the presence of non- or poorly dissolved fragments, making the solution heterogeneous, and would lead to additional difficulties when performing light scattering measurements. The presence of salt impurities from Na CMC synthesis can also significantly modify the behaviour of Na CMC in solution.

2-3.4. Influence of some external factors on Na CMC solution behaviour

After having reviewed the influence of Na CMC sample intrinsic characteristic on its behaviour in solution, the influence of two external factors which are key for this thesis is investigated: salt addition and sonication.

2-3.4.1. Salt addition

NaCl is the salt whose influence on Na CMC solutions has been studied the most. It is thus used here to explain the most common mechanisms occurring when salts are added into Na CMC solutions. The behaviour of other salts is then compared to the one of NaCl.

Figure 2-48 shows the influence of Na CMC and NaCl concentrations on Na CMC solution flow behaviour. When NaCl is added to solutions of low Na CMC concentration, the viscosity of the solutions decreases.[19,30,41,87,119,126,150] This is commonly explained by the fact that the Na^+ ions brought by NaCl screen the negative charges of the COO^- groups on Na CMC chains. As the number of charges on Na CMC chains decreases, they become more coiled. As coiled chains show less resistance to flow than extended chains (*i.e.* polymer chains in absence of NaCl), the viscosity of the solution decreases. Thus, as NaCl concentration increases, the behaviour of the solution becomes closer to the one of neutral polymer chains.[81,151,152] As seen from Figure 2-48, at high Na CMC concentrations, the addition of NaCl to the solution does not modify its flow behaviour. Indeed, at such high Na CMC concentrations, electrostatic interactions are expected to be screened (see Sections 2-2.1 and 2-2.2) so that salt-free Na CMC solutions behave like solutions of neutral polymers.

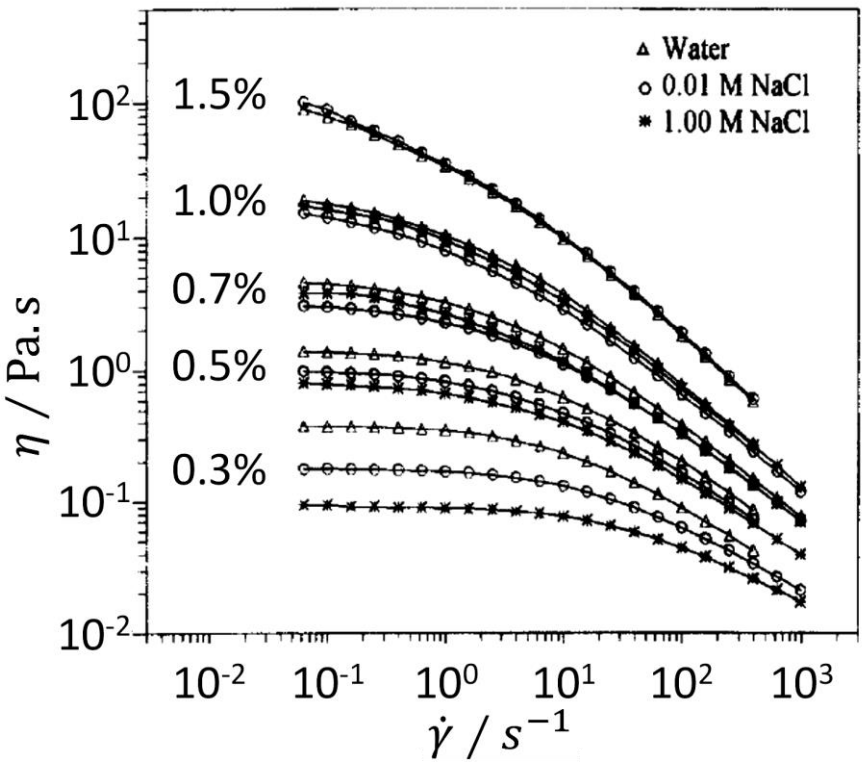

Figure 2-48: Influence of Na CMC and NaCl concentrations on Na CMC solution flow curves. The investigated Na CMC sample has a molecular weight of 2.09 × 106 g/mol and a DS of 0.99. Reprinted from Kulicke *et al*,[30] Copyright © 1996 Elsevier Ltd, with permission from Elsevier.

The influence of salt addition on $\eta_{sp} = f(c_{Na\ CMC})$ data is shown in Figure 2-49. As previously seen with the flow curves, at high Na CMC concentrations, salt addition has no effect on the observed rheological behaviour, where Na CMC solutions with and without added salt behave like neutral polymer solutions. At low Na CMC concentrations, Na CMC solution viscosity decreases upon NaCl addition. Above a critical NaCl concentration, all charges along Na CMC chains are screened and the Na CMC solutions behave like neutral polymer solutions. Hence, in Figure 2-49, a power law exponent of 1.3, characteristic for neutral polymer solutions in the semi-dilute non-entangled regime, is found for the semi-dilute non-entangled regime when NaCl concentration is above 0.05 M.

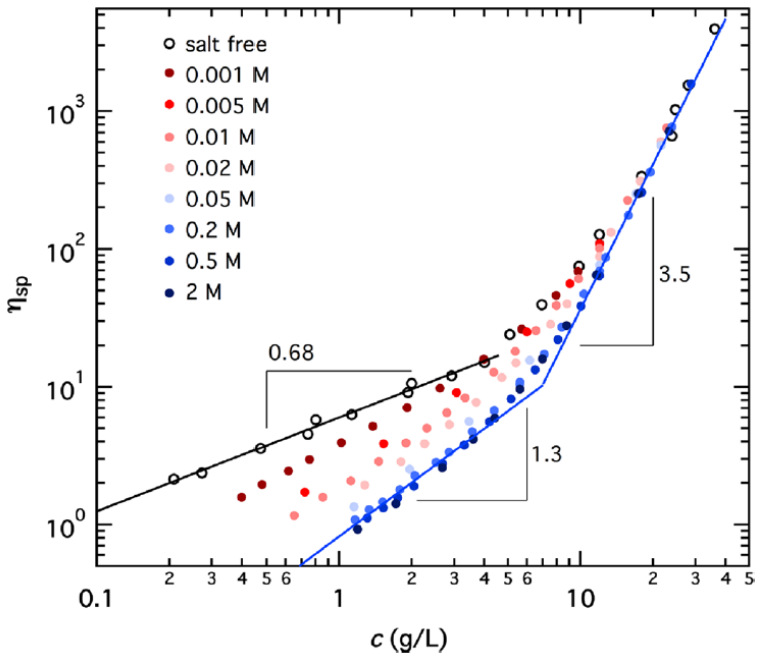

Figure 2-49: Na CMC and NaCl concentration dependence of the specific viscosity η_{sp}. Na CMC characteristics (from the supplier): M_w = 250,000 g/mol; DS = 1.15-1.45; supplier: Sigma Aldrich. Reprinted with permission from Lopez *et al*,[15] Copyright © 2017 American Chemical Society.

A couple of articles[107,119,153] mention that Na CMC becomes less soluble at high NaCl concentrations. Brown and Henley[119] thus observed flocculation in their solutions when NaCl concentration was above 0.2 M, while Hoogendam *et al.*[107] observed more 'scaly particles' upon increasing NaCl concentration, and Pals and Hermans[153] obtained more turbid solutions at high NaCl concentrations.

When other monovalent salts are added, the behaviour of Na CMC solutions is identical to the one observed in presence of the same concentration of NaCl.[41,149-151] Studied monovalent salts include LiCl, KCl and CsCl.

For multivalent salts, the outcomes are salt-dependent. They are summarised in Table 2-7. For the salts found in several articles, the outcomes are even source-dependent. This could either come from the fact that the studies were performed over different salt concentrations and/or at different Na CMC concentrations, or from the differences in the studied Na CMC samples. For example, Heinze *et al.*[94] have shown that heterogeneously substituted Na CMC samples were much less influenced by the addition of salts than homogeneously substituted ones of similar DS. Indeed, such samples would contain more non-substituted monomer glucose units, which cannot interact with ions as they are not charged.

Table 2-7: Influence of the addition of multivalent salts on Na CMC solutions.

Ion	Salt	Studied parameter(s)	Main outcome(s)	Comment(s) from the cited article/ *from the present authors*	Ref
CATIONS					
Al^{3+}	?	*Flow curve vs* c_{salt}	$c_{salt} \nearrow \Longrightarrow \eta \nearrow$ Gelation at high c_{salt}	*Data not shown.* See Fe^{3+} from the same reference for detailed explanations.	147
	$Al_2(SO_4)_3$	$\eta = f(c_{salt})$	$c_{salt} \nearrow \Longrightarrow \eta \nearrow$		41
		$\eta_{rel} = f(Al^{3+}/COO^-)$	$c_{salt} \nearrow \Longrightarrow \eta_{rel} \searrow$ Gelation at high c_{salt}	↘ in η: would be due to the shielding of COO^- groups by Al^{3+} ions. The chains would then be less extended. The ↘ in η is stronger than for Ca^{2+} ions as the charge is higher for the same anion/cation ratio. Gelation: cross-linking of Na CMC chains by Ca^{2+} ions.	94
		$\eta = f(c_{salt})$	$c_{salt} \nearrow \Longrightarrow \eta \nearrow$	The aluminium salt would be successively hydrolysed and polymerised. The OH groups of the resulting polymer chains would then bind Na CMC chains through H bonds. See paper for further details.	126
Ba^{2+}	$BaCl_2$	$\eta = f(c_{salt})$	$c_{salt} \nearrow \Longrightarrow \eta \searrow$	The ↘ in η is much stronger than for NaCl, even if the comparison is made at identical ionic strengths.	41
Ca^{2+}	$CaCl_2$	$\eta = f(c_{salt})$	$c_{salt} \nearrow \Longrightarrow \eta \searrow \nearrow \searrow$	1st ↘ in η: Ca^{2+} ions screen the charges. Repulsive interactions are reduced, molecules shrink and $\eta \searrow$. ↗ in η: polymer coils would extend as there would be repulsive interactions between the excess of positive charges outside the polymer coils. It could also be due to the formation of superstructures *via* bridging Ca^{2+} ions. 2nd ↘ in η: due to phase separation (flocculation occurs). Depending on the conditions, it can be reversible (*i.e.* precipitates can be dissolved again by adding some water) or irreversible.	87
			$c_{salt} \nearrow \Longrightarrow \eta \searrow$	The ↘ in η is much stronger than for NaCl, even if the comparison is made at identical ionic strengths.	41
		$\eta_{rel} = f(Ca^{2+}/COO^-)$	$c_{salt} \nearrow \Longrightarrow \eta_{rel} \searrow$ Gelation	↘ in η: would be due to the shielding of COO^- groups by Ca^{2+} ions. The chains would then be less extended. The ↘ in η is less strong than for Al^{3+} ions as the	94

			at high c_{salt}	charge is lower for the same anion/cation ratio. Gelation: cross-linking of Na CMC chains by Ca^{2+} ions.	
Co^{2+}	$Co(NO_3)_2$	$\eta = f(c_{salt})$	$c_{salt} \nearrow \Longrightarrow \eta \searrow$	The ↘ in η is much stronger than for NaCl, even if the comparison is made at identical ionic strengths.	41
Cu^{2+}	?	*Flow curve vs* Cu^{2+}/COO^-	$c_{salt} \nearrow \Longrightarrow \eta \nearrow$ Gelation at high C_{salt}	*Data not shown.* See Fe^{3+} from the same reference for detailed explanations.	147
	$CuCl_2$	$\eta = f(c_{salt})$	$c_{salt} \nearrow \Longrightarrow \eta \searrow$ Gelation at high c_{salt}	↘ in η: as COO^- groups electrostatically shielded, Na CMC chains adopt a less expanded conformation.	126
Fe^{3+}	?	*Flow curve vs* Fe^{3+}/COO^-	$c_{salt} \nearrow \Longrightarrow \eta \nearrow$ Gelation at high C_{salt}	↗ in η: Fe^{3+} ions link Na CMC chains together but their concentration is not high enough to form a 3D-network. Gelation: formation of a strong 3D-network due to the cross-linking action of Fe^{3+} ions.	147
	$FeCl_3$	$\eta = f(c_{salt})$	$c_{salt} \nearrow \Longrightarrow \eta \searrow$ Gelation at high C_{salt}	↘ in η: as COO^- groups electrostatically shielded, Na CMC chains adopt a less expanded conformation.	126
Pb^{2+}	?	$\eta = f(c_{salt})$	$c_{salt} \nearrow$ $\Longrightarrow \eta \searrow \nearrow \searrow$	*Data not shown.* See Ca^{2+} from the same reference for detailed explanations.	87
ANIONS					
PO_4^{3-}	Na_3PO_4	$J = (c_{salt})$	$c_{salt} \nearrow \Longrightarrow J \searrow$ ⇒Na CMC gels more difficult to deform	*The studied Na CMC products were Na CMC gels in a Na_3PO_4/HCl buffer. These results should be taken carefully as the outcomes with NaCl presented in the article are opposite to the ones of other publications.*	154
HPO_4^{2-} /PO_4^{3-}	KH_2PO_4/ Na_2HPO_4	$J = f(c_{salt})$	$c_{salt} \nearrow \Longrightarrow J \searrow$ ⇒Na CMC gels more difficult to deform	*The studied Na CMC products were Na CMC gels in a KH_2PO_4/Na_2HPO_4 buffers.* *These results should be taken carefully as the outcomes with NaCl presented in the article are opposite to the ones of other publications.*	154
$P_2O_7^{4-}$	$Na_4P_2O_7$	$\eta = f(c_{salt})$	$c_{salt} \nearrow \Longrightarrow \eta \searrow$	The ↘ in η is identical to a similar solution of NaCl (pH around 10; identical concentration of Na^+ ions).	41

?: data not provided in the paper; *J*: compliance (higher values of *J* correspond to more deformable materials)

The SLS measurements performed by Trap and Hermans[122] on Na CMC solutions containing different salt concentrations show that the excess Rayleigh ratio increases with

the amount of added salt (see Figure 2-35.B). This is consistent with the fact that polymer chains get more coiled as the salt concentration increases, and scatter more the light. The power law exponent describing the concentration-dependence of the excess Rayleigh ratio at the highest NaCl concentrations is around 0.7; which is consistent with the behaviour reported for sodium poly(styrene sulfonate) solutions in 0.05 M NaCl by Tanahatoe and Kuil,[34] shown in Figure 2-19.B and discussed in Section 2-2.3.3, but different from the expected value of 1.[40,74]

All the studies of Na CMC in presence of different amounts of added salt in the dilute regime show that the radius of gyration of the chains decreases when the amount of added salt increases.[107,119-121] Such a decrease in the size of Na CMC chains upon salt addition is consistent with the coiling of the polymer chains as the charges on the polyions get screened by the added salt (see Section 2-2).

Dogsa *et al.*[13] studied the behaviour of 2% *w/v* Na CMC solutions in 0.1 M electrolyte using SAXS and LS. Compared to the SANS profiles obtained by Lopez and co-workers[1,14] (see Figure 2-36), Dogsa *et al.*'s SAXS profiles[13] do not exhibit any correlation peak. Indeed, the correlation peak characteristic for polyelectrolytes has been shown to disappear upon salt addition.[72,155]

Regarding their DLS measurements, Dogsa *et al.*'s reported the presence of both the fast and the slow relaxation modes typically observed for polyelectrolytes even if their Na CMC solutions contained 0.1 M electrolyte. This is consistent with the behaviour reported for polyelectrolytes (see Section 2-2.3.2). The IAC data were fitted using a sum of a single exponential and a stretched exponential to describe the fast and the slow relaxation modes, respectively. The fast mode was found to be diffusive, while the slow mode exhibited a q^3-dependence; suggesting that the size of the domains was large and that internal relaxation modes were also probed (see Section 2-2.3.2).

2-3.4.2. Sonication

Sonication is used to break the chains of cellulose derivatives, including Na CMC, before NMR measurements to characterise the substitution along the chains.[30,87,156] Indeed, contrary to chemical and enzymatic hydrolyses, no additional component is added to the Na CMC solutions which can then be directly analysed with NMR. It has been shown that the substitution pattern is not altered by sonication.[30,87,156] Apart from this usage, to my knowledge, only two studies about the influence of sonication on Na CMC solutions

have been published.[45,46] Hence, as sonication is an important technique used in Chapter 4, the present review has been extended to polymer solutions in general.

Ultrasound is defined as high frequency sound-waves that are above ~ 20 kHz, which is beyond the human hearing perception.[43,44,157,158] Depending on their frequencies, they can be divided into two main classes:[43,44] (i) destructive ultrasound (also referred as power or high-intensity ultrasound) at low frequencies (20 kHz-2 MHz[44] depending on references), and (ii) non-destructive ultrasound (also referred as diagnostic or low-intensity ultrasound) at high frequencies (above 5-10 MHz[44]). The former has been widely used to chemically and/or physically modify polymers.[43,44,159] During sonication, cavitation occurs, which corresponds to the creation and the growth of bubbles in the liquid submitted to sonication. Bubble sizes increase in a sinusoidal way until a critical size is reached, whereupon the bubbles become unstable and collapse.[44,159] At this stage, both the local temperature and the local pressure are extremely high (*i.e.* ~ 5,000°C and 1,000 atm,[157] respectively), and the cooling rate following the collapse is very quick (*i.e.* about 10^{10} $K.s^{-1}$). These points are termed hot spots,[44,159] and may damage the polymer chains, creating ions and radicals.[44] The main mechanism attributed to polymer chain breakage is however not related to these hot spots, but to the high shear- and strain-rates created by cavitation over broader length-scales (*i.e.* micrometres) causing chain extension and scission.[44,157,159,160] Breakage usually occurs in the middle of the polymer chains, which is a structurally weak point, and/or where chemical bonds are weaker.[44-46,159,161] Mechanical-induced scission only occurs for polymer chains whose molecular weight M_w is high enough.[43,159,160] A critical M_w of around 30,000-40,000 g/mol has been determined.[159,160]

Mechanical degradation of polymer chains has been reported for a wide range of both synthetic polymers and biopolymers.[159,161] A number of different factors influencing the breakage of the chains and their effects are summarised in Table 2-8. When available, for each factor, outcomes of investigations on Na CMC are provided after the commonly reported effects have been described.

Table 2-8: Example of factors influencing polymer chain mechanical breakage upon sonication. The results obtained from investigations on Na CMC are provided when available.

Factor	Influence on breakage
Cavitation	Cavitation is a necessary condition for breakage to occur.[159]
Temperature	Low temperatures (4-45°C[43]) favour breakage as cavitation bubbles collapse less violently at higher temperatures.[43,159]

	Indeed, there is more vapour in the bubbles; which cushions their collapse.[43,159] The lower the temperature, the more breakage and the faster it is.[158,159]
Polymer concentration	Low polymer concentrations favour breakage as the chains are more extended and possibly less or not entangled, and they can more freely move around the bubbles where the high shears and strains are located.[159] A study on Na CMC reported similar results,[46] while another showed the existence of an optimum concentration.[45] The optimum was explained by the fact that low concentrated Na CMC solutions have a low viscosity inducing a decrease in the shear forces, while highly concentrated Na CMC solutions have a high viscosity which damps the collapse of bubbles.[45]
Frequency	Portenlänger and Heusinger's[160] investigations on dextran solutions have shown that a frequency of 35 kHz induced significantly more mechanical breakage than frequencies between 500 kHz and 1.6 MHz, which gave comparable results as γ-radiations. The latter results suggests that higher frequencies induce reaction rather than mechanical degradation.[160] Meanwhile, Koda *et al.*'s[161] investigations on five different aquasoluble polymers at 20 and 500 kHz and under constant delivered ultrasonic power (*i.e.* opposed to constant electrical or input powers; see paragraphs following this Table) have shown that higher frequencies led to more significant breakage. Using a radical scavenger, they showed that the significant increase in chain degradation at high frequencies was due to the increase in radical degradation at high frequencies. They also showed that radical degradation occurred at low frequencies, though to a much lower extent than at high frequencies. The apparent discrepancy with the results reported by Portenlänger and Heusinger[160] on dextrans is likely to come from the fact that they did not keep the delivered ultrasonic power constant so that the delivered ultrasonic power was lower at higher frequencies.[161] However, Mohod and Gogate[46] found that the degradation was significantly more pronounced at 20 kHz than at 204 or 694 kHz for both Na CMC and polyvinyl alcohol (*N.B:* the ultrasonic dissipated powers were higher for the highest frequencies)[46] So the influence of the frequency on the degradation may differ from one system to another.
Solvent volatility	Low solvent volatility favours breakage. In a similar way as for the temperature, cavitation bubbles in volatile solvents contain more vapour, leading to a weaker collapse of the bubbles.[159]
Solvent surface tension	Low surface tension solvents favour breakage.[43]
Viscosity	Low viscosity favours breakage.[43,46] Indeed, if the viscosity is high, bubble explosion is damped. This has been demonstrated by independent studies of bubble dynamics, where an increase

	in the viscosity led to a decrease in the pressure when the bubbles collapse upon cavitation.[46] In the context of this thesis, the viscosity is controlled by both the polymer M_w and concentration, so that determining the contribution of each of these factors on the overall behaviour of the studied systems is not trivial.
M_w	The higher M_w, the more significant and the faster the degradation.[43,159,160] There is a critical M_w about 30,000-40,000 g/mol under which no breakage occur.[43,159,160] Above this critical value, higher M_w polymers are more broken than lower M_w ones. Under this value, polymer chains are small enough to follow the high elongational flows so that they do not undergo mechanical scission. They can still be broken by radical reactions.[160] The results about mechanical degradation were confirmed for Na CMC.[45] Experiments were even performed on solutions of identical viscosities made with different M_w Na CMC samples to exclude the effect of the solution viscosity.[45]
Polymer conformation	Linear polymers are more easily broken than linear ones as they are more easily extended upon elongational flows.[43,161]
Polymer hydrophobicity (for aquasoluble polymer)	Polymers which are more hydrophobic may be more easily degraded as they would tend to gather at the surface of the bubbles.[161]
Sonication mean and ultrasonic intensity	Ultrasound probes are more efficient at breaking the chains compared to ultrasound baths widely available in the laboratories and categorised as 'cleaning baths', as ultrasound probe energy inputs are higher. Typical intensity values are 5 $W.cm^{-2}$ or below, and 14-500 $W.cm^{-2}$ for probes and cleaning baths, respectively;[159,162-164] further details about the determination of such values are provided below this Table. For pectins, it has been shown that the degradation increased with the energy input for intensities ranging from 121 to 302 $W.cm^{-2}$ and plateaued above 302 $W.cm^{-2}$.[158] For both Na CMC and polyvinyl alcohol solutions, a probe and a bath with similar dissipated ultrasound (frequency: 20 kHz) were compared. Results showed that degradation was more pronounced when the probe was used and attributed to a higher local activity of cavitation. It was however noted that the power density was 30 times higher for the probe than for the bath.[46]
Horn depth (for sonication probes)	The horn depth influences both the rate and the extent of polymer chain degradation. Indeed, the flow patterns generated in the solution depends on the position of the horn in the solution, which needs to be optimised to obtain homogeneous degradation. This has been shown for both Na CMC and polyvinyl alcohol.[46]
Air injection	Upon air injection, the initial degradation rate of Na CMC chains is higher. This is thought to be due to the fact that the

	injected air bubbles act as *nuclei* for the cavitation process. However, after long sonication times, chain degradation is more significant without air than upon air injection. Air injection may add too much gas in the systems which would reduce the intensity of cavitation at collapse and/or would affect the ultrasound wave propagation, thus decreasing the energy available for cavitation.[46]
Salt addition	Upon NaCl addition, degradation of Na CMC and polyvinyl alcohol is promoted. This is more significant for polyvinyl alcohol and explained by the fact that salt addition would push hydrophobic polyvinyl alcohol towards the bubble interfaces so that polyvinyl alcohol chains would experience more the high shear rates and strains.[46] For the more hydrophilic Na CMC, it is suggested that NaCl addition could lower the attenuation of ultrasound waves.[46]
Surfactant addition	Addition of Sodium Lauryl Sulfate to Na CMC solutions led to a decrease in the degradation compared to surfactant-free solutions as the growth, the coalescence and the stability of the cavitation bubbles were modified.[46]

Numerous ultrasonication studies report the sonication intensity either as the electrical consumption of the generator or as the electrical energy it provides.[45,160,164] The ultrasound energy actually transferred to the medium I is however different than these values as it not only depends on the generator performance (energy input, frequency) but also on factors such as the size and the geometry of the sonication mean, the properties of the medium (surface tension, viscosity, vapour pressure, presence of solid particles and/or dissolved gas) and environmental conditions (temperature, pressure).[164,165] Hence, to compare experiments, the sonication intensity I actually transferred to the medium should be estimated.[162-165] Calorimetric methods are the most commonly used methods for this purpose.[46,162-165] They are based on the assumption that all the mechanical energy is transferred into heat[162,165] so that I can be determined by measuring the temperature increase dT/dt at the beginning of the sonication process using Eqs 2-25 and 2-26.[162-165]

$$P = m\, c_P \frac{dT}{dt} \tag{2-25}$$

$$I = \frac{P}{S_{emitting\ surface}} \tag{2-26}$$

where P is the ultrasonic power (also termed acoustic power or power output), m is the mass of the sonicated medium, c_P is its heat capacity and $S_{emitting}$ surface is the area of the emitting surface (*e. g.* $S_{emitting}$ area = πr^2 for a horn tip of radius r[163]).Examples of values found in the literature for various geometries and sizes of sonication means are provided in Table 2-9.

Table 2-9: Examples of values of sonication intensities *I* actually transferred to the sonication medium.

Sonication mean	Dimensions*	Frequency (kHz)	Electrical power (W)	Model; manufacturer	Sonicated system	*T* (°C)	*I* (W.cm²)	Ref
Probe	1.2 cm	20	600	V1A; Sonics & Materials Inc. Danbury CT	10% *w/w* soy protein aqueous suspensions	*n/a*	45-52	162
Bath	300 × 150 × 150 mm	40	300	SO375T; Sonomatic			2	
Bath	*n/a*	100	500 (512[§])	ES01/06/92; Undatim Ultrasonics S.A.			< 1	
Probe	*n/a*	*n/a*	20	S3000; Misonix Incorporated	Soybean suspensions in hexane, isopropanol or hexane:isopropanol	25	16.4-47.6[#]	163
Bath	*n/a*	*n/a*	20	Fungsonics mod. 28 L; Fungilab S.A.	Pork loin in a saturated NaCl brine	2	5.2	164
Probe	0.6 cm	100	20	*n/a*; Sonics & Materials Inc. Connecticut			14.7-21.3[#]	
	1.3 cm						29.2-75.8[#]	

*Provided dimensions correspond to the internal dimensions and to the tip diameter for sonication baths and probes, respectively. [§]Effective frequency provided by the authors. [#]The different values of *I* were obtained by varying the electrical power of the transducer. *n/a*: non-available. Ref: reference.

Investigations on carrageenan solutions at 48 kHz showed a significant decrease in the shear-viscosity.[43] The decrease in the shear-viscosity was only temporary,[43] and I propose that aggregates and/or polyion clusters usually observed in polyelectrolyte solutions could

have been physically broken and would build-up again at rest. Such changes, rather than chain breakage would be consistent with results obtained for walnut protein isolates, where sonication did not induce any change in M_w but broke down protein aggregates.[157] The sonicated samples were further characterised and it was shown that the structure of the proteins had been modified; suggesting that physical bonds could have been broken.[157] A LS study of hyaluronan solutions sonicated in a bath also suggested that polymer aggregates can be broken down upon sonication.[166]

2-4. Conclusions

Using the scaling law description of polyelectrolyte chains, three or four concentration regimes are predicted for low or high M_w polyelectrolyte solutions, which are the dilute regime, the semi-dilute regime (divided into a non-entangled and an entangled regime for high M_w polyelectrolytes) and the concentrated regime. The concentration dependence of the solution specific viscosity can be described by power laws whose exponents are characteristic for each concentration regime; thus allowing the determination of the concentration regimes and the associated crossover concentrations. The power law exponents obtained for salt-free Na CMC solutions are in agreement with the predicted values. The value obtained for the semi-dilute non-entangled regime is however slightly larger than the predicted value; which is thought to come from Na CMC semi-flexible nature and/or its polydispersity. It has also been found that the crossover concentration between the semi-dilute and the concentrated regimes, c^{**}, does not follow the expected M_w dependence, suggesting that the model proposed by the scaling laws to describe the polyelectrolyte chains at this transition and above is not sufficient. This outcome is further supported by SANS experiments on Na CMC solutions and the anomalous concentration dependence of the terminal modulus reported for quaternized poly(vinyl pyridine) solutions.

DLS experiments performed on polyelectrolyte solutions probe one relaxation mode at low concentrations, which is attributed to the coupled diffusion of counterions and polyions when polyion charges are not screened, and to the diffusion of screened polyions when charges are screened. When the polyelectrolyte concentration is increased, a second relaxation mode characterised by a longer relaxation time, hence called slow relaxation mode, appears. Its origin is still not understood, but it is commonly attributed to polyion clusters termed ‘domains’. The other relaxation mode, referred as fast relation mode, is

still attributed to the coupled diffusion between counterions and polyions. The fast relaxation mode diffusion coefficient increases as the polyelectrolyte concentration increases because polyion chains and counterions are getting closer to each other, and eventually reaches a plateau. The crossover concentrations marking the beginning of this plateau and the appearance of the slow relaxation mode are also probed by SLS and they have not been assigned yet. For high M_w polyelectrolytes, a third crossover concentration can be observed for the slow relaxation mode, but this crossover concentration is not probed by SLS; which suggests that this transition is related to changes in solution dynamics rather than structure, and I have suggested it may be assigned to the entanglement concentration. A combined rheology and light scattering study could help understanding what the crossover concentrations probed with LS correspond to.

Despite the origin of the slow relaxation mode being unknown yet, and the discrepancies observed between the investigated polyelectrolyte systems, a few common features have been established. The slow relaxation mode is not due to the presence of impurities. An ageing study performed over a couple of years has shown that the slow relaxation mode could weaken over time until an equilibrium state is established. This weakening of the slow mode would be caused by polyions leaving the domains while the domain sizes remain constant; implying that the arrangement of the polyions in a domain is such that a decrease in the number of chains involved in a domain does not induce any change in the domain size. It would be interesting to investigate this ageing behaviour for other systems as the present studies which do not report any ageing behaviour may not have been performed over time-scale that are long enough to probe ageing. Filtration decreases the size of the domains, and can possibly remove them, or, at least, reduce their size below the lower limit that can be probed by LS. Forces applied during either centrifugation or ultracentrifugation seem to be high enough to break the interactions responsible for polyion cohesion in the domains. The domains may reappear after centrifugation, further supporting the fact that domains correspond to a metastable equilibrium in solution. Salt addition leads to a decrease in the size of the domains. At low polyelectrolyte concentrations and/or for low M_w polyelectrolytes, the domains even disappear upon salt addition. This disappearance of the domains could be due to a change in the concentration regime from a polyelectrolyte semi-dilute concentration regime to a screened dilute concentration regime, where only one relaxation mode is expected. A combined LS and rheological study could help answering this question too. It could be interesting to

investigate other techniques that could break the domains to collect more information about their properties and getting closer to understand their nature and origin.

The review of Na CMC characteristics has highlighted that both batch inter- and intra-variabilities can be significant. Such variabilities include differences in substitution (average DS and substitution homogeneity along polyion chains) and crystallinity, which are key to the behaviour of Na CMC in solution as non- or poorly substituted Na CMC fractions cannot undergo full dissolution, leading to more complex sample preparation for light scattering measurements. The presence of salt impurities coming from Na CMC synthesis has also been shown to significantly alter the rheological behaviour. Finally, the broad M_w distribution typically reported for Na CMC samples makes the comparison with monodisperse synthetic polyelectrolytes more complicated and could be at the origin of the opposite concentration dependence observed for the onset of the shear-thinning behaviour compared to monodisperse synthetic polyelectrolyte systems.

The literature review has also demonstrated that no extensive LS investigation has been performed on salt-free Na CMC solutions in the semi-dilute regime. In fact, no extensive DLS study of Na CMC solutions has been carried out so far. The influence of sonication on Na CMC solutions under the polyelectrolyte perspective has not been studied either. The next two Chapters report two studies of Na CMC behaviour in water combining both LS and rheology. The first of them, Chapter 3, investigates the behaviour of salt-free semi-dilute Na CMC solutions, while the second one, Chapter 4, studies the influence of sonication on Na CMC solutions with and without added salt.

Chapter 3: Characterisation of Sodium Carboxymethyl Cellulose (Na CMC) aqueous solutions using rheology and light scattering

The content of this Chapter has been submitted to *ACS Applied Polymer Materials* under the title 'Characterization of Sodium Carboxymethyl Cellulose (Na CMC) Aqueous Solutions to Support Complex Product Formulation – a Rheology and Light Scattering Study', and is currently under review.

3-1. Introduction

Sodium Carboxymethyl Cellulose (Na CMC) is widely used in industry for its thickening and swelling properties.[1,4,5] The Na CMC global market represented 1.2 billion USD in 2014[4] and keeps expanding with a compounded annual growth rate around 4%.[4,5] Application areas include pharmaceutical, food, home and personal care products as well as those of the paper industry, paint, water treatment and mineral processing.[1,4,5]

Na CMC is a linear, negatively charged, water-soluble, semi-flexible polymer derived from cellulose,[1,15,28] which is the most abundant organic polymer on Earth.[1,2] Na CMC has the same linear backbone as cellulose (*i.e. D*-glucose monomers linked by β-1,4 glucosidic bonds) with some of the hydroxyl groups of the raw material cellulose substituted by carboxymethyl groups.[2,26,88] On each monomer, all three hydroxyl groups can, in principle, be substituted.[26] However, full substitution is rarely achieved.[26] Commercial Na CMCs typically have an average of 0.4-1.5 substituted hydroxyl groups per monomer, which is referred to as its absolute Degree of Substitution (DS).[18,26] It is the presence of these carboxymethyl groups that makes Na CMC soluble in water.[28-30,82,83] However, if the DS is too low, or if the substitution along the chains is not homogeneous so that large parts of the chains are poorly or non-substituted, Na CMC does not fully solubilise in water.[26,29,30,82,83,88] Heterogeneously substituted (or blocky) Na CMCs are commonly used in laundry detergents as their low solubility facilitates deposition on fabric and enhances stain removal,[16,167] while homogeneously substituted Na CMCs are commonly used in toothpaste.[168] Because the raw material from which Na CMC is synthesised comes from natural sources, there is a great variability in the size of the polymer chains in Na CMC samples, as characterised by large polydispersity

indices M_w/M_n.[1,3,24,25] Common values of M_w/M_n are around 1.7-3.6,[1,3,24,25] but values as high as 8.5 and 8.7 have been reported.[24]

The influence of Na CMC characteristics on its rheological behaviour has been extensively studied in aqueous solutions. The rheological behaviour of Na CMC in water, with or without other compounds (*e.g.* salts,[15,30,41,81,126] sugars,[41,132] or surfactants[81,118]), or in solvents such glycerin/water mixtures,[32] propylene glycol/water mixtures[36] or cadoxen[145] has been characterised. Studies investigating the swelling properties of Na CMC[169] and its ability to form films on its own, or in association with other polymers, have also been performed. Only a few light scattering (LS) studies have been performed on Na CMC solutions, and none, to the best of my knowledge, have been performed on Na CMC solutions without added salt. Several Static Light Scattering (SLS) studies were performed in the 1950-1960s[119,121,122] on Na CMC in the presence of NaCl and focused on the intrinsic properties of the Na CMC polymer without the effects of charge. Also, three recent light scattering studies that combine LS with other experimental techniques have been published: Dogsa *et al.*[13] studied Na CMC chain conformation as a function of pH while keeping the ionic strength constant at 0.1 M, Guillot *et al.*[118] investigated the behaviour of Na CMC in the presence of a surfactant, and Hoogendam *et al.*[107] characterised the conformation of Na CMC chains in the presence of an electrolyte, using Size Exclusion Chromatography (SEC) coupled to a Multiple Angle Laser Light Scattering (MALLS) detector.

Generally, both SLS and Dynamic Light Scattering (DLS) have been widely used to characterise polyelectrolytes in aqueous solution. Synthetic polyelectrolytes such as sodium poly(styrene sulfonate) (Na PSS),[66] poly(methacrylic acid) (PMA)[170] or poly(*N*-methyl-2-vinylpyridinium chloride) (PMPVP),[31] as well as natural polyelectrolytes such as DNA,[72,171] chitosan,[35] xanthan[36,37] or hyaluronan[37] have been investigated. For polyelectrolyte solutions above their overlap concentrations, either without added salt or at relatively low salt concentrations so that charges along the chains are not fully screened, DLS typically reveals two relaxation modes. These modes include: (i) a fast mode which is usually attributed to the coupling between counterions and polyions[31,36] (as the smaller counterions diffuse within the solution, they exert a drag on the oppositely charged polyions) and (ii) a slow mode, whose origin is not fully understood, but is usually attributed to the presence of aggregates or clusters of polyelectrolyte chains, commonly termed 'domains'.[31,36]

The relaxation rate of the fast mode is usually q^2-dependent (q is the scattering vector defined as $q = \frac{4\pi n \sin(\theta/2)}{\lambda}$, with n the refractive index, θ the scattering angle and λ the laser excitation wavelength); implying it has diffusive character.[32,33,35,37,172] The fast mode relaxation time τ_f is typically around a few μs and the corresponding diffusion coefficient $D_f \sim 10^{-6}$ cm^2.s^{-1}.[22,69] The slow mode is characterised by significantly longer relaxation times τ_s, that are typically in the range of 1 ms to 10 s.[22,69] The slow mode has commonly been found to also exhibit a q^2-dependence,[32,33,35,37,172] for which a diffusion coefficient can be calculated[35] and an apparent hydrodynamic radius of the domains can be estimated.[35] However, other q-dependences have been observed for the slow mode,[33,37] where it has been suggested that the characteristic size of the domains, L, is large compared to the probed length-scale so that $qL >> 1$ and internal relaxations within the domains are also probed.[22,69]

To understand the nature of the slow mode, the influence of both the polymer intrinsic properties (*e.g.* M_w,[31,33,37] degree of ionisation[71,76,77]) and the experimental conditions (*e.g.* polyelectrolyte concentration,[22,31,37] sample filtration,[22,79] centrifugation,[36,80] dialysis,[73,76] salt addition,[32,76,78] backbone solvation,[71,75,78] pH[13,76]) have been extensively studied. Nevertheless, there appears to be relatively few outcomes that can be generalised across all the investigated systems. For example, some studies show that, at a given polyelectrolyte concentration, the size of the domains does not vary with M_w[31,33] while another shows it does.[37] In a similar way, a study shows that at a given M_w, $R_{g,app}$*(domains)* increases with the polyelectrolyte concentration,[22] while others show that it does not[31,37] (see Section 2-2.3.4 and Figure 2-21). However, there does seem to be an agreement on the fact that both filtration and centrifugation can modify the domains.[22,36,79,80] Filtration using small pore size filters can even fully remove them[79,80] or, at least, reduce their size to a level that is below the length-scales probed by LS in the particular experiment.[80] Ultracentrifugation has also recently been shown to remove the domains, suggesting that centrifugal forces can break the cohesive interactions in the domains.[36] This observation was suggested to support the idea that the domains result from electrostatic forces and are formed by polyelectrolyte chains sharing counterions.[36] It has also been suggested that they are temporal, in that the polyelectrolyte chains of a domain are continually exchanged with polyelectrolyte chains present in the rest of the solution.[32,36] In some cases, it has been reported that the number of chains forming a domain decreases over long periods of time.[70]

Finally, a third relaxation mode is sometimes observed in polyelectrolyte solutions,[69-73] which is generally either slower than the slow mode,[71,72] or situated between the fast and the slow modes.[69-71] The reported origin of this relaxation varies significantly between different systems.[69-73] For example, as an intermediate mode, it has been attributed to the motion of polyelectrolyte chain sections that do not belong to the domains,[69] or to the motion of hydrophobic domains formed by uncharged segments of the polyelectrolyte backbone,[71] while as an 'ultra-slow' mode, it has been attributed to loose aggregates of polyelectrolyte chains.[72]

The present work combines viscosity measurements with SLS and DLS over a wide range of polymer concentrations for salt-free aqueous Na CMC solutions. The solution viscosity is studied as a function of polymer concentration. The obtained results are compared to the predictions of the scaling theory for polyelectrolytes and to recent results from literature; leading to the identification of two concentration regimes and to their assignment to the semi-dilute non-entangled and entangled regimes. Moreover, a comprehensive SLS-DLS study is performed over a similar range of concentrations, where the properties of the excess Rayleigh ratio determined from SLS and the three relaxation modes observed in DLS are investigated.

3-2. Materials and methods

3-2.1. Materials

Na CMC of average molecular weight 700,000 g/mol and DS 0.8-0.95 (supplier specification) was obtained from Sigma-Aldrich (product number: 419338; lot number: MKBR1032V). Using the acid wash method from the ASTM,[173] the DS was found to be 0.85 ± 0.03. The moisture content of the polymer powder was $8.4 \pm 0.2\%$, which was taken into account for the preparation of the polyelectrolyte solutions.[173] 'Ultrapure' water type I (called deionised DI water in the following) was obtained from either a Milli-Q® Advantage A10 ultrapure water station (Merck Millipore) or a PURELAB® Option Q station (Elga). Isopropanol from VWR® Chemicals (AnalaR NORMAPUR® ACS, Reag. Ph. Eur. analytical reagent; product number: 20842.323) and toluene from Fisher Chemical (analytical reagent; product number: T/2300/17) were used.

3-2.2. Methods

3-2.2.1. Optical microscopy

Optical microscopy was performed using a Zeiss LSM700 inverted confocal microscope (Carl Zeiss Microscopy) using both phase contrast and differential interference contrast (DIC) techniques.

3-2.2.2. Rheology measurements

Initially, stock solutions of 0.037, 0.18, 0.68 and 0.73% Na CMC (all concentrations quoted in this Chapter are in *wt*%) were prepared by adding the appropriate amounts of Na CMC powder to filtered DI water (using non-sterile Fisherbrand® syringe filters with 0.2 μm pore-size nylon membranes) under stirring with the help of a magnetic stirrer at 850 rpm. Stirring was pursued for 2 h. These initial solutions were diluted to 0.018-0.48% Na CMC and kept overnight before rheology measurements were carried out.

All rheology measurements were performed at 25°C using a Discovery HR-2 rheometer (TA Instruments) equipped with a bob and cup geometry (bob with a conical end). Preliminary measurements of the time-evolution of the viscosity for different constant shear-stress values (data not shown) were performed to determine the most suitable shear-stress range and time parameters for flow curve acquisition; these include the equilibration time Δt_{eq}, which is the time during which the shear-stress is applied before data acquisition to allow a steady flow to be achieved, and the averaging time Δt_{av}, which is the time during which data are taken and averaged. All viscosities were measured using the stress-controlled mode. Δt_{eq} was set to 200 s for Na CMC concentrations up to 0.18% and to 30 s for all other concentrations. For each solution, flow curve data were collected using Δt_{av} = 200 s and Δt_{av} = 300 s to confirm that the value of Δt_{eq} was adequate and a steady flow had indeed been achieved.

3-2.2.3. Light scattering measurements

To avoid dust contamination, all glassware were washed with filtered DI water (nylon-membrane filters mentioned in Section 3-2.2.2) and filtered isopropanol (non-sterile Fisherbrand® syringe filters with 0.2 μm pore-size PTFE membranes) before being dried in a dust-free environment at *ca.* 50°C. Solutions ranging from 0.018 to 0.92% Na CMC were prepared directly by mixing the appropriate amounts of Na CMC powder and filtered DI water. The preparation procedure was the same as that used for the rheology

samples, except that the solutions prepared for LS were transferred into glass vials (rimless Pyrex® culture tubes 75 × 10 mm), suitable for LS, and then kept overnight before the measurements. During the sample preparation tests for the LS measurements, using filtration and/or centrifugation to try to remove contamination (*e.g.* dust), the solutions were filtered using a P5 (1.0-1.6 μm pore size) VitraPOR® Borosilicate 3.3 filter tunnel (ROBU®) before being transferred into LS tubes, and/or centrifuged directly in the LS tubes using a Heraeus™ Megafuge™ 16R Centrifuge (Thermo Scientific™) equipped with a Rotor swing-out TX-400 4 × 400 mL (Thermo Scientific™); both procedures are described in detail in Section 3-3.3. The reference (*i.e.* toluene) and solvent (*i.e.* water) samples required for excess Rayleigh ratio ΔR calculations were filtered through previously mentioned PTFE and nylon filters, respectively.

LS measurements were performed at 25.0 ± 0.5°C using a 3D LS spectrometer (LS Instruments, Switzerland) equipped with a HeNe laser (λ = 632.8 nm, power: 21 mW), an automated laser attenuator and two avalanche photodiode (APD) detectors. All measurements were performed with vertically polarised incident and vertically polarised detected light and in pseudo-cross correlation mode, which removed after-pulsing effects and allowed the investigation of lag times τ as low as 25 ns. All samples were transparent and it was confirmed that multiple scattering did not have to be taken into account; thus, all measurements were performed using a standard '2D mode'. The measurements were performed within a few days following solution preparation and did not last more than a week, which is important since Na CMC solution properties such as the viscosity have been shown to change over time.[12,41,42] Further details about the measurement process and data analysis are given in Section 3-3.3.

3-2.2.4. Fitting of the data

All fits were performed with Origin® and the Levenberg Marquardt algorithm with 'instrumental weights' was used.

3-3. Results and discussion

3-3.1. Optical microscopy of Na CMC solutions

It became evident upon the initial preparation of the Na CMC solutions that a very small proportion of non-dissolved cellulose residuals remained, even after extended mixing.

Microscopy was used to understand their nature and categorise them based upon different observed morphologies, with examples shown in Figure 3-1. The presence of similar residuals in Na CMC solutions was reported as early as 1942 by Höppler.[113] Further investigations on Na CMC samples with a low DS (around 0.7) were performed more recently by Jardeby and co-workers,[29,82,83] who concluded that these residuals were made of non- or poorly-substituted cellulose originating from less reactive cellulose fragments in the raw material used for Na CMC synthesis. Because of their lower DS, these residuals could not undergo full dissolution and would exist in solution as fibres ($DS_{residuals} \approx 0.1$), 'ballooned' fibres ($DS_{residuals} \approx 0.3$-05) or gel particles ($DS_{residuals} \approx 0.5$-0.6).[29] The presence of undissolved residuals in Na CMC solutions for samples with DS values as high as 0.95 has previously been reported.[28,91] In the following, the term 'particulates' will be used for the residuals observed in the studied samples.

Consistent with Jardeby and co-workers's observations[29,82,83], microscopy reveals the existence of particulates as fibres (Figure 3-1.A), swollen and ballooned fibres (Figure 3-1.B), or swollen ring-like fragments (Figure 3-1.C) at more advanced dissolution stages. It is worth noting that studying these particulates using optical microscopy can be difficult. As an example, Figure AI-1 shows the same particulates as in Figure 3-1.C for different *foci*. Moreover, similar morphologies to those shown in Figure 3-1.D were observed in microcrystalline cellulose suspensions, as shown in Figure AI-2; which supports assigning these to non- or poorly substituted cellulose fragments.

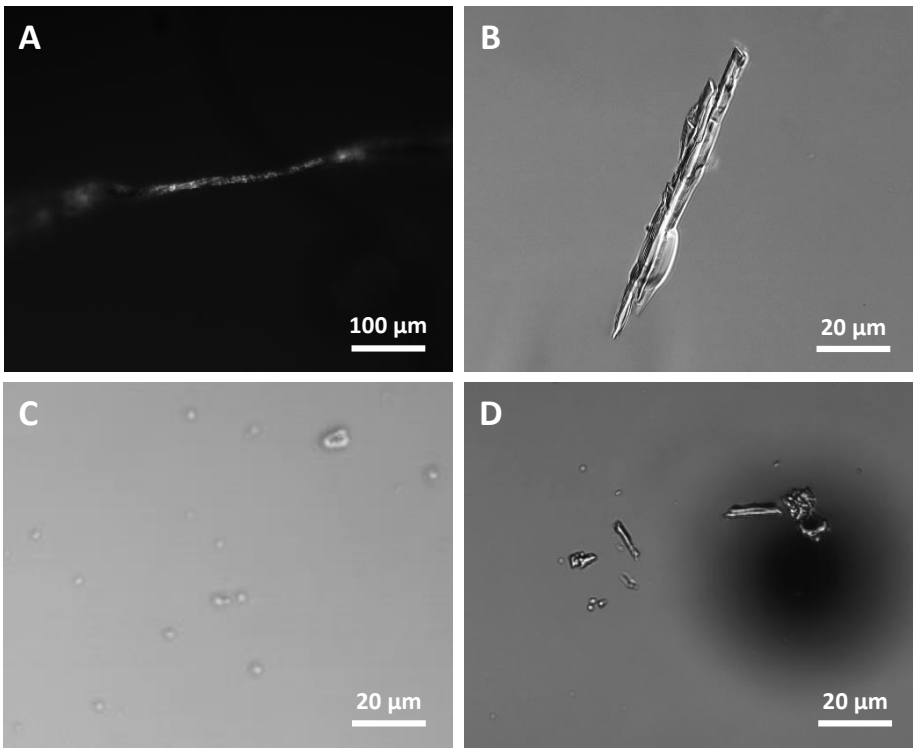

Figure 3-1: Examples of particulates observed in Na CMC solutions under the microscope. **A.** 0.18% solution; **B.** 1.8% solution; **C, D.** 0.018% solution (the black spot in D belongs to the background and not to the sample).

3-3.2. Concentration dependence of Na CMC solution viscosity

The scaling model for solutions of uncharged flexible polymers in good solvents classifies their behaviour into three concentration regimes: dilute, semi-dilute and concentrated.[49,51] In the dilute regime, the polymer chains are well separated and can be described as a sequence of thermal 'blobs' of size ξ_T*:* for length-scales smaller than ξ_T (*i.e.* within the blobs), the excluded volume interactions are weaker than the thermal energy kT and chains adopt a nearly ideal chain conformation, while for length-scales larger than ξ_T, the excluded volume interactions are stronger than kT and the chains can be viewed as self-avoiding walks of thermal blobs.[49] As the semi-dilute regime is entered at the overlap concentration c^*, a new length-scale, the correlation length ξ, approximately corresponding to the distance between polymer chains and defining so-called correlation blobs, is introduced.[49] At length-scales smaller than ξ, the chain conformations are the same as in the dilute regime, while for length-scales larger than ξ, the excluded volume interactions are screened and each chain can be viewed as a random walk of correlation blobs.[49] As the polymer concentration is further increased, the distance between polymer chains and correspondingly ξ decrease,[51,61] and when ξ becomes smaller than ξ_T, the polymer chains behave like ideal chains at all length-scales; this is called the concentrated

regime[51,61] and the concentration at which it is entered is called c^{**}. Moreover, if the polymer molecular weight is high enough, the chains in the semi-dilute and concentrated solutions can be entangled, and the crossover concentration between the semi-dilute non-entangled and entangled regimes is then called the entanglement concentration c_e.

A common method to identify these concentration regimes is to plot the specific viscosity η_{sp} (Eq. 3-1) as a function of the polymer concentration, where η_{sp} is defined as:

$$\eta_{sp} = (\eta_0 - \eta_s)/\eta_s \quad (3\text{-}1)$$

with η_0 the polymer solution zero-shear viscosity and η_s the solvent viscosity. According to the scaling laws for polymer solutions,[15,48] each concentration regime is characterised by a power law $\eta_{sp} \sim c^b$, with a characteristic exponent b that depends not only on the concentration regime, but also on the solvent quality (*e.g.* theta solvent, good solvent).[15,48] For an uncharged flexible polymer in a good solvent, the predicted values of the exponent b for the dilute, the semi-dilute non-entangled, the semi-dilute entangled and the concentrated regimes are 1, 1.3, 3.9 and 3.75, respectively.[15,48]

Importantly, similar concentration regimes have been observed for polyelectrolytes in salt-free solutions.[15,48] The relevant length-scales are here defined by the effects of electrostatic interactions.[20,51] The key length-scale of the polyelectrolyte scaling theory[174] is that characterising so called electrostatic blobs of size ξ_e. Within these blobs, electrostatic interactions are screened and chains act as if they were uncharged, whereas on length-scales larger than ξ_e, the chains adopt stretched directed random walk configurations in the dilute regime due to repulsive interactions between the electrostatic blobs.[1,174] Within the semi-dilute regime, neighbouring chains screen electrostatic interactions on length-scales above the correlation length ξ, where chains behave like random walks of correlation blobs.[20,174] The power law exponent in the dilute regime is predicted to be 1 for salt-free polyelectrolyte solutions, as for neutral solutions, but c^* is typically much lower for polyelectrolyte chains of similar molecular weight due to the significant charge-induced chain stretching.[48] The power law exponents of the semi-dilute non-entangled and entangled regimes are predicted to be 0.5 and 1.5, respectively, while the power law exponent of the concentrated regime should be identical to that observed for neutral polymers (3.75) since the charges of the polyelectrolyte chains are fully screened in this regime.[15,47,48]

Examples of Na CMC solution flow curves spanning the full range of investigated concentrations are shown in Figure 3-2. Flow curves obtained with Δt_{av} = 200 s and Δt_{av} = 300 s superimposed well (data not shown); which confirms that the time parameters used for the measurements were appropriate, and the measured viscosities were at steady-state. All solutions are shown to exhibit shear-thinning behaviour. The values of η_0 were obtained by fitting the flow curves with the Carreau model[1] (also shown in Figure 3-2). The equation as well as the fitting parameters corresponding to the curves shown in Figure 3-2 are provided in Section AI-2.1. The values of η_0 were combined with the experimentally determined solvent viscosity η_s = 0.948 ± 0.002 mPa.s to calculate the specific viscosities η_{sp} (Eq. 3-1), which are shown in Figure 3-3 as a function of the Na CMC concentration.

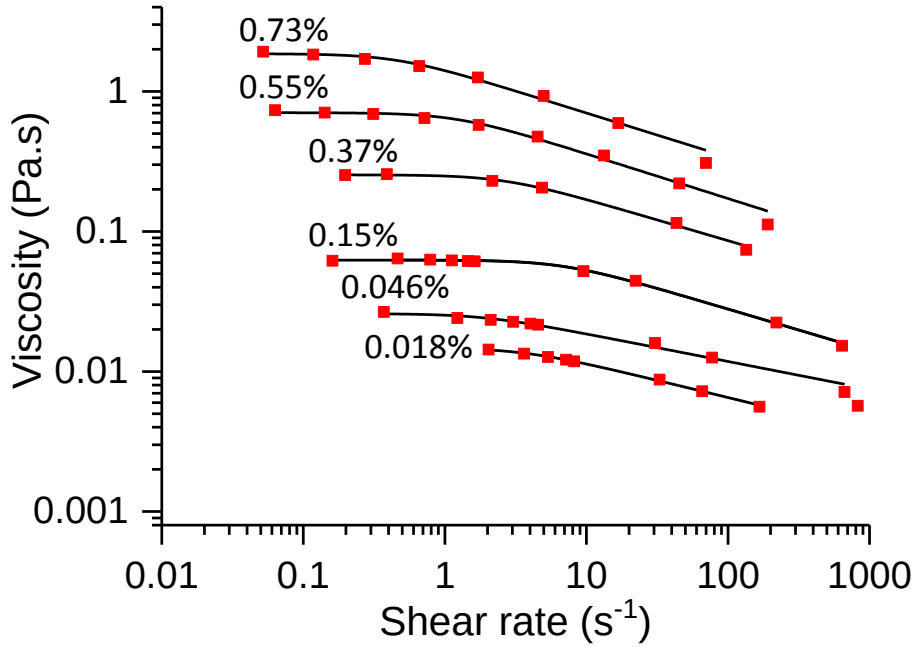

Figure 3-2: Examples of viscosity curves across the studied range of concentrations. Δt_{av} = 200 s. The black lines are fits to the Carreau model, used to determine the values of the zero-shear viscosity η_0.[1]

For the studied range of Na CMC concentrations, the increase in η_{sp} with $c_{Na\ CMC}$ may be described using three different power laws (dashed lines in Figure 3-3). The determined power law exponents are shown below the fits in Figure 3-3 and were found to be consistent with those previously reported for other Na CMC solutions.[1,15,143,175] However, a comparison to the exponents theoretically predicted by the scaling theory for polyelectrolytes[14,15] (values in brackets in Figure 3-3) clearly shows that the exponent value found for the semi-dilute non-entangled regime is higher than the prediction from scaling theory. Lopez *et al.*[15] highlighted that the presence of residual salts leads to higher

power law exponent values in this regime, which can be as high as 1. Their experiments were conducted on solutions prepared with purified Na CMC samples as well as Na CMC samples containing low amounts of residual salts, where the value of the power law exponent for the semi-dilute non-entangled regime was measured to be 0.68 ± 0.02. These authors argue that Na CMC samples characterised by similar exponents can effectively be considered as salt-free.[15] The exponent of the present Na CMC sample in the semi-dilute non-entangled regime is found to be 0.74 ± 0.04, thus similar to the value found by Lopez *et al.* within experimental error, and can therefore also be considered effectively salt-free. For salt-free Na CMC solutions, Lopez *et al.*[15] also suggested that both polydispersity and chain rigidity could contribute to the discrepancy observed between experimental and predicted power law exponent values in the semi-dilute non-entangled regime. The scaling laws for polyelectrolytes have indeed been established for flexible polymer chains, while it is known that Na CMC polymer chains are semi-flexible.[15,47]

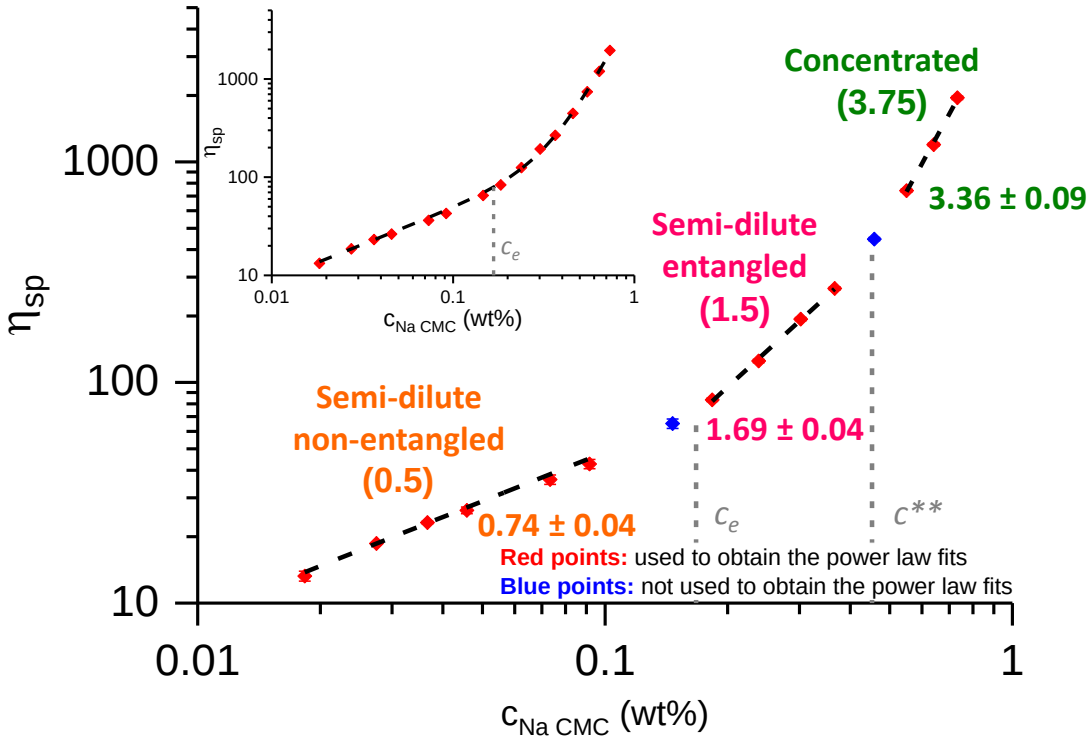

Figure 3-3: Determination of the concentration regimes from the specific viscosity η_{sp} *vs* Na CMC concentration $c_{Na\ CMC}$ data. Dashed lines: best power law fits; the corresponding power law exponents are provided below the fitting curves. Theoretical values from the polyelectrolyte scaling laws are given in brackets below the name of each concentration regime. The inset shows the same data set fitted using Eq. 3-2b where b = 0.74 and c_e = 0.17 *wt*% (values obtained from the best power law fits). The fit with the power law exponent predicted by the scaling law is shown in Figure AI-3.

The crossover concentrations are shown in Table 3-1. It is worth noting that as non-fractionated Na CMC samples are generally polydisperse,[1] the transitions between different concentration regimes are expected to be characterised by a concentration range instead of a single characteristic concentration. Thus, the concentrations determined using the power law fitting approach should be viewed only as estimates. Because the exponents of the best power law fits are different from those predicted by the scaling laws, the crossover concentrations c^*, c_e, and c^{**}, calculated as the intersections between the power law fits of two successive concentration regimes, differ depending on whether theoretical or best fit exponents are considered (*i.e.* upper and lower lines of Table 3-1 respectively). The fits of the semi-dilute non-entangled concentration regime obtained with both theoretical and best fit exponents were extrapolated to $\eta_{sp} = 1$ to obtain the values of the overlap concentrations. These processes are illustrated in Figure AI-3.

Table 3-1: Crossover concentrations calculated with different methods.

Calculation method	c^* (%)	c_e (%)	c^{**} (%)
Scaling law fits	7.7×10^{-5}	0.10	0.46
Best power law fits	5.2×10^{-4}	0.17	0.45

By studying how the crossover concentrations and the specific viscosity behave with Na CMC molecular weight, Lopez and co-workers[1,15] concluded that the scaling laws of salt-free polyelectrolyte solutions may not be the most appropriate model to describe salt-free Na CMC solutions above c^*. Their study[15] indicated that there may be only one crossover concentration, instead of the two separate concentrations, c_e and c^{**}. This hypothesis was reinforced by the absence of the expected change in the Small Angle Neutron Scattering (SANS) profile at c^{**}, which suggests that the current description of such systems based on the electrostatic blobs and the correlation length is not sufficient to describe them,[1] as well as by the fact that viscosity data could be successfully fitted outside the dilute regime using a simple expression (Eq. 3-2a) that contains only one characteristic concentration within the fitting regime, chosen as the entanglement concentration c_e determined as discussed above. Eq. 3-2a[15] is a simple parameterisation of the η_{sp} *vs* $c_{Na\,CMC}$ data above c^*, which uses a single characteristic concentration c_e outside the dilute regime and includes two parameters γ and q to describe the power law exponents in the non-entangled and entangled regimes. To account for variations in the shape of η_{sp} *vs* $c_{Na\,CMC}$ as the behaviour transitions from the low to high concentration power law behaviour, a final parameter Q is introduced.

$$\eta_{sp} = \eta_{sp}(c^*) \cdot (c_{Na\,CMC}/c^*)^{\gamma} \cdot (1 + Q(c_{Na\,CMC}/c_e)^q) \quad (3\text{-}2a)$$

An attempt to fit the present data outside of the dilute regime with Eq. 3-2b, adapted from Eq. 3-2a to avoid any assumption on the values of $\eta_{sp}(c^*)$ and c^*, is shown in the inset to Figure 3-3. Here γ is the exponent of the best power law fit within the semi-dilute non-entangled regime (*i.e.* $\gamma = 0.74$), c_e is the entanglement concentration determined from the scaling law analysis described above (see value in Table 3-1), and *A*, *Q* and *q* are fitting parameters.

$$\eta_{sp} = A \cdot c_{Na\,CMC}{}^{\gamma} \cdot (1 + Q(c_{Na\,CMC}/c_e)^q) \quad (3\text{-}2b)$$

The fit is also shown in Figure AI-3, where it is compared to that using the exponent predicted from scaling theory (*i.e.* $\gamma = 0.5$) and where all parameters are provided for both fits. Eq. 3-2b is found to fit the data well, which supports the possibility that there may be only one crossover concentration above the overlap concentration. It is worth noting that the existence of the concentrated regime has also been questioned for another polyelectrolyte system by Dou and Colby.[174] While the graph of η_{sp} *vs* $c_{polymer}$ was consistent with the scaling law predictions, the concentration-dependence of the terminal modulus *G* did not show the expected inflection at c^{**}.

In summary, a detailed analysis of the concentration dependence of the specific viscosity has been performed above the overlap concentration. The present data can be described using a set of power laws as predicted from the scaling laws for polyelectrolytes. The determined power law exponents slightly differ from the theoretical predictions, but are consistent with those previously determined for Na CMC samples of varying M_w and DS.[1,14,15] Importantly, the same data can be alternatively described using a simpler approach which interpolates between a low and a high concentration power law behaviour using only a single crossover concentration. This concentration is assigned to that characterising the onset of entanglements within the semi-dilute regime.

3-3.3. Optimisation of light scattering measurements

LS measurements are very difficult to perform for Na CMC concentrations below 0.018% due to the low scattering intensity. It was thus decided to limit the LS study to Na CMC concentrations starting from 0.018% and covering the concentration range investigated with viscosity measurements (see Section 3-3.2).

Sample preparation

LS measurements ideally require samples free of dust and residual components.[39,76] Observations of the Na CMC solutions using optical microscopy, however, showed the presence of particulates (see Figure 3-1). Thus, the possibility of removing these particulates from the solutions prior to performing the LS measurements was investigated. Filtration and centrifugation are the two most commonly used techniques for this purpose.[13,39,76] 0.2 μm pore-size syringe filters were tried first. However, the scattering intensities of the Na CMC solutions after filtering using such filters were very close to those of pure water (data not shown). This result clearly demonstrated that these filters are not appropriate for sample preparation, which is consistent with the fact that the characteristic size of the 'domains' responsible for the slow relaxation mode scattering contribution was determined to be around 400 nm (see Section 3-3.5 and Figure 3-15).

Jardeby and co-workers have previously isolated particulates from Na CMC solutions (see Figure 3-1 and Jardeby and co-workers' papers[29,82,83]) using filters, and the same filter types (*i.e.* ROBU® VitraPOR® Borosilicate 3.3 filter tunnels) were thus tried in the present study, using the smallest available pore size (1.0-1.6 μm). Centrifugation tests were also carried out, and were performed directly in the LS cells to prevent any contamination of dust due to the sample transfer into the cells.[76] The centrifugation acceleration and deceleration speeds were set to the lowest available values to minimise any modification of the solution structure.[76,80] For the same reason, the Relative Centrifuge Force (RCF) and the centrifugation times were varied to ensure that none of the chosen values modified the solution behaviour significantly, as several studies have shown that centrifugation can alter the solution properties.[36,69] Both the filtration and centrifugation trials were performed on 0.018% Na CMC solutions. The effectiveness of these preparation protocols to remove dust and residual components were evaluated using LS. The intensity auto-correlation data corresponding to a range of different preparation protocols are shown in Figure 3-4.

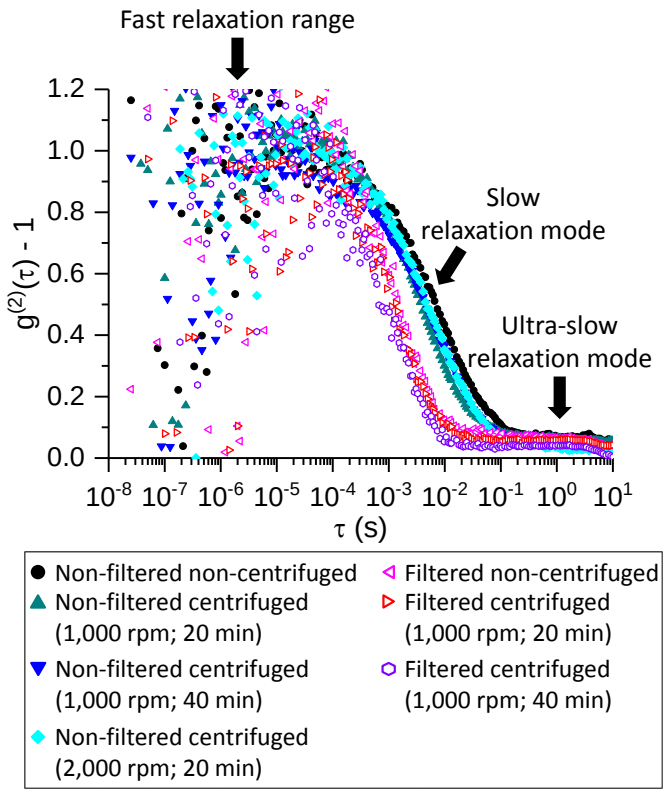

Figure 3-4: Normalised intensity auto-correlation data at 90° scattering angle collected during sample purification trials (*i.e.* centrifugation and/or filtration) for a 0.018% Na CMC solution. Each data series is an average of 30-s measurements (See details about normalisation and averaging in Section AI-3.2).

All intensity auto-correlation data exhibit two decays: (i) a main decay with a relaxation time around either 0.01 s or 0.003 s, and (ii) a secondary decay at much longer relaxation times. The main relaxation (i) was assigned to the slow relaxation normally reported for salt-free polyelectrolyte solutions above c^*, and thought to be due to the presence of polyelectrolyte aggregates here termed 'domains',[32,38] as discussed in Sections 2-2.3 and 3-1. None of the investigated centrifugation parameters modified the value of the relaxation time τ_s of the slow mode significantly, which demonstrates that the behaviour of the Na CMC solutions was not altered by the centrifugation procedure. Conversely, filtration led to a significant decrease in τ_s, suggesting that the compositions and/or the structures of the solutions were considerably modified. This observation is in agreement both with previous literature on light scattering of salt-free polyelectrolyte solutions[22,80] and with an observed 12.2 ± 0.6% decrease of the viscosity upon filtration (data not shown). The origin of the secondary decay, referred to here as the ultra-slow mode, is not clear. The corresponding relaxation times are long, suggesting that the ultra-slow mode is due to the presence of large particulates present in solution (see Section 3-3.5 for a more detailed discussion). As neither centrifugation nor filtration completely removed

the ultra-slow mode, and filtration even significantly altered the slow relaxation mode, the LS measurements were performed using unprocessed Na CMC solutions. The next two sub-sections describe how data collection and processing were adapted to account for the presence of the ultra-slow mode. Importantly, this approach has the clear advantage that it allowed detailed light scattering measurements to be performed on the original Na CMC solutions which are relevant for industrial applications.

Measurement settings

For each solution, preliminary measurements at different angles were performed to identify the most appropriate measurement durations. DLS measurements need to be long enough so that the determination of the intensity auto-correlation data is reliable. However, particularly for the lower concentration range, where the scattering is weak, the acquisition times that can be used are limited since scattering from particulates (assumed to be responsible for the ultra-slow mode) will eventually interfere with the scattering from the Na CMC solution. Indeed, the intensity auto-correlation data in Figures 3-5.A-C demonstrate that the effects of the ultra-slow mode increase with the measurement duration, which is consistent with the interpretation that more of the particulates responsible for the ultra-slow mode enter the scattering volume during long measurements as compared to short ones. Also, as shown in Figure 3-5, for measurements at a fixed acquisition time, the ultra-slow mode becomes more significant for lower scattering angles, which is consistent with the fact that a larger object will show a higher scattering intensity and thus contribute more at lower scattering angles. Thus, at a scattering angle of 30° (data not shown), it was not possible to obtain high quality measurements for the longest measurement durations.

From a practical viewpoint, more but shorter measurements can be performed at each scattering angle so that measurements that are significantly impacted by scattering from particulates can be discarded. Subsequently, the remaining data are averaged across several independent measurements to enable good statistics for samples at low concentrations, where the intrinsic scattering is low, without significant effects of scattering from particulates.

Figure 3-5.D shows that the normalised scattering intensity I_{norm} (calculated as $I_{norm} = \frac{measured\ count\ rate \times sin(\theta)}{laser\ intensity}$) depends on the acquisition time only at longer times, where particulates enter the scattering volume. Appropriate acquisition times were

thus determined for each angle and each solution. It is worth noting that individual SLS measurements were performed over shorter periods of time than DLS measurements to further minimise the influence of particulates.

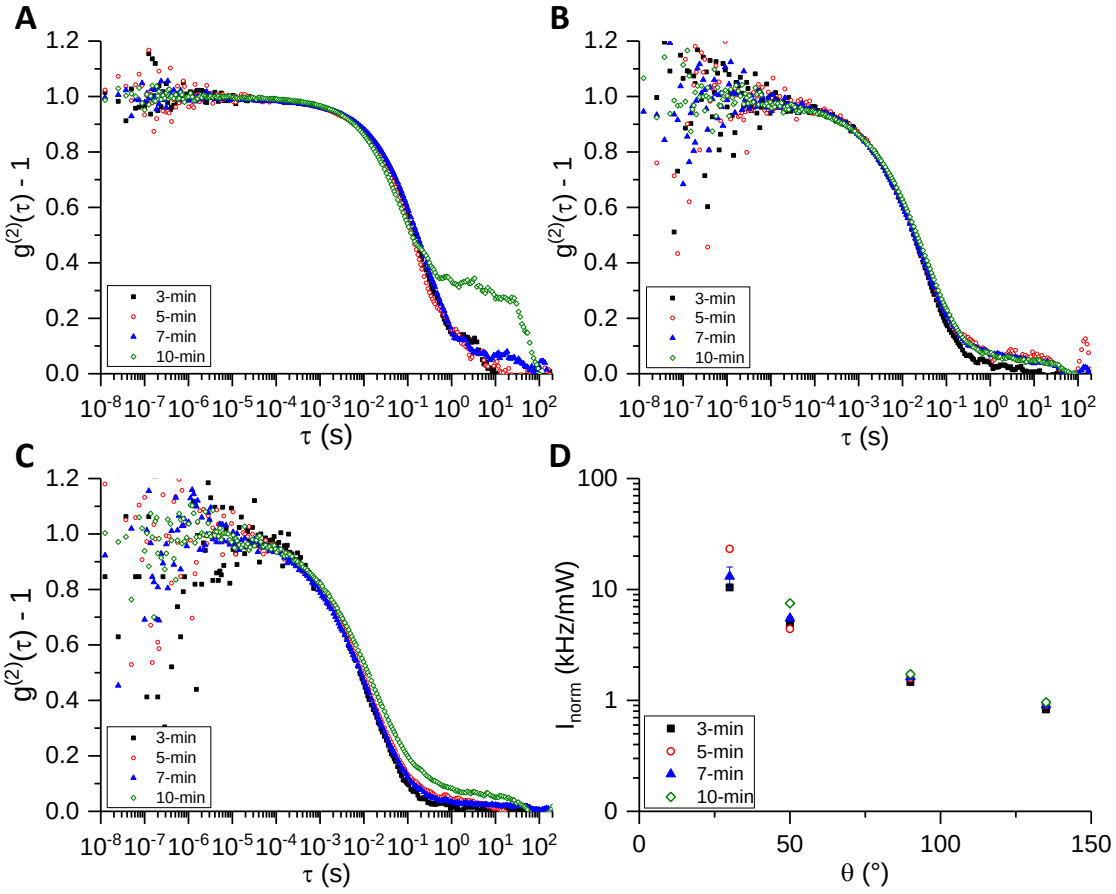

Figure 3-5: Influence of measurement duration on the light scattering data collected for a 0.073% Na CMC solution. **A. B. C.** Averaged normalised intensity auto-correlation data collected over different periods of time at scattering angles of 50, 90 and 135°, respectively. **D.** Normalised scattering intensity I_{norm} as a function of the scattering angle θ. Error bars represent the standard error (plotted only when there were at least 3 proper quality measurements).

Data processing

The LS data need to be collected within the linear range of the detector to be reliable. As a consequence of the presence of particulates in the solutions, extra precautions were required to make sure this condition was always met, as explained in detail in Section AI-3.1. Hence, the first data processing step was to remove all measurements during which the scattering intensities were outside the detector linear range, which occurred for some experimental runs influenced by the stronger scattering contribution from particulates. Subsequently, the scattering traces (*i.e.* scattering intensity over time) were investigated and traces which contained clear contributions to the scattering from particulates, as identified by sharp peaks with significantly higher intensity than the intensity fluctuations

corresponding to the contributions from the intrinsic solutions, were removed. This trace check was performed for all DLS measurements, while it was only performed for the measurements where the scattering was far above the mean for SLS data.

The obtained SLS data were used to calculate the excess Rayleigh ratio ΔR using Eq. 3-3[65]

$$\Delta R(\theta) = \frac{I_{norm,sample}(\theta) - I_{norm,water}(\theta)}{I_{norm,toluene}(\theta)} \left(\frac{n_{sample}}{n_{toluene}}\right)^2 R_{toluene} \quad (3\text{-}3)$$

where n_{sample} and $n_{toluene}$ are the measured sample refractive index and the toluene refractive index respectively, and R_{toluene} is the Rayleigh ratio of toluene at λ = 632.8 nm.

For DLS on the solutions with low polymer concentration (0.018-0.073%), the intensity auto-correlation data from multiple experimental runs were averaged to obtain the final intensity auto-correlation curves. The data processing methodology is summarised in Figure AI-5.

The way of fitting the data depended on the Na CMC concentration. As an example of the data fitting approaches, Figure 3-6 shows raw and processed intensity auto-correlation data for solutions of low (0.018-0.073%; Figures 3-6.A_1 and A_2), intermediate (0.18-0.37%; Figures 6.B_1 and B_2) and high (0.55-0.92%; Figures 3-6.C_1, C_2 and C_3) Na CMC concentrations. Figures 3-6.A_1, B_1 and C_1 show the intensity auto-correlation data of individual measurements at a given angle while Figures 3-6.A_2, B_2, C_2 and C_3 illustrate the fitting of these data sets (*i.e.* the averaged intensity auto-correlation data for Figure 3-6.A_2 and individual measurement data for all other Figures 3-6.B_2, C_2 and C_3). Eq. 3-4[13,38] could be used to fit all the intensity auto-correlation data, where *f*, *s* and *us* refer to the fast, slow and ultra-slow mode respectively, A_i is the amplitude of the mode *i*, β_i is the stretching coefficient of the mode *i* and $\tau_{e,i}$ is an effective relaxation time of the mode *i*. The average relaxation time τ_i of the mode *i* is linked to $\tau_{e,i}$ with $\tau_i = \frac{\tau_{e,i}}{\beta_i}\Gamma\left(\frac{1}{\beta_i}\right)$ where Γ is the gamma function.[13,38]

$$g^{(2)}(\tau) - 1 = \left[A_f e^{-\left(\frac{\tau}{\tau_f}\right)} + A_s e^{-\left(\frac{\tau}{\tau_{e,s}}\right)^{\beta_s}} + A_{us} e^{-\left(\frac{\tau}{\tau_{e,us}}\right)^{\beta_{us}}}\right]^2 \quad (3\text{-}4)$$

The fast mode could not be observed for the three least concentrated solutions (Figure 3-6.A_2), so here A_f was set to 0 and only the slow and the ultra-slow modes were fitted. For the high Na CMC concentrations, it was not possible to obtain a satisfactory fit with Eq. 3-4. Therefore, the contributions of the fast and the slow modes were determined using two different fits as detailed in Section AI-3.2 and Figure AI-5, and illustrated in Figures 3-6.C_2 and C_3.

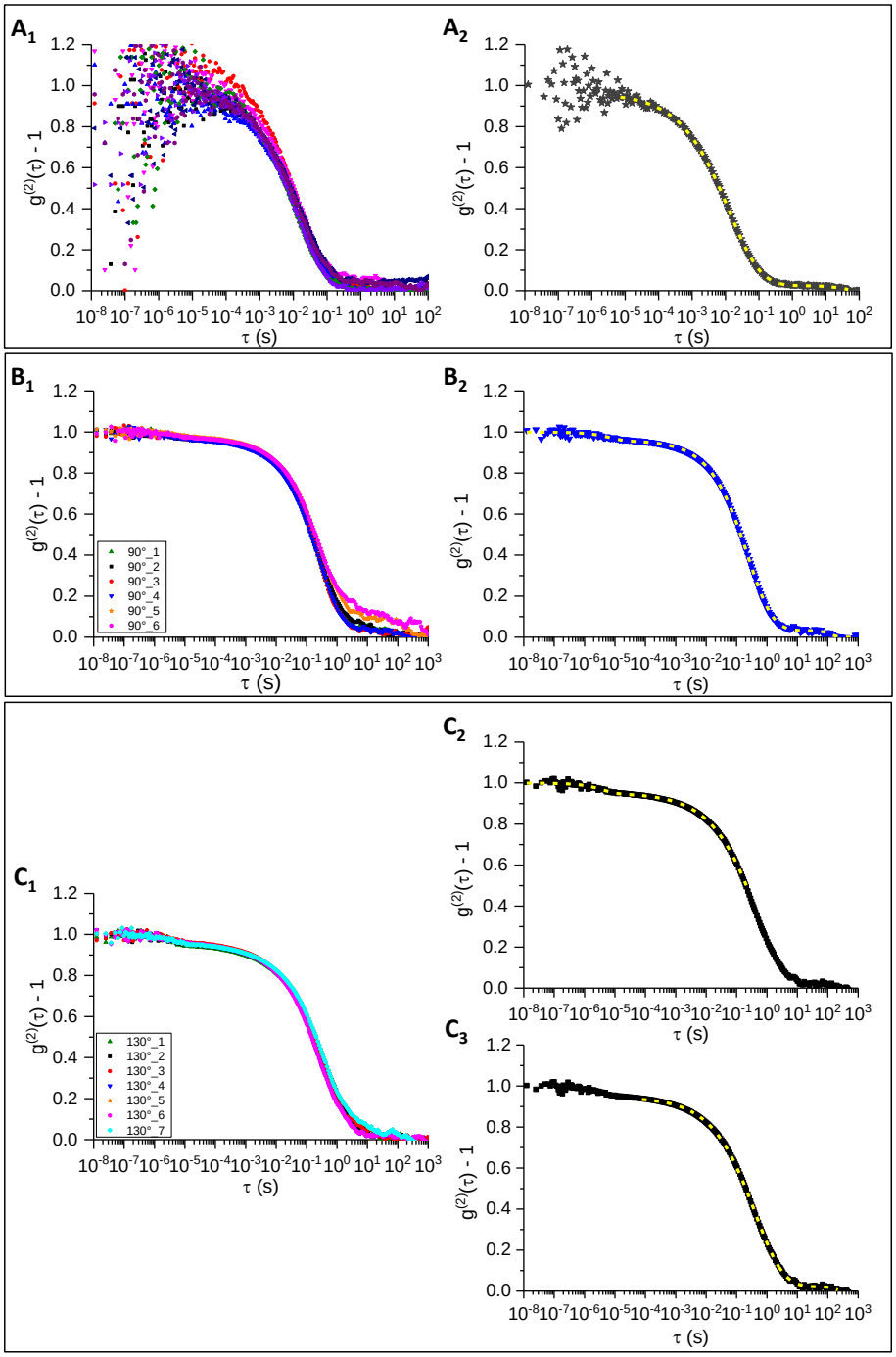

Figure 3-6: Measurement reproducibility and data processing for **A.** low Na CMC concentrations (0.073%); **B.** intermediate Na CMC concentrations (0.37%) and **C.** high Na CMC concentrations (0.55%). **A_1.** Individual intensity auto-correlation data at 130°; **A_2.** Averaged intensity auto-correlation data at 130° and corresponding fit (yellow dashed line); **B_1.** Individual intensity-autocorrelation data at 90°; **B_2.** Intensity auto-correlation data of measurement 4 and corresponding fit (yellow dashed line); **C_1.** Individual intensity auto-correlation data at 130°; **C_2.** Intensity auto-correlation data of measurement 2 and fit of the fast and the slow modes (yellow dashed line). **C_3.** Intensity auto-correlation data of measurement 2 and fit of the slow and the ultra-slow modes (yellow dashed line). Fit residuals given in Figure AI-6.

The residuals of the fits shown in Figure 3-6 are displayed in Figure AI-6 and demonstrate that the data are successfully fitted using the approach described above. Nonetheless, it is

worth noting that the fitting of the fast mode, when visible, was not as accurate as that of the slow mode; which is both due to its very low amplitude (see Section 3-3.5) and to generally noisy data at the relevant short lag times. The fast mode can however be adequately described using either a single or a stretched exponential with a stretching parameter β near 1. To restrict the number of fitting parameters, a single exponential was used in all fits, which corresponds to what is commonly used for this relaxation contribution in the literature.[21,32]

3-3.4. Static light scattering measurements

The excess Rayleigh ratio ΔR, calculated from SLS data, is plotted as a function of scattering wave-vector q in Figure 3-7.A. ΔR increases with increasing Na CMC concentration and decreases with increasing q, following an approximate power law relationship (see dashed lines in Figure 3-7.A). At low q and high $c_{Na\ CMC}$, the data points are more scattered and fall above the power law fits; the likely reason for this behaviour is the presence of the sample particulates which provide an additional scattering contribution that is most prominent at small scattering angles. The power law exponent values obtained from the data fitting are shown in Figure 3-7.B for samples of varying Na CMC concentrations. No significant concentration dependence of the power law exponents is observed, and their average value across the concentration range is estimated as -2.36 ± 0.05. Similar values have been observed for other polyelectrolytes such as PMPVP[31] (d_f = 2.2 ± 0.2) or poly(*N*-benzyl-2-vinylpyridinium bromide)[32] (d_f = 2.7). This power law exponent has sometimes been interpreted as the fractal dimension of the system. However, given the relatively small q-range and the fact that observing an approximate power law does not necessarily indicate a fractal behaviour, this interpretation must be considered with care. In addition, Zhang *et al.*[176] have shown that the value of the exponent for a polyelectrolyte can vary significantly depending on the experimental conditions (*e.g.* solvent nature) and suggested that the structure of the domains is not universal.

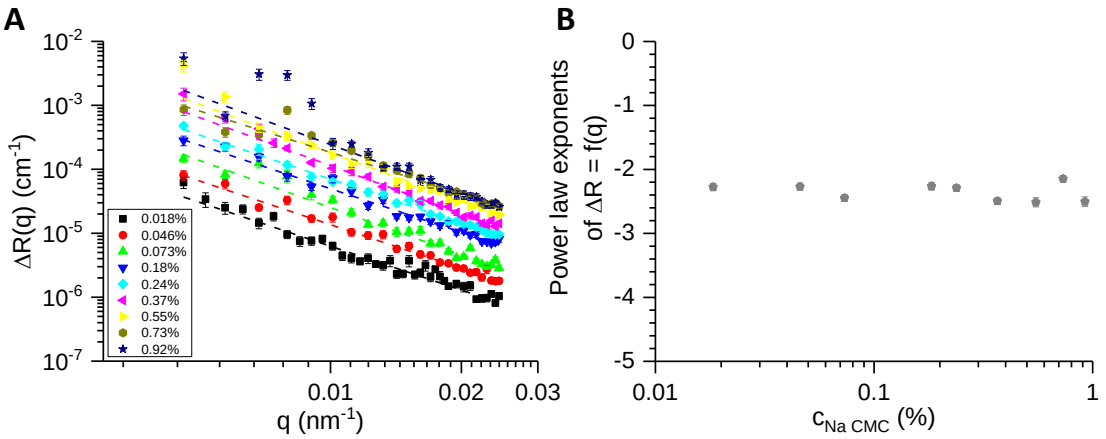

Figure 3-7: q- and $c_{Na\ CMC}$-dependence of the excess Rayleigh ratio ΔR. **A.** Excess Rayleigh ratio ΔR as a function of the scattering vector q for all the studied concentrations. The dashed lines are power law fits. **B.** Exponents of the power law fits shown on A.

To determine the excess Rayleigh ratio in the zero wave-vector limit $q = 0$, $\Delta R(0)$, Zimm plots ($[K.c_{Na\ CMC}/\Delta R] = f(q^2)$ where K is an optical contrast constant[40] (see Eq. AI-3)) were produced, for which an example is shown in Figure AI-9.A. However, for most of the studied solutions, the $q = 0$ intercepts were slightly negative, which indicates the presence of excess scattering at low q and thus the presence of large structures.[40] Berry ($[K.c_{Na\ CMC}/\Delta R]^{0.5} = f(q^2)$)[40] and Guinier ($\ln[K.c_{Na\ CMC}/\Delta R] = f(q^2)$)[40] plots were also considered as they might be more successful at linearizing the data at low q values[40] and examples are shown in Figure AI-9. As the linear part covered a wider range of q values for Berry plots as compared to Guinier plots, further calculations were performed with the data obtained from the Berry plots. Ioan *et al.*[38] obtained similar Berry plots for dextran solutions above c^*. It is also worth noting that, as shown in Section AI-3.5.3, the same behaviour was observed for the proportion of the excess Rayleigh ratio corresponding to the slow mode; which suggests that the observed behaviour of the total excess Rayleigh ratio is mainly driven by the domains responsible for the slow mode.

The obtained values of $\Delta R(0)$, as well as the values of ΔR at different angles, are plotted as a function of Na CMC concentration in Figure 3-8. For each angle, the data $\Delta R = f(c_{Na\ CMC})$ were fitted using power laws (dashed lines in Figure 3-8), and the power law exponents for all angles were found to be 0.91 ± 0.02. Sedlák and Amis obtained similar results, though their power law exponents were slightly above 1.[66]

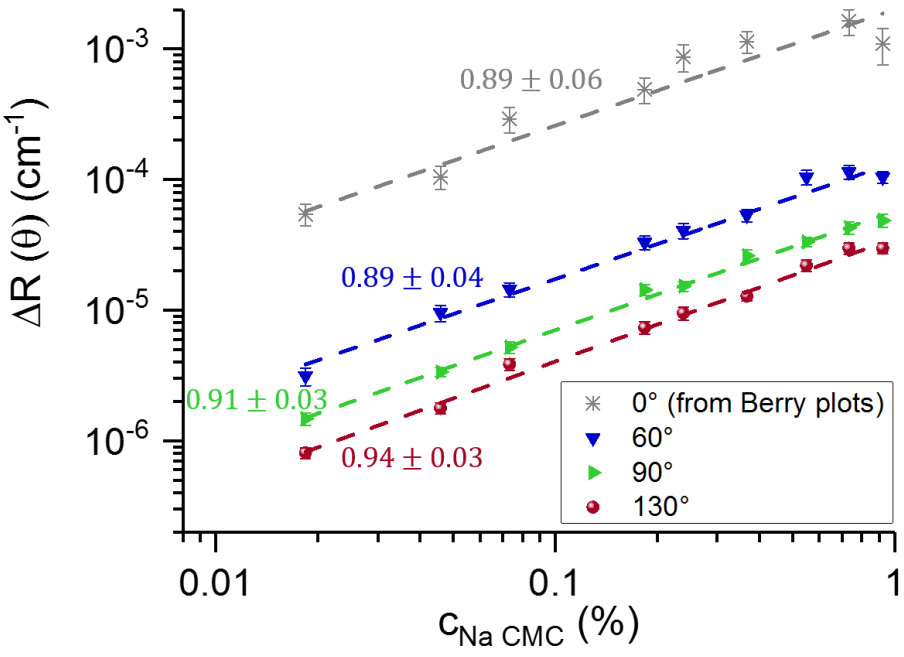

Figure 3-8: Concentration dependence of the excess Rayleigh ratio $\Delta R(\theta)$ at different angles. The values of the excess Rayleigh ratios at 0° (or $q = 0$) were obtained by linear extrapolation of the Berry plots at low q^2 values. Dashed lines are power law fits whose exponent values are provided next to each fit.

In conclusion, it is found that $\Delta R \sim q^{\alpha}$ across the investigated concentration range with a concentration-independent power law exponent $\alpha = -2.36 \pm 0.05$. It is also found that $\Delta R(\theta) \sim c_{Na\ CMC}{}^{\alpha'}$ with a consistent power law exponent $\alpha' \sim 0.9$. Thus, from SLS, no evidence for a change in structure across the investigated concentration range is found.

3-3.5. Dynamic light scattering measurements

Examples of normalised intensity auto-correlation data at different scattering angles for three solutions, illustrating low, intermediate and high Na CMC concentrations, are shown in Figure 3-9. For each solution, the characteristic relaxation time of the slow mode is shifted towards longer times as the scattering angle decreases.[32] However, for some data sets, the amplitude of the ultra-slow mode is significant; particularly for the two lowest scattering angles shown in Figure 3-9.B. To address this issue, the ultra-slow mode was accounted for in the fitting procedure, as described in Section 3-3.3 and Figure AI-5. Also, as discussed previously (Section 3-3.3), the fast mode cannot be observed for the least concentrated solutions, despite their concentrations being above the overlap concentration c^*, which is likely due to it being hidden in the noise observed at low lag times τ. When the fast mode can be observed (at higher concentrations), its relative amplitude (compared to the slow mode) increases for increasing scattering angles.[32] This

is explicitly shown in Figure AI-10 and agrees with the commonly observed behaviour for polyelectrolytes.[35,37] Figure AI-10, however, also shows that the relative amplitude of the fast mode is concentration-independent, which is different from the behaviour reported for some polyelectrolytes.[32,35,37,172]

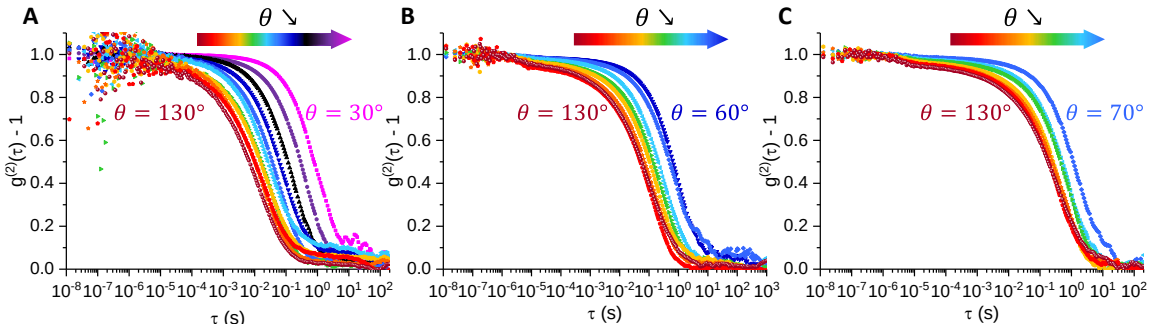

Figure 3-9: Normalised intensity auto-correlation data for a wide range of angles in steps of 10°, for three different Na CMC concentrations. Shown data are averaged intensity auto-correlation data for A, while they are angle-representative data for B and C. **A.** 0.073% Na CMC solution (low concentration range). **B.** 0.37% Na CMC solution (intermediate concentration range). **C.** 0.55% Na CMC (high concentration range).

Intensity auto-correlation data for each solution are compared at three given scattering angles (60°, 90° and 130°) in Figure 3-10. The relaxation time of the fast mode is concentration-independent.[32,172] The relaxation time of the slow mode, conversely, increases across the concentration range.[32,172]

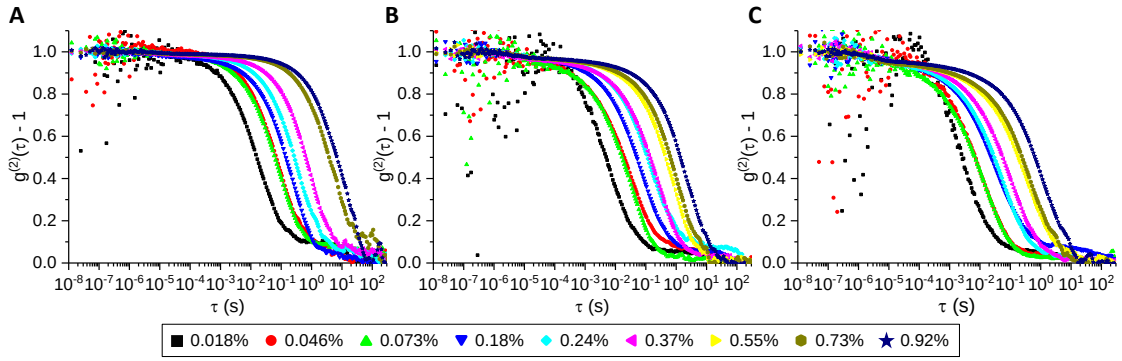

Figure 3-10: Normalised intensity auto-correlation data over the full range of concentrations at three different scattering angles. The data are averaged intensity auto-correlation data for 0.018, 0.046 and 0.073% Na CMC, while they are angle-representative curves for all the other Na CMC concentrations. **A.** 60°. **B.** 90°. **C.** 130°.

Ultra-slow mode

The ultra-slow mode is characterised by a long relaxation time and was present in all solutions at all scattering angles. Moreover, neither filtration nor centrifugation were able to remove this decay to a significant degree (see Section 3-3.3). As mentioned in Section 3-3.3, the presence of particulates in the Na CMC solutions (see Figure 3-1) could

explain the presence of the ultra-slow mode. The size of the smallest particulates determined by optical microscopy (Figure 3-1.C) is in the range of 1-10 μm, but difficulty in determining the size using optical microscopy made exact size determination difficult (see Section 3-3.1). While the smallest particulates could pass through the glass filter (pore size: 1.0-1.6 μm), some larger particulates may also go through if they have the ability to deform and change shape during filtration. Assuming the diffusion of these 1-10 μm-diameter particulates solution is Brownian in the 0.018% Na CMC solution and the viscosity they experience is that of the solution (see Eq. 3-7), the corresponding relaxation times at a scattering angle of 90° would be in the range of 0.09-0.9 s, while they would be in the range of 12-120 s for the 0.73% Na CMC solution under the same hypotheses. For both Na CMC concentrations, these relaxation times are longer than the relaxation times of the slow mode, but smaller than those observed for the ultra-slow mode (Figure 3-10.B). The assumptions behind this simple argument, including simple Brownian motion, a spherical particle shape and the fact that the particulates experience the viscosity of the solution are most unlikely to be all true. Even more likely, the strong contribution to the resulting scattering of the largest particulates, such as the fibre shown in Figure 3-1.A, would, in effect, hide the contribution from smaller particulates, and result in the very long observed relaxation times.

The amplitude of the ultra-slow mode was typically higher for lower Na CMC concentrations (see Figure 3-10), which is reasonable since, at low Na CMC concentrations, the scattering of the Na CMC solutions themselves would be very weak and the particulates would thus be observed to a greater degree. In addition, these solutions have lower viscosities, meaning that particulates would move faster and their scattering is more likely to be detected within the set acquisition time. Moreover, the values of the ultra-slow mode fitting parameters vary significantly between repeat measurements, which strongly suggests that the ultra-slow mode relaxation time is too long compared with measurement durations to collect statistically reliable data for this mode. Thus, the fitting of the ultra-slow mode was only used to effectively remove its contribution from the results of the two other modes, and the corresponding fitting parameters have not been included.

Fast mode

The contribution of the fast mode to the total excess Rayleigh ratio ΔR_f (called fast mode amplitude by Sedlák[80]) is q-independent within experimental error as shown in

Figure AI-11 and is proportional to the Na CMC concentration. A similar q-independence of ΔR_f was found for Na PSS in an organic solvent, *N*-methylformamide, and in the presence of various amounts of NaCl[78] as well as for poly(acrylic acid) (PAA) in water.[76]

The q- and $c_{Na\ CMC}$-concentration dependences of the fast relaxation time τ_f are shown in Figure 3-11. The curves of $\tau_f = f(q)$ superimpose well within the experimental error for all the studied solutions, which confirms that the fast-mode is independent of Na CMC concentration (as discussed in relation to Figure 3-10). The q-dependent data can be fitted by a power law with an exponent value of 2.5 ± 0.3. This is close to the usually reported value of 2,[35,37] and characteristic for a diffusive process; this small discrepancy is thought to be due to the difficulties encountered in the fitting of the fast mode (see Section 3-3.3).

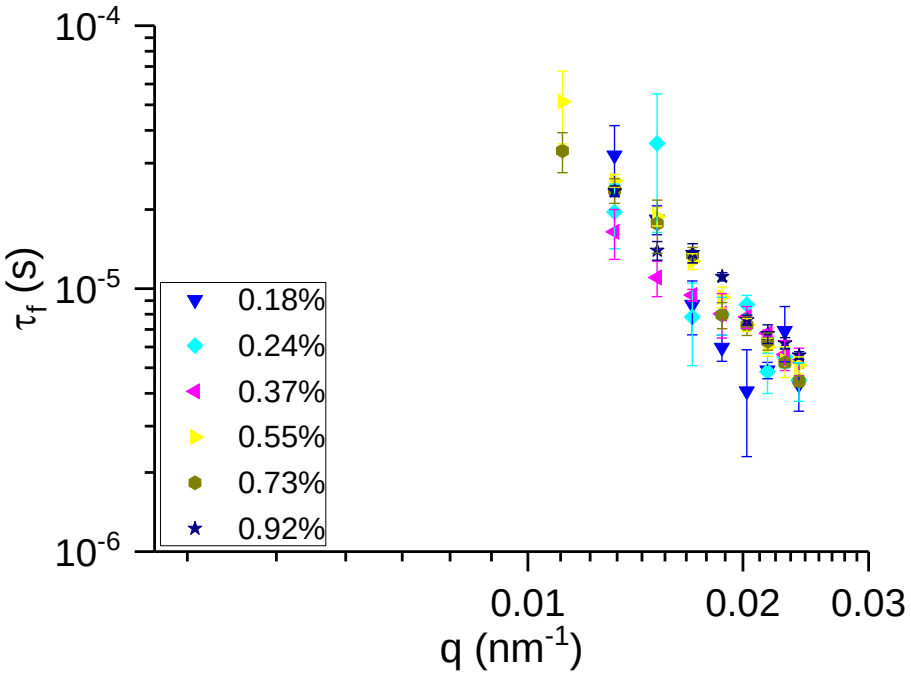

Figure 3-11: q- and $c_{Na\ CMC}$-dependences of the fast mode. Fast relaxation time τ_f as a function of the scattering vector q for solution concentrations of 0.18% Na CMC and above. The curves were fitted with power laws which are not represented for clarity. The average exponent across all concentrations is -2.5 ± 0.3.

Considering the fast mode as a diffusive process, attempts were made to calculate the fast mode diffusion coefficient D_f. The different methods used are explained below and further illustrated in Figure AI-12. For each solution, the data $\tau_f^{-1} = f(q^2)$ were fitted using Eq. 3-5.

$$\tau_f^{-1} = A + D_f q^2 \qquad (3\text{-}5)$$

where A is the intercept of the linear curve and is either set to be free or set to 0. Eq. 3-5 with $A = 0$ is expected for simple diffusive behaviour[39,72] while Eq. 3-5 with $A \neq 0$

accounts for a small uncertainty in the determined values of τ_f (see Section 3-3.3). As shown in Figure 3-12, which displays the values of D_f obtained using different calculation methods, the two methods used to determine D_f lead to consistent results within the accuracy of the data. Two other calculation methods were also investigated: D_f values were computed at each angle with $D_f = \tau_f^{-1} q^{-2}$ (equivalent to Eq. 3-5 with $A = 0$)[33] before being fitted as a function of q^2 with Eq. 3-6 for $B = 0$ and $B \neq 0$.

$$D_f = D_f(q^2 = 0) + Bq^2 \quad (3\text{-}6)$$

The results of these calculations are also shown in Figure 3-12. The values of D_f obtained from all four calculation methods are close to each other and are of the same order of magnitude as those generally observed for other polyelectrolytes[33,84,171,176] (*i.e.* around 10^{-6} cm^2.s^{-1}). A value of D_f of $(3.1 \pm 0.2) \times 10^{-6}$ cm^2.s^{-1} is obtained using Eq. 3-5 with $A = 0$ and Eq. 3-6 with $B = 0$; which are the simplest methods and correspond to what is expected for diffusive behaviour.

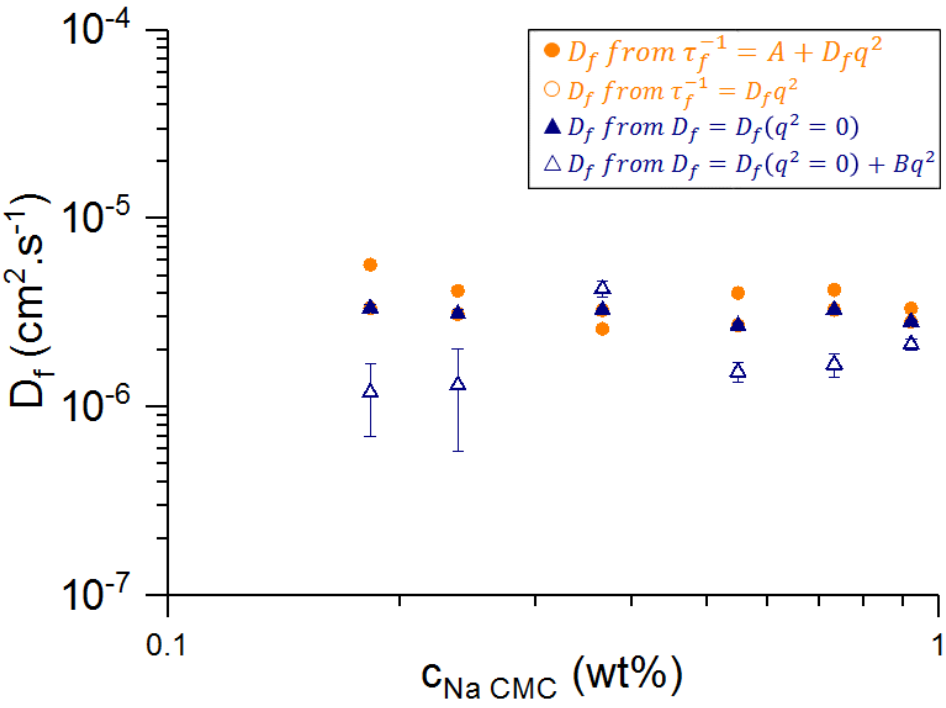

Figure 3-12: Fast mode diffusion coefficients as a function of Na CMC concentration. The calculation methods are explicitly shown in Figure AI-12.

Slow mode

The contribution of the slow mode to the total excess Rayleigh ratio ΔR_s (called slow mode amplitude by Sedlák)[80] is q-dependent, as shown in Figure AI-13, and is proportional to the Na CMC concentration. A q-dependence of ΔR_s has been observed for Na PSS in water without added salt[21] as well as in an organic solvent in the presence of

salt.[78] The q- and $c_{Na\,CMC}$-concentration dependences of the slow relaxation time τ_s are shown in Figure 3-13. It is found that as the Na CMC concentration is increased, the relaxation time τ_s also increases. The q- and $c_{Na\,CMC}$-concentration dependences of the stretching exponent β_s (see Eq. 3-4) are illustrated in the inset of Figure 3-13 for a few Na CMC concentrations. Within the accuracy of the measurements, β_s is independent of Na CMC concentration, but decreases with q. Its value is around 0.7; which is in agreement with the value found by Dogsa *et al.*[13] for Na CMC solutions of smaller DS and M_w, as well as with values usually found for polyelectrolyte solutions whose slow mode is successfully fitted with a stretched exponential.[37,38]

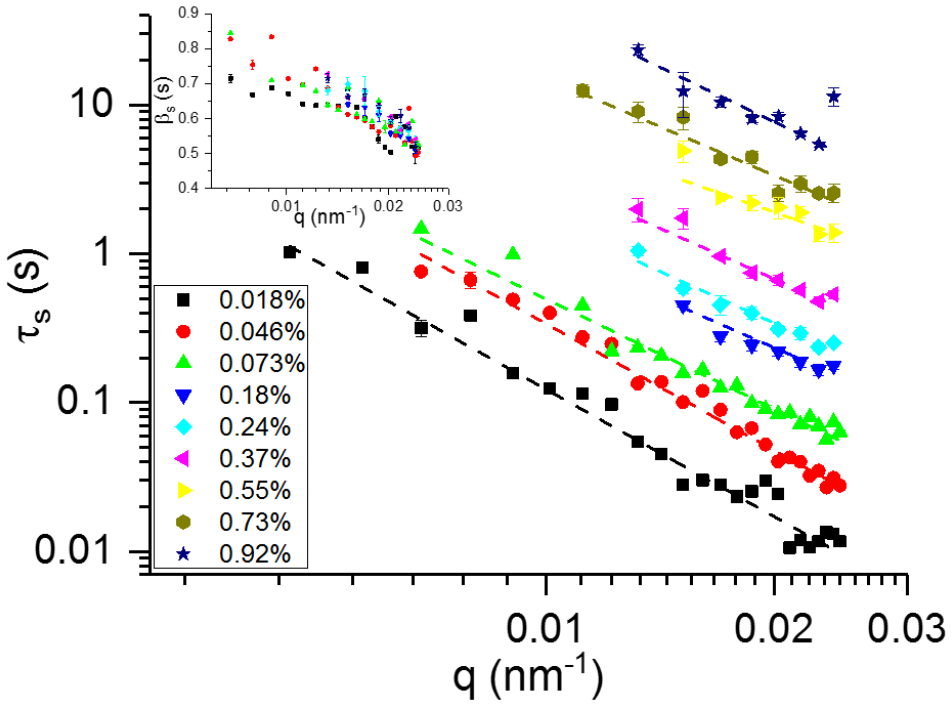

Figure 3-13: q- and $c_{Na\,CMC}$-dependence of the slow mode. Slow mode relaxation time τ_s as a function of the scattering vector q for all studied concentrations. Dashed lines are power law fits. The average exponent value across all concentrations is -2.4 ± 0.2. Exponent values are shown in Figure AI-14. Inset shows the stretching coefficient β_s as a function of q, for a few Na CMC concentrations.

The relationship between the slow mode relaxation time and Na CMC concentration is also shown in Figure 3-14.A, which presents τ_s at 90° scattering angle as a function of $c_{Na\,CMC}$ across the studied range of concentrations, as well as in Figure AI-15 which shows the concentration dependence of τ_s at two other scattering angles. Figures 3-13, 3-14.A and Figure AI-15 all confirm that including the ultra-slow mode in the fits is successful in removing its influence on the τ_s values. Figure 3-14.A also compares $\tau_s(90°)$ with the specific viscosity η_{sp} and shows that they exhibit a similar concentration dependence,

suggesting that the slow mode is related to the viscosity of the solutions across the studied concentration range. A similar result was found by Esquenet and Buhler[37] for high molecular weight xanthan and hyaluronan samples (average molecular weights of 4.2×10^6 and 2×10^6 g/mol respectively) in 0.1 M NaCl. In the present case, the *q*-dependence of the slow mode can be described using power laws, where the average value of power law exponents across all concentrations is -2.4 ± 0.2 (the exponent values for each studied concentrations are given in Figure AI-14). Similarly to the fast mode, the exponent is close to 2; thus suggesting that the slow mode is also related to a diffusive process. There is, however, a slight concentration dependence with greater values at low concentrations, likely due to the increased difficulty in determining τ_s for very dilute solutions and/or to the presence of additional relaxation contributions (*e.g.* relaxation contributions of internal modes). These effects are also illustrated in the data representation shown in Figure AI-16.

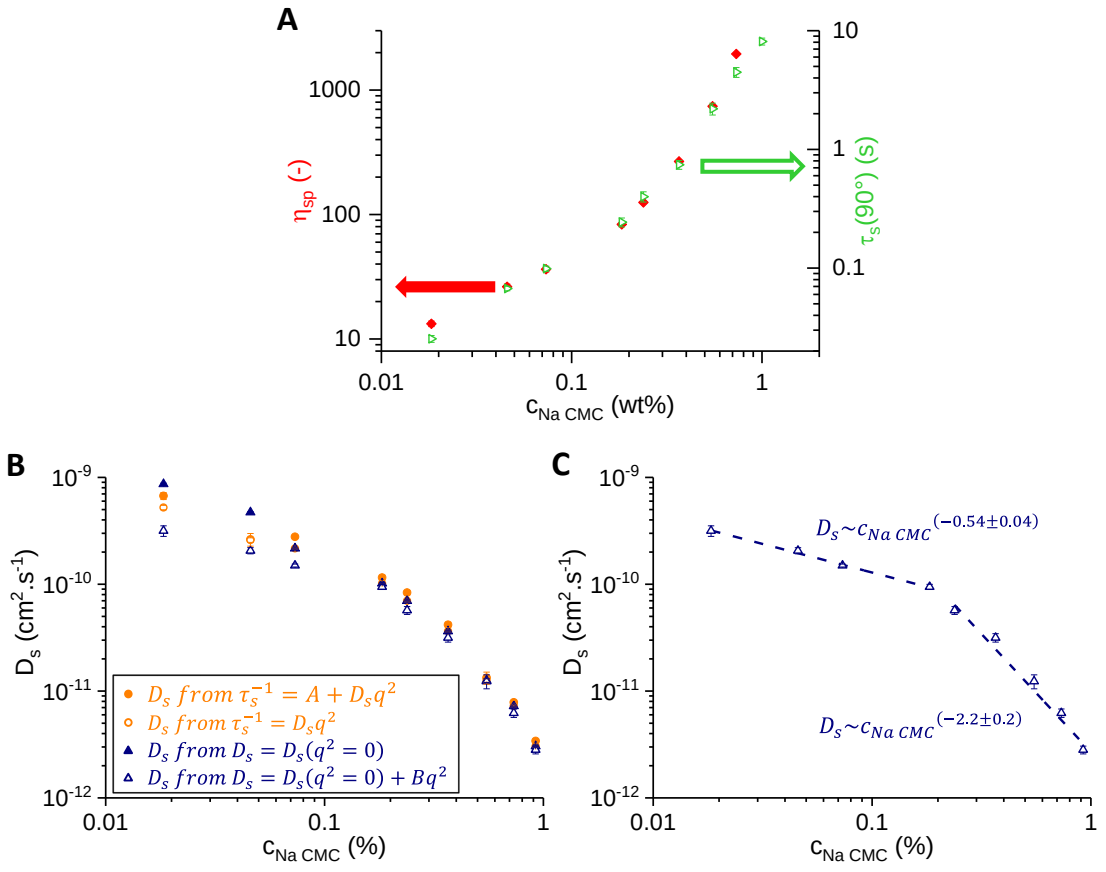

Figure 3-14: Polymer concentration dependences for the slow mode relaxation time τ_s and slow mode diffusion coefficient D_s. **A.** Concentration dependence of the slow mode relaxation time τ_s at 90° scattering angle and the specific viscosity. **B.** Concentration dependence of D_s for D_s values calculated with four methods (as shown for the fast mode). **C.** Concentration dependence of D_s, with the D_s values retained for further calculations (D_s values from $D_s = D_s(q^2 = 0) + Bq^2$). Dashed lines are the best power law fits of $D_s = f(c_{Na\ CMC})$.

The same methods as for the fast mode were used to calculate the diffusion coefficient D_s of the slow mode (see previous subsection for more details). Values of D_s obtained with the four methods are shown in Figure 3-14.B. For the most concentrated solutions, the D_s values are very close, regardless of the calculation method. For the three least concentrated solutions, the values are somewhat different from each other. This discrepancy is most likely due to the fact that the slow mode is not strictly q^2-dependent at these low concentrations (see Figures AI-16 and AI-17 illustrating the D_s calculation methods for a low and a high Na CMC concentrations respectively) which is usually attributed to the large size of the domains and to their polydispersity.[21,32]

$D_s = f(c_{Na\ CMC})$ suggests a change in the concentration behaviour for an intermediate concentration, where the behaviour can be approximately described by power laws at both low and high concentrations, as shown in Figure 3-14.C which displays the values of D_s obtained using Eq. 3-6. The equivalent graphs obtained for the three other calculation methods are shown in Figure AI-18, where the fitting parameters for all four methods are reported in Table AI-2. This type of behaviour has previously been observed in the literature for high molecular weight polyelectrolytes in salt-free solutions above c^*.[66,170] The power law exponent of the fit describing the low concentration region is -0.54 ± 0.04, which is in a similar range compared to the values of -0.35 and -0.7 obtained by Sedlák and co-workers obtained for Na PSS[66] and poly(methacrylic acid), respectively.[170] The power law exponent describing the high concentration region is -2.2 ± 0.2; which is much higher than the values of -0.83 and 1.4 found for the two previously cited polyelectrolytes.[66,170] It has however been shown that the value of the power law exponent υ of the relationship $D_s \sim c^{\nu}$ increases with the polymer molecular weight.[33]

The crossover concentration determined from the intercept of the two power laws for the present system is ~ 0.21% (as determined from the fits shown in Figure 3-14.C; the values obtained using the other methods are similar and can be found in Table AI-2; as for the crossover concentrations determined from rheology data (see Section 3-3.2), these concentrations are only estimates of where a change in behaviour occurs). Sedlák and Amis[66] found a similar crossover concentration in Na PSS solutions. They also observed that this crossover concentration does not correspond to c^{**} predicted by the version of the scaling laws for polyelectrolytes improved by Odijk.[66] The crossover concentration for the present system is close to the entanglement concentration c_e = 0.17%, as calculated using the scaling laws; so it is reasonable to assume that they both correspond to the onset

of entanglements. This is in agreement with the previously observed similarity in the behaviour of the specific viscosity and the slow mode relaxation time shown in Figure 3-14.A. The fact that the change in concentration behaviour of D_s *vs* $c_{Na\ CMC}$ is not observed for low molecular weight polymers[66,170] is consistent with this hypothesis, since low molecular weight polymer chains are too short to be entangled.

Using the values of D_s plotted in Figure 3-14.C (*i.e.* assuming the slow mode is diffusive), the apparent hydrodynamic radii $R_{H,app}$ of the domains were estimated using Eq. 3-7.

$$R_{H,app} = \frac{kT}{6\pi\eta D_s} \tag{3-7}$$

where k is the Boltzmann constant, T the temperature and η the solution viscosity. The obtained values of $R_{H,app}$ are plotted in Figure 3-15 together with the estimated values of the apparent radii of gyration of the domains $R_{g,app}$ obtained from the Berry plots of the excess Rayleigh ratio associated with the slow mode ΔR_s. Details on the determination of $R_{g,app}$ are provided in Section AI-3.5.3. $R_{g,app}$ is relatively independent of the Na CMC concentration and an average value of 200 ± 20 nm is estimated across the studied range of concentrations. This value is of the same order of magnitude as the one obtained for a ~ 900,000 g/mol hyaluronan sample in 0.1 M NaCl.[37] $R_{g,app}$ has also been found to be independent of the polyelectrolyte concentration above c^* for two hyaluronan samples of smaller M_w,[37] for PMPVP[31] and for chitosan in an electrolyte solution,[35] while they have been found to increase with the polyelectrolyte concentration for Na PSS.[22,32,68] It is worth noting that Buhler and Rinaudo[35] highlight the fact that R_g is likely to increase with the polyelectrolyte concentration and to be larger than $R_{g,app}$. The values of $R_{H,app}$ in the present study are of the same order of magnitude as $R_{g,app}$. It is found that the values decrease over the studied range of concentration; which is different from the results of Buhler and Rinaudo[35] who studied chitosan in the presence of a background electrolyte and found that $R_{H,app}$ instead increased with increasing chitosan concentration.

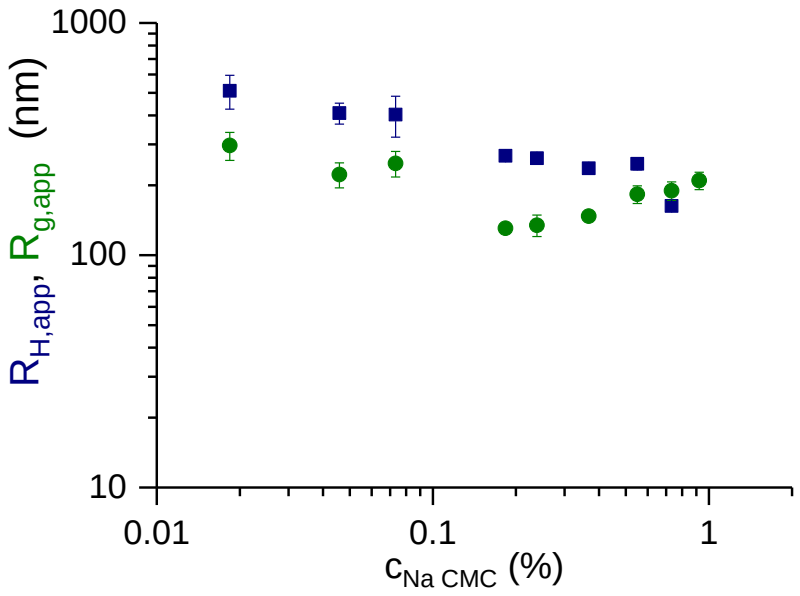

Figure 3-15: Apparent hydrodynamic radius $R_{H,app}$ (blue squares) and apparent radius of gyration $R_{g,app}$ (green circles) of the domains as a function of Na CMC concentration.

3-4. Conclusions

In this Chapter, the behaviour of Na CMC in aqueous solutions without added salt was investigated for a wide range of concentrations, using rheology and light scattering measurements.

For the studied concentration range, the concentration dependence of the specific viscosity could be described by the scaling theory for polyelectrolytes using a set of power laws. Three concentration regimes were identified: semi-dilute non-entangled, semi-dilute entangled and concentrated. The so-determined power law exponents slightly differed from the theoretically predicted values but were consistent with those previously found for Na CMC. Alternatively, the data could be described using a simple empirical equation which links two power law behaviours only including one crossover concentration. The success of this approach suggests that only the semi-dilute non-entangled and entangled regimes are observed.

To further test this, Na CMC solutions covering the same concentration range were investigated using both SLS and DLS. The excess Rayleigh ratio, as determined from SLS, was found to vary linearly with Na CMC concentration. For all the studied solutions, it followed a power law relationship with the scattering wave vector q and a power law exponent of -2.36 ± 0.05, which was independent of the Na CMC concentration. Three relaxation modes were observed in DLS measurements. The two fastest modes were

identified as the fast and slow relaxation modes commonly observed for polyelectrolytes. The third, and slowest mode, was attributed to poorly substituted undissolved cellulose fragments. As filtration (or centrifugation) did not sufficiently remove these fragments, and importantly did alter the solution behaviour, both data collection and processing were adapted to account for the presence of this mode; thus allowing the detailed LS characterisation to be performed on the original Na CMC solutions, which are relevant for industrial applications. The diffusion coefficient D_f of the fast relaxation mode was found to be concentration-independent and equal to $(3.1 \pm 0.2) \times 10^{-6}$ $cm^2.s^{-1}$. The relaxation time of the slow mode showed a similar crossover behaviour to that found for the specific viscosity. Interestingly, no such change in behaviour with Na CMC concentration was observed in the excess Rayleigh ratio, determined from static light scattering, suggesting that the origin of the observed behaviour mainly originates from a change in dynamics.

Chapter 4: Ultrasonication-induced changes in Sodium Carboxymethyl Cellulose (Na CMC) solutions characterised with rheology, Size Exclusion Chromatography (SEC) and Light Scattering (LS)

4-1. Introduction

Ultrasound is defined as high frequency sound-waves that are above the human hearing perception (*i.e.* above ~ 20 kHz).[43,44,157,158] Depending on their frequencies, they can be divided into two main classes:[43,44] (i) power ultrasound (also referred as destructive or high-intensity ultrasound) within the low frequency range (18-100 kHz[43] or 20 kHz-2 MHz[44] depending on references) and (ii) diagnostic ultrasound (also referred as destructive or low-intensity ultrasound) within the high frequency range (above 5-10 MHz[44]). The former, also called sonochemistry,[44,159] has been widely used to modify polymers,[43,44,159] where such modifications may be chemical and/or physical.[44,157,159] During sonication, cavitation occurs, corresponding to the creation of bubbles in the liquid subjected to sonication, where the size of the bubbles vary. Upon sonication, bubble sizes increase until a critical size is reached, whereupon the bubbles become unstable and collapse.[44,159] At this stage, both the local temperature and the local pressure are extremely high (*i.e.* ~ 5,000°C and 1,000 atm,[157] respectively), and the cooling rate following the collapse is very quick (*i.e.* about 10^{10} $K.s^{-1}$). These events are termed hot spots,[44,159] and may damage the polymer chains, creating highly reactive radical species and/or ions.[44]

The main mechanism attributed to polymer chain breakage is however not related to these hot spots, but to the high shear- and strain-rates created by cavitation, which typically cause effects on length-scales of micrometres, causing chain extension and scission.[44,157,159,160] Breakage usually occurs in the middle of the polymer chains as it is a structurally weak point, and/or where bonds are weaker.[44-46,159,161] Mechanically-induced scission only occurs for polymer chains whose molecular weight M_w is high enough,[43,159,160] and values around 30,000-40,000 g/mol have been found for this critical molecular weight.[159,160]

Upon sonication, mechanical degradation of polymer chains has been reported for a wide range of both synthetic polymers and biopolymers.[159,161] The solution viscosity is often

observed to decrease with sonication time, which may be due to the reduction in the size of the polymer chains. For pectin, a weakening of the shear-thinning behaviour at high shear-rates has been reported.[158] Investigations on carrageenan solutions at 23, 48 and 83 kHz showed a significant decrease in the shear-viscosity at 48 kHz only, suggesting that no degradation had occurred at either 23 or 83 kHz.[43] The decrease in the shear-viscosity was temporary,[43] and I propose that aggregates and/or polyion clusters usually observed in polyelectrolyte solutions could have been physically broken and would build-up again at rest. Such changes, rather than chain breakage would agree with results obtained for walnut proteins, where sonication did not induce any change in M_w but broke down protein aggregates.[157] It was suggested that physical bonds could have been broken, and such structural changes were responsible for changes in walnut protein properties such as water-solubility which was increased.[157] A Light Scattering (LS) study of hyaluronan solutions sonicated in a bath also suggested that polymer aggregates were broken down.[166] In that study, a single relaxation mode, attributed to the diffusion of polymer aggregates, was observed in LS. [166] The corresponding diffusion coefficient increased upon sonication time; the increase was very fast at the beginning of sonication and slowed down afterwards. After long sonication times, the authors suggested that polymer chains may also be broken, however to a small extent.[166]

Size Exclusion Chromatography (SEC) is a separation technique based on the volume of the objects present in a sample.[177-179] As the volume occupied by polymer chains varies with their molecular weight, it can be used to determine the molecular weight distribution of polymer samples.[177-179] It has thus been widely used in sonication studies to follow the breakage of polymer chains during sonication.[45,158-161] However, as highlighted in Section 2-2, the size of polyelectrolyte chains not only varies with M_w, but also with the polyelectrolyte concentration and with salt addition. Hence, great care needs to be exercised to measure the molecular weight of polyelectrolytes properly. Detailed explanations will be provided in Section 4-2.2.3, where the methods are explained.

SEC has also been widely used to investigate the presence of protein aggregates and aggregation phenomena,[180-184] especially in the pharmaceutical field, where the presence of aggregates in drugs can cause serious effects in patients.[180,181] LS detectors are often used as detectors to detect the compounds after they have been separated as well as to determine their size and study their conformation.[180,181,183] However, as already mentioned above, samples need to be diluted in an appropriate solvent for SEC

measurements, which may affect the aggregates. Moreover, aggregates may interact with the chromatographic column, leading to unreliable determination of their size and conformation.[185] Hence, it has been advised to use other techniques such as LS measurements on bulk solutions to assess the reliability of the obtained SEC data.[181,183,184]

The previous Dynamic Light Scattering (DLS) investigations of salt-free Na CMC solutions shown in Chapter 3 highlighted the presence of a fast and a slow relaxation mode, as typically reported for polyelectrolytes within the semi-dilute regime (see Section 2-2.3.2). A weak third mode exhibiting an even slower relaxation was also found. Usually, purification methods were not successful at fully removing this mode, and also significantly altered the slow relaxation mode. Thus, data collection and processing were adapted to take account of the presence of this ultra-slow mode, and the measurements were thus performed on original Na CMC solutions. It was also demonstrated that, in the semi-dilute regime, the slow relaxation mode observed in DLS measurements, and the specific viscosity of Na CMC solutions, were both probing solution dynamics characterised by the transition from non-entangled to entangled concentration regimes and Static Light Scattering (SLS) measurements did not probe any qualitative change in the solution structure across the same concentration range.

The origin of the slow relaxation mode observed in LS is not well understood (see Section 2-2.3.4). Sonicating Na CMC solutions allowed getting new insights regarding the nature of the slow relaxation mode and its relationship to the rheological behaviour of Na CMC solutions. To study the effect of sonication on Na CMC solutions, rheology, SEC and LS measurements were combined. The elution behaviour of Na CMC samples during SEC measurements was first investigated to check the reliability of the method and its appropriateness to determine the molecular weight distribution of the polymer chains in the samples. The influence of sonication on Na CMC solutions prepared at three different concentrations was then investigated using both rheology and light scattering. Subsequently, both SEC and LS on dilute solutions were used to assess whether the polymer chains were broken upon sonication. Finally, additional investigations including salt addition, ageing and solution heating were performed to further elucidate the effect of sonication on Na CMC solution in general as well as on the behaviour of the slow relaxation mode in particular.

4-2. Materials and methods

4-2.1. Materials

The investigated sample was identical to the one studied in Chapter 3 (see Section 3-2.1 for details). Also, deionised water obtained from the same water stations was used for all experiments (see Section 3-2.1).

Sodium nitrate ($NaNO_3$; reference: S5022-1kg), sodium phosphate (NaH_2PO_4, $2H_2O$; reference: 71500-1kg), sodium azide (NaN_3; references: 71289-5g and 71289-50g), sodium chloride (NaCl; reference: S7653-1kg), all from Sigma, as well as isopropanol from VWR® Chemicals (AnalaR NORMAPUR® ACS, Reag. Ph. Eur. analytical reagent; reference: 20842.323), and sodium hydroxide from Merck (NaOH; reference: 1.06498.1000) were used.

An Acrylamide Tertiary Butyl Sulfonic Acid-Polyacrylamide *co*-polymer (*co*-ATBS-PAM) of high molecular weight (~ 10^7 g/mol) and high anionicity from SNF (reference: Flopaam AN 132 VHM) was used to determine the void volume of the SEC column.

4-2.2. Methods

4-2.2.1. Sample preparation

Na CMC solutions were prepared in conical flasks by batches of 150 g. The required amount of Na CMC powder was added to the appropriate amount of DI water under magnetic stirring at 850 rpm. Stirring was pursued for 2 h and the solutions were stored overnight before further use. Na CMC concentrations are given in %*wt*. They take into account the Na CMC powder moisture content.

Batches were divided in 40 mL vials. 21 g of the stock solution was poured in each vial for ultrasonication. Samples from the same batch were sonicated simultaneously in a Fisherbrand FB11002 sonication bath (frequency: 40 kHz; power: 140 W; internal dimensions (width × depth × height): 137 × 240 × 100 mm;[186] Fisherbrand) containing ~ 1.1 L of DI water for various amounts of time. The bath temperature was maintained below 50°C using ice packs which were changed every 30 min. A preliminary study had shown that maintaining the Na CMC solutions at temperatures below 60°C for 1 h did not have any influence on their rheological behaviour (data not shown). Changes in the

Na CMC solution behaviour after ultrasonication are thus expected to be caused by ultrasonication rather than to the solution being heated to temperatures up to 50°C.

0.18% Na CMC samples of 21 g were also sonicated at an amplitude of 40% with a Fisherbrand 505 Sonic Dismembrator (frequency: 20 kHz; power: 500 W; Fisherbrand) equipped with a 6.3 mm diameter microtip probe. To prevent solutions from heating up, sonication was performed in a pulsing rather than in a continuous way, alternating 30 s sonication periods with 30 s breaks. Moreover, solutions had been placed in the fridge before sonication and were placed in an ice bath which had a temperature below 20°C at all times.

45 g of 0.18% Na CMC were heated at 80°C in a round-bottom flask equipped with a refrigerant for 1 h (the solutions were effectively heated up for 1 h 20 min as the time was counted when the solution temperature reached 80°C). The solutions were then cooled to room temperature in an ice bath, and the solution masses were checked. The mass loss was about 0.2%, and an appropriate amount of DI water was added to compensate for this.

All experimental conditions were tested in duplicate, *i.e.* on two separate solutions coming from different batches.

4-2.2.2. pH measurements

pH measurements were performed with an Orion™ 8102BNUWP ROSS Ultra™ pH electrode (ThermoFisher Scientific) connected to an Orion Star™ A321 portable pH-meter (ThermoFisher Scientific). The electrode was calibrated with the pH 4.01, 7.00 and 10.01 buffers provided in the Orion™ ROSS™ All-in-One™ pH buffer kit (ThermoFisher Scientific). The temperature of the buffers and the eluent was monitored with a Fisherbrand™ Traceable™ digital thermometer (Fisherbrand), and the measurements were performed under light magnetic stirring; the sample containers being isolated from the stirring plate by a piece of cardboard to prevent the temperature from increasing.

4-2.2.3. Size Exclusion Chromatography measurements

The principle and precautions for polyelectrolytes

SEC separates compounds according to their size, from which M_w can be estimated. Hence, to determine reliable M_w distributions, the polymer chains should not interact with

(i) each other (*i.e.* the concentration must be low enough so that the solutions belong to the dilute regime, but high enough to be detected by the detector placed after the column), (ii) the eluent or (iii) the packing inside the column. Solutions should also be free from aggregates, though care must be exercised during filtration so that no significant amount of polymer is removed. As explained within Section 2-2.1, in the dilute regime, the size of polyelectrolyte chains in salt-free solutions changes with polyelectrolyte concentration. Indeed, as the polyelectrolyte concentration increases, the chains become less and less extended to minimise repulsive interactions between similarly charged chains. To measure reliable sizes, salt must be added so that the charges alongside the chains are screened. Finally, according to Hoogendam *et al.*,[107] preparing Na CMC solutions in water first, and diluting them afterwards with a salt solution at appropriate salt concentration, minimises aggregate formation.

The size exclusion chromatograph used for these experiments was only available for a limited period of time and under restricted use. Hence, whenever possible, preliminary LS measurements were performed prior to SEC measurements to check the conditions required to collect reliable data were met (see discussion in the paragraph above). Table 4-1 summarises these conditions and indicates how they were checked in the present study. It also provides more details on some unwanted phenomena that can occur during SEC measurements and lead to biased results.

Table 4-1: Summary of the parameters of importance to collect reliable SEC data for polyelectrolyte systems and proposed experiments to ensure SEC data reliability.

Parameters	Proposed experiments	Objectives/hypotheses	Technique
Eluent type	Compare the chosen eluent with NaCl	Results should be the same indicating polymer chain conformation is similar in both solvents	LS
Eluent concentration	Try different salt concentrations	Salt concentration needs to be high enough so that all the charges on the polymer chains are screened[177]	LS
Polymer concentration	Try different polymer concentrations	Polymer concentration needs to be: - Low enough so that the solution concentration belongs to the dilute regime of concentrations, meaning that the polymer chains	LS SEC

		do not interact with each other (otherwise, their hydrodynamic volume will be smaller and the 'domains' usually observed for polyelectrolyte solutions could be present) - High enough so that the polymer chains can be detected - Not too high to avoid overloading effects, adsorption on the column packing (favoured at low salt concentrations due to possible electrostatic interactions and at high salt concentrations as hydrophobic interactions appear; hydrogen bonding can also occur), shear-scission of the polymer chains in the column (occurs especially at high flow rates and for high molecular weight polymers), viscosity fingering effect (when the viscosity of the injected sample is significantly higher than the one of the eluent, local viscosities are different; fractions of the samples are retained for longer periods of time in the column and appear smaller than they truly are)[177,178]	
Injection volume	Try different injection volumes	The elution volume should not vary with the volume of sample injected in the size exclusion chromatograph	SEC
Filtration	Compare a non-filtered sample with samples filtered through different pore-size membranes	Filtration should remove both impurities and dust but not the polymer itself	LS

Method

The eluent used for SEC measurements was a 0.2 M $NaNO_3$, 0.01 M $NaNH_2PO_4$, 0.05% *w/v* NaN_3 (pH 7) solution as recommended by the column manufacturer[187] (NaN_3 was added to avoid bacterial growth). The eluent was prepared in 1 L volumetric flasks before being filtered through a 0.2-µm pore size nylon membrane using a Nalgene™ Rapid-Flow™ Sterile Disposable Filter Unit (reference: 164-0020; ThermoFisher Scientific). The pH was checked and adjusted to 7.0 ± 0.1 with a 1 M NaOH solution filtered through nylon filters (non-sterile Fisherbrand® syringe filters with 0.2 µm pore-size nylon membranes).

Unless otherwise specified, the samples for SEC measurements were prepared by diluting the Na CMC solutions to 0.14% with a 0.8 M $NaNO_3$, 0.04 M $NaNH_2PO_4$, 0.2% *w/v* NaN_3 solution, and with DI water for Na CMC solutions above 0.18% so that the background electrolyte concentrations correspond to the ones of the eluent. It is worth noting that it was a volume dilution; the Na CMC concentrations provided for the diluted solutions were estimated considering that the density of the initial Na CMC solutions is 1. The solutions were stirred for 30 min, rested for about 2 h and filtered through 0.8 µm pore size surfactant-free cellulose-acetate membranes (sterile Minisart™ NML syringe filters; Sartorius™) directly into 2 mL clear glass autosampler screw thread vials (Thermo Scientific).

The SEC measurements were performed with a 1260 Infinity II Multi-Detector GPC/SEC size exclusion chromatograph (Agilent Technologies) equipped with a guard column (PL aquagel-OH Guard, 8 µm, 50 × 7.5 mm; Agilent Technologies) and two columns (PL aquagel-OH MIXED-H, 8 µm, 7.5 × 300 mm; Agilent Technologies) mounted in series. Detection was carried out with a Differential Refractive Index (DRI) detector (1260 Infinity; Agilent Technologies) as well as a UV detector (1260 Infinity II; Agilent Technologies) set to 290 nm to allow the detection of oxidation products expected to contain carbonyl groups.[25] The temperature was set to 30°C, the flow rate was 1 mL/min and, unless otherwise specified, the injection volume was 100 µL. A set of polyethylene glycol/oxide (PEG/PEO) standards with M_p ranging from 106 to 1.5 × 10^6 g/mol[188] (EasiVial PEG/PEO calibration kit; reference: PL2080-0201; Agilent Technologies; the molecular weight data from the manufacturer certificate of analysis are provided in Table AII-3) were used for the calibration of the column, which was checked with a broad

dextran standard (M_w = 32,000 g/mol ± 20%; reference: PL2080-0700; Agilent Technologies).

Data analysis is described in details in Section 4-3.1.

4-2.2.4. Light scattering measurements

The samples for LS measurements were prepared by diluting the 0.14% solutions previously prepared for SEC measurements to 0.0069% with a 0.8 M $NaNO_3$, 0.04 M $NaNH_2PO_4$, 0.2% *w/v* NaN_3 solution and water so that the background electrolyte concentrations correspond to the ones of the eluent used for SEC. As for the solutions prepared for SEC, the dilution was performed per volume and the Na CMC concentrations were estimated considering that the density of the initial solutions was 1. They were stirred for 30 min, rested for at least 1 h, and filtered with 0.8 µm cellulose-acetate filters (26 mm Minisart® Syringe filters; Sartorius; 1.2 µm surfactant free cellulose-acetate filters from the same manufacturer were also used during the preliminary measurements) directly into the LS cells (rimless Pyrex® culture tubes 75 × 10 mm; cleaning process described in Section 3-2.2.3).

LS measurements were performed under the same conditions as the one detailed in Section 3-2.2.3, except that the laser had been replaced by a Diode-Pumped Solid State (DPSS) laser (λ = 660 nm, maximum power: 100 mW; Colbolt Flamenco™ 100; Cobolt).

4-2.2.5. Rheology measurements

Rheology measurements were performed at 25°C with a MCR301 rheometer (Anton-Paar) equipped with a bob (CC27) and cup geometry. The stress was varied logarithmically from 0.01 to 10 Pa (5 points/decade) to measure the steady-state viscosity. The equilibrium time Δt_{eq} and averaging time Δt_{av} were set to 200 s and 60 s respectively (see Section 3-2.2.2 for further details).

4-2.2.6. Fitting of the data

All fits were performed with Origin® using the Levenberg Marquardt algorithm with 'instrumental weights' or 'no weight'. The former weighing method was used for data sets where the experimental error was available, while the latter method was used for data sets where no experimental error was available.

4-3. Results and discussion

4-3.1. Checking the elution conditions

Preliminary DLS measurements were performed across a wide range of concentrations in the eluent considered for SEC measurements (*i.e.* in 0.2 M $NaNO_3$ and 0.01 M NaH_2PO_4) to determine the dilute regime, and the corresponding intensity auto-correlation data collected at 90° scattering angles are shown in Figure 4-1.A. The data from the 0.0009-0.045% Na CMC solutions superimpose on top of each other, while the data from the 0.09% and 0.18% Na CMC solutions begin to deviate from this behaviour and exhibit an additional slow relaxation mode. The data were best described by a sum of two exponentials (*i.e.* Eq. 3-4 with $A_{us} = 0$). The exponential function fitting the fastest relaxation mode was a single exponential (*i.e.* $\beta = 1$), while the one fitting the second relaxation mode was a stretched exponential (*i.e.* $0 < \beta < 1$). Such a description of the data suggests that the slow mode is present in all solutions.

Assuming a diffusive behaviour for the fast relaxation mode, the diffusion coefficients were calculated from the associated relaxation times and are given in Figure 4-1.B. The intensity auto-correlation data collected at 30° are displayed in Figure 4-1.C for a few of the studied concentrations, and confirm the presence of the slow relaxation mode. Similarly to 90°, the fast mode diffusion coefficients were determined and are also plotted in Figure 4-1.B. The values obtained at both angles are very close to each other, as expected for relaxation modes associated with diffusive behaviours (see Sections 2-2.3 and 3-3.5). The values of the apparent diffusion coefficient associated with the slow mode were also calculated for the 30° data and are shown in Figure 4-1.B. It is worth noting that the absence of data for D_s at a given concentration does not mean that there is no slow relaxation mode at that concentration, but is simply due to the fact that no data were collected at 30° for that concentration. As previously discussed, a slow mode was indeed observed from the intensity auto-correlation data collected at 90° for all concentrations.

Figure 4-1.D shows the SLS data for the same measured solutions. Like D_f and D_s (see Figure 4-1.B), a change in behaviour is observed at a concentration of about 0.02% Na CMC. This change in behaviour is similar to the one reported by Tanahatoe and Kuil[34,68] for sodium poly(styrene sulfonate) in NaCl, and may be assigned to the crossover concentration c_a, as defined in Section 2-2.3.2 and seen in Figure 2-15. The behaviour above this crossover concentration corresponds to that observed in the region marked

with a question mark in Figure 2-15 and for which the attribution to either the dilute or the semi-dilute regime has not been confirmed.

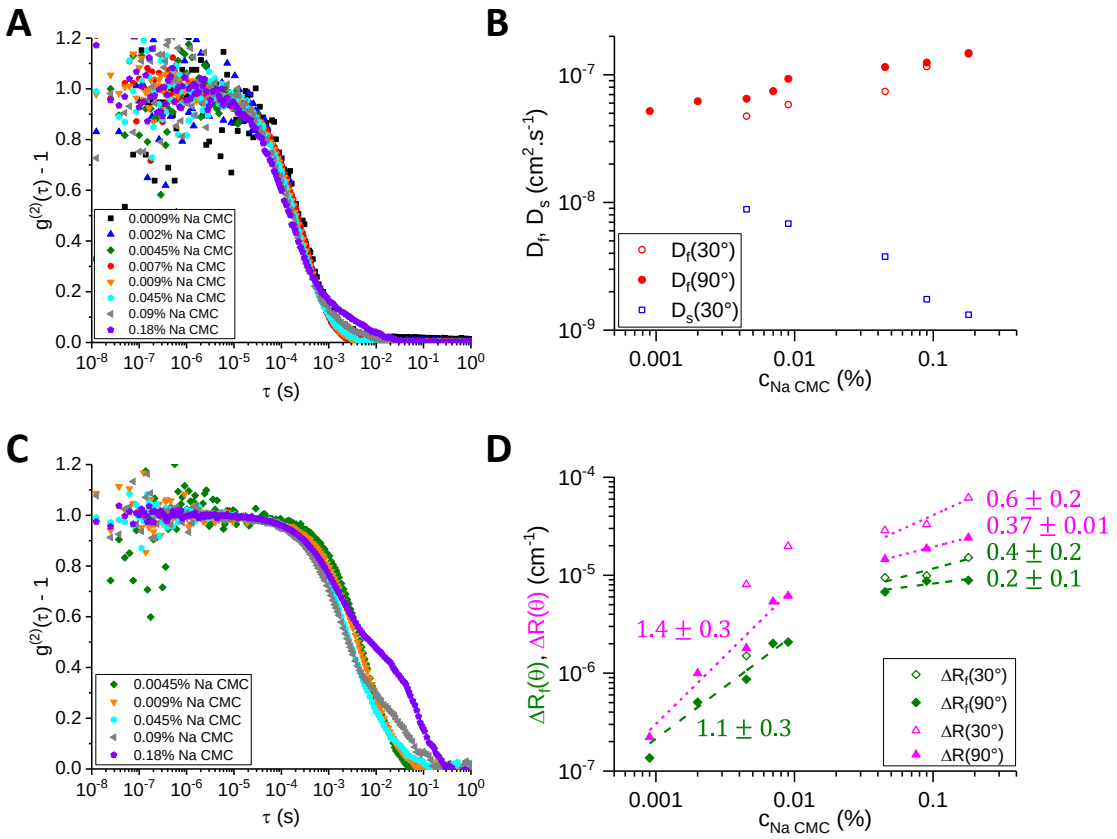

Figure 4-1: Light scattering of Na CMC solutions in 0.2 M $NaNO_3$ and 0.01 M NaH_2PO_4 and filtered with 0.8 µm pore size filters (apart from the 0.0045% Na CMC solution at 30° scattering angle which was not filtered). **A** & **C.** Intensity auto-correlation data from DLS measurements of Na CMC solutions at 90° and and 30° scattering angles, respectively. **B.** Diffusion coefficients of the fast and the slow relaxation modes, D_f and D_s respectively, calculated from the corresponding relaxation times, obtained from fitting the data shown in A and C, and assuming a diffusive behaviour. For the slow mode, the values of D_s are not shown at 90° as its amplitude at the lowest Na CMC concentrations was too small to obtain reliable values. A slow mode was observed for all the studied concentrations. Hence, the fact that no value is shown on the graph at a given concentration does not mean that there is no slow mode, but is simply due to the fact that no data were collected at 30° for that Na CMC concentration. **D.** Contribution of the fast mode to the excess Rayleigh ratio ΔR_f and total excess Rayleigh ratio ΔR at 30° and 90°, corresponding to the data shown in A and C. The dashed lines are power law fits of the data. The slopes are indicated next to the corresponding curves. The fitting parameters are provided in Table AII-1.

Below the crossover concentration, the solutions should thus belong to the dilute regime, where no slow mode is observed in DLS and an exponent of 1 is expected for the concentration dependence of the excess Rayleigh ratio $\Delta R(\theta)$ (see Section 2-2.3.3). The fact that a slow mode is still observed in this low concentration region could be due to the pore size of the filters not being small enough to fully remove the domains, although 0.8-µm pore size filters would most probably be required in a first instance to prevent the

filters from getting clogged by the non- or poorly substituted cellulose fragments present in the Na CMC solutions. Another explanation may be that the domains thought to be responsible for the presence of the slow mode need more time to 'dissolve' in the solutions upon dilution and salt addition. Moreover, the presence of the slow mode is most likely the reason why the power law exponent of the power law describing $\Delta R(\theta) = f(c_{Na\ CMC})$ is higher than the expected value of 1, as it would add a contribution to the scattering of the screened individual polyelectrolyte chains. The fact that the value of the power law exponent describing the concentration dependence of the contribution of the fast relaxation mode to the excess Rayleigh ratio $\Delta R_f(\theta)$ is 1.1 ± 0.3, thus equalling 1 within the experimental error, confirms the hypothesis of the contribution of the slow mode to the total scattering of the solution leading to a deviation from the expected $\Delta R(\theta) \sim c_{Na\ CMC}$ behaviour in the dilute regime.

The identified range of concentrations corresponding to the dilute regime is a bit higher than the one that can be estimated from the previous study of salt-free Na CMC solutions (see Section 3-3.2 and Table 3-1). Indeed, the overlap concentration c^* was estimated to be about 5.2×10^{-4}% Na CMC in absence of salt using the best power law fits to the viscosity data. It is generally observed that $c^*(salt) \approx 10c^*(salt\text{-}free)$[15,48] hence, the overlap concentration in fully screened Na CMC solutions is expected to be around 0.0052%. The discrepancy between this value and the value of 0.02% found here most probably comes from the high uncertainties associated with both values.

Other parameters such as filtration, eluent concentration and type were investigated using DLS, and the corresponding intensity auto-correlation data are shown in Figure AII-1. Figure AII-1.A gives the intensity auto-correlation data at 90° obtained for a 0.0045% Na CMC solution. In addition to the fast and the slow relaxation modes previously reported for the 0.0045% Na CMC solution in 0.2 M $NaNO_3$ and 0.01 M NaH_2PO_4 filtered with the 0.8 μm-pore size filters (see above discussion and Figure 4-1), the non-filtered 0.0045% Na CMC solution exhibits a third relaxation mode attributed to the presence of the particulates, as its relaxation time is of the same order of magnitude as the one usually observed for the ultra-slow mode found in salt-free solutions (see Section 3-3.5). Filters with pore sizes of 0.8 and 1.2 μm were both efficient at removing this third relaxation mode and had no significant effect on the fast main relaxation mode; suggesting that only a negligible fraction of the polymer had been retained by the filter. Measurements at smaller scattering angles (data not shown) showed

that the 1.2-µm pore-size filters were not as efficient as the 0.8-µm ones to remove the ultra-slow mode. Filters with smaller pore sizes were also tried (data not shown), but they were dismissed as they significantly modified the fast main relaxation mode. 0.8-µm pore size filters were thus selected for filtration prior to SEC and LS measurements on Na CMC solutions prepared in the eluent.

Doubling the eluent concentration or replacing it by a NaCl solution had no effect either on the solution behaviour as observed by DLS; showing that the selected eluent does not have any specific interactions with the polymer chains and that its concentration is high enough to screen the charges along the polymer chains. Figure AII-1.B confirms that the chosen eluent concentration would still be appropriate for higher Na CMC concentrations in terms of charge screening, but they would belong to a concentration regime where polymer chains experience strong repulsion as explained in the Section 2-2.3.2 and shown in Figure 4-1.D.

Based on these preliminary DLS experiments, the first Na CMC concentrations investigated with SEC measurements were 0.0009, 0.002, 0.0045 and 0.007%. The chromatograms obtained from the DRI detector are shown in Figure 4-2. Two peaks whose heights are not proportional to Na CMC concentration can be seen at high elution volumes. The elution peak related to the presently investigated high molecular Na CMC sample would be expected at much lower elution volumes (*i.e.* around 13-14 mL according to the elution behaviour of the PEG/PEO standards used to calibrate the column which have similar molecular weights as the one expected for the present Na CMC sample). Moreover, both their heights and areas should be proportional to Na CMC concentration as the DRI detector response is proportional to the solute concentration.[177]

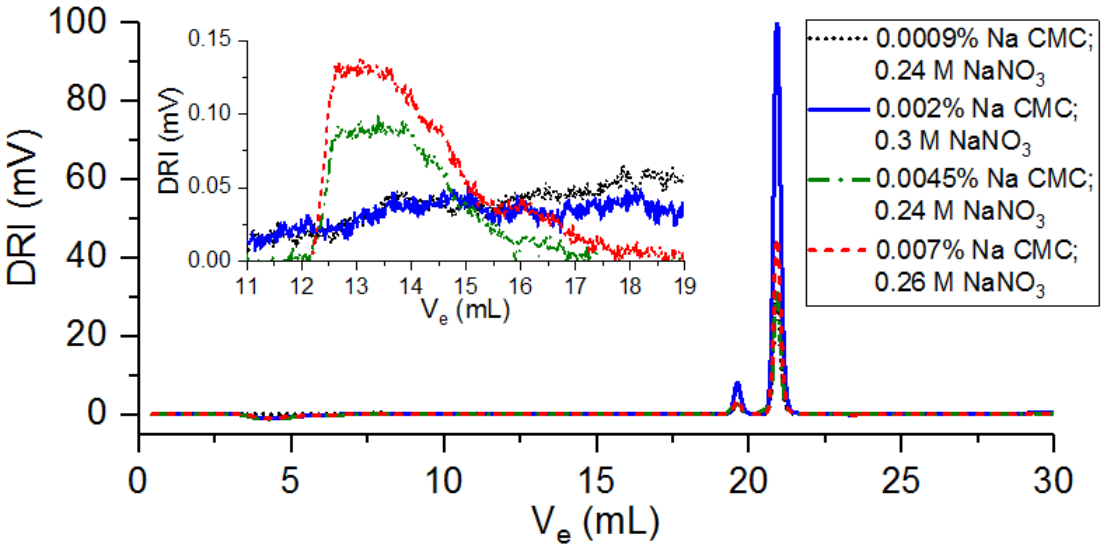

Figure 4-2: Size exclusion chromatogram obtained for the dilute Na CMC solutions studied by DLS (see Figure 4-1) showing the DRI signal as a function of the elution time. The injection volume was 50 µL. The inset is a zoom of the chromatogram for elution times ranging from 11 to 19 min. Due to a mistake during dilution, the background electrolyte concentrations were higher than that of the eluent, as reported in the legend of the Figure (only $NaNO_3$ concentrations are reported; NaH_2PO_4 and NaN_3 varied accordingly).

In the initial run, a mistake was made during dilution, and the background electrolyte concentrations did not match that of the eluent. The effective background electrolyte concentrations were thus calculated, and it can be noticed that the heights and areas of the two observed peaks seem to vary with the electrolyte concentration; suggesting that these peaks could be assigned to the salt peaks (also termed eluent peaks or solvent peaks) commonly observed in SEC.[177,189,190] Such peaks may be caused by the establishment of Donnan equilibria in the column.[177,190] They can also occur when there is a difference between the composition of the eluent and the composition of the background electrolyte of the sample; which was the case in the present study, even when the dilution was mistake-free. Indeed, neither the pH of the background electrolyte solution used to dilute the Na CMC solutions nor the pH of the actual SEC samples were adjusted to 7 contrary to the eluent. Furthermore, it has been reported that such peaks can be observed even if the background electrolyte solution and the eluent match each other perfectly.[190] It is worth noting that such peaks still appeared when a background electrolyte solution at 0.2 M $NaNO_3$ prepared from the 0.8 M $NaNO_3$, 0.04 M $NaNH_2PO_4$, 0.2% *w/v* NaN_3 solution used to dilute the Na CMC solutions was injected; confirming their assignment as salt peaks. They will therefore be ignored for the rest of the study.

The inset in Figure 4-2 is an enlargement of the chromatogram in the 11-19 mL region. The chromatograms of the two least concentrated solutions are noisy, while the chromatograms of the two most concentrated solutions each exhibit a peak, whose area and height increase with Na CMC concentration. Thus, these peaks are likely to be related to Na CMC. As they are just above the noise, quantification would not be reliable. The DRI detector sensitivity is known to be poor for low polymer concentrations.[191] The Na CMC concentration thus had to be increased to allow better detection with the available detectors. It however needs to be kept in mind that the investigated solutions will enter the semi-dilute concentration regime.

Solutions with higher Na CMC concentrations (*i.e.* 0.007-0.14% Na CMC) were injected, and the injected volume was also varied. No main peak was evident on the UV chromatograms (data not shown) apart from those attributed to the salt peaks (see discussion above). The wavelength of the UV detector was chosen to detect the presence of carbonyl groups resulting from oxidation of Na CMC polymer chains.[25] The absence of such peaks shows that the Na CMC chains have not undergone any oxidation process. The DRI chromatograms obtained for these more concentrated Na CMC solutions are shown in Figure 4-3.

Both the area and the height of the overall elution peak increase with the amount of Na CMC injected in the column. For the same mass of Na CMC injected (*e.g.* 50 µL of the 0.09% Na CMC solution *vs* 100 µL of the 0.045% Na CMC solution) the obtained chromatograms superimpose on top of each other; confirming the proportionality between the effective polymer concentration in the column and the response of the DRI detector. The chromatogram of a high molecular weight *co*-ATBS-PAM polymer is also presented in Figure 4-3. The average molecular weight of this polymer was about 10^7 g/mol, which is expected to be just beyond the upper limit of the column separation capabilities. This polymer is thus expected to be excluded from the column and to come out at the void volume V_0. The tailed shape of the obtained chromatogram confirms that the polymer was excluded;[192,193] it could thus be used to determine V_0. Such a shape is due to the transport of high M_w polymers in the other parts of the size exclusion chromatograph (*e.g.* junctions, capillary tubing, cell detectors) than the column.[192,193] The fluid velocity is the highest in the centre of the tubes, while it is very low near the walls. Thus, the polymer chains in the centre are more quickly transported throughout the tubes, while those near the walls need longer to go through; leading to the observed tailed peak.[192,193]

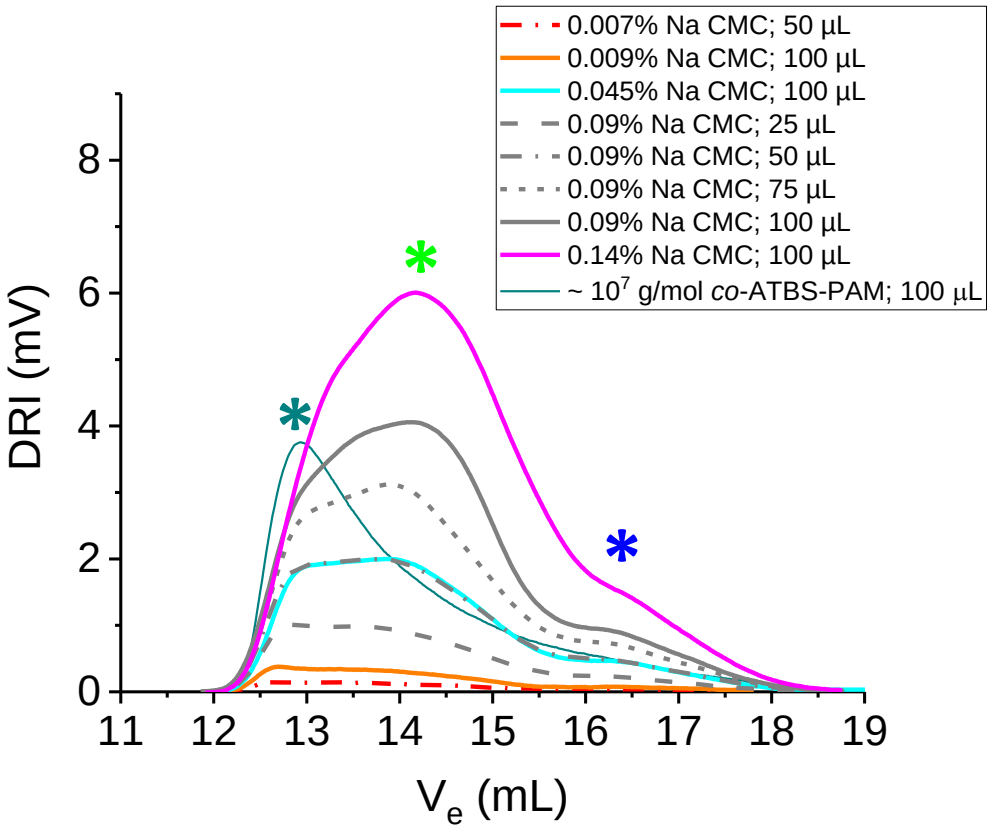

Figure 4-3: Influence of Na CMC concentration and injection volume on Na CMC elution behaviour. The elution behaviour of a high molecular weight *co*-ATBS-PAM used to determine the void volume V_0 of the column is also shown. * indicate the hypothetic positions of the three peaks the overall elution peaks could be the sum of.

The overall shape of the peak attributed to Na CMC suggests that it could be the sum of three peaks. The hypothetic positions of these suggested peaks are indicated by asterisks in Figure 4-3. Considering the chromatogram of the high M_w sample, the first of these three peaks (*i.e.* the one corresponding to the lowest elution volume) would most probably be related to 'objects' present in the Na CMC solutions being excluded from the column and eluting at the void volume. The shape of the *co*-ATBS-PAM sample peak suggests that an Exponentially Modified Gaussian (EMG or GaussMod in Origin software) model could be appropriate for the deconvolution of the overall Na CMC peak. This model is a Gaussian to which an exponential decay has been added, allowing the description of the tail exhibited by the peak; this model has been widely used to fit chromatographic peaks,[194] including peaks of compounds eluting at the void volume.[192] The equations of the Gaussian and the EMG models are provided as Eqs AII-1 and AII-2, respectively.

The fitting of the *co*-ATBS-PAM elution peak is shown in Figure AII-2 and the void volume V_0 is found to be 12.6 mL. An example of Na CMC peak deconvolution with the EMG model is shown in Figure 4-4.A. The sum of the three peaks provided by the model

is in agreement with the experimental data. The *co*-ATBS-PAM peak is also shown in the Figure and corresponds to the first peak obtained from the deconvolution; consistent with the hypothesis that the Na CMC solutions contain some large objects that are excluded from the column. Comparisons of the results obtained from deconvolution with the EMG and the Gaussian models are shown in Figure AII-3 for the same 0.14%. Na CMC solution as well as for a 0.009% Na CMC solution. Though the Gaussian model is successful at deconvoluting the overall peak for the 0.14% Na CMC solution, it does not work for the 0.009% Na CMC solution. Moreover, the residuals from fitting with the Gaussian model are always higher than the ones obtained from fitting with the EMG model.

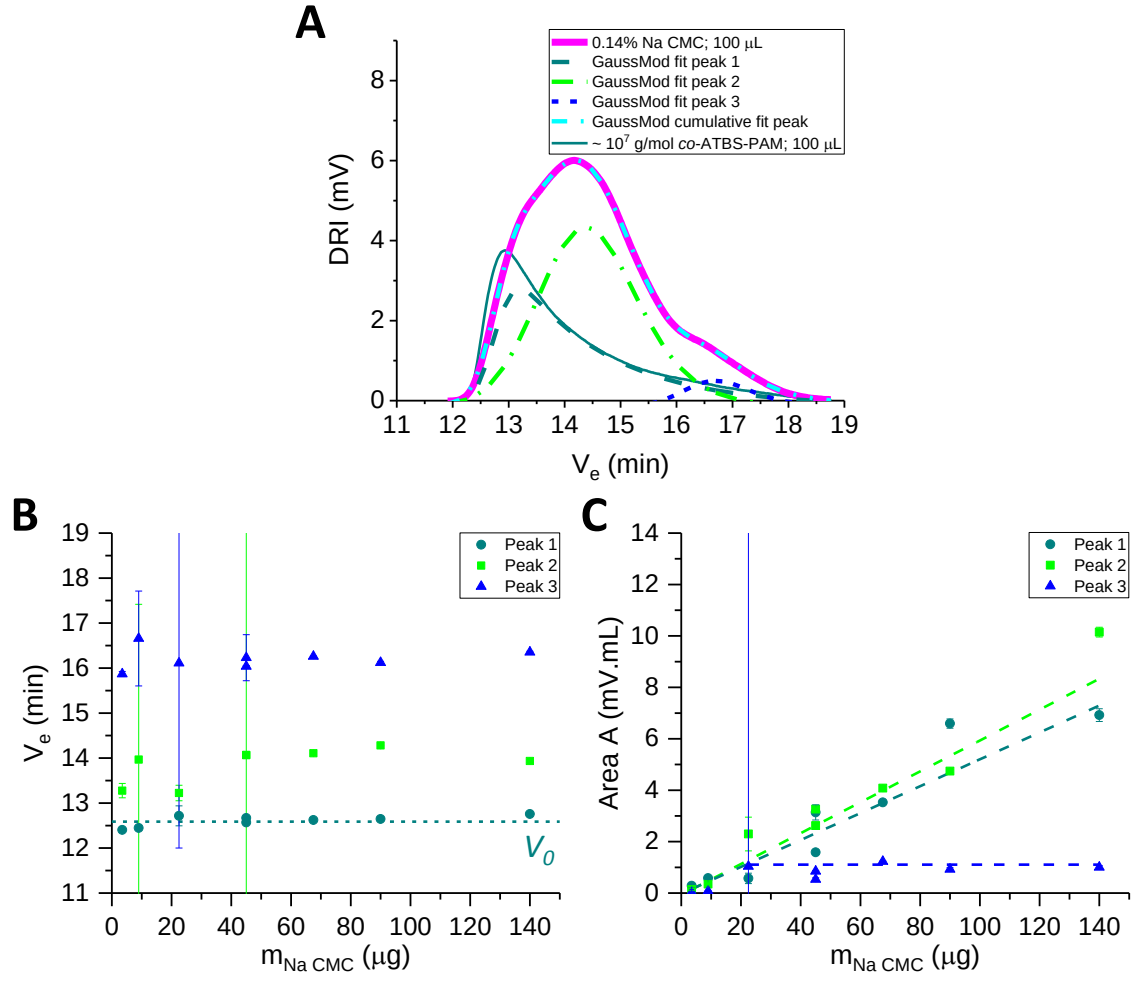

Figure 4-4: Deconvolution of SEC data. **A.** Example of peak deconvolution with the EMG model for the 0.14% Na CMC solution. The elution peak of the high molecular weight *co*-ATBS-PAM allowing the determination of the void volume is also shown. The fitting of this peak with the EMG model is shown in Figure AII-2. **B.** Elution volume of each of the peaks obtained from the EMG deconvolution as a function of the injected mass of Na CMC. The short dashed line represents the void volume V_0 calculated from the elution peak of the high molecular weight *co*-ATBS-PAM. **C.** Area under each of the peaks obtained from the EMG deconvolution as a function of the injected mass Na CMC. The dashed lines are fits of the data points to the zero- and one-degree order polynomial models for peaks 1 & 2 and peak 3 respectively. The fitting parameters are shown in Table AII-2. Errors bars shown on B and C are standard errors from the fits.

Two key parameters, the elution volume V_e and the peak area A, obtained from the deconvolution of the chromatograms presented in Figure 4-3 are shown as a function of the injected mass of Na CMC in Figures 4-4.B and C, respectively. The error bars represent the standard error from the fits and are sometimes fairly large. Indeed, peak deconvolution is complex, especially when the peaks are not clearly identifiable initially as is the case here. The elution volume of the first peak does not change with the injected amount of Na CMC, again consistent with its attribution to the void volume. The elution volume of the second peak seems to increase slightly with the injected amount of Na CMC, and may be attributed to the polyelectrolyte chains. Indeed, as discussed before about the LS and shown in Figure 4-1, most of the investigated concentrations are in the region where strong inter-chain interactions occur, so that the size of the chains is expected to decrease with the polyelectrolyte concentration (see Section 2-2), hence leading to higher elution volumes. It is worth noting that it is not possible to fully assess the polyion conformation in the column from the LS data as the solutions undergo further dilution in the eluent and interactions with column could take place. Figure 4-4.C shows that the areas of these first two peaks increase proportionally to the injected amount of Na CMC, as the experimental data can be described by first order polynomial models (the obtained fitting parameters are available in Table AII-2). This proportionality between the signal detector and the effective Na CMC concentration in the column is in agreement with the behaviour expected from a DRI detector, whose response is proportional to the solute concentration.[177]

The elution volume of the third peak does not change with the injected amount of Na CMC, while the associated area increases across the three lowest injected amounts of Na CMC and remains constant across the higher concentration range. This behaviour suggests that other phenomena in addition to exclusion or retention (usually termed 'non-size exclusion effects') occur in the column, such as adsorption on the column packing, shear-degradation and/or 'viscous fingering'.[177,178,189] Adsorption on the column packing is favoured when the eluent electrolyte concentration is too low and/or pH is not appropriate, as electrostatic interactions occur between charged groups on the column packing and the charged polymer chains.[177,178,180,185] Regarding the eluent concentration, it is unlikely that such electrostatic interactions occur in the present case. However, adsorption also occurs when the eluent electrolyte concentration is high, as hydrophobic interactions are enhanced and favour polyelectrolyte chain adsorption on the packing

throughout their hydrophobic parts (*e.g.* poorly substituted sections of Na CMC chains in the present case) and/or as hydrogen bonding can occur between the polyelectrolyte chains and the column packing.[177,178,180,185] The column used for this study was a PL aquagel-OH MIXED-H. Though the composition of the packing is kept confidential by the manufacturer, it is known that the packing possesses hydroxyl groups,[189,195] which could form hydrogen bonds with Na CMC.

Adsorption in the column can be temporary or definitive.[185] When adsorption is quickly reversible compared to the SEC run, it does not affect the polymer recovery, but leads to an increase in the elution volume, usually associated with peak broadening, skewing and/or tailing.[185] When it is irreversible, or when the reversibility occurs over longer timescales, the polymer recovery is uncomplete, but the elution peak related to the polymer chains which are not adsorbed is not affected.[185] In the present case, adsorption would mainly be rapidly reversible and lead to the observed broadening/tailing of the overall Na CMC elution peak. At low Na CMC concentrations, there would not be enough polymer chains to adsorb on all the available sites, while above a certain concentration, all the sites available for adsorption would be covered and the amount of adsorbed polymer would remain the same. It is worth noting that an increase in the column pressure was observed during the experiments, suggesting that longer-term adsorption could occur too.

Shear-degradation is particularly frequent for high molecular weight polymers at high concentrations and under high flow rates.[177,179,196,197] It arises from the fact that, due to the packing in the column, high shear-rates can be experienced by the polymer chains in the column; *e.g.* shear-rates as high as 0.8-1.6 × 10^4 s^{-1} were estimated for column packings with 5 μm-diameter particles.[197] The shear-rate in the column depends on the packing particle size, the flow rate and the column diameter.[179,197] High shear-rates may also be experienced in other parts of the instrument such as the injection valve, the capillary tubing connecting the injection valve to the column and the column to the detectors, and the column frits.[197] Using equations provided by Barth and Carlin[197] and by Cave *et al.*[179] (Eqs. AII-3 and AII-4 respectively), the shear-rates under the chromatographic conditions used in this study are estimated around 10^3 s^{-1} and 2-20 × 10^2 s^{-1} respectively. Whether shear-degradation occurs or not depends on the nature of the polymer, its molecular weight and the flow rate, while the polymer-concentration dependence of the shear-degradation varies from one polymer to another.[178,197] Shear-

degradation of polymers of similar (or even lower) molecular weight polymers has been observed under milder SEC conditions than the ones used here;[179,197] so the hypothesis of shear-degradation occurring in the column should not be rejected. It is worth noting that Yu *et al.*[196] showed that it is the shear-stress which controls the degradation rather than the shear-rate or the energy input. They proposed two mechanisms for shear-degradation: (i) stretching of the polymer chains under flow (usually observed at low polymer concentrations) and (ii) breakage where 'entanglements' are present in solutions (higher polymer concentrations, where polymer chain stretching is in effect limited due to the high polymer concentration) as 'entanglements' are regions of high energy.[196,197] It is worth noting that it is not clear from the literature whether the word 'entanglements' is used in the same way as it is defined by the scaling laws, and may also refer to interpenetrated chains in the semi-dilute non-entangled concentration regime. Using the zero-shear viscosity of a 0.18% Na CMC solution in 2 M NaCl, the upper estimation of the shear-rate in the column and the relationship $\eta = \sigma/\dot{\gamma}$ where η is the viscosity of the Na CMC solution, σ the shear-stress and and $\dot{\gamma}$ the shear-rate, an upper estimation of the shear-stress of 22 Pa is obtained. This value is significantly lower than the shear-stresses investigated by D'Almeida and Dias[198] for high M_w Na CMC solutions and which did not lead to Na CMC chain degradation.

'Viscous fingering' (also termed 'viscosity effect') occurs when the viscosities of the eluent and that of the injected solutions significantly differ from each other as the flow in the column is uneven, leading to presence of a side peak on the rear of the polymer peak.[177,189,197] It is often difficult to differentiate these three phenomena (*i.e.* adsorption, shear-degradation and viscous fingering), and they may be combined.[177,178] The present data do not allow to definitively establish the origin of this third peak.

Using polymer standards to calibrate the column with a DRI detector only allows a relative determination of the molecular weight of the polymers of unknown molecular weight.[177] Moreover, in the present case, the injected samples are in the semi-dilute regime; so the effective size of the polymer chains is going to be smaller than the one they are in in the dilute regime. Hence, looking at the calibration in terms of molecular weight would not provide much valuable information for the study of the present samples. However, in effect, SEC does not separate the compounds according to their molecular weight but to their hydrodynamic volume. The corresponding radius is the viscometric radius R_η, defined as given in Eq. 4-1. Note, often R_η is termed the hydrodynamic radius

in SEC literature,[177,179] but the term hydrodynamic radius will be kept for the radius determined with the Stokes-Einstein equation (Eq. 2-19) from DLS.

$$R_\eta = \left(\frac{3[\eta]M_w}{10N_A\pi}\right)^{1/3} \quad (4\text{-}1)$$

where $[\eta]$ is the polymer intrinsic viscosity, M_w its molecular weight and N_A is the Avogadro number.[55,177] The hydrodynamic radius R_H obtained from DLS measurements (also referred as Stokes radius) is given by Eq 2-19. In the data reported in literature, the values of R_η and R_H are usually close to each other; R_H being either identical to R_η or smaller.[55] It was thus attempted to attribute the SEC peaks based on the comparison of the polymer standard radii and the values of the hydrodynamic radii evaluated from DLS measurements.

As a first approximation, R_H was estimated for the polymer standards with the relationship established by Devanand and Selser[199] (Eq. 4-2) for PEO in water from the values of M_w determined by light scattering and provided by Agilent for the batch used in this study (values provided in Table AII-3).

$$R_H = 0.145{M_w}^{0.571} \quad (4\text{-}2)$$

The calculated values of R_H were plotted against the elution time measured by SEC for the high molecular weight PEG/PEO standards and are shown in Figure 4-5, where each data point corresponds to a polymer standard. The same data are presented in Figure AII-4.A where each data point is labelled with the corresponding polymer ID. Such data could be fitted to a third order polynomial model (black dashed line in Figure 4-5; model parameters provided in Table AII-4). It is worth noting that these values were estimated in water while the SEC measurements were performed in a 0.2 M $NaNO_3$, 0.01 M $NaNH_2PO_4$, 0.05% *w/v* NaN_3 eluent. The effective hydrodynamic radii of the PEG/PEO standards in the present experimental conditions are likely to differ slightly from these values. Figure AII-4 shows the previously calculated values of the hydrodynamic radius together with values of the viscometric radius calculated for different solvents from the molecular weight data provided by the PEG/PEO manufacturer (see Table AII-3). In agreement with the behaviour reported for most polymers,[55] in water, the estimated values of R_H are smaller than the ones of R_η. Compared to the values calculated in water, the values of R_η are unchanged in 0.02% NaN_3, while they are smaller in 0.1 N $NaNO_3$ and in 0.4 N NaOH, decreasing as the ionic strength increases. Considering all these calculations, the values of R_H of the PEO/PEG standards

for the present experimental conditions are thus very likely to be lower than the ones calculated in water and shown in Figure 4-5.

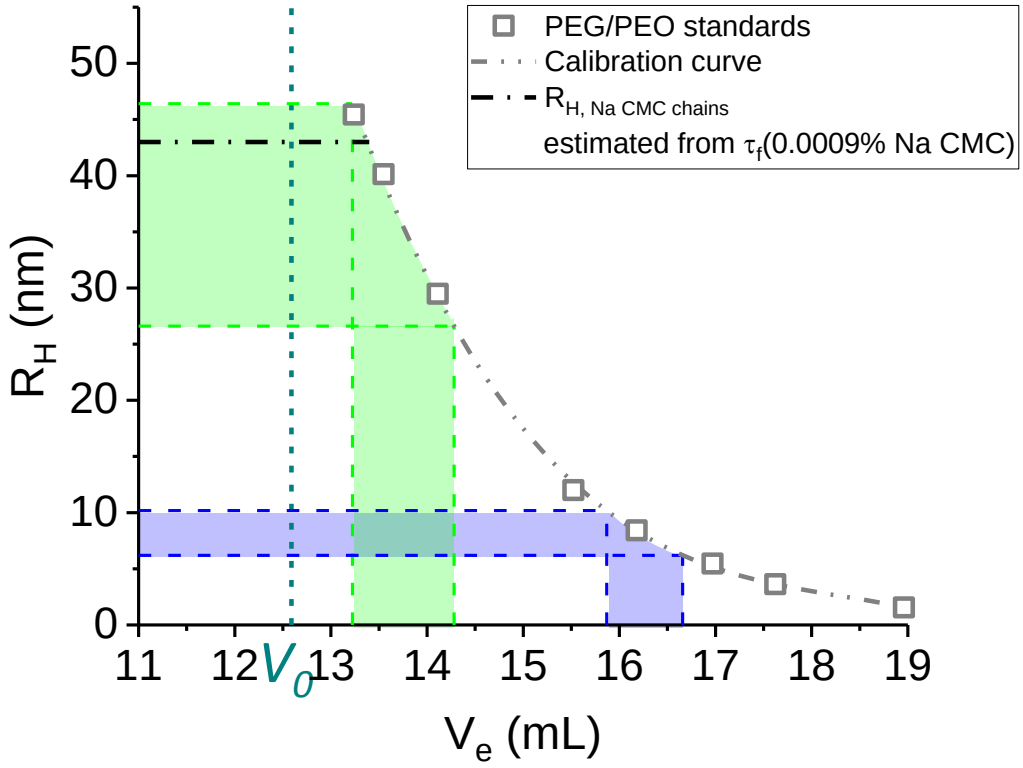

Figure 4-5: Calibration curve $R_H = f(V_e)$ with R_H the hydrodynamic radii of the PEO/PEG standards calculated with Eq. 4-2 from the M_w values measured by DLS and provided by the supplier, and V_e the elution volume of the PEO/PEG standards. The calibration curve is a third order polynomial model and its equation is given in Table AII-4. The short dashed turquoise line represents the void volume V_0. The green and the blue areas show the relationship between the elution volumes determined for the 2nd and the 3rd peaks for the previously studied range of concentrations (values shown in Figure 4-4.B) and the ranges of hydrodynamic radius values they correspond to according to the calibration curve. The black dashed-dotted line represent the hydrodynamic radius estimated from the fast relaxation time determined at 90° scattering angle for the 0.0009% Na CMC solution (see Figure 4-1).

Because of the presence of the slow relaxation mode, even for concentrations that are likely to be in the dilute regime (see discussion about the LS data shown in Figure 4-1), it is difficult to estimate the hydrodynamic radius of the Na CMC polymer chains $R_{H,\ Na\ CMC\ \ chains}$. Amongst all the collected data, those obtained from the lowest investigated Na CMC concentrations should give the closest possible approximation of $R_{H,\ Na\ CMC\ chains}$. Using the diffusion coefficient of the fast relaxation mode at 90° scattering angle shown in Figure 4-1.B and the Stokes-Einstein equation (Eq. 2-19), it is found that $R_{H,\ Na\ CMC\ chains} \approx 43$ nm. This value is displayed in Figure 4-5 as the black dashed-dotted line, and shows that the approximated size of Na CMC chains is between those of the two

highest M_w PEO/PEG standards, *i.e.* between 1,067,000 and 1,327,000 g/mol. The average M_w of the studied Na CMC sample would thus be higher than the value of 700,000 g/mol provided by the manufacturer. Such a result would however be in agreement with the value of 1.2×10^6 g/mol obtained from intrinsic viscosity measurements in 0.1 M NaCl by Lopez *et al.*[15] on a similar Na CMC sample. It is worth noting that, as discussed before, the calibration curve is most likely to lead to an overestimation of the size, and the determination of M_w is relative in the present case, as the calibration was performed using other polymers than the one studied.

According to the manufacturer specification, the highest molecular weight that can be separated by the column is 10^7 g/mol. Using the same equation as the one used to calculate the hydrodynamic radii of the PEG/PEO standards in water (*i.e.* Eq 4-2), a size of *ca.* 145 nm was estimated for the largest objects that can be separated by the column, meaning that objects whose size is larger than this value would be excluded from the column. The same precautions as the ones discussed in the previous paragraph apply, so that is most likely that this size is, in effect, lower than 145 nm.

The ranges of elution volumes covered by the second and third peaks obtained from SEC measurements investigating the influence of the injected amount of Na CMC (data shown in Figures 4-3 and 4-4) are reported in Figure 4-5. The black dashed-dotted line showing an approximation of $R_{H,\ Na\ CMC\ chains}$ is within the size range covered by the 2nd peak obtained from the SEC measurements; suggesting that the 2nd peak could correspond to the elution of the Na CMC chains. The hydrodynamic radius R_H associated with the slow mode cannot be calculated from the DLS data shown in Figure 4-1, as the viscosity of the solution is not known. Indeed, due to their length-scales, the domains associated with the slow mode are most likely to experience a viscosity which is close to that of the solution rather than the viscosity of the solvent itself. Hence, the viscosity of the solution could be used to estimate the viscosity of the continuous phase, in turn used in the calculation of the apparent hydrodynamic radius of the domains (Eq. 2-19; see Section 3-3.5).[35] Using the data collected for a 0.18% Na CMC solution containing 2 M NaCl, the apparent hydrodynamic radius of the domains is estimated to be *ca.* 150 nm in the presence of high salt concentrations; which is above the maximum size that can be separated by the column and confirms the attribution of the first SEC peak to the domains.

Finally, the reproducibility of SEC measurements was checked. The chromatograms of three different 0.14% Na CMC solutions are shown in Figure AII-5.A. The elution

profiles are similar. The elution volumes and peak areas obtained from peak deconvolution, displayed in Figures AII-6.A and B respectively, confirm that there is no significant difference in the elution behaviour. Samples analysed with SEC the day after they were prepared, D_1, as well as samples filtered and analysed on D_1, show no significant difference either, as seen from the chromatograms shown in Figure AII-5.B and the elution parameters from Figure AII-6.

In conclusion, LS investigations allowed the determination of the regime where there is no strong repulsive interaction between Na CMC chains. A slow mode is however still present and thought to be either due to the presence of some particulates in the solutions, or due to a lack of 'dissolution' of the domains typically observed at higher concentrations. SEC measurements performed on such solutions showed that the DRI detector is not sensitive enough to detect Na CMC chains at these low concentrations. Solutions at higher Na CMC concentrations, where strong repulsive inter-chain interactions occur, could be detected and were used to investigate the influence of Na CMC concentration on the elution behaviour. The overall shape of the obtained elution envelopes suggests that they are the sum of three peaks, which was confirmed by the successful deconvolution with the EMG model. The first peak, corresponding to the void volume of the column, was assigned to the domains remaining in the solutions as shown by the DLS measurements. The second peak was attributed to the polyions, and the third one to non-exclusion effects.

4-3.2. Sonication study

Rheology and DLS investigations of the sonicated solutions

Figures 4-6.A, B and C show the influence of sonication on the rheological behaviour of 0.18%, 0.46% and 0.73% Na CMC solutions, respectively. As usually reported for Na CMC solutions (see Section 2-3.2.2), the non-sonicated solutions exhibit a shear-thinning behaviour which can be described with the Carreau model (Eq. 2-3), where the zero-shear viscosity η_0 describes the viscosity plateau at low shear-rates, the time constant τ corresponds to the inverse of the shear-rate characterising the onset of the shear-thinning behaviour, and the exponent p describes the behaviour of the viscosity as a function of the shear-rate in the shear-thinning region. By definition, the higher τ, the lower the shear-rate from which the shear-thinning behaviour is observed, and the higher p, the stiffer the slope of $\eta = f(\text{shear-rate})$. Solutions exhibiting a strong shear-thinning

behaviour are thus characterised by high values of τ and p, while solutions exhibiting a weak shear-thinning behaviour are characterised by low values of τ and p. Finally, Newtonian solutions, whose viscosity is shear-rate independent, are simply described by a constant corresponding to η_0, and no τ nor p parameter is defined.

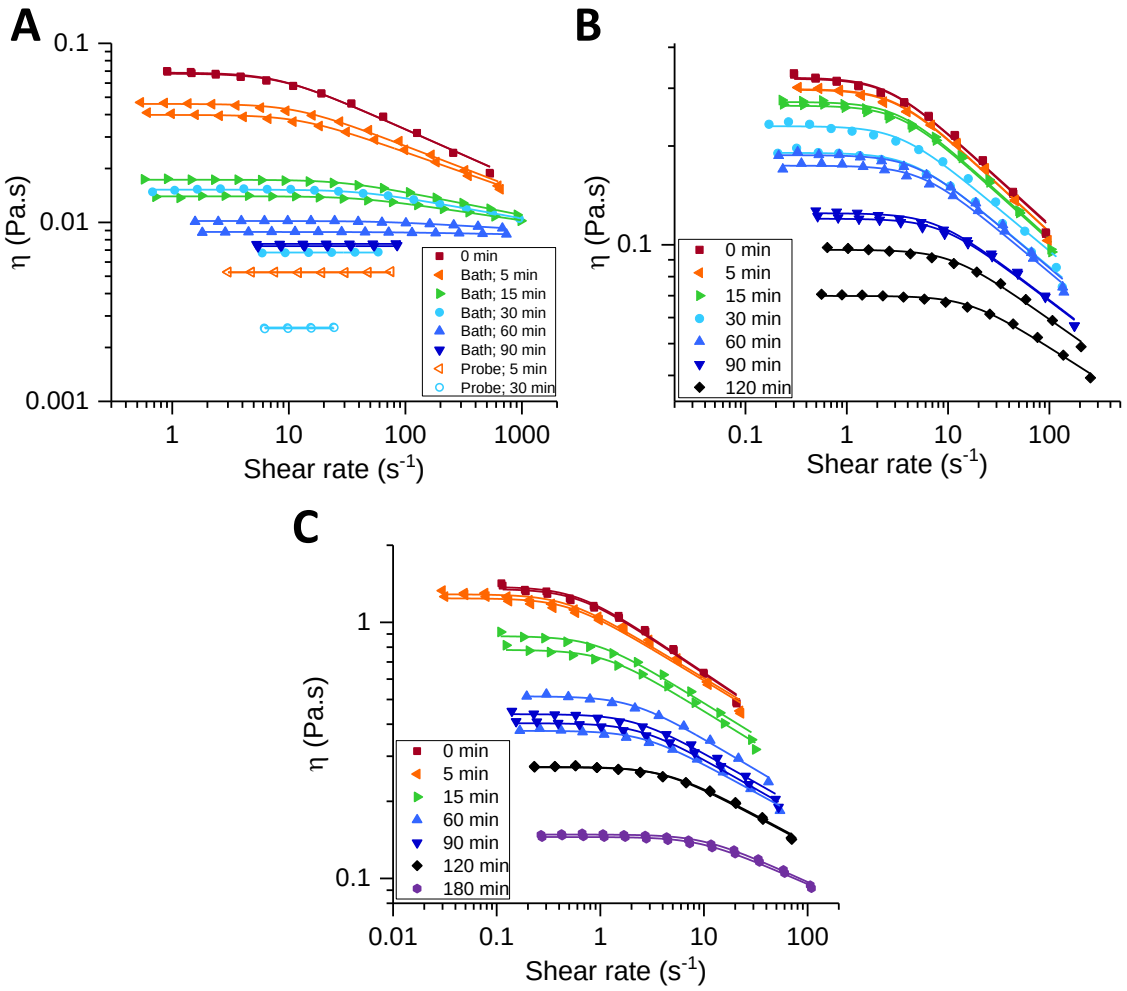

Figure 4-6: Flow behaviour of the non- and sonicated 0.18% (**A**), 0.46% (**B**) and 0.73% (**C**) Na CMC solutions. Samples were either sonicated in the bath (full symbols) or with the probe (empty symbols). Lines are fits to the Carreau model or to constants for data exhibiting shear-thinning or Newtonian behaviours, respectively. Each set of experimental conditions (*i.e.* sonication time and Na CMC concentration) were investigated in duplicates.

Figure 4-6 indicates that the solution viscosity decreases, and the shear-thinning behaviour lessens, when the sonication time increases, as previously reported for pectin.[158] After 30-60 min sonication in the bath, the behaviour of the 0.18% Na CMC solution is nearly Newtonian, while it becomes Newtonian after less than 5 min when the sonication probe is used (Figure 4-6.A). This difference is most likely to be due to the significantly higher energy input of the probe compared to the bath (see Section 2-3.4.2 and Table 2-9).[46,158,159] It is worth noting that the sonication process is more reproducible

with the probe than with the bath, where parameters such as the location of the vial, the number of vials and the amount of water in the bath are likely to influence sonication reproducibility.[166,200] These data sets were fitted to the Carreau model or to a constant depending on whether they exhibited a shear-thinning or a Newtonian behaviour, and the resulting parameters are shown in Figure 4-7.

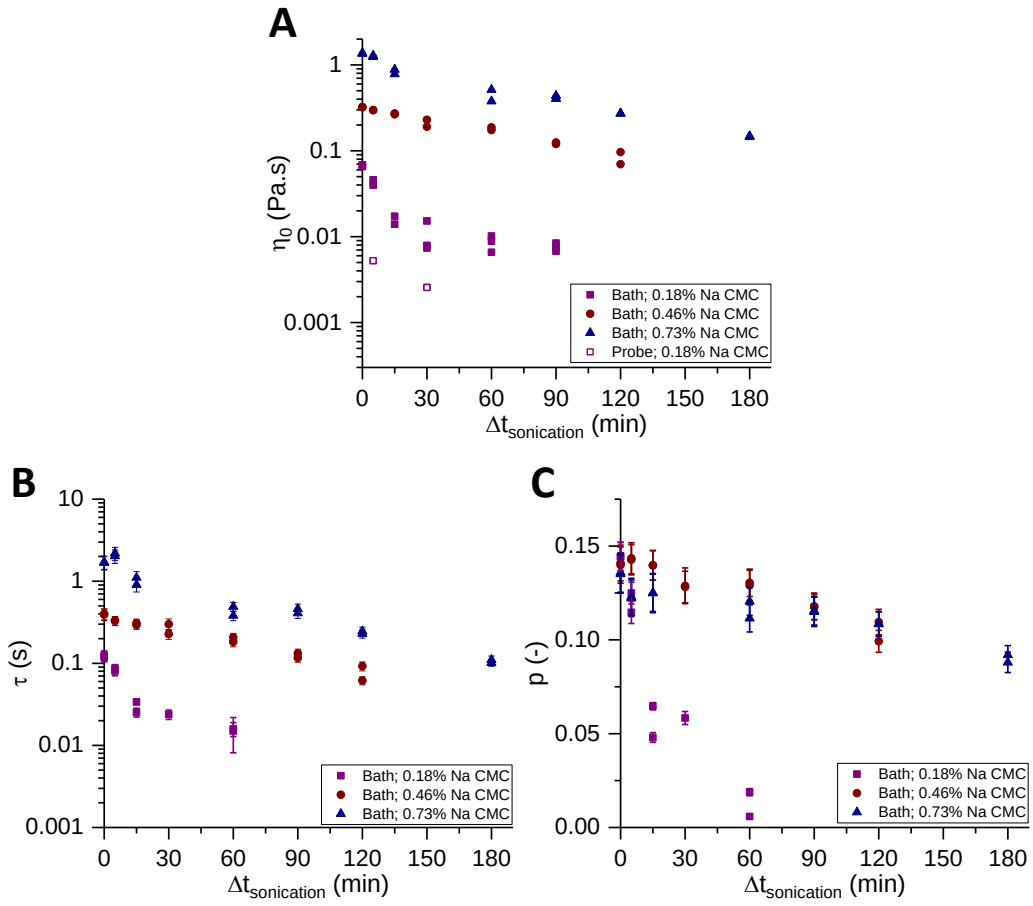

Figure 4-7: Fitting parameters obtained from fitting the viscosity curves of the non- and sonicated 0.18%, 0.46% and 0.73% solutions shown in Figure 4-6. **A.** Zero-shear viscosity from fits to the Carreau model or a constant for solutions exhibiting a shear-thinning or a Newtonian behaviour respectively. **C.** Carreau model time parameter τ corresponding to the inverse of the shear-rate at which the shear-thinning behaviour begins. **D.** Carreau model exponent p describing the viscosity *vs* shear-rate behaviour in the shear-thinning region. Each set of experimental conditions (*i.e.* sonication time and Na CMC concentration) were investigated in duplicates. It is worth noting that curves fitted using a constant do not appear on C. nor D. as no such parameter is available. Lin-lin representations of B and C are shown in Figure AII-7.

For all Na CMC concentrations, the solution viscosity decreases and the shear-thinning behaviour weakens under sonication, as η_0, τ and p decrease with the sonication time. However, despite investigating longer sonication times, no Newtonian behaviour was observed for 0.46% nor 0.73% Na CMC solutions for the investigated sonication times, and the Carreau model parameters seem to follow very similar trends for both solutions.

Indeed, the slopes of $\eta_0 = f(\Delta t_{sonication})$ and $\tau = f(\Delta t_{sonication})$ are alike in the log-lin plots shown in Figures 4-7.B and C for both 0.46% and 0.73% Na CMC solutions, while it is higher for 0.18% Na CMC solutions and a plateau seems to appear at long sonication time. For the third parameter of the Carreau model, *p*, the values at a given sonication time are identical for both 0.46% and 0.73% Na CMC solutions, while they are significantly lower for 0.18% Na CMC solutions from 15-min sonication times and disappear for solutions subjected to the highest investigated sonication times. The origin of the difference in behaviour between the 0.18% Na CMC solutions and the two more concentrated Na CMC solutions could be the fact they belong to two different concentration regimes. According to Section 3-2.2.2 and Figure 3-3, the 0.18% Na CMC solution belongs to the upper region of the semi-dilute non-entangled regime, while both the 0.46% and the 0.73% Na CMC solutions belong to the semi-dilute entangled regime.

The shear-thinning behaviour of polymer solutions is usually attributed to the alignment of the polymer chains in the flow direction.[87] The shear-thinning behaviour is stronger when the chains are entangled as entanglements need additional shear to be overcome.[87] It is worth noting that polymer chains get entangled only if their molecular weight is high enough.[30] At this stage of the study, the decrease in the viscosity and in the shear-thinning behaviour caused by sonication could be attributed to a change in the polymer chain conformation and/or a breakage of the chains. Regarding the latter, it has indeed been shown for solutions made with different M_w Na CMC samples that the solution viscosity decreases and the shear-thinning behaviour weakens when M_w decreases.[30,87]

The solutions exhibiting the most extreme rheological behaviours were also studied with DLS and the main outcomes of these investigations are displayed in Figure 4-8. Figure 4-8.A shows the intensity auto-correlation data of 0.18% Na CMC solutions at 90° scattering angle; the equivalent data collected for the 0.46% and 0.73% Na CMC solutions are shown in Figure AII-8. The three previously reported relaxation modes can be seen: (i) the fast relaxation time τ_f at lag times of *ca.* 10^5-10^6 s, (ii) the slow relaxation time τ_s at intermediate lag times, and (iii) the ultra-slow relaxation time τ_{us} at lag times of *ca.* 10^1-10^2 s. For the same reasons as discussed in the previous Chapter (see Section 3-3.3), the ultra-slow mode is taken into account for data fitting but the obtained fitting parameters are not discussed.

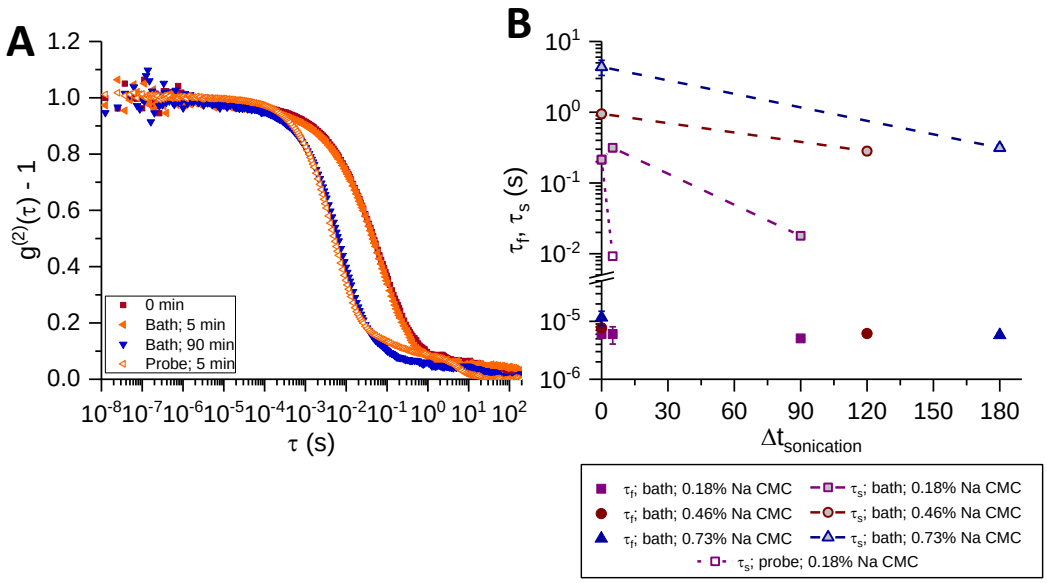

Figure 4-8: Dynamic light scattering at 90° scattering angle of sonicated and non-sonicated 0.18%, 0.46% and 0.73% Na CMC solutions. Full and empty symbols represent solutions sonicated with the bath and the probe, respectively. **A.** Examples of intensity auto-correlation data collected for 0.18% Na CMC solutions. **B.** Relaxation times τ_f and τ_s of the fast and the slow modes, respectively. The values of τ_f obtained for the 0.18% Na CMC solution sonicated with the probe are not provided as the intensity auto-correlation data were too noisy at low lag times to be properly fitted. In fact, measurements were performed over shorter periods of time to minimise the influence of the ultra-slow mode which was particularly significant and thought to be caused by the presence of some particles detached from the probe during sonication. Dashed and dotted lines are guide-to-the-eye.

Figure 4-8.B shows the fast and slow relaxation times τ_f and τ_s as a function of the sonication time for 0.18%, 0.46% and 0.73% Na CMC solutions, representing the different behaviours previously observed with rheology measurements. While the fast mode remains unchanged upon sonication, the relaxation time of the slow mode τ_s significantly decreases upon sonication. The only exception is the 5-min sonicated 0.18% Na CMC solution, for which the ultra-slow mode was particularly important, and corrections from ultra-slow mode fitting may not have been accurate enough to observe changes upon sonication, which are expected to be small after such a short sonication time using the bath. Hence, because of the presence of the particulates in Na CMC solutions (thought to be the cause of the ultra-slow mode) rheology seems to be a more sensitive technique to probe the early onset of changes caused by sonication.

The obtained results are comparable to the ones obtained by Reed *et al.*[166] for hyaluronan. Upon sonication, they reported an increase in the diffusion coefficient of the single relaxation mode they observed, and suggested thatit was due to a breakage of aggregates formed by polymer chains.[166] The fact that they only observed one relaxation mode in

their salt-free solutions compared to the present Na CMC solutions may be due to the small amplitude of the fast mode; hence, if measurements were not carried out over long enough periods of time, the small mode may have been overlooked.

It was shown in Section 3-3.5 and in Figure 3-14 that the solution viscosity and the slow relaxation mode observed by DLS were correlated. The fact that sonication induces a decrease in both of them confirms this correlation. Moreover, despite having only a couple of points for each Na CMC concentration, it appears that the decrease of the slow relaxation time τ_s upon sonication observed for both 0.46% and 0.73% Na CMC solutions follows a similar pattern as the one observed for the rheological behaviour, while its reduction is much more significant for the 0.18% Na CMC solution. Here too, the use of the sonication probe magnifies the observed changes as the slow mode relaxation time of the 5-min sonicated 0.18% Na CMC solution is more than an order of magnitude shorter than the one of the 5-min bath-sonicated solution.

The apparent hydrodynamic radii associated with the slow mode were estimated using the values of the zero-shear viscosity η_0 determined with the Carreau model (data in Figure 4-6.B) and the values of the slow relaxation time determined at 90° scattering angle (data in Figure 4-8.B). The obtained values are shown in Table 4-2. The values of $R_{H,app}$ for the non-sonicated solutions are identical within the experimental error at the three studied concentrations, and are similar to the ones reported in the previous study (see Section 3-3.5 and Figure 3-15). For the bath-sonicated solutions, the errors on $R_{H,app}$ are high and it is difficult to conclude on the influence of sonication, although a slight decrease in $R_{H,app}$ upon sonication can be observed after 90 min sonication for the 0.18% solution and after 180 min for the 0.73% solution. The value obtained for the 5-min probe-sonicated 0.18% Na CMC solution is significantly smaller than the one obtained for the original 0.18% Na CMC solution, which appears to confirm a measureable decrease in $R_{H,app}$ upon high cavitational activities. The sonication probe is indeed expected to induce higher local cavitational activities compared to the bath (see Section 2-3.4.2).[46] To understand what this decrease means, SLS data were also examined.

Table 4-2: Values of the apparent hydrodynamic radius $R_{H,app}$ estimated for the slow mode of the non- and sonicated solutions using Eq. 2-19 with η_c the zero-shear viscosity of the solution determined from the Carreau model and the diffusion coefficient calculated at 90° scattering angle from the relaxation time of the slow mode.

$c_{Na\ CMC}$ (%)	$\Delta t_{sonication}$ (min)	Sonication mean	$R_{H,app}$ (nm)
0.18	0	-	$(2.2 \pm 0.2) \times 10^2$
0.18	90	Bath	1.7×10^2
0.46	0	-	$(2.1 \pm 0.3) \times 10^2$
0.46	120	Bath	$(2.1 \pm 0.3) \times 10^2$
0.73	0	-	$(2.3 \pm 0.6) \times 10^2$
0.73	180	Bath	$(1.5 \pm 0.2) \times 10^2$
0.18	5	Probe	$(1.24 \pm 0.02) \times 10^2$

Standard errors were estimated from the standard error on the zero-shear viscosity (standard error from fitting) and the one on the slow relaxation time (standard error of the mean on the slow relaxation times of all the successful DLS measurements). As only two DLS measurements were successful for the 90-min sonicated 0.18% Na CMC solution, the standard error could not be estimated.

The excess Rayleigh ratio ΔR was calculated from short LS measurements. The results obtained for the non- and sonicated 0.18% Na CMC solutions are shown in Figure 4-9.A, while the results obtained for the 0.46% and 0.73% Na CMC solutions are shown in Figures AII-9.B and C. No change in the excess Rayleigh ratio is observed upon sonication. Without added salt, the excess Rayleigh ratio contribution from the fast mode is negligible compared to the one of the slow mode, and the total excess Rayleigh ratio can be assigned to that resulting from the slow mode (see Section 2-2.3).[66] Data shown in Figure AII-9, where the excess Rayleigh ratio of the slow mode is plotted at 90° scattering angle, confirm this assumption. The fact that the excess Rayleigh ratio does not change upon sonication suggests that the associated apparent radius of gyration $R_{g,app}$ does not change either. The contributions of the fast and the slow modes to the total excess Rayleigh ratio, ΔR_f and ΔR_s respectively, were calculated from the SLS data collected during the long DLS measurements performed at 90° scattering angle. As seen in Figure 4-9.B, ΔR_f is negligible compared to ΔR_s, and neither ΔR_f nor ΔR_s is modified upon

sonication; confirming that $R_{g,app}$ associated with the slow mode is not modified by sonication.

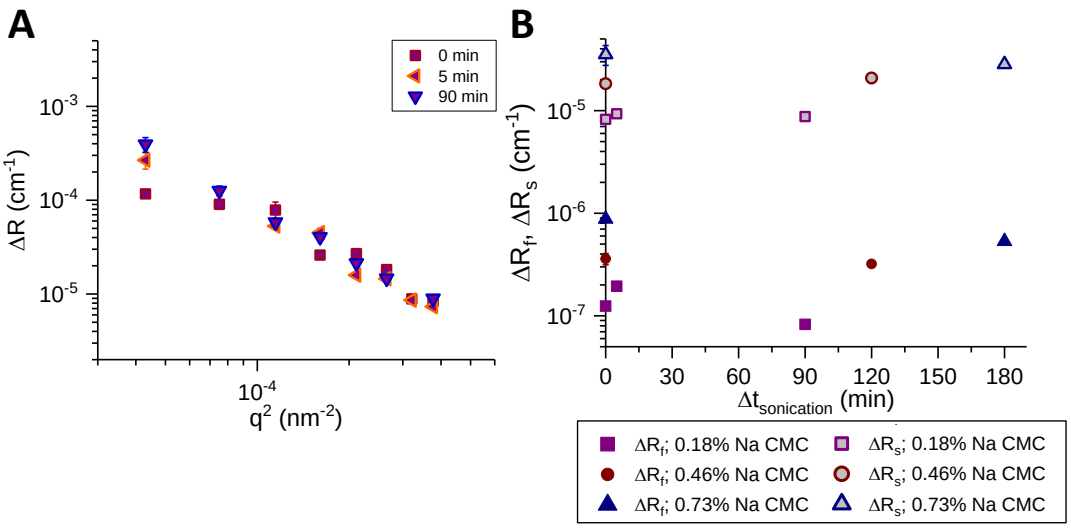

Figure 4-9: SLS data from non- and bath-sonicated solutions. **A.** SLS data from non- and bath-sonicated 0.18% Na CMC solutions. The total excess Rayleigh ratio ΔR is plotted against the squared scattering vector q^2. The same data are shown in Figure AII-9.A with the value of the excess Rayleigh ratio obtained from the SLS data collected during the long DLS measurements at 90° scattering angle as well as the contribution of the slow mode to the excess Rayleigh ratio determined from these DLS measurements. Equivalent data for the 0.46% and 0.73% Na CMC solutions are shown in Figures AII-9.B and C, respectively. **B.** Contributions of the fast and the slow modes to the excess Rayleigh ratio (ΔR_f and ΔR_s respectively) as a function of sonication time and Na CMC concentration. These contributions were determined from the long DLS measurements at 90° scattering angle.

DLS measurements show that $R_{H,app}$*(domains)* decreases upon sonication while SLS measurements show that $R_{g,app}$*(domains)* remains constant, suggesting that the size of the domains is not modified during sonication. Furthermore, the scattering intensity is proportional to the solute concentration and M_w ($\Delta R \sim c_{solute} M_w$).[177] The fact that ΔR_s and $R_{g,app}$*(domains)* are unchanged upon sonication thus implies that the domain concentration remains constant too. At first sight, these results seem contradictory. Solvent molecules may, to a certain extent, pass through the domains.[67,70] This phenomenon is referred as draining.[67,70] If there were fewer polymer chains in domains of unmodified size, more solvent molecules could pass through the domains, so that $R_{H,app}$ would decrease while $R_{g,app}$ would remain the same. Similar findings were reported by Sedlák[70] upon ageing. He however also observed a decrease in ΔR_s explained by the reduction in contrast between the bulk solution and the domains as polyions left the latter. The extent to which ΔR_s decreased in that study depended on polyelectrolyte solutions, but ΔR_s was typically divided by 2 after 240 days.[70] In the present work, it may be that the presence of the particulates in Na CMC solutions prevents such a decrease in ΔR_s

upon sonication from being observed. Indeed, the experimental error on the present data due to the presence of the particulates is higher than that on data collected on synthetic polyelectrolyte solutions which could be purified before LS measurements without significantly altering them.

Owing to the experimental error and the presence of the particulates, it may also be that the decrease in $R_{g,app}$ cannot be seen. In such a case, both $R_{g,app}$ and $R_{H,app}$ would decrease simultaneously. Furthermore, it is worth noting that the validity of the Stokes-Einstein equation to estimate $R_{H,app}$*(domains)* can also be questioned. Indeed, it assumes a purely diffusive behaviour while the relaxation mode associated with the domains has often been shown to exhibit more complex behaviours due to the large size of the domains. Moreover, the viscosity experienced by the domains (*i.e.* the viscosity of the continuous phase η_c; see Eq. 2-19) may not be exactly the one of the solution.

To conclude this Section, Na CMC solution viscosity decreases upon sonication and their shear-thinning behaviour weakens. For 0.18% Na CMC solutions, the shear-thinning behaviour fully disappears after about 30 min sonication in the bath. This change becomes faster when the sonication bath is exchanged for a sonication probe, since the energy input of the probe is higher than the one of the bath. The modifications of the rheological behaviour are correlated with the decrease in the slow mode relaxation time observed using DLS measurements. The extent of the modifications seem to be concentration-dependent as the effects of sonication on semi-dilute non-entangled solutions (*i.e.* 0.18% Na CMC) are more pronounced than on entangled solutions (*i.e.* 0.46% and 0.73% Na CMC). A decrease in $R_{H,app}$ is found while $R_{g,app}$ and the contribution of the slow mode to the excess Rayleigh ratio remain constant within the experimental error. The latter findings imply that the concentration and the size of the domains are relatively unchanged upon sonication. One way to account for the decrease in $R_{H,app}$ is that the number of polyelectrolyte chains within the domains decreases. It is worth reminding that there is some uncertainty on the values of $R_{H,app}$, as $R_{H,app}$ calculations with the Stokes-Einstein equation rely on hypotheses that may not be applicable in the present case. The change in the slow mode relaxation time upon sonication is however clear.

At this stage, polymer chain breakage cannot be ruled out, though, as it would also lead to the observed changes in the solution rheological behaviour. The influence of chain breakage on LS data is more complex to establish as results related to the slow relaxation mode, and especially to the size of the domains, vary from one study to another. The next

SEC and LS experiments should bring more insights to understand the effects of sonication on the studied solutions.

SEC and complementary LS investigations

To further understand the influence of sonication on Na CMC solutions, both the non-sonicated and sonicated solutions were diluted with a 0.8 M $NaNO_3$, 0.04 M $NaNH_2PO_4$, 0.2% *w/v* NaN_3 solution to obtain 0.14% Na CMC solutions in the eluent selected for the SEC measurements. Examples of chromatograms obtained for a 0.18% Na CMC solution sonicated by 15 g fractions and a 0.73% Na CMC solution are shown in Figures 4-10.A and B, respectively. The overall elution peak is shifted towards higher elution volumes as sonication time is increased. As for the rheology data collected on the original Na CMC solutions, the fact that some samples do not follow the general trend most likely comes from the small variability of bath sonication.

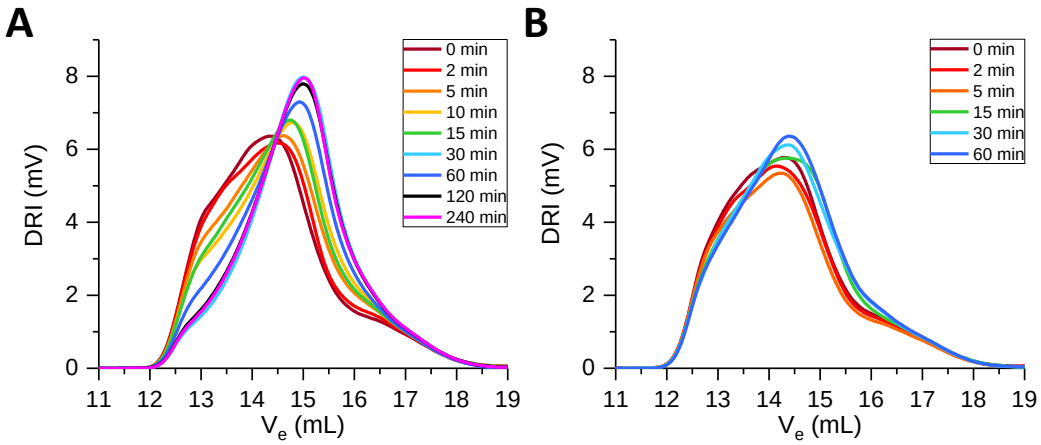

Figure 4-10: Elution of 0.18% (**A**) and 0.73% (**B**) Na CMC solutions after sonication for various durations and dilution to 0.14% with the eluent. The 0.18% Na CMC solution was sonicated by fractions of 15 g instead of the usual 21 g.

As described in Section 4-3.1, the obtained data were deconvoluted into three peaks using the EMG model. The elution volumes V_e and the peak areas A obtained for the deconvoluted peaks for both 0.18% and 0.73% Na CMC solutions are shown as a function of sonication time in Figures 4-11.A and B. For clarity, the error bars representing the fitting standard error are not shown. They were significant for a few data points, which is not surprising as deconvoluting three peaks is a complex process. For all sonication times, the elution volumes obtained for each of the three peaks are constant within the experimental error. The elution volume of the first peak appears to correspond to the void volume V_0, consistent with the non-sonicated samples, and again was attributed to the slow mode observed with light scattering (see Section 4-3.1). Even if the size of the

domains has changed upon sonication (and dilution in the eluent), their size still remains above the maximum size that can be separated by the column (estimated to be around 145 nm). The area of this peak, however, decreases upon sonication, while the area of the second peak, attributed to the Na CMC polyions, increases. As it has been shown in Section 4-3.1, the area of the first two peaks is proportional to the mass of Na CMC, this behaviour suggests that the large domains associated with peak 1 contain fewer polymer chains. The freed polyions would then elute later from the column, *i.e.* at the elution time corresponding to the second peak. The fact that the elution volume corresponding to the position of the second peak is not altered with time suggests that the polymer chains are not broken upon sonication. Such a result would be in agreement with those of D'Almeida and Dias,[198] who showed that Na CMC could bear stresses as high as 1,900 Pa without getting broken as the M_w was not modified, where they explained the observed decrease in the solution viscosity by the breakage of 'macromolecular aggregates' present in solution, which can be assigned to the domains. The peak parameters remain constant for the last peak, attributed to polymer chain adsorption on column packing, shear-degradation and/or viscosity effects in the column. If the polymer chains were to be broken upon sonication, shear-degradation would probably become less important as the polymer chains would get smaller, leading to a lessening of the peak with sonication time. As it is not the case, the hypothesis of polymer chains adsorbing onto the column packing seems more plausible to explain the third peak.

These SEC data seem to indicate that no significant breakage occurs upon bath-sonication, if any. They also appear to confirm the previously suggested hypothesis that the number of polyions involved in the domains decreases upon sonication, while the number of free polyions in solution increases. The fact that the domains still elute at the void volume supports the idea that their size is not affected by sonication. These experiments can however not exclude a change in the domain size as (i) the domains are most probably smaller compared to the original solutions as the solutions analysed with SEC contain high amounts of salts,[23,34] and (ii) a decrease in the size of the domains to a value which is still above the maximum size which can be separated by the column would not measurable.

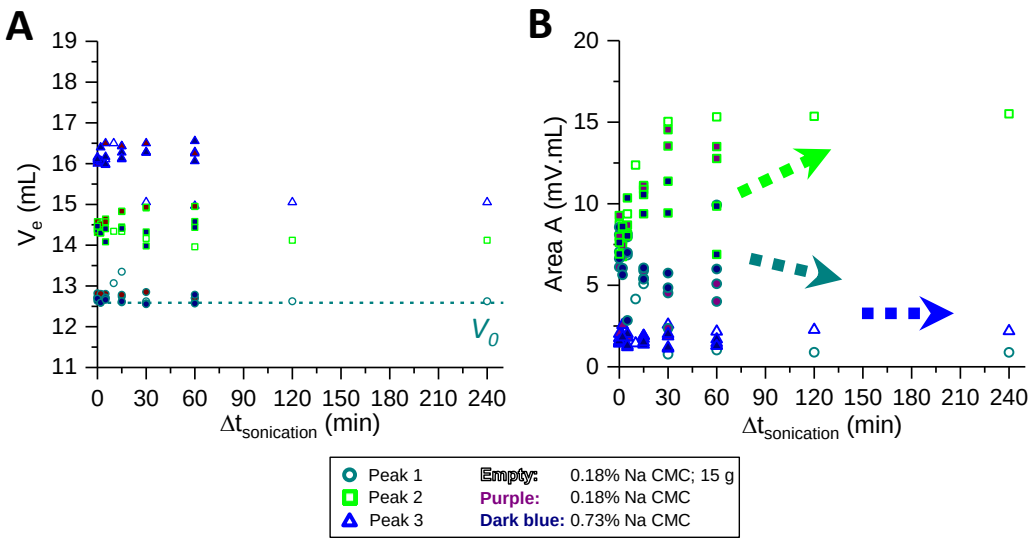

Figure 4-11: Elution volume V_e (**A**) and area A (**B**) of the three peaks obtained from deconvolution of the chromatograms of the 0.18% and 0.73% Na CMC solutions after dilution to 0.14% with the eluent as a function of the sonication time. In A, the short dashed line represents the void volume V_0. In B, the arrows highlight the evolution of the area of each of the peak as a function of the sonication time. The 0.18% Na CMC solution sonicated by fractions of 15 g instead of the usual 21 g is represented by empty symbols. Other sets of experimental conditions (*i.e.* sonication time and Na CMC concentration) were investigated in duplicates. For clarity, the error bars representing the standard errors from the deconvolution with the EMG model are not represented.

SEC samples from 0.18% and 0.73% solutions and representing the extreme behaviours (*i.e.* non-sonicated solutions and solutions sonicated for the longest times) were investigated with LS to understand the behaviour of the bulk solutions, free from probable interactions with the SEC column. These samples were in the concentrated salt conditions used to screen the polymer charges, and not in pure water as for the samples whose results are shown in Figures 4-8 and 4-9. Examples of raw data collected on samples made from 0.73% Na CMC solutions are shown in Figure 4-12.A, while Figure 4-12.B summarises the outcomes of the experiments, giving the fast and the slow relaxation times as a function the scattering angle for non- and sonicated samples made from both 0.18% and 0.73% solutions. As for the original salt-free solutions (see previous Section), the relaxation time of the fast mode does not change upon sonication, and the relaxation time of the slow mode decreases upon sonication.

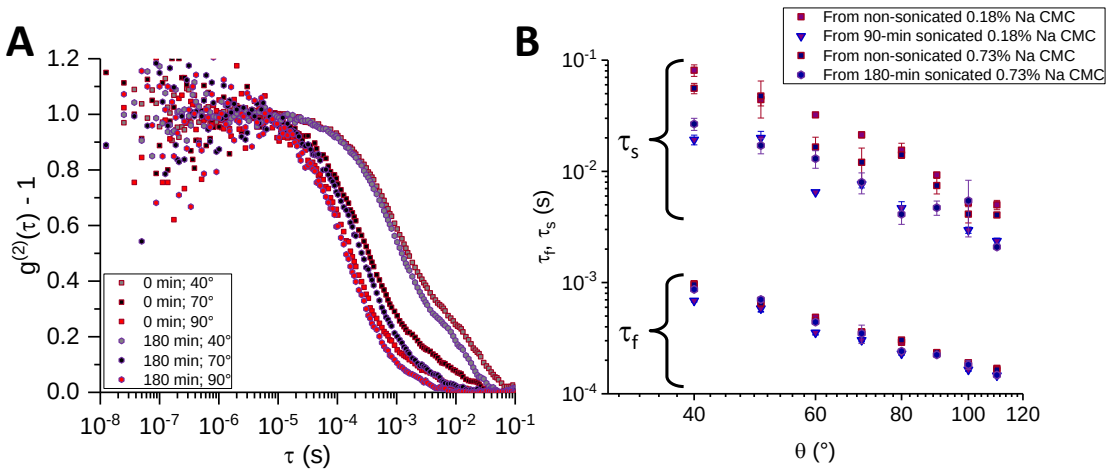

Figure 4-12: DLS of SEC samples (*i.e.* 0.14% Na CMC solutions in the eluent). **A.** Intensity auto-correlation data at 40°, 70° and 90° scattering angles of SEC samples made from non- and 180-min sonicated 0.73% Na CMC solutions. **B.** Fast and slow relaxation times τ_f and τ_s of SEC samples made from non- and sonicated 0.18% and 0.73% Na CMC solutions. Figure AII-10.A shows the same data as well as the data from a 5-min sonicated 0.18% Na CMC solution, which are not shown here to prevent the Figure from being overcrowded.

The intensity auto-correlation data shown in Figure 4-12.A suggest that the relative amplitudes of the fast and the slow modes do not change significantly upon sonication. The scattering contributions of the fast and the slow modes to the total excess Rayleigh ratio, ΔR_f and ΔR_s respectively, were calculated and are shown in Figure 4-13. As for the original salt-free solutions, ΔR_f and ΔR_s do not change upon sonication within the accuracy of the measurements. It is worth noting that, in this case, ΔR_f and ΔR_s are equal for all solutions; which is due to Na CMC concentration being identical for all solutions as they have all been diluted to 0.14% Na CMC in the eluent before LS measurements. The apparent radii of gyration of the domains $R_{g,app}$ estimated using Berry plots (see Sections 3-3.5 and AI-3.5.3) for the original salt-free non-sonicated 0.18% Na CMC solution and the solution obtained from its dilution to 0.14% Na CMC in the eluent are ~ 265 nm and ~ 115 nm, respectively. This decrease in the domain size between the original salt-free solutions and the solutions used for SEC and additional LS measurements is caused by the addition of salt (see Section 2-2.3.4).[23,32,34] The $R_{g,app}$ value found for the domains present in the solutions used for SEC suggests that the domains would not all be excluded from the column (the distribution of sizes of the domains is indeed expected to be polydisperse[70]). However, as discussed before, the upper size limit of 145 nm for separation by the column is very likely to be overestimated. Moreover, this size is based on the calculation of the hydrodynamic radii R_H of PEG/PEO standards, and it is not known how these radii would compare to the apparent radii of

gyration $R_{g,app}$ of the domains. Nevertheless, it cannot be fully excluded that some of the domains elute later than the void volume, but before the free polyions.

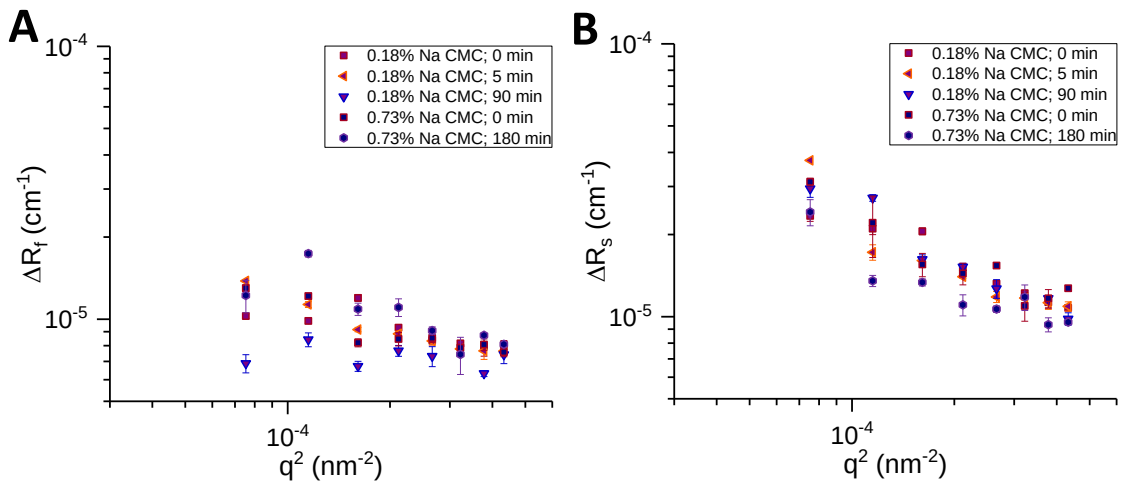

Figure 4-13: Contributions to the excess Rayleigh ratio of the fast (**A**) and the low mode (**B**) for the 0.18% and 0.73% non- and bath-sonicated solutions. Error bars are standard errors of the mean calculated from the independent LS measurements performed at each angle.

Together with the SEC data, the SLS results suggests that while the number of polyions outside of the domains increases with sonication time, the actual size of the domains is approximately constant. This behaviour would indicate that the energy provided and/or the high shear-rates and strains generated by cavitation during sonication remove the polymer chains from the domains. The way the polymer chains are organised in the domains would be such that taking apart some polymer chains would not modify their size. Similarly to the original salt-free solutions, this suggested behaviour cannot be fully confirmed as there are uncertainties on the determination of $R_{g,app}$ and $R_{H,app}$.

To double-check that the polymer chains have not been broken during sonication, the 0.14% solutions were diluted to 0.007% in the eluent. Such a low concentration is indeed thought to be within the dilute regime, though a slow relaxation mode is still observed and attributed to some residuals from the domains initial present in the salt-free solutions (see detailed discussion in Section 4-3.1). Examples of the fast relaxation times observed for these solutions are shown in Figure 4-14. The data points are scattered at the lowest studied angle. This issue is due to the difficulty of collecting good quality data for solutions at such low concentrations and, despite all the precautions taken to minimise the influence of the larger 'objects' present in the solution, I did not manage to fully erase their influence (see Section 4-3.1). Nevertheless, their effect decreases as the scattering angle increases, and all the series superimpose on top of each other at higher angles;

meaning that there is no significant breakage of the polymer chains upon sonication. If there was any significant breakage, it would have led to significantly smaller values of τ_f (although, owing to the fact that the measurements were performed at the limits of the technique sensitivity, it cannot be ascertained that there was no breakage at all). It is worth pointing out that, as discussed in Section 2-2.3.2, this is only true in the dilute regime, whose boundary could not be fully confirmed. If the selected 0.007% Na CMC concentration were to belong to a higher concentration regime, the breakage of the polymer chains would be overlooked as τ_f is no longer M_w-dependent outside the dilute regime.

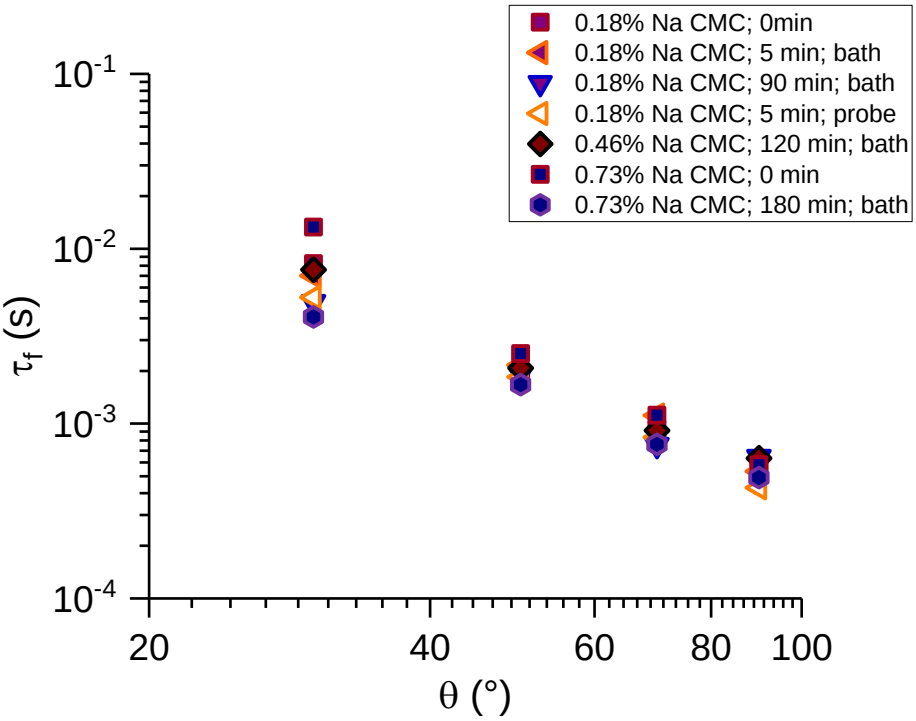

Figure 4-14: Fast relaxation time from DLS measurements on 0.007% Na CMC solutions in the SEC eluent made from non- and sonicated 0.18%, and 0.46% and 0.73% Na CMC solutions. Sonication conditions are indicated in the Figure.

To conclude this Section, sonication induces a significant decrease in Na CMC solution viscosities and in the shear-thinning behaviour, as well as in the slow mode relaxation time and in $R_{H,app}$*(domains)* probed by DLS. Meanwhile, no change in structure, including $R_{g,app}$*(domains)*, is probed by SLS. Moreover, SEC measurements suggest that there would be more polyions free in the bulk solution as sonication time increases. According to these results, it is proposed that the high energy/forces generated during sonication remove polyions from the domains. The arrangement of the chains in the domains would be such that removing polyions would not modify their size (*i.e.* $R_{g,app}$*(domains)*

constant). Water molecules would however be able to go through the domains more easily, leading to a decrease in $R_{H,app}$*(domains)*. Having more polyions free in solution and looser domains could explain the observed decrease in Na CMC solution viscosity and weakening in the shear-thinning behaviour as free polyions would more easily align in the direction of flow and looser domains would be more deformable, facilitating flow. This explanation, which can explain the combined rheology, LS and SEC results, cannot however be fully confirmed due to the uncertainties in the determination of $R_{g,app}$ and $R_{H,app}$. It is worth pointing out that a less careful analysis of the SEC data may have led to the conclusions that the polymer chains are degraded during sonication, though some non-significant breakage of the chains cannot be fully excluded.

4-3.3. Further investigations

To obtain a better understanding regarding the effects of sonication on Na CMC solutions as well as about the nature of the slow mode and the related domains, additional experiments including salt addition, solution heating and ageing were carried out.

Figure 4-15 illustrates the influence of sonication on the behaviour of a 0.18% Na CMC solution in 2 M NaCl. As seen from Figure 4-15.A, NaCl addition in a 0.18% Na CMC solution leads to a decrease in the solution viscosity and lessens its shear-thinning behaviour. This in agreement with the literature on Na CMC[19,87] as well as about polyelectrolytes in general.[60] In DLS experiments, salt addition leads to an increase in the fast relaxation mode and a decrease of the slow relaxation mode, as reported in the literature for other polyelectrolytes (see Section 2-2.3) and already observed during the preliminary LS measurements shown in Section 4-3.1. A number of the investigations conducted on polyelectrolytes have shown that the slow mode disappears when the salt concentration is high enough to screen the charges on the polyelectrolyte chains,[23,32,201] but Sedlák[23] has extensively studied this behaviour and shown that for high M_w sodium poly(styrene sulfonate) solutions at high concentrations, the interactions responsible for the formation of the slow mode cannot be completely removed and the slow mode never entirely disappears. This behaviour was also found by Buhler and Rinaudo[35] for chitosan.

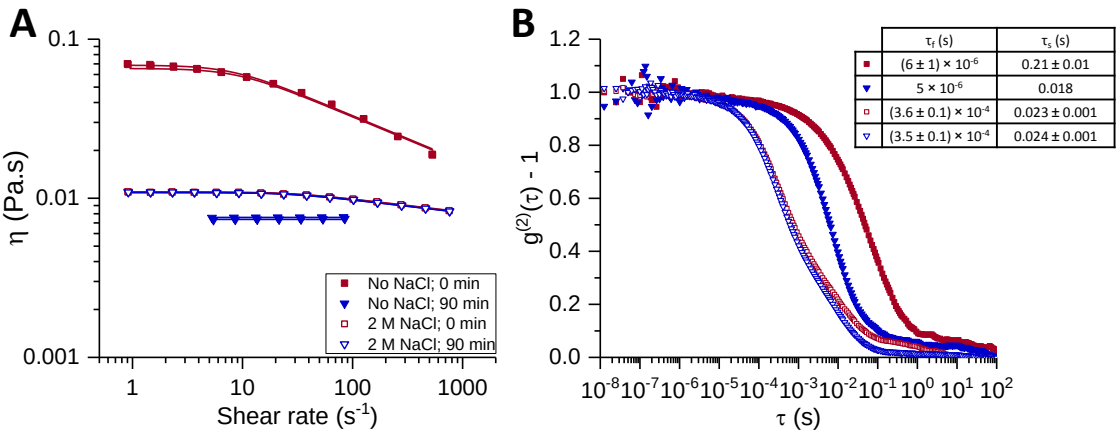

Figure 4-15: Behaviour of non- and 90-min sonicated 0.18% Na CMC solutions with and without added NaCl investigated using rheology (**A**) and DLS at 90° scattering angle (**B**). Experimental parameters were tested in duplicate. The lines in A are fits of the experimental data to the Carreau model. The data shown for the salt-free solutions are identical to those shown in Figures 4-6.A and 4-7.A.

The Na CMC solutions containing 2 M NaCl were bath-sonicated during 90 min, and no change in either the rheology nor in the DLS behaviour was observed. This consistency in behaviour is in apparent disagreement with Mohod's and Gogate's[46] findings, where the viscosity of Na CMC solutions containing various amounts of NaCl decreased upon sonication. However, in that case, the decrease in viscosity was attributed to the degradation of Na CMC chains rather than to that of the domains. The fact that sonication performed in presence of a high amount of NaCl does not induce any change in either the rheological nor the DLS behaviour seems to confirm that electrostatic interactions are responsible for the cohesion of the domains giving rise to the slow mode; which is already suggested by the fact that the domains typically tend to disappear upon salt addition.[23,32,34,36]

Nierling and Nordmeier[69] indicated that the slow mode present in poly(diallyl-*N*,*N*-dimethylammonium chloride) solutions could be removed by centrifugal forces, and more recently, Cao and Zhang[36] also showed that ultracentrifugation forces led to the disappearance of the slow mode. Both studies suggested that the centripetal forces are large enough to overcome electrostatic interaction energies,[36] that are assumed to be responsible for holding the chains together in the domains.[36,69] In the present case, the high shear-rates and strains generated by cavitation and/or the energy applied during sonication would be high enough to take some of the polymer chains apart from the domains. It can be seen in Figure AII-11 that heating Na CMC at 80°C during 1 h has a similar affect, though it is much less efficient.

Finally, the sonicated solutions were kept for a month and characterised again with DLS. Figure 4-16 and Figure AII-12 show that slow mode has partially or fully recovered upon ageing. Such a result can be compared to the viscosity recovery of pectin solutions reported by Ogutu *et al.*[43] after sonication (see Section 2-3.4.2). Nierling and Nordmeier[69] also observed a recovery of the slow mode they observed in their poly(diallyl-*N*,*N*-dimethylammonium chloride) solutions after the slow mode had disappeared upon centrifugation. The recovery process was noticeable after 4 days but took 21 days to be fully completed.[69] This change not only confirms the fact that the polymer chains have not been broken upon sonication, but also the temporal nature of the aggregates.[32,36] Cao and Zhang[32] thus suggested that the domains were formed by polyelectrolyte chains that would be constantly exchanged between the bulk and the domains, as repulsion between similarly charged chains would make chains leave the domains while electrostatic interactions holding the chains together in the domains (see discussion about salt addition above and in Section 2-2.3) would make chains join the domains. According to them, shared counterions would be responsible for the existence and cohesion of the domains. This idea had already been suggested before.[32]

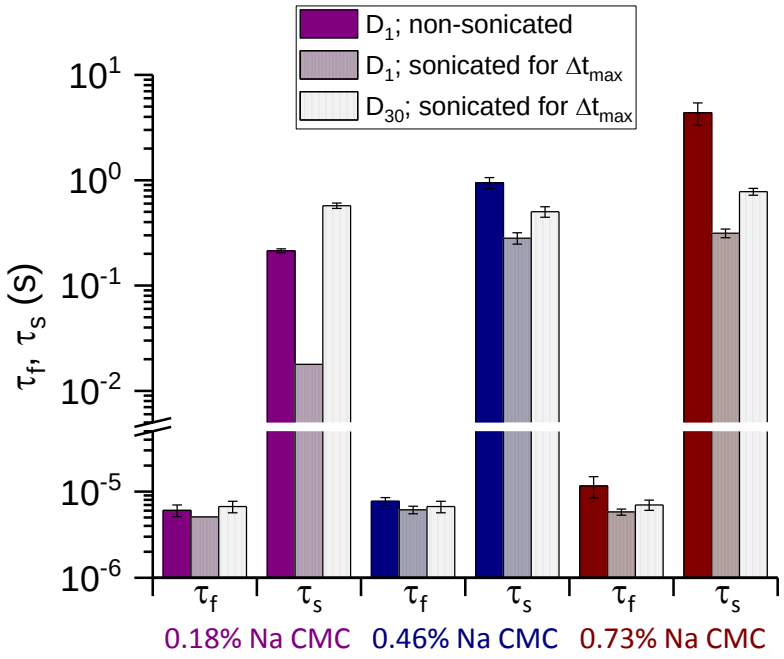

Figure 4-16: Fast and slow relaxation times τ_f and τ_s probed by DLS at 90° scattering angle of 30-day old sonicated solutions. For comparison, the data of the non- and 1-day old sonicated solutions already presented in Figure 4-8.B are also shown. The sonicated solutions shown in this Figure were sonicated for Δt_{max} (*i.e.* 90 min, 120 min and 180 min for the 0.18%, 0.46% and 0.73% Na CMC solutions, respectively). Examples of the intensity auto-correlation data from which the parameters shown in this Figure were extracted are shown in Figures AII-12.A, B and C.

The fact that the slow mode recovers over time tends to confirm that Na CMC chains are not significantly broken upon the mild sonication conditions used in this study. As discussed in the first part of Section 4-3.2, sonication showed similarities to the ageing observed by Sedlák[70] for sodium poly(styrene sulfonate), suggesting that it could be a way to accelerate ageing. In Sedlák's experiments,[70] the relaxation time related to the slow mode decreased and reached a steady value after periods of time ranging from a couple of hundreds to more than thousand days depending on the studied solutions. Sedlák[70] proposed that a metastable equilibrium was achieved after these long periods of time. The fact that the slow relaxation mode recovers after sonication suggests that sonication has taken the Na CMC solutions beyond this metastable equilibrium, and they would subsequently evolve towards this equilibrium.

4-4. Conclusions

In this work, the influence of sonication on semi-dilute Na CMC solutions was studied using rheology, SEC and LS.

Initial LS and SEC investigations were performed on 0.0009-0.18% Na CMC solutions in the eluent pre-selected for SEC measurements. The concentration dependence of the diffusion coefficient of the fast relaxation mode observed with DLS and the SLS data changed at a concentration of *ca.* 0.02% Na CMC, as reported for other polyelectrolyte solutions going from the dilute regime to a concentration regime which has not been definitely assigned yet where chains start interacting with each other. Below this concentration, the slow relaxation mode was unexpectedly still observed and the exponent of the power law describing the concentration-dependence of the excess Rayleigh ratio ΔR obtained from SLS measurements was higher than the expected value of 1 because of the additional contribution coming from the slow mode. In this dilute regime, the DRI detector of the Size Exclusion Chromatograph was however not sensitive enough to perform any quantitative measurement. When Na CMC concentration was increased, and thus entered the region where inter-polyion interactions occurred, the obtained elution peak could be deconvoluted into three peaks: (i) a peak corresponding to the void volume of the column and assigned to the domains present in Na CMC solutions, too large to be retained by the column, (ii) a peak assigned to the polyions, and (iii) a peak attributed to interactions with the column packing.

During sonication, both the viscosity and the shear-thinning behaviour of the investigated Na CMC solutions decreased. Upon long enough sonication times, 0.18% Na CMC solutions lost their shear-thinning behaviour and exhibited a simple Newtonian behaviour. The use of a sonication probe, whose energy input is much greater than the sonication bath, significantly enhanced the kinetics. In parallel to the decrease in the viscosity, the slow mode relaxation time observed by DLS decreased with sonication time; confirming the relationship between the slow relaxation mode and the solution viscosity previously established for semi-dilute salt-free solutions established in Chapter 3. The behaviour of the semi-dilute entangled 0.46% and 0.73% Na CMC solutions was similar, while the 0.18% Na CMC solution, belonging to the upper range of the semi-dilute non-entangled regime, clearly exhibited a different behaviour as kinetics was higher and allowed the shear-thinning behaviour to disappear upon long-enough relaxation times. SLS measurements did not probe any change in the structure of the solution, suggesting that the size of the domains was not affected by sonication. Meanwhile, the apparent hydrodynamic radius of the domains determined from DLS data decreased. These last two results need to be considered with caution because (i) changes in the scattering intensity may have been overlooked by the presence of the non- or poorly substituted cellulose fractions in the solutions, and (ii) the calculation of the hydrodynamic radius uses the Stokes-Einstein which may not be fully applicable to domains.

SEC measurements performed on samples prepared in the eluent highlighted that the elution volume of the three peaks did not change upon sonication. However, the area of the first peak, attributed to the large domains, decreased, while the area of the second one, attributed to the polyions, increased. Meanwhile, SLS on these solutions, as for the original salt-free solutions, did not measure any change with sonication either. Combined with the data collected on the original (*i.e.* eluent-free) solutions, it was suggested that the high shear-rates and strains and/or energy input generated during sonication would be high enough to take polyions apart from the domains without modifying the domain size. Water molecules would then be able to pass through the domains more easily, leading to the decrease in the apparent hydrodynamic radius observed upon sonication for the salt-free solutions. Further dilution of the solutions to the regime where there is no strong inter-chain interaction supported the absence of significant breakage of Na CMC chains

upon sonication, if any, as already suggested by the fact that the elution volume of the second peak, attributed to the polyions, remained constant.

Additional experiments indicated that 0.18% Na CMC solutions containing enough salt to screen all the charges were not affected by sonication, strengthening the hypothesis of the domains being held together by electrostatic interactions. DLS measurements performed after a month on 0.18%, 0.46% and 0.73% Na CMC solutions led to partial or full recovery of the slow relaxation mode, confirming the fact that no significant polyion breakage had occurred if any, and supporting the temporality of the domains.

Chapter 5: Conclusions and perspectives

The aim of this thesis was to investigate structure-property relationships of Sodium Carboxymethyl Cellulose (Na CMC) in solutions with and without added salt using both rheology and light scattering. The key findings are reported in this Chapter, together with suggestions of investigations to complement the present work.

In Chapter 3, the determination of the concentration dependence of salt-free Na CMC solution specific viscosity across the investigated concentration range has allowed the identification of three concentration regimes according to the polyelectrolyte scaling laws: the semi-dilute non-entangled, semi-dilute entangled and concentrated regimes. The data could alternatively be described by a simpler model which interpolates two power laws and uses a single crossover concentration assigned to the onset of entanglements c_e. This modelling of the data, recently proposed in the literature for Na CMC solutions, suggests that the description of polyelectrolyte chains with the electrostatic and correlation blob concepts is not sufficient to describe the chain behaviour at high concentrations. The absence of transition between the semi-dilute and the concentrated regimes, at least across the studied range of Na CMC concentrations, is further supported by the light scattering experiments, which do not detect any change in behaviour in the corresponding concentration range.

DLS revealed three relaxation modes. The two fastest relaxation modes were attributed to the fast and the slow relaxation modes typically observed in semi-dilute polyelectrolyte solutions. The fast mode was associated with the coupled diffusion between counterions and polyions. The slow mode is not predicted by the polyelectrolyte scaling laws and its origin is still not fully understood. Its observation is commonly attributed to the presence of polyion clusters, termed ‘domains’. The third relaxation mode was characterised by relaxation times of hundreds of seconds and attributed to the presence of non- or poorly dissolved cellulose fragments. As filtration significantly altered the behaviour of the solutions without significantly removing these residuals, data collection and processing were adapted to account for this additional mode, allowing light scattering measurements to be performed on original Na CMC solutions, which are relevant for industrial applications. This method could be used to investigate the behaviour of other systems,

especially those which are altered by purification techniques used to remove dust or large particles prior to LS measurements.

Because the relaxation times associated with the third relaxation mode were particularly long and the measurement durations were not long enough to collect statistically reliable data for this mode, it could not be further investigated. Indeed, the order of magnitude of the relaxation times for this third mode is hundreds of seconds, which would require standard DLS measurements to be carried out over tens of hours to collect statistically reliable data. Differential Dynamic Microscopy (DDM), which uses an optical microscope to perform DLS experiments, could overcome this issue and help understanding what the third relaxation mode corresponds to. DDM indeed combines time and space averaging, thus significantly reducing the measurement duration needed to collect reliable data and allowing the investigation of larger objects.

Both the slow mode relaxation time and the solution specific viscosity exhibited a similar concentration dependence. The concentration dependence of the slow relaxation time exhibited a change in behaviour in the concentration range assigned to the onset of polymer chain entanglement. No concentration dependence was detected by SLS in this region; further supporting the fact that this transition is related to changes in solution dynamics rather than structure. The characteristics of this transition concentration correspond to the highest crossover observed by Sedlák and Amis[66] in salt-free high M_w sodium poly(styrene sulfonate) solutions but not in low M_w solutions, which could not be assigned at the time of their experiments. All these elements strongly suggest that this transition concentration corresponds to the entanglement concentration. It would be interesting to perform combined rheology and LS measurements on solutions prepared with polyelectrolytes with characteristics that can be fully controlled. Synthetic monodisperse polyelectrolytes with a well-defined ionisation degree would be ideal candidates for this purpose. Furthermore, the behaviour of a sample with a M_w below the entanglement molecular weight should be compared with the behaviour of a high M_w sample where polymer chains can get entangled. Thus, such a combined rheology and LS study could be extended towards lower polyelectrolyte concentrations. Indeed, this would help understanding what the two other crossover concentrations reported in the literature for LS measurements correspond to, when only one crossover concentration is probed by rheology.

In Chapter 4, it was shown that sonicating Na CMC solutions led to a decrease in the solution viscosity and a weakening of the shear-thinning behaviour. Meanwhile, DLS probed a decrease in the relaxation time of the slow mode. Such results are consistent with the correlation between the solution viscosity and the slow relaxation time found in the previous investigation of salt-free semi-dilute Na CMC solutions. Upon sonication, the behaviour of the investigated semi-dilute non-entangled solution differed from the two studied semi-dilute entangled solutions. In particular, the semi-dilute non-entangled solution exhibited a Newtonian behaviour after about 30-min sonication, while the flow behaviour of the two other solutions remained shear-thinning even after significantly longer sonication times. As the concentration selected for the investigated non-entangled solution was very close to the entanglement transition, it would be interesting to perform additional sonication experiments on solutions with concentrations significantly below the entanglement transition to strengthen these results. The fast relaxation mode remained unchanged upon sonication. Moreover, SLS did not detect any change, suggesting that the size of the domains remain constant upon sonication, and that sonication induces changes in solution dynamics rather than structure.

Complementary Size Exclusion Chromatography (SEC) and LS measurements on samples diluted with an electrolyte solution suggested that there is no significant breakage of Na CMC chains, if any, under the investigated sonication conditions. SEC measurements brought further evidence that the proportion of Na CMC chains involved in the domains decreases upon sonication. This result, combined with the SLS data showing that the size of the domains remains constant under sonication, suggests that the shear-strains applied during sonication are strong enough to overcome the interactions responsible for the cohesion of the domains, so that some chains are forced to leave the domains. This also suggests that the arrangement of the chains within the domains would be such that taking some of them apart does not induce any significant change in the domain size. With this hypothesis, the domains are looser and deform more easily under flow; thus leading to the observed decrease in the shear-thinning behaviour. The present LS findings are similar to those of polyelectrolyte solution ageing studies. Hence, sonication may be useful to simulate and/or study ageing phenomena. Here too, it would be interesting to confirm these results with polyelectrolytes having well-controlled characteristics.

To further confirm that the number of Na CMC chains involved in the domains decreases upon sonication, SANS measurements could be performed on both non- and sonicated solutions. As Na CMC chains leave the domains, the number of chains participating to the network of mesh-size ξ increases (*N.B.* ξ is the correlation length; see Sections 2-2.1 and 2-3.2.1). Hence, similarly to what is observed when Na CMC concentration increases (see Section 2-3.2.1), one would expect the SANS profile of sonicated solutions to exhibit a higher scattering intensity in the high q region (characteristic for an increase in the Na CMC chains involved in the network rather than in the domains), and/or a shift of the correlation peak towards larger q values (characteristic for a decrease in ξ), as compared to non-sonicated solutions.

Sonication had no effect on Na CMC solutions containing enough salt to screen Na CMC charges as both the rheology and LS data were identical before and after sonication. Such results further support that the interactions responsible for the cohesion of the domains would be based on electrostatic interactions. It is worth noting that DLS measurements on such solutions probed two relaxation modes, as may be observed for high M_w polyelectrolyte and/or high polyelectrolyte concentrations, and despite the slow relaxation mode typically disappearing upon salt addition. The disappearance of the slow relaxation mode that can be observed when adding salt may be due to the fact that salt addition induces a change in the concentration regime from a salt-free concentration regime to a screened dilute concentration regime. Combined rheology and LS experiments with and without added salt would confirm this hypothesis. From a broader perspective, the investigation of Na CMC solutions with added salts would provide interesting insights for the formulation of the complex products it enters the composition.

After a month rest, a partial or full recovery of the slow relaxation mode was observed for the sonicated solutions. Such behaviour further supports the absence of Na CMC chain degradation without completely ruling it out. It also reinforces the hypothesis that domains correspond to a metastable equilibrium and that sonication brings Na CMC solutions beyond the equilibrium which, according to ageing studies reported in the literature, may only be achieved after months or years. An ageing study of non-sonicated solutions could be carried out to compare the influence of both ageing and sonication on Na CMC solutions.

It is worth noting that to facilitate both the comparison of the present data with those from the literature and the replication of the experiments, the ultrasound energy actually

transferred to the medium during the sonication experiments should be estimated as explained in Section 2-3.4.2. It will be quantified for publication of the sonication study.

The detectors of the size exclusion chromatograph used in this study were not sensitive enough to allow SEC investigations to be performed on dilute Na CMC solutions and fully confirm the absence of Na CMC chain breakage. Measurements on dilute Na CMC solutions with a size exclusion chromatograph equipped with a viscometer and/or a light scattering detector would help confirm that the tested sonication conditions do not induce any significant polymer chain breakage, if any. The approach used for the SEC measurements offered the possibility of studying the domains. Flow Field Flow Fractionation (FFFF), which is another technique commonly used to investigate M_w distributions of polymers, but also of the size distribution of larger 'objects', could complement SEC experiments. As FFFF columns do not contain any packing, larger objects can be studied, and prior filtration is not necessary. The original solutions may thus be studied without prior dilution and filtration (it is worth noting that the samples would still undergo dilution in the eluent in the FFFF column). Such an instrument might even be used to characterize the domains directly in water. Coupled with a light scattering detector, not only may the size distribution of the domains be characterised, but also their shape. The proportion of both free chains and chains involved in the domains might also be determined as they would elute out of the column at very different times due to the size difference.

The Na CMC samples were filtered before SEC measurements to prevent the column from getting clogged. The addition of salt in Na CMC solutions lowered their viscosity enough so that they could be filtered without being significantly altered. The filtration was moreover successful at making the ultra-slow mode reported in the investigation of the salt-free solutions disappear. This suggests that salt could be added to Na CMC to purify them. Once filtered, the Na CMC solutions with added salt could then be dialysed to remove the salt, and, if necessary, concentrated to reach higher concentrations. It is worth noting, though, that this heavy process may modify the behaviour of the obtained purified samples, and that the study of such samples may no longer be relevant for understanding the behaviour of the original samples.

The present work has established a link between Na CMC solution rheological behaviour and the presence of the domains. Rheo-small angle light scattering measurements performed on both non- and sonicated solutions may help understanding the origin of the

shear-thinning behaviour in polyelectrolyte solutions. Such measurements should preferably be performed with polyelectrolytes having well-defined characteristics, as the contribution of the non- or poorly dissolved matters in Na CMC solutions would contribute to the scattering, and it would not be possible to correct for their contribution in absence of simultaneous DLS measurements.

References

1. Lopez, C. G.; Rogers, S. E.; Colby, R. H.; Graham, P.; Cabral, J. T. Structure of Sodium Carboxymethyl Cellulose Aqueous Solutions: A SANS and Rheology Study. *Journal of Polymer Science, Part B: Polymer Physics* **2015,** *53*, 492-501.

2. Joshi, G.; Naithani, S.; Varshney, V. K.; Bisht, S. S.; Rana, V.; Gupta, P. K. Synthesis and characterization of carboxymethyl cellulose from office waste paper: A greener approach towards waste management. *Waste Management* **2015,** *38*, 33-40.

3. Zhao, G. H.; Kapur, N.; Carlin, B.; Selinger, E.; Guthrie, J. T. Characterisation of the interactive properties of microcrystalline cellulose–carboxymethyl cellulose hydrogels. *International Journal of Pharmaceutics* **2011,** *415*, 95-101.

4. MarketsAndMarkets. Carboxymethyl Cellulose Market by Application (Food & Beverages, Pharmaceutical & Cosmetics, Oil & Gas, Paper, Detergents, and Others (Mining, Textiles Processing, Ceramics, Paints, Construction, and Adhesives)) - Trends & Forecasts to 2020 http://www.marketsandmarkets.com/Market-Reports/carboxymethyl-cellulose-market-16412328.html?gclid=EAIaIQobChMIyaiA976x1wIV1TLTCh34mwWpEAAYASAAEgLmvfD_BwE (accessed Nov 9, 2017).

5. Transparency Market Research. Carboxymethyl Cellulose Market for Food and Beverages, Oil Drilling Fluids, Paper Processing, Personal Care, Paints & Adhesives, and Other End-users - Global Industry Analysis, Size, Share, Growth, Trends and Forecast, 2013 - 2019. https://www.prnewswire.com/news-releases/carboxymethyl-cellulose-market-will-reach-us10398-million-by-2019-expanding-food-and-beverage-industry-to-drive-global-market-transparency-market-research-522683771.html (accessed Nov 9, 2017).

6. Grand View Research. Carboxymethyl Cellulose Market Analysis By Application (Cosmetics & Pharmaceuticals, Food & Beverages, Oil & Gas, Paper & Board, Detergents), By Region, And Segment Forecasts, 2018 - 2025. https://www.grandviewresearch.com/industry-analysis/carboxymethyl-cellulose-cmc-market (accessed Sept 20, 2018).

7. Global Market Insights. Carboxymethyl Cellulose Market worth over $1.7bn by 2024. https://www.gminsights.com/pressrelease/carboxymethyl-cellulose-cmc-market (accessed Sept 20,2018).

8. Pader, M., Dentifrice rheology. In *Rheological properties of cosmetics and toiletries.*, Laba, D., Ed. CRC Press: New-York, 1993; pp 247-273.

9. Rosen, M. R., Oral care: formulating products and practices for health and beauty. In *Harry's Cosmeticology, Volume 3 (9th Edition)*, Chemical Publishing Company Inc.: 2015; Vol. 3, pp 1443-1482.

10. Ho Tan Tai, L., Liquid Detergents. In *Formulating Detergents and Personal Care Products - A Guide to Product Development*, AOCS Press: Champaign, 2000; pp 156-173.

11. Arancibia, C.; Bayarri, S.; Costell, E. Effect of hydrocolloid on rheology and microstructure of high-protein soy desserts. *Journal of Food Science and Technology* **2015,** *52*, 6435-6444.

12. Arinaitwe, E.; Pawlik, M. Dilute solution properties of carboxymethyl celluloses of various molecular weights and degrees of substitution. *Carbohydrate Polymers* **2014,** *99*, 423-431.

13. Dogsa, I.; Tomšič, M.; Orehek, J.; Benigar, E.; Jamnik, A.; Stopar, D. Amorphous supramolecular structure of carboxymethyl cellulose in aqueous solution at different pH values as determined by rheology, small angle X-ray and light scattering. *Carbohydrate Polymers* **2014,** *111*, 492-504.

14. Lopez, C. G.; Colby, R. H.; Cabral, J. T. Electrostatic and Hydrophobic Interactions in NaCMC Aqueous Solutions: Effect of Degree of Substitution. *Macromolecules* **2018,** *51*, 3165-3175.

15. Lopez, C. G.; Colby, R. H.; Graham, P.; Cabral, J. T. Viscosity and Scaling of Semiflexible Polyelectrolyte NaCMC in Aqueous Salt Solutions. *Macromolecules* **2017,** *50*, 332-338.

16. Hulskotter, F.; Scialla, S.; Loughnane, B. J.; Brooker, A. T.; Ure, C.; Ebert, S. R.; Ludolph, B.; Wigbers, C.; Maas, S.; Boeckh, D.; Eidamshaus, C. Cleaning compositions containing a polyetheramine, a soil release polymer, and a carboxymethylcellulose. US 9,193,939 B2 Nov 24, 2015.

17. Nicolae, A.; Radu, G.-L.; Belc, N. Effect of sodium carboxymethyl cellulose on gluten-free dough rheology. *Journal of Food Engineering* **2016,** *168*, 16-19.

18. Savadkoohi, S.; Farahnaky, A. Small deformation viscoelastic and thermal behaviours of pomegranate seed pips CMC gels. *Journal of Food Science and Technology* **2014,** *52*, 1-10.

19. Savadkoohi, S.; Mesbahi, G.; Niakousari, M.; Farahnaky, A. A New Study on the Steady Shear Flow, Thermal and Functional Properties of Beet Pulp Carboxymethyl Cellulose. *Journal of Food Processing and Preservation* **2014,** *38*, 2117-2128.

20. Dobrynin, A. V.; Rubinstein, M. Theory of polyelectrolytes in solutions and at surfaces. *Progress in Polymer Science* **2005,** *30*, 1049-1118.

21. Sedlák, M. What Can Be Seen by Static and Dynamic Light Scattering in Polyelectrolyte Solutions and Mixtures? *Langmuir* **1999,** *15*, 4045-4051.

22. Sedlák, M. Domain structure of polyelectrolyte solutions: is it real? *Macromolecules* **1993,** *26*, 1158-1162.

23. Sedlák, M. The ionic strength dependence of the structure and dynamics of polyelectrolyte solutions as seen by light scattering: The slow mode dilemma. *The Journal of Chemical Physics* **1996,** *105*, 10123-10133.

24. Cheng, H. N.; Takai, M.; Ekong, E. A. Rheology of carboxymethylcellulose made from bacterial cellulose. *Macromolecular Symposia* **1999,** *140*, 145-153.

25. Eremeeva, T. E.; Bykova, T. O. SEC of mono-carboxymethyl cellulose (CMC) in a wide range of pH; Mark–Houwink constants. *Carbohydrate Polymers* **1998,** *36*, 319-326.

26. Almlöf Ambjörnsson, H.; Schenzel, K.; Germgård, U. Carboxymethyl Cellulose Produced at Different Mercerization Conditions and Characterized by NIR FT Raman

Spectroscopy in Combination with Multivariate Analytical Methods. *BioResources* **2013,** *8*, 1918-1932.

27. Kamide, K.; Okajima, K.; Kowsaka, K.; Matsui, T.; Nomura, S.; Hikichi, K. Effect of the Distribution of Substitution of the Sodium Salt of Carboxymethylcellulose on its Absorbency toward Aqueous Liquid. *Polymer Journal* **1985,** *17*, 909-918.

28. Barba, C.; Montané, D.; Rinaudo, M.; Farriol, X. Synthesis and characterization of carboxymethylcelluloses (CMC) from non-wood fibers I. Accessibility of cellulose fibers and CMC synthesis. *Cellulose* **2002,** *9*, 319-326.

29. Jardeby, K.; Germgård, U.; Kreutz, B.; Heinze, T.; Heinze, U.; Lennholm, H. Effect of pulp composition on the characteristics of residuals in CMC made from such pulps. *Cellulose* **2005,** *12*, 385-393.

30. Kulicke, W.-M.; Kull, A. H.; Kull, W.; Thielking, H.; Engelhardt, J.; Pannek, J.-B. Characterization of aqueous carboxymethylcellulose solutions in terms of their molecular structure and its influence on rheological behaviour. *Polymer* **1996,** *37*, 2723-2731.

31. Ermi, B. D.; Amis, E. J. Domain Structures in Low Ionic Strength Polyelectrolyte Solutions. *Macromolecules* **1998,** *31*, 7378-7384.

32. Förster, S.; Schmidt, M.; Antonietti, M. Static and dynamic light scattering by aqueous polyelectrolyte solutions: effect of molecular weight, charge density and added salt. *Polymer* **1990,** *31*, 781-792.

33. Sedlák, M.; Amis, E. J. Dynamics of moderately concentrated salt-free polyelectrolyte solutions: Molecular weight dependence. *The Journal of Chemical Physics* **1992,** *96*, 817-825.

34. Tanahatoe, J. J.; Kuil, M. E. Light Scattering on Semidilute Polyelectrolyte Solutions: Ionic Strength and Polyelectrolyte Concentration Dependence. *The Journal of Physical Chemistry B* **1997,** *101*, 10839-10844.

35. Buhler, E.; Rinaudo, M. Structural and Dynamical Properties of Semirigid Polyelectrolyte Solutions: A Light-Scattering Study. *Macromolecules* **2000,** *33*, 2098-2106.

36. Cao, Z.; Zhang, G. Insight into dynamics of polyelectrolyte chains in salt-free solutions by laser light scattering and analytical ultracentrifugation. *Polymer* **2014,** *55*, 6789-6794.

37. Esquenet, C.; Buhler, E. Aggregation Behavior in Semidilute Rigid and Semirigid Polysaccharide Solutions. *Macromolecules* **2002,** *35*, 3708-3716.

38. Ioan, C. E.; Aberle, T.; Burchard, W. Light Scattering and Viscosity Behavior of Dextran in Semidilute Solution. *Macromolecules* **2001,** *34*, 326-336.

39. Schärtl, W., *Light Scattering from Polymer Solutions and Nanoparticle Dispersions*. Springer: Berlin, 2007.

40. Burchard, W., Light Scattering. In *Physical techniques for the study of food biopolymers*, Ross-Murphy, S. B., Ed. Blackie Academic & Professional: London, 1994; pp 151-213.

41. Francis, P. S. Solution properties of water-soluble polymers. I. Control of aggregation of sodium carboxymethylcellulose (CMC) by choice of solvent and/or electrolyte. *Journal of Applied Polymer Science* **1961,** *5*, 261-270.

42. Lohmander, U.; Strömberg, R. Non-newtonian flow of dilute sodium carboxymethyl cellulose solutions at different ionic strengths and of dilute solutions of cellulose nitrate and polystyrene in moderately viscous solvents studied by capillary viscometry · Experimental results. *Die Makromolekulare Chemie* **1964,** *72*, 143-158.

43. Ogutu, F. O.; Tai-Hua, M.; Rizwan, E.; Miao, Z.; Hong-Nan, S. Ultrasonic Modification of Selected Polysaccharides-Review. *Journal of Food Processing & Technology* **2015,** *6*, 446.

44. Paulusse, J. M. J.; Sijbesma, R. P. Ultrasound in polymer chemistry: Revival of an established technique. *Journal of Polymer Science Part A: Polymer Chemistry* **2006,** *44*, 5445-5453.

45. Grönroos, A.; Pirkonen, P.; Ruppert, O. Ultrasonic depolymerization of aqueous carboxymethylcellulose. *Ultrasonics Sonochemistry* **2004,** *11*, 9-12.

46. Mohod, A. V.; Gogate, P. R. Ultrasonic degradation of polymers: Effect of operating parameters and intensification using additives for carboxymethyl cellulose (CMC) and polyvinyl alcohol (PVA). *Ultrasonics Sonochemistry* **2011,** *18*, 727-734.

47. Dobrynin, A. V.; Colby, R. H.; Rubinstein, M. Scaling Theory of Polyelectrolyte Solutions. *Macromolecules* **1995,** *28*, 1859-1871.

48. Colby, R. Structure and linear viscoelasticity of flexible polymer solutions: comparison of polyelectrolyte and neutral polymer solutions. *Rheologica Acta* **2010,** *49*, 425-442.

49. Rubinstein, M.; Colby, R. H., *Polymer physics*. Oxford University Press: New-York, 2003.

50. Dou, S.; Colby, R. H. Charge density effects in salt-free polyelectrolyte solution rheology. *Journal of Polymer Science, Part B: Polymer Physics* **2006,** *44*, 2001-2013.

51. Strobl, G., *The Physics of Polymers. Concepts for understanding their structures and behavior*. 3rd ed.; Springer: Berlin, 2007.

52. Dobrynin, A. V. Theory and simulations of charged polymers: From solution properties to polymeric nanomaterials. *Current Opinion in Colloid & Interface Science* **2008,** *13*, 376-388.

53. Combet, J. Structure des solutions de polyélectrolytes : apport de la diffusion des rayons X et des neutrons aux petits angles. *JDN* **2010,** *11*, 153-176.

54. Lorchat, P. Structure des solutions aqueuses de polyélectrolytes fortement chargés. PhD Thesis, Université de Strasbourg, Strasbourg, 2012.

55. Smith, M. J.; Haidar, I. A.; Striegel, A. M. Measuring the size of polymers with negative radii using MALS/QELS: an exploration of the thermodynamic radius. *Analyst* **2007,** *132*, 455-460.

56. Colby, R. H.; Boris, D. C.; Krause, W. E.; Dou, S. Shear thinning of unentangled flexible polymer liquids. *Rheologica Acta* **2007,** *46*, 569-575.

57. Lapasin, R.; Pricl, S., *Rheology of industrial polysaccharides: Theory and applications*. Chapman & Hall: 1995.

58. Risica, D.; Barbetta, A.; Vischetti, L.; Cametti, C.; Dentini, M. Rheological properties of guar and its methyl, hydroxypropyl and hydroxypropyl-methyl derivatives in semidilute and concentrated aqueous solutions. *Polymer* **2010,** *51*, 1972-1982.

59. Gauri, V.; Koelling, K. W. Extensional rheology of concentrated poly(ethylene oxide) solutions. *Rheologica Acta* **1997,** *36*, 555-567.

60. Boris, D. C.; Colby, R. H. Rheology of Sulfonated Polystyrene Solutions. *Macromolecules* **1998,** *31*, 5746-5755.

61. Rubinstein, M.; Colby, R. H.; Dobrynin, A. V. Dynamics of Semidilute Polyelectrolyte Solutions. *Physical Review Letters* **1994,** *73*, 2776-2779.

62. Berne, B. J.; Pecora, R., *Dynamic light scattering: with applications to chemistry, biology and physics*. Dover Publications: 2000.

63. Frisken, B., Light scattering tutorial. 2001.

64. Mattsson, J., Lecture notes for "Soft matter characterisation" module. University of Leeds, 2014.

65. Vaccaro, A. Light scattering: fundamentals. http://www.lsinstruments.ch/technology/slide_shows/ (accessed Nov 1, 2017).

66. Sedlák, M.; Amis, E. J. Concentration and molecular weight regime diagram of salt-free polyelectrolyte solutions as studied by light scattering. *The Journal of Chemical Physics* **1992,** *96*, 826-834.

67. Reed, W. F., Light-Scattering Results on Polyelectrolyte Conformations, Diffusion, and Interparticle Interactions and Correlations. In *Macro-ion Characterization*, American Chemical Society: 1993; Vol. 548, pp 297-314.

68. Tanahatoe, J. J.; Kuil, M. E. Light Scattering on Semidilute Polyelectrolyte Solutions: Molar Mass and Polyelectrolyte Concentration Dependence. *The Journal of Physical Chemistry B* **1997,** *101*, 9233-9239.

69. Nierling, W.; Nordmeier, E. Studies on Polyelectrolyte Solutions VII. Fast, Heterogeneous, and Slow Diffusion Modes of Poly(diallyl-*N*,*N*-dimethylammonium chloride) in Aqueous Alcoholic Salt Solvents. *Polymer Journal* **1997,** *29*, 795-806.

70. Sedlák, M. Long-time stability of multimacroion domains in polyelectrolyte solutions. *The Journal of Chemical Physics* **2002,** *116*, 5246-5255.

71. Topp, A.; Belkoura, L.; Woermann, D. Effect of Charge Density on the Dynamic Behavior of Polyelectrolytes in Aqueous Solution. *Macromolecules* **1996,** *29*, 5392-5397.

72. Borsali, R.; Nguyen, H.; Pecora, R. Small-Angle Neutron Scattering and Dynamic Light Scattering from a Polyelectrolyte Solution: DNA. *Macromolecules* **1998,** *31*, 1548-1555.

73. Cong, R.; Temyanko, E.; Russo, P. S.; Edwin, N.; Uppu, R. M. Dynamics of Poly(styrenesulfonate) Sodium Salt in Aqueous Solution. *Macromolecules* **2006,** *39*, 731-739.

74. Slootmaekers, D.; De Jonghe, C.; Reynaers, H.; Varkevisser, F. A.; Bloys van Treslong, C. J. Static light scattering from κ-carrageenan solutions. *International Journal of Biological Macromolecules* **1988,** *10*, 160-168.

75. Ermi, B. D.; Amis, E. J. Influence of Backbone Solvation on Small Angle Neutron Scattering from Polyelectrolyte Solutions. *Macromolecules* **1997,** *30*, 6937-6942.

76. Sedlák, M. Generation of multimacroion domains in polyelectrolyte solutions by change of ionic strength or pH (macroion charge). *The Journal of Chemical Physics* **2002,** *116*, 5256-5262.

77. Zhou, K.; Li, J.; Lu, Y.; Zhang, G.; Xie, Z.; Wu, C. Re-examination of Dynamics of Polyeletrolytes in Salt-Free Dilute Solutions by Designing and Using a Novel Neutral−Charged−Neutral Reversible Polymer. *Macromolecules* **2009,** *42*, 7146-7154.

78. Sehgal, A.; Seery, T. A. P. The Ordinary−Extraordinary Transition Revisited: A Model Polyelectrolyte in a Highly Polar Organic Solvent. *Macromolecules* **1998,** *31*, 7340-7346.

79. Ghosh, S.; Peitzsch, R. M.; Reed, W. F. Aggregates and other particles as the origin of the "extraordinary" diffusional phase in polyelectrolyte solutions. *Biopolymers* **1992,** *32*, 1105-1122.

80. Sedlák, M. Mechanical properties and stability of multimacroion domains in polyelectrolyte solutions. *The Journal of Chemical Physics* **2002,** *116*, 5236-5245.

81. Kästner, U.; Hoffmann, H.; Dönges, R.; Hilbig, J. Structure and solution properties of sodium carboxymethyl cellulose. *Colloids and Surfaces A: Physicochemical and Engineering Aspects* **1997,** *123–124*, 307-328.

82. Jardeby, K.; Lennholm, H.; Germgård, U. Characterisation of the undissolved residuals in CMC-solutions. *Cellulose* **2004,** *11*, 195-202.

83. Jardeby, K.; Germgård, U.; Kreutz, B.; Heinze, T.; Heinze, U.; Lennholm, H. The influence of fibre wall thickness on the undissolved residuals in CMC solutions. *Cellulose* **2005,** *12*, 167-175.

84. Ermi, B. D.; Amis, E. J. Model Solutions for Studies of Salt-Free Polyelectrolytes. *Macromolecules* **1996,** *29*, 2701-2703.

85. Sedlak, M. On the "Filterable Aggregates and Other Particles" Interpretation of the Slow Polyelectrolyte Mode. *Macromolecules* **1995,** *28*, 793-794.

86. Graessley, W. W. Polymer chain dimensions and the dependence of viscoelastic properties on concentration, molecular weight and solvent power. *Polymer* **1980,** *21*, 258-262.

87. Clasen, C.; Kulicke, W. M. Determination of viscoelastic and rheo-optical material functions of water-soluble cellulose derivatives. *Progress in Polymer Science* **2001,** *26*, 1839-1919.

88. Enebro, J.; Momcilovic, D.; Siika-aho, M.; Karlsson, S. A New Approach for Studying Correlations between the Chemical Structure and the Rheological Properties in Carboxymethyl Cellulose. *Biomacromolecules* **2007,** *8*, 3253-3257.

89. Kumsah, C. A.; Pass, G.; Phillips, G. O. The interaction between sodium carboxymethylcellulose and water. *Journal of Solution Chemistry* **1976,** *5*, 799-806.

90. Mutalik, V.; Manjeshwar, L. S.; Wali, A.; Sairam, M.; Sreedhar, B.; Raju, K. V. S. N.; Aminabhavi, T. M. Aqueous-solution and solid-film properties of poly(vinyl alcohol), poly(vinyl pyrrolidone), gelatin, starch, and carboxymethylcellulose polymers. *Journal of Applied Polymer Science* **2007,** *106*, 765-774.

91. Siqueira, E. J.; Brochier Salon, M. C.; Mauret, E. The effects of sodium chloride (NaCl) and residues of cellulosic fibres derived from sodium carboxymethylcellulose (NaCMC) synthesis on thermal and mechanical properties of CMC films. *Industrial Crops and Products* **2015,** *72*, 87-96.

92. Vais, A. E.; Palazoglu, T. K.; Sandeep, K. P.; Daubert, C. R. Rheological characterization of carboxymethylcellulose solution under aseptic processing conditions. *Journal of Food Process Engineering* **2002,** *25*, 41-61.

93. Yaşar, F.; Toğrul, H.; Arslan, N. Flow properties of cellulose and carboxymethyl cellulose from orange peel. *Journal of Food Engineering* **2007,** *81*, 187-199.

94. Heinze, T.; Heinze, U.; Klemm, D. Viscosity behaviour of multivalent metal ion-containing carboxymethyl cellulose solutions. *Die Angewandte Makromolekulare Chemie* **1994,** *220*, 123-132.

95. Käuper, P.; Kulicke, W.-M.; Horner, S.; Saake, B.; Puls, J.; Kunze, J.; Fink, H.-P.; Heinze, U.; Heinze, T.; Klohr, E.-A.; Thielking, H.; Koch, W. Development and evaluation of methods for determining the pattern of functionalization in sodium carboxymethylcelluloses. *Die Angewandte Makromolekulare Chemie* **1998,** *260*, 53-63.

96. Kulicke, W. M.; Lange, S.; Heins, D., Advantages of Determining the Molar Mass Distributions of Water-Soluble Polymers and Polyelectrolytes with FFFF-MALLS and SEC-MALLS. In *Chromatography of Polymers*, American Chemical Society: 1999; Vol. 731, pp 114-140.

97. Rinaudo, M.; Danhelka, J.; Milas, M. A new approach to characterising carboxymethylcelluloses by size exclusion chromatography. *Carbohydrate Polymers* **1993,** *21*, 1-5.

98. Heinze, T.; Koschella, A. Carboxymethyl Ethers of Cellulose and Starch – A Review. *Macromolecular Symposia* **2005,** *223*, 13-40.

99. Reuben, J.; Conner, H. T. Analysis of the carbon-13 n.m.r. spectrum of hydrolyzed *O*-(carboxymethyl)cellulose: monomer composition and substitution patterns. *Carbohydrate Research* **1983,** *115*, 1-13.

100. Silva, D. A.; de Paula, R. C. M.; Feitosa, J. P. A.; de Brito, A. C. F.; Maciel, J. S.; Paula, H. C. B. Carboxymethylation of cashew tree exudate polysaccharide. *Carbohydrate Polymers* **2004,** *58*, 163-171.

101. Heinze, T.; Erler, U.; Nehls, I.; Klemm, D. Determination of the substituent pattern of heterogeneously and homogeneously synthesized carboxymethyl cellulose by using high-performance liquid chromatography. *Die Angewandte Makromolekulare Chemie* **1994,** *215*, 93-106.

102. Zhang, G.; Zhang, L.; Deng, H.; Sun, P. Preparation and characterization of sodium carboxymethyl cellulose from cotton stalk using microwave heating. *Journal of Chemical Technology & Biotechnology* **2011,** *86*, 584-589.

103. Ünlü, C. H. Carboxymethylcellulose from recycled newspaper in aqueous medium. *Carbohydrate Polymers* **2013,** *97*, 159-164.

104. Adinugraha, M. P.; Marseno, D. W.; Haryadi Synthesis and characterization of sodium carboxymethylcellulose from cavendish banana pseudo stem (*Musa cavendishii* LAMBERT). *Carbohydrate Polymers* **2005,** *62*, 164-169.

105. Toğrul, H.; Arslan, N. Production of carboxymethyl cellulose from sugar beet pulp cellulose and rheological behaviour of carboxymethyl cellulose. *Carbohydrate Polymers* **2003,** *54*, 73-82.

106. Heinze, T.; Röttig, K.; Nehls, I. Synthesis of 2,3-*O*-carboxymethylcellulose. *Macromolecular Rapid Communications* **1994,** *15*, 311-317.

107. Hoogendam, C. W.; de Keizer, A.; Cohen Stuart, M. A.; Bijsterbosch, B. H.; Smit, J. A. M.; van Dijk, J. A. P. P.; van der Horst, P. M.; Batelaan, J. G. Persistence Length of Carboxymethyl Cellulose As Evaluated from Size Exclusion Chromatography and Potentiometric Titrations. *Macromolecules* **1998,** *31*, 6297-6309.

108. Cheng, G.; Varanasi, P.; Li, C.; Liu, H.; Melnichenko, Y. B.; Simmons, B. A.; Kent, M. S.; Singh, S. Transition of Cellulose Crystalline Structure and Surface Morphology of Biomass as a Function of Ionic Liquid Pretreatment and Its Relation to Enzymatic Hydrolysis. *Biomacromolecules* **2011,** *12*, 933-941.

109. O'Sullivan, A. C. Cellulose: the structure slowly unravels. *Cellulose* **1997,** *4*, 173-207.

110. Baker, A. A.; Helbert, W.; Sugiyama, J.; Miles, M. J. High-Resolution Atomic Force Microscopy of Native *Valonia* Cellulose I Microcrystals. *Journal of Structural Biology* **1997,** *119*, 129-138.

111. Dürig, G.; Banderet, A. Sur la structure des solutions aqueuses de carboxymethylcellulose. *Helvetica Chimica Acta* **1950,** *33*, 1106-1118.

112. Xiquan, L.; Tingzhu, Q.; Shaoqui, Q. Kinetics of the carboxymethylation of cellulose in the isopropyl alcohol system. *Acta Polymerica* **1990,** *41*, 220-222.

113. Höppler, F. Rheometrie und Kolloidik des Systems Natriumzelluloseglykolat—Wasser. *Kolloid-Zeitschrift* **1942,** *98*, 348-358.

114. Lindman, B.; Karlström, G.; Stigsson, L. On the mechanism of dissolution of cellulose. *Journal of Molecular Liquids* **2010,** *156*, 76-81.

115. Medronho, B.; Romano, A.; Miguel, M. G.; Stigsson, L.; Lindman, B. Rationalizing cellulose (in)solubility: reviewing basic physicochemical aspects and role of hydrophobic interactions. *Cellulose* **2012,** *19*, 581-587.

116. Lindman, B.; Medronho, B., *The Subtleties of Dissolution and Regeneration of Cellulose: Breaking and Making Hydrogen Bonds*. 2015.

117. Medronho, B.; Lindman, B. Competing forces during cellulose dissolution: From solvents to mechanisms. *Current Opinion in Colloid & Interface Science* **2014,** *19*, 32-40.

118. Guillot, S.; Delsanti, M.; Désert, S.; Langevin, D. Surfactant-Induced Collapse of Polymer Chains and Monodisperse Growth of Aggregates near the Precipitation Boundary in Carboxymethylcellulose−DTAB Aqueous Solutions. *Langmuir* **2003,** *19*, 230-237.

119. Brown, W.; Henley, D. Studies on cellulose derivatives. Part IV. The configuration of the polyelectrolyte sodium carboxymethyl cellulose in aqueous sodium chloride solutions. *Die Makromolekulare Chemie* **1964,** *79*, 68-88.

120. Brown, W.; Henley, D.; Öhman, J. Sodium carboxymethyl cellulose, an experimental study of the influence of molecular weight and ionic strength on polyelectrolyte configuration. *Arkiv för Kemi* **1964,** *22*, 189-206.

121. Schneider, N. S.; Doty, P. Macro-ions. IV. The Ionic Strength Dependence of the Molecular Properties of Sodium Carboxymethylcellulose. *The Journal of Physical Chemistry* **1954,** *58*, 762-769.

122. Trap, H. J. L.; Hermans, J. J. Light-Scattering by Polymethacrylic Acid and Carboxymethylcellulose in Various Solvents. *The Journal of Physical Chemistry* **1954,** *58*, 757-761.

123. Castelain, C.; Doublier, J. L.; Lefebvre, J. A study of the viscosity of cellulose derivatives in aqueous solutions. *Carbohydrate Polymers* **1987,** *7*, 1-16.

124. Dapía, S.; Tovar, C. A.; Santos, V.; Parajó, J. C. Rheological behaviour of carboxymethylcellulose manufactured from TCF-bleached Milox pulps. *Food Hydrocolloids* **2005,** *19*, 313-320.

125. Ghannam, M. T.; Esmail, M. N. Rheological properties of carboxymethyl cellulose. *Journal of Applied Polymer Science* **1997,** *64*, 289-301.

126. Yang, X.; Zhu, W. Viscosity properties of sodium carboxymethylcellulose solutions. *Cellulose* **2007,** *14*, 409-417.

127. Benchabane, A.; Bekkour, K. Rheological properties of carboxymethyl cellulose (CMC) solutions. *Colloid and Polymer Science* **2008,** *286*, 1173-1180.

128. Edali, M.; Esmail, M. N.; Vatistas, G. H. Rheological properties of high concentrations of carboxymethyl cellulose solutions. *Journal of Applied Polymer Science* **2001,** *79*, 1787-1801.

129. Balmaceda, E.; Rha, C.; Huang, F. Rheological properties of hydrocolloids. *Journal of Food Science* **1973,** *38*, 1169-1173.

130. Abdelrahim, K. A.; Ramaswamy, H. S. High temperature/pressure rheology of carboxymethyl cellulose (CMC). *Food Research International* **1995,** *28*, 285-290.

131. Abdelrahim, K. A.; Ramaswamy, H. S.; Doyon, G.; Toupin, C. Effects of concentration and temperature on carboxymethylcellulose rheology. *International Journal of Food Science & Technology* **1994,** *29*, 243-253.

132. Cancela, M. A.; Álvarez, E.; Maceiras, R. Effects of temperature and concentration on carboxymethylcellulose with sucrose rheology. *Journal of Food Engineering* **2005,** *71*, 419-424.

133. Gómez-Díaz, D.; Navaza, J. M. Rheology of aqueous solutions of food additives: Effect of concentration, temperature and blending. *Journal of Food Engineering* **2003,** *56*, 387-392.

134. Elfak, A. M.; Pass, G.; Phillips, G. O. The effect of shear rate on the viscosity of solutions of sodium carboxymethylcellulose and κ-carrageenan. *Journal of the Science of Food and Agriculture* **1979,** *30*, 724-730.

135. Yaseen, E. I.; Herald, T. J.; Aramouni, F. M.; Alavi, S. Rheological properties of selected gum solutions. *Food Research International* **2005,** *38*, 111-119.

136. Renaud, M.; Belgacem, M. N.; Rinaudo, M. Rheological behaviour of polysaccharide aqueous solutions. *Polymer* **2005,** *46*, 12348-12358.

137. Escudier, M. P.; Gouldson, I. W.; Pereira, A. S.; Pinho, F. T.; Poole, R. J. On the reproducibility of the rheology of shear-thinning liquids. *Journal of Non-Newtonian Fluid Mechanics* **2001,** *97*, 99-124.

138. Tam, K. C.; Tiu, C. Improved correlation for shear-dependent viscosity of polyelectrolyte solutions. *Journal of Non-Newtonian Fluid Mechanics* **1993,** *46*, 275-288.

139. Salt, D. L.; Ryan, N. W.; Christiansen, E. B. The rheology of carboxymethylcellulose dispersions in water. *Journal of Colloid Science* **1951,** *6*, 146-154.

140. Elfak, A. M.; Pass, G.; Phillips, G. O. The viscosity of dilute solutions of κ-carrageenan and sodium carboxymethylcellulose. *Journal of the Science of Food and Agriculture* **1978,** *29*, 557-562.

141. Muller, F. L.; Davidson, J. F. Rheology of Shear Thinning Polymer Solutions. *Industrial & Engineering Chemistry Research* **1994,** *33*, 2364-2367.

142. Piližota, V.; Šubarić, D.; Lovrić, T. Rheological properties of CMC dispersions at low temperatures. *Food Technology and Biotechnology* **1996,** *34*.

143. Truzzolillo, D.; Cametti, C.; Sennato, S. Dielectric properties of differently flexible polyions: a scaling approach. *Physical Chemistry Chemical Physics* **2009,** *11*, 1780-1786.

144. Li, W.; Sun, B.; Wu, P. Study on hydrogen bonds of carboxymethyl cellulose sodium film with two-dimensional correlation infrared spectroscopy. *Carbohydrate Polymers* **2009,** *78*, 454-461.

145. Okatova, O. V.; Lavrenko, P. N.; Dautzenberg, H.; Filipp, B. N.; Tsvetkov, V. N. Polyelectrolyte effects in diffusion and viscosity phenomena in water-cadoxene solutions of carboxymethylcellulose. *Polymer Science U.S.S.R.* **1990,** *32*, 533-539.

146. Kulicke, W.-M.; Reinhardt, U.; Fuller, G. G.; Arendt, O. Characterization of the flow properties of sodium carboxymethylcellulose via mechanical and optical techniques. *Rheologica Acta* **1999,** *38*, 26-33.

147. deButts, E. H.; Hudy, J. A.; Elliott, J. H. Rheology of Sodium Carboxymethylcellulose Solutions. *Industrial & Engineering Chemistry* **1957,** *49*, 94-98.

148. Kamide, K.; Saito, M. Light Scattering and Viscometric Study of Cellulose in Aqueous Lithium Hydroxide. *Polymer Journal* **1986,** *18*, 569-579.

149. Matsumoto, T.; Mashiko, K. Influence of added salt on dynamic viscoelasticity of carboxymethylcellulose aqueous systems. *Polymer Engineering & Science* **1988,** *28*, 393-402.

150. Rinaudo, M.; Mils, M. Polyelectroyte behavior of a bacterial polysaccharide from *Xanthomonas campestris:* Comparison with carboxymethylcellulose. *Biopolymers* **1978,** *17*, 2663-2678.

151. Basu, S.; Das Gupta, P. C. Studies on polyelectrolytes. I. Sodium carboxymethylcellulose. *Journal of Colloid Science* **1952,** *7*, 53-70.

152. Fujita, H.; Homma, T. Non-Newtonian viscosities in dilute aqueous solutions of sodium carboxymethylcellulose. *Journal of Polymer Science* **1955,** *15*, 277-295.

153. Pals, D. T. F.; Hermans, J. J. Sodium salts of pectin and of carboxy methyl cellulose in aqueous sodium chloride. I. Viscosities. *Recueil des Travaux Chimiques des Pays-Bas* **1952,** *71*, 433-457.

154. Bonferoni, M. C.; Rossi, S.; Ferrari, F.; Bertoni, M.; Caramella, C. Influence of medium on dissolution-erosion behaviour of Na carboxymethylcellulose and on viscoelastic properties of gels. *International Journal of Pharmaceutics* **1995,** *117*, 41-48.

155. Prabhu, V. M. Counterion structure and dynamics in polyelectrolyte solutions. *Current Opinion in Colloid & Interface Science* **2005,** *10*, 2-8.

156. Kulicke, W.-M.; Otto, M.; Baar, A. Improved NMR characterization of high-molecular-weight polymers and polyelectrolytes through the use of preliminary ultrasonic degradation. *Die Makromolekulare Chemie* **1993,** *194*, 751-765.

157. Zhu, Z.; Zhu, W.; Yi, J.; Liu, N.; Cao, Y.; Lu, J.; Decker, E. A.; McClements, D. J. Effects of sonication on the physicochemical and functional properties of walnut protein isolate. *Food Research International* **2018,** *106*, 853-861.

158. Liu, D. The influence of ultrasound on the structure, rheological properties and degradation path of citrus pectin. *Proceedings of Meetings on Acoustics* **2013,** *19*, 045092.

159. Suslick, K. S.; Price, G. J. Applications of ultrasound to materials chemistry. *Annual Review of Materials Science* **1999,** *29*, 295-326.

160. Portenlänger, G.; Heusinger, H. The influence of frequency on the mechanical and radical effects for the ultrasonic degradation of dextranes. *Ultrasonics Sonochemistry* **1997,** *4*, 127-130.

161. Koda, S.; Taguchi, K.; Futamura, K. Effects of frequency and a radical scavenger on ultrasonic degradation of water-soluble polymers. *Ultrasonics Sonochemistry* **2011,** *18*, 276-281.

162. Jambrak, A. R.; Lelas, V.; Mason, T. J.; Krešić, G.; Badanjak, M. Physical properties of ultrasound treated soy proteins. *Journal of Food Engineering* **2009,** *93*, 386-393.

163. Li, H.; Pordesimo, L.; Weiss, J. High intensity ultrasound-assisted extraction of oil from soybeans. *Food Research International* **2004,** *37*, 731-738.

164. Cárcel, J. A.; Benedito, J.; Bon, J.; Mulet, A. High intensity ultrasound effects on meat brining. *Meat Science* **2007,** *76*, 611-619.

165. Raso, J.; Mañas, P.; Pagán, R.; Sala, F. J. Influence of different factors on the output power transferred into medium by ultrasound. *Ultrasonics Sonochemistry* **1999,** *5*, 157-162.

166. Reed, C. E.; Li, X.; Reed, W. F. The effects of pH on hyaluronate as observed by light scattering. *Biopolymers* **1989,** *28*, 1981-2000.

167. Lant, N. J. Laundry detergent composition comprising a highly water-soluble carboxymethyl cellulose particle. US 8,193,143 B2 Jun 5, 2012.

168. Cash, M. J.; Cowan, P. J.; Kroon, G. Soluble, associative carboxymethylcellulose, method of making, and uses thereof. US 2004/0158058 A1 Aug 12, 2004.

169. Waring, M. J.; Parsons, D. Physico-chemical characterisation of carboxymethylated spun cellulose fibres. *Biomaterials* **2001,** *22*, 903-912.

170. Sedlák, M.; Koňák, Č.; Štěpánek, P.; Jakeš, J. Semidilute solutions of poly(methacrylic acid) in the absence of salt: Dynamic light-scattering study. *Polymer* **1987,** *28*, 873-880.

171. Wissenburg, P.; Odijk, T.; Cirkel, P.; Mandel, M. Multimolecular aggregation of mononucleosomal DNA in concentrated isotropic solutions. *Macromolecules* **1995,** *28*, 2315-2328.

172. Schmidt, M. Static and dynamic light scattering by an aqueous polyelectrolyte solution without added salt: Quaternized poly(2-vinylpyridine). *Die Makromolekulare Chemie, Rapid Communications* **1989,** *10*, 89-96.

173. ASTM D1439-03(2008), Standard Test Methods for Sodium Carboxymethylcellulose. In *Annual book of ASTM standards*, ASTM International: Philadelphia, 2010; Vol. 6.03, pp 245-250.

174. Dou, S.; Colby, R. H. Charge density effects in salt-free polyelectrolyte solution rheology. *Journal of Polymer Science, Part B: Polymer Physics* **2006,** *44*, 2001-2013.

175. Truzzolillo, D.; Bordi, F.; Cametti, C.; Sennato, S. Counterion condensation of differently flexible polyelectrolytes in aqueous solutions in the dilute and semidilute regime. *Physical Review E* **2009,** *79*, 011804.

176. Zhang, Y.; Douglas, J. F.; Ermi, B. D.; Amis, E. J. Influence of counterion valency on the scattering properties of highly charged polyelectrolyte solutions. *The Journal of Chemical Physics* **2001,** *114*, 3299-3313.

177. Mori, S.; Barth, H. G., *Size exclusion chromatography*. Springer-Verlag: 1999.

178. Barth, H. G. A Practical Approach to Steric Exclusion Chromatography of Water-Soluble Polymers. *Journal of Chromatographic Science* **1980,** *18*, 409-429.

179. Cave, R. A.; Seabrook, S. A.; Gidley, M. J.; Gilbert, R. G. Characterization of Starch by Size-Exclusion Chromatography: The Limitations Imposed by Shear Scission. *Biomacromolecules* **2009,** *10*, 2245-2253.

180. Carpenter, J. F.; Randolph, T. W.; Jiskoot, W.; Crommelin, D. J. A.; Middaugh, C. R.; Winter, G. Potential inaccurate quantitation and sizing of protein aggregates by size exclusion chromatography: Essential need to use orthogonal methods to assure the quality of therapeutic protein products. *Journal of Pharmaceutical Sciences* **2010,** *99*, 2200-2208.

181. Mahler, H.-C.; Friess, W.; Grauschopf, U.; Kiese, S. Protein aggregation: Pathways, induction factors and analysis. *Journal of Pharmaceutical Sciences* **2009,** *98*, 2909-2934.

182. Li, Y.; Weiss, W. F.; Roberts, C. J. Characterization of high-molecular-weight nonnative aggregates and aggregation kinetics by size exclusion chromatography with inline multi-angle laser light scattering. *Journal of Pharmaceutical Sciences* **2009,** *98*, 3997-4016.

183. Sahin, E.; Roberts, C. J., Size-Exclusion Chromatography with Multi-angle Light Scattering for Elucidating Protein Aggregation Mechanisms. In *Therapeutic Proteins: Methods and Protocols*, Voynov, V.; Caravella, J. A., Eds. Humana Press: Totowa, NJ, 2012; pp 403-423.

184. Philo, J. S. Is any measurement method optimal for all aggregate sizes and types? *The AAPS Journal* **2006,** *8*, E564-E571.

185. Arakawa, T.; Ejima, D.; Li, T.; Philo, J. S. The critical role of mobile phase composition in size exclusion chromatography of protein pharmaceuticals. *Journal of Pharmaceutical Sciences* **2010,** *99*, 1674-1692.

186. Fisher Scientific. https://www.fishersci.ie/webfiles/uk/web-docs/0137_LC.pdf (accessed Aug 29, 2018).

187. Agilent Technologies. An Analysis of food by GPC/SEC. http://hpst.cz/sites/default/files/attachments/5991-2029en.pdf (accessed May 18, 2017).

188. Agilent Technologies. PEG/PEO Calibration Kits. https://www.agilent.com/en/products/gpc-sec/gpc-sec-standards/polystyrene-standards/easivial (accessed May 15, 2017).

189. Wu, C.-S., *Column handbook for size exclusion chromatography*. Academic Press: 1999; p 637.

190. Neddermeyer, P. A.; Rogers, L. B. Column efficiency and electrolyte effects of inorganic salts in aqueous gel chromatography. *Analytical Chemistry* **1969,** *41*, 94-102.

191. Ochi, A.; Hossain, K. S.; Magoshi, J.; Nemoto, N. Rheology and Dynamic Light Scattering of Silk Fibroin Solution Extracted from the Middle Division of *Bombyx mori* Silkworm. *Biomacromolecules* **2002,** *3*, 1187-1196.

192. Busnel, J. P.; Foucault, F.; Denis, L.; Lee, W.; Chang, T. Investigation and interpretation of band broadening in size exclusion chromatography. *Journal of Chromatography A* **2001,** *930*, 61-71.

193. Felinger, A.; Pasti, L.; Dondi, F.; van Hulst, M.; Schoenmakers, P. J.; Martin, M. Stochastic Theory of Size Exclusion Chromatography: Peak Shape Analysis on Single Columns. *Analytical Chemistry* **2005,** *77*, 3138-3148.

194. Di Marco, V. B.; Bombi, G. G. Mathematical functions for the representation of chromatographic peaks. *Journal of Chromatography A* **2001,** *931*, 1-30.

195. Štulík, K.; Pacáková, V.; Tichá, M. Some potentialities and drawbacks of contemporary size-exclusion chromatography. *Journal of Biochemical and Biophysical Methods* **2003,** *56*, 1-13.

196. Yu, J. F. S.; Zakin, J. L.; Patterson, G. K. Mechanical degradation of high molecular weight polymers in dilute solution. *Journal of Applied Polymer Science* **1979,** *23*, 2493-2512.

197. Barth, H. G.; Carlin, F. J. A Review of Polymer Shear Degradation in Size-Exclusion Chromatography. *Journal of Liquid Chromatography* **1984,** *7*, 1717-1738.

198. D'Almeida, A. R.; Dias, M. L. Comparative study of shear degradation of carboxymethylcellulose and poly(ethylene oxide) in aqueous solution. *Polymer Degradation and Stability* **1997,** *56*, 331-337.

199. Devanand, K.; Selser, J. C. Asymptotic behavior and long-range interactions in aqueous solutions of poly(ethylene oxide). *Macromolecules* **1991,** *24*, 5943-5947.

200. Nascentes, C. C.; Korn, M.; Sousa, C. S.; Arruda, M. A. Z. Use of ultrasonic baths for analytical applications: a new approach for optimisation conditions. *Journal of the Brazilian Chemical Society* **2001,** *12*, 57-63.

201. Prabhu, V. M.; Amis, E. J.; Bossev, D. P.; Rosov, N. Counterion associative behavior with flexible polyelectrolytes. *The Journal of Chemical Physics* **2004,** *121*, 4424-4429.

202. Shakun, M.; Maier, H.; Heinze, T.; Kilz, P.; Radke, W. Molar mass characterization of sodium carboxymethyl cellulose by SEC-MALLS. *Carbohydrate Polymers* **2013,** *95*, 550-559.

203. OriginLab®. Gauss. https://www.originlab.com/doc/Origin-Help/Gauss-FitFunc (accessed Aug 4, 2018).

204. OriginLab®. GaussMod. https://www.originlab.com/doc/Origin-Help/GaussMod-FitFunc (accessed Aug 4, 2018).

Appendixes

Appendix I: Supplementary information to Chapter 3

As in Chapter 3, all concentrations are in *wt*%.

AI-1. Optical microscopy of Na CMC solutions and microcrystalline cellulose suspensions

To investigate the particulates observed in all the studied Na CMC solutions (see Sections 3-3.1, 3-3.3 and 3-3.5), both Na CMC solutions and microcrystalline cellulose suspensions were observed with a microscope using phase contrast and differential interference contrast techniques (see Section 3-2.2.1 for details about the instrument). A few of the collected images are shown in Figures AI-1 and AI-2.

Figure AI-1.A is a wider view of Figure 3-1.C and shows the particulates observed in a 0.018% Na CMC solution. Figures A I-1.A' and A" are images of the same particulates using different *foci*. In Figure AI-1.A, the particulates have a relatively well-defined contour, while in Figures AI-1.A' and A", they appear to consist of a core surrounded by a thick ring and resemble the swollen rings observed by Jardeby *et al.*[83] Such particulates are thought to be poorly substituted cellulose fragments which cannot undergo full dissolution.[83] Depending on the image used for sizing, the size of the particulates is estimated to be around 1-10 µm; larger sizes are found when the particulates are sized using Figure AI-1.A".

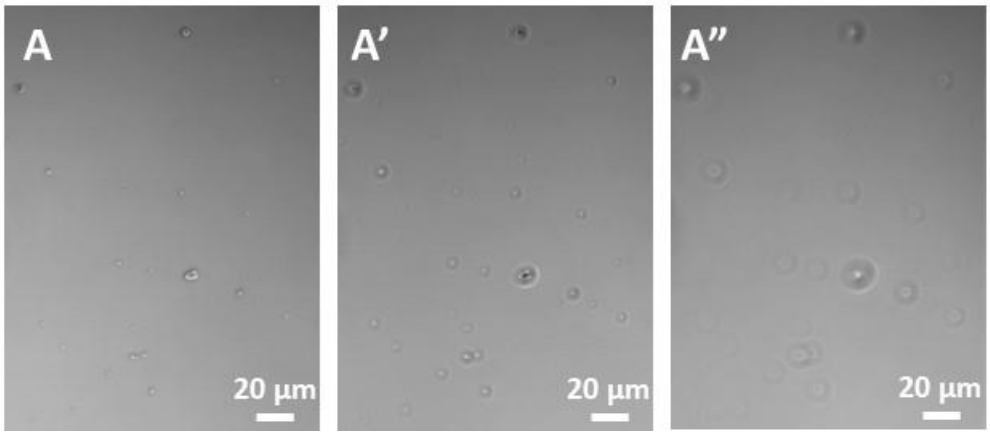

Figure AI-1: Small particulates observed in a 0.018% Na CMC solution**.** A, A' and A" show the same particulates observed with different *foci*. A is a wider view of Figure 3-1.C.

To further investigate the suggested origin of the observed particulates as non- or poorly substituted cellulose, a complementary microscopy investigation was performed on

suspensions of microcrystalline cellulose (microcrystalline cellulose powder from cotton linters; product number: 1001938731; Sigma Aldrich); the corresponding images are shown in Figure AI-2. Particulates with different sizes and shapes are observed. It is noted that these look similar to some of the particulates shown in Figure 3-1.D, which strengthens the hypothesis that the particulates observed in the Na CMC solutions are poorly or non-substituted cellulose fragments.

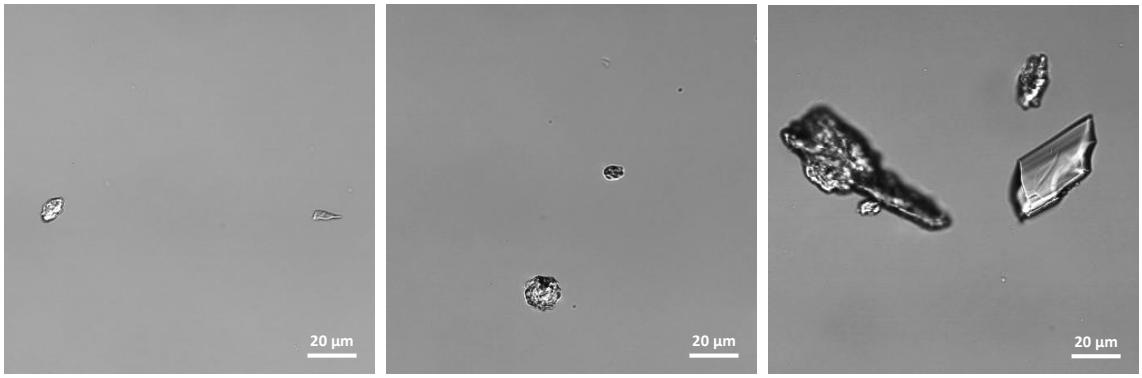

Figure AI-2: Examples of particulates observed with a phase contrast microscope in microcrystalline cellulose suspensions.

AI-2. Rheology measurements

AI-2.1. Data collection and further calculations

To identify the optimal experimental parameters for the viscosity measurements, the time-dependence of the solution viscosity was measured for different shear stresses. This procedure allowed the determination of the time required to reach a steady-state flow, the equilibrium time Δt_{eq}, which was subsequently set to 200 s and 30 s for solutions with $c_{Na\ CMC} \leq 0.37\%$ and $c_{Na\ CMC} \geq 0.46\%$, respectively. For each solution, data were collected using averaging times Δt_{av} of both 200 and 300 s to check that acquisition time parameters did not influence the collected data. As the data obtained for both averaging times were identical, it was concluded that steady-state flows were achieved and only the data collected using Δt_{av} = 200 s were used.

The viscosity curves shown in Figure 3-2 were fitted with the Carreau model[1] (Eq. AI-1):

$$\eta(\dot{\gamma}) = \frac{\eta_0}{(1+(\tau\dot{\gamma})^2)^p} \quad \text{(AI-1)}$$

where η_0 is the zero-shear viscosity and corresponds to the viscosity plateau observed at low shear rates, τ is a time constant which corresponds to the inverse of the shear-rate characterising the shear-thinning behaviour onset and p is an exponent which describes

the behaviour of the viscosity as a function of the shear-rate in the shear-thinning region. The fitting parameters obtained for the curves shown in Figure 3-2 are shown in Table AI-1.

Table AI-1: Fitting parameters obtained with the Carreau model for the data shown in Figure 3-2.

$c_{Na\ CMC}$ (%)	η_0 (Pa.s)	τ (s)	p (-)	χ_{red}^2	R_{adj}^2
0.018	$(1.47 \pm 0.02) \times 10^{-2}$	0.28 ± 0.03	0.123 ± 0.004	1.85×10^{-8}	0.998
0.046	$(2.59 \pm 0.08) \times 10^{-2}$	0.5 ± 0.2	0.099 ± 0.009	6.71×10^{-7}	0.983
0.15	$(6.26 \pm 0.06) \times 10^{-2}$	0.15 ± 0.02	0.150 ± 0.009	1.31×10^{-6}	0.996
0.37	0.254 ± 0.004	0.38 ± 0.07	0.15 ± 0.01	2.87×10^{-5}	0.995
0.55	0.69 ± 0.02	0.7 ± 0.2	0.17 ± 0.02	6.17×10^{-4}	0.990
0.73	1.85 ± 0.05	1.9 ± 0.5	0.17 ± 0.02	4.83×10^{-3}	0.989

The accuracy of the zero-shear viscosity measurements was estimated for two selected Na CMC concentrations: 0.018% and 0.18%. For each of these concentrations, rheology measurements were performed on 3 different batches. The obtained zero-shear values were averaged, and both the standard error and the relative error were determined. The relative errors calculated for the 0.018% and 0.18% solutions were used to calculate the standard errors for the solutions of Na CMC concentrations below and above 0.18% respectively. These standard errors are the errors represented by the error bars in Figure 3-3 as well as in Figure AI-3.

AI-2.2. Fitting of the $\eta_{sp} = f(c_{Na\ CMC})$ data, and identification of the different concentration regimes and crossover concentrations

Figure AI-3 includes the same data as Figure 3-3. Figure AI-3.A is identical to Figure 3-3, except that the power law describing the semi-dilute non-entangled regime has been extrapolated to $\eta_{sp} = 1$ to determine the overlap concentration c^* provided in Table 3-1. Figure AI-3.B is similar to Figure AI-3.A, except that the power law fits are obtained using fixed exponent values corresponding to the theoretical values predicted by the scaling laws (see the discussion in Section 3-3.2). Figure AI-3.C is identical to the inset of Figure 3-3 and shows the fit of the data to Eq. 3-2b (also shown in the Figure) with the power law exponent describing the behaviour in the semi-dilute non-entangled regime set to the value found with the best power law fits (*i.e.* $\gamma = 0.74$). Similarly, Figure AI-3.D shows the data fitted to Eq 3-2b with the power law exponent set to the value predicted by the scaling laws (*i.e.* $\gamma = 0.5$).

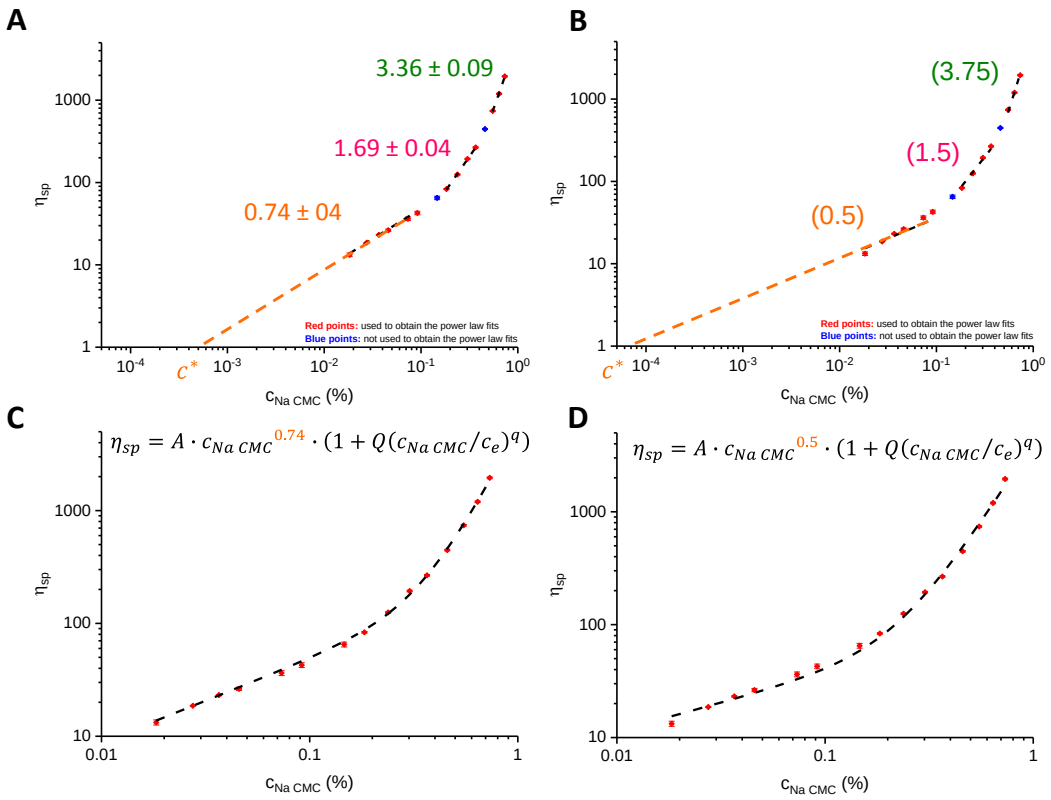

Figure AI-3: Illustration of the methods used to calculate the crossover concentrations. **A.** Calculation of c^* using the best fit power law exponents. The orange dashed line shows how the fit of the semi-dilute non-entangled regime was extrapolated to 1 to determine $c(\eta_{sp} = 1)$, which corresponds to c^*. **B.** Calculation of the overlap concentration c^* based on the power law exponent predicted by the scaling laws of polyelectrolytes in salt-free solutions. The orange dashed line shows how the fit of the semi-dilute non-entangled regime was extrapolated to 1 to determine $c(\eta_{sp} = 1)$, which corresponds to c^*. **C.** Fit of $\eta_{sp} = f(c_{Na\ CMC})$ from the semi-dilute regime with Eq. 3-2b (see Section 3-3.2). The values of γ and c_e are the ones obtained from the best power law fits (*i.e.* $\gamma = 0.74$ and $c_e = 0.17$ *wt*%). The values of the free fitting parameters A, Q and q are $266 \pm 4\%^{-0.74}$, 0.122 ± 0.006 and 2.82 ± 0.07 respectively. **D.** Fit of $\eta_{sp} = f(c_{Na\ CMC})$ from the semi-dilute regime with Eq. 3-2b (see Section 3-3.2). The values of γ and c_e are the ones obtained from the scaling law fits (*i.e.* $\gamma = 0.5$ and $c_e = 0.10$ *wt*%). The values of the free fitting parameters A, Q and q are $114 \pm 3\%^{-0.5}$, 0.14 ± 0.03 and 2.40 ± 0.09 respectively.

AI-3. Light scattering measurements

AI-3.1. Linear range of the detector

To be reliable, Light Scattering (LS) data need to be collected within the linear range of the detector. The instrument used for the measurements has an automated attenuator which adapts the laser intensity to result in a scattering intensity which is as high as possible but within the linear range of detector. To do this, the laser intensity is set to a given value for a certain amount of time and the scattering intensity measured. The laser intensity is increased step-by-step until an optimum scattering intensity is achieved.

However, as explained in Section 3-3.3, particulates, which scatter significantly, sometimes enter the scattering volume. When the duration used to test the laser intensity is shorter than the time-scale for particulates to enter the scattering volume, the laser intensity is set to a value for which the upper limit of the linear range of the detector is reached during the actual measurements, particularly at the lowest scattering angles. This saturation is illustrated in Figure AI-4.A, showing the scattering intensity of a 0.73% Na CMC solution over time. Thus, at the lowest angles, the scattering intensity was not set with the automated mode, but to a value far below the upper limit of the linear range of the detector, as illustrated in Figure AI-4.B, where the experimental conditions are identical to the ones used to obtain Figure AI-4.A except that the scattering intensity was set to 25 kHz.

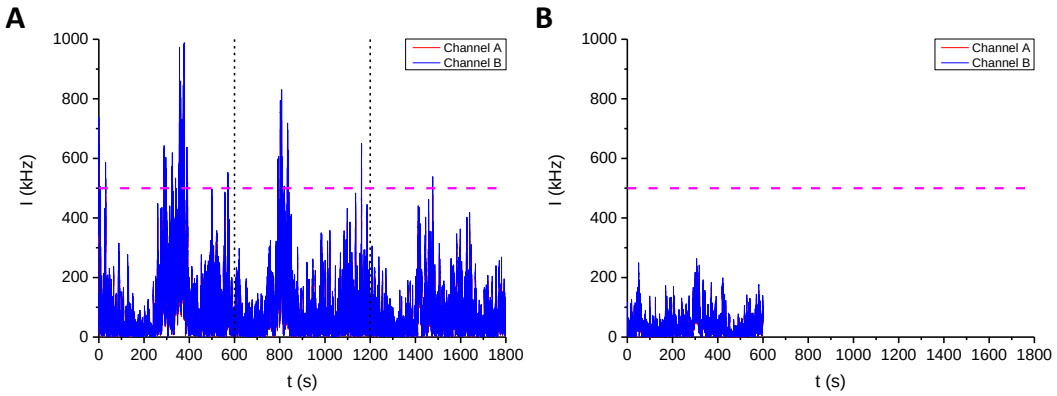

Figure AI-4: Scattering intensity (or count rate) as a function of time for a 0.073% Na CMC solution at θ = 30° and for Δt_{meas} = 10 min. **A.** Scattering intensity *I*, as automatically set by the light scattering device (3 measurements shown; they are separated from each other by black dashed lines). **B.** Scattering intensity *I* set to 25 kHz (1 measurement shown). The pink dashed line represents the upper limit of the linear regime of the detector which is 500 kHz. The instrument used for the measurements is equipped with two avalanche photodiode (APD) detectors used in pseudo-correlation mode and referred here as Channels A and B.

AI-3.2.Light Scattering (LS) data processing

The method used for LS data processing is summarised in Figure AI-5. Depending on the Na CMC concentration, it consists of 3 to 4 main steps: (i) selection of the measurements for data analysis (*i.e.* measurements whose scattering intensities are within the linear range of the detector and which have not been significantly impacted by the particulates) and normalisation of the intensity autocorrelation data (IAC) to intercept 1, (ii) averaging of the IAC data for $c_{Na\,CMC} \leq 0.078\%$, (iii) fitting of the IAC data, and (iv) error estimation.

For $c_{Na\ CMC} \leq 0.37\%$, IAC data fitting with Eq. 3-4 (see Section 3-3.3; also shown in the 'IAC data fitting and error estimation' box) was first performed without the ultra-slow mode (*i.e.* corresponding data not selected and $A_{us} = 0$). The so-obtained values were then used to initialise the fitting parameters for the final fits.

For $c_{Na\ CMC} \leq 0.073\%$, the error was estimated for 3 angles only (a low, an intermediate and a high angle). For each angle, 3 measurements were randomly chosen and their IAC data averaged; this was repeated on 5 different groups and the standard errors were estimated for these 5 sets of fitting parameters. These errors are represented by the error bars in Figure 3-13, and in Figure AI-13. These determined errors are used in the calculations of the diffusion coefficients of the slow mode D_s in the following way: the error calculated for the low angles is applied to all angles below the intermediate angle, while the error calculated for the intermediate angle is applied to all angles up to the high angle.

For $c_{Na\ CMC} > 0.073\%$, the errors were estimated directly by calculating the standard error for the average relaxation time of the slow mode τ_s determined from the fitting parameter $\tau_{e,s}$ (effective relaxation time for the slow mode), as well as for all the other fitting parameters.

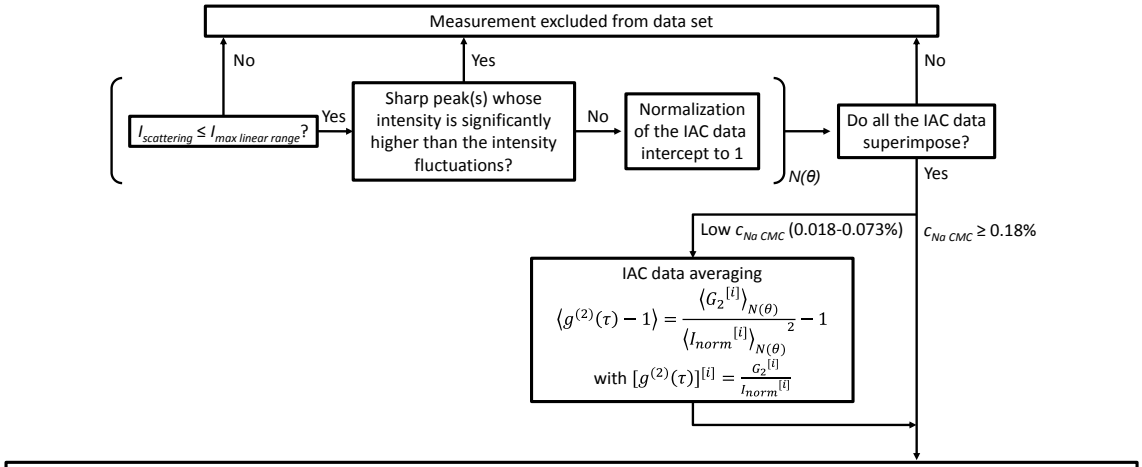

IAC data fitting and error estimation

$$g^{(2)}(\tau) - 1 = \left[A_f e^{-\left(\frac{\tau}{\tau_f}\right)} + A_s e^{-\left(\frac{\tau}{\tau_{e,s}}\right)^{\beta_s}} + A_{us} e^{-\left(\frac{\tau}{\tau_{e,us}}\right)^{\beta_{us}}}\right]^2 \text{ with } A_f = 0 \text{ for } c_{Na\,CMC} \leq 0.073\%$$

$c_{Na\ CMC}$ range (%)	Initial fit			Final fit(s)				Fitted data	Error estimation
	Fitted mode(s)	$A_i \neq 0$	$A_i = 0$	Fitted mode(s)	$A_i \neq 0$	$A_i = 0$	Related Figure		
0.018-0.073	*s*	A_s	A_f, A_{us}	*s*, *us*	A_s, A_{us}	A_f	3-6.A_2	Average IAC data ⟹ 1 set of fitting parameters at the angle *θ*	For 3 angles *θ*; see main text
0.18-0.37	*f*, *s*	A_f, A_s	A_{us}	*f*, *s*, *us*	A_f, A_s, A_{us}	-	3-6.B_2	Individual IAC data ⟹ 1 set of fitting parameters/measurement ⟹ N_i sets of fitting parameters at the angle *θ*	Calculation of the standard error
0.55-0.92	N.A.			*f*, *s*	A_f, A_s	A_{us}	3-6.C_2		
				s, *us*	A_s, A_{us}	A_f	3-6.C_3		

Figure AI-5: Illustration of the method used to process the DLS data collected at an angle *θ*. *N(θ)*: number of measurements performed at the angle *θ*; IAC data: intensity auto-correlation data; I_{norm}: normalised scattering intensity; *f*, *s* and *us*: fast, slow and ultra-slow modes, respectively, A_i: amplitude of the mode *i*.

AI-3.3.Dynamic Light Scattering (DLS) data fitting

Figure AI-6 shows the graphs of the residuals of the fits shown in Figure 3-6. The residuals were calculated with Eq. AI-2, where $\left[g^{(2)}(\tau) - 1\right]_{exp}$ is the experimental intensity auto-correlation data and $\left[g^{(2)}(\tau) - 1\right]_{fit}$ is the intensity auto-correlation data calculated with the fitting parameters obtained by fitting the experimental data to Eq. 3-4.

$$Residuals = \left[g^{(2)}(\tau) - 1\right]_{exp} - \left[g^{(2)}(\tau) - 1\right]_{fit} \quad \text{(AI-2)}$$

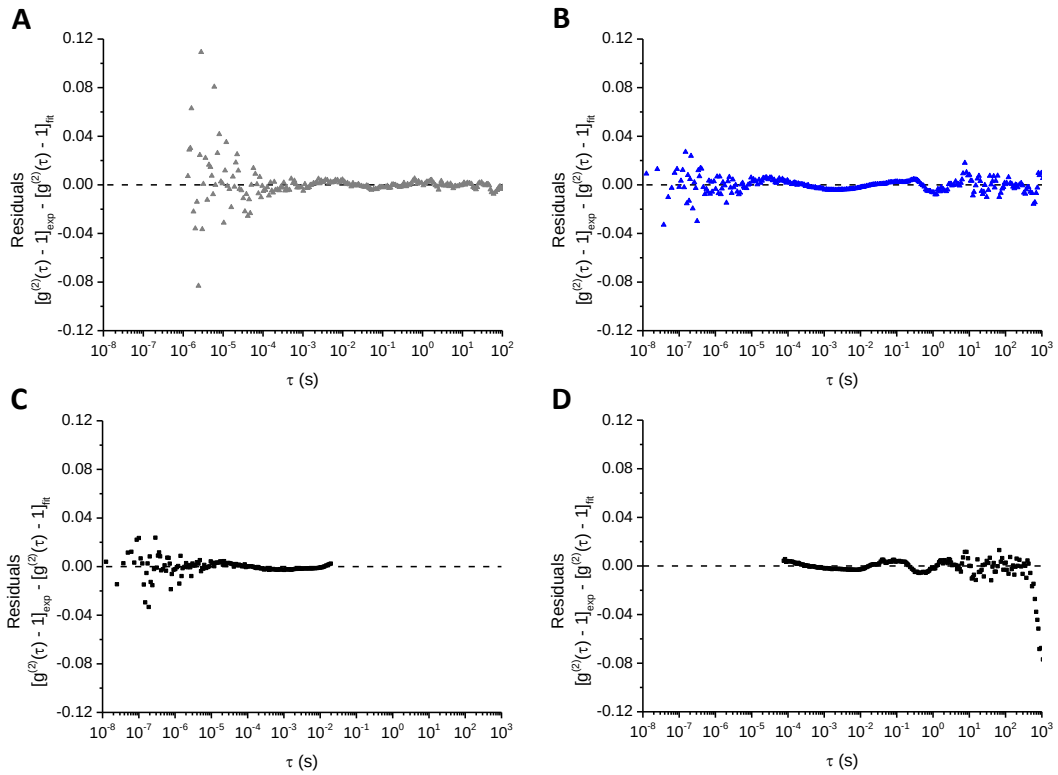

Figure AI-6: Residuals of the fits shown in Figure 3-6. **A.** Low Na CMC concentration (0.073% Na CMC; 130°): residuals of the fit of the slow and the ultra-slow modes; **B.** Intermediate Na CMC concentration (0.37% Na CMC; 90°); residuals of the fit of the fast, slow and ultra-slow modes; **C. D.** High Na CMC concentration (0.55% Na CMC; 130°): residuals of the fit of the slow and the fast mode (C) and of the slow and the ultra-slow mode (D).

AI-3.4.Static Light Scattering (SLS)

The LS spectrometer used for the experiments allowed simultaneous collection of both DLS and SLS data. The SLS data presented in the Chapter 3 come from the short measurements specifically performed to collect SLS data so that the influence of the particulates on such data is minimised. However, to calculate the contributions of the fast and the slow modes to the total excess Rayleigh ratio, as well as to estimate the apparent radius of gyration $R_{g,app}$ of the domains responsible for the slow mode, SLS data collected during the longer DLS measurements for which the relative amplitudes of each mode were known from fitting the intensity auto-correlation data to Eq. 3-4 were used. The excess Rayleigh ratios ΔR obtained for both SLS and DLS measurements are shown in Figure AI-7.A. For each solution, both SLS and DLS data superimpose well. Hence, the SLS data collected during the DLS measurements are not more impacted by the presence of the particulates than the data collected during the actual SLS measurements, and can thus be used for further calculations. The values of the power law exponents describing

ΔR = f(q) shown in Figure AI-7.B confirm that there is no significant difference between the two data sets.

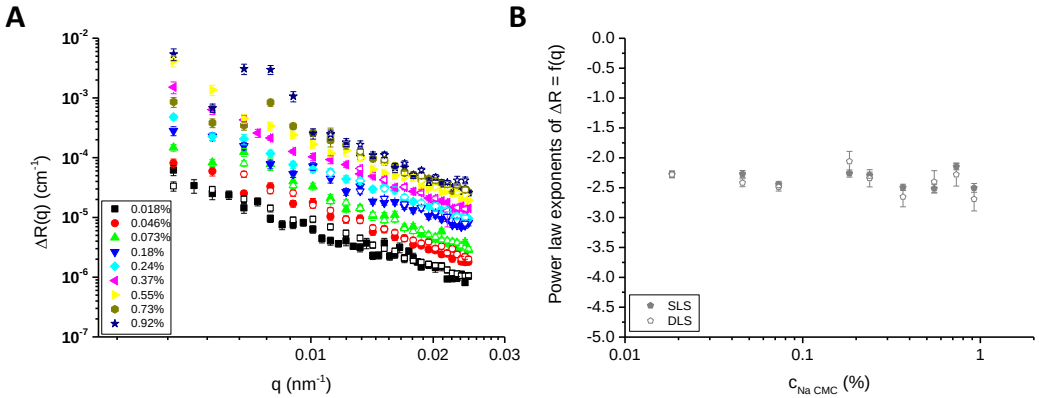

Figure AI-7: Comparison between the excess Rayleigh ratio *ΔR* values obtained during SLS and DLS measurements (*i.e.* short and long measurements respectively). **A.** *q*- and $c_{Na\ CMC}$-dependence of the excess Rayleigh ratio *ΔR* for both SLS (full symbols) and DLS (empty symbols) measurements. **B.** Power law fit exponents of the curves *ΔR(q) = f(q)* for both SLS (full symbols) and DLS (empty symbols) measurements. For clarity, the power law fits have not been represented in A.

Zimm ($[K.c_{Na\ CMC}/\Delta R] = f(q^2)$),[40] Berry ($[K.c_{Na\ CMC}/\Delta R]^{0.5} = f(q^2)$),[40] and Guinier ($\ln[K.c_{Na\ CMC}/\Delta R] = f(q^2)$)[40] plots were produced using the SLS data. The optical constant *K* was calculated using Eq. AI-3,[40] where λ is the wavelength of the laser excitation, *n* the refractive index of the solution, *dn/dc* the refractive index increment and θ the scattering angle.

$$K = \frac{4\pi^2}{\lambda^2} n^2 \left(\frac{dn}{dc}\right)^2 \qquad \text{(AI-3)}$$

The refractive index values *n* of the Na CMC solutions were determined with an Abbe refractometer (Prisma Refractometer, Ceti). They were plotted as a function of $c_{Na\ CMC}$ and fitted to a first order polynomial model as shown in Figure AI-8. The fitting parameters and their associated errors are shown in the Figure. The intercept corresponds to the value of the refractive index *n* in absence of Na CMC (*i.e.* n_{water}) while the slope corresponds to the refractive index increment *dn/dc* of Na CMC in water. The values of *n* used for the determination of variables such as *K* and *q* were calculated with Eq. AI-3. The value of *dn/dc* is 0.0017%$^{-1}$. To compare this result with the literature, Na CMC solution density was set to 1 g/mL so that *dn/dc* = 0.17 mL/g. This value is slightly higher than the values reported in the literature such as $(dn/dc)_{950\ nm}$ = 0.144 mL/g for a Na CMC sample of DS 1.23 in water,[118] and *dn/dc* = 0.156 mL/g for Na CMC samples of various M_w and DS in either NaCl or aqueous ammonium acetate solutions.[202] The small difference observed between the present experimental value and the ones from the

literature can most likely be accounted for by the small variation in the solution densities and by differences in the probing wavelengths.

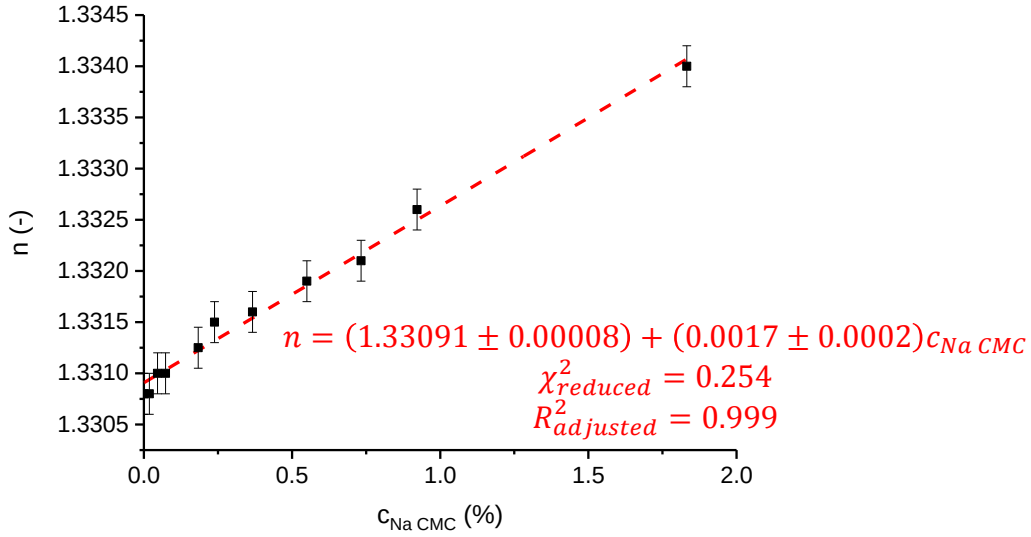

Figure AI-8: Refractive index measurements. The dashed line represents the linear fit of the experimental data points.

The graph of the reciprocal of the excess Rayleigh ratio as a function of q^2 and the Zimm plot shown in Figures AI-9.A and B respectively exhibit a small negative intercept. This is characteristic for excess scattering and often observed when large scatterers are present in solution.[40] In such cases, linearization of the data can be achieved with the Berry and the Guinier plots such as the ones presented in Figures AI-9.C and D. As the linear region is wider for the Berry plots than for the Guinier plots, the zero-angle excess Rayleigh ratios $\Delta R(0)$ were determined from the Berry plots.

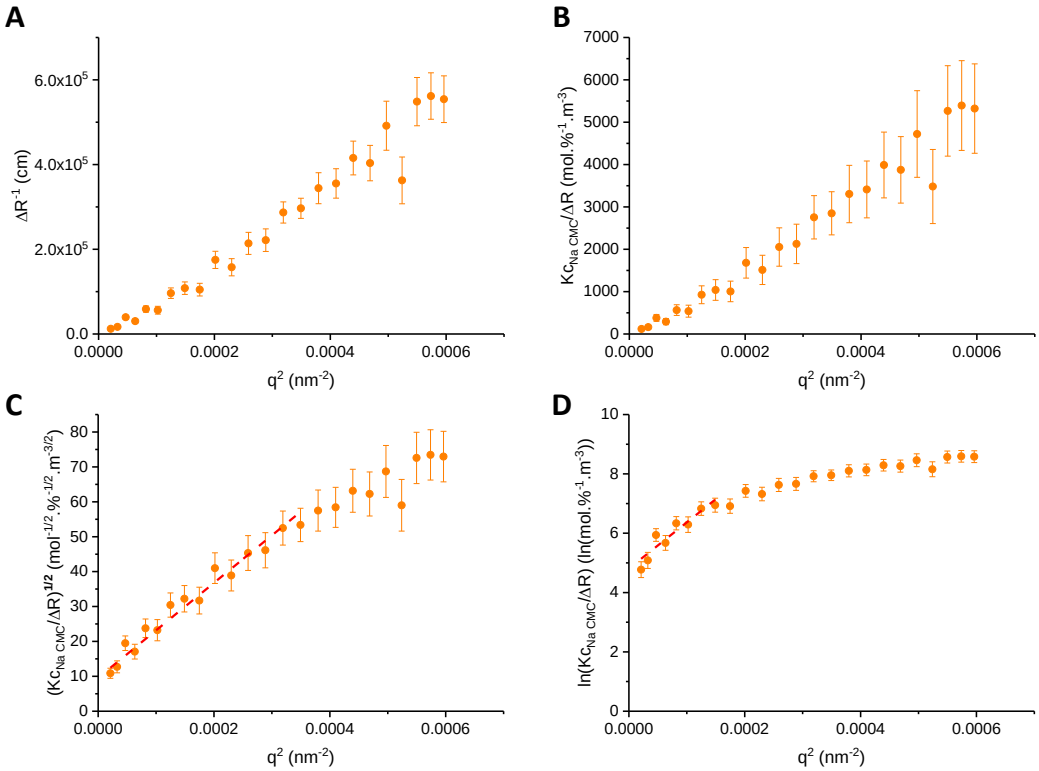

Figure AI-9: Determination of the excess Rayleigh ratio at q^2 = 0 for the 0.046% Na CMC solution. **A.** Graph of $\Delta R^{-1} = f(q^2)$; **B.** Zimm plot; **C.** Berry plot; **D.** Guinier plot. The red dashed-lines are linear fits of the curves.

AI-3.5.Dynamic Light Scattering (DLS)

AI-3.5.1.Calculation of the contributions of the fast and the slow modes to the total excess Rayleigh ratio

The contributions of the fast and the slow modes to the total excess Rayleigh ratio were calculated using Eq. AI-4.[70] Hence, the contribution ΔR_i of the mode i to the total excess Rayleigh ratio ΔR is given by:

$$\Delta R_i = \frac{A_i \, \Delta R}{A_i + A_j + A_k} \qquad \text{(AI-4)}$$

where A_i, A_j and A_k are the amplitudes of the modes i, j and k respectively obtained from fitting the IAC data to Eq. 3-4. For $c_{Na\ CMC} \leq 0.073\%$, where one set of averaged IAC data was available for each angle, one value of ΔR_i was obtained for each angle. The errors were estimated for the same 3 angles as for the DLS fitting parameter data (see Section AI-3.2) and are represented by the error bars in Figure AI-13. For $c_{Na\ CMC} > 0.073\%$, the values of ΔR_i were calculated for each measurement and averaged. Standard errors could thus be determined for each angle as for the DLS fitting parameter data, and are represented by the error bars in Figures AI-10, AI-11 and AI-13.

For $c_{Na\ CMC}$ > 0.55%, the IAC data could not be directly fitted to a sum of 3 exponentials (see Section AI-3.2 as well as Section 3-3.3). Hence, the fast and the slow modes were fitted together to provide the data for the fast mode and relative amplitudes $A_{f,1}$ and $A_{s,1}$ for the fast and the slow modes respectively, while the slow and the ultra-slow modes were fitted together to provide the data for the slow mode and relative amplitudes $A_{s,2}$ and $A_{us,2}$ for the slow and the ultra-slow modes respectively. The relative amplitudes of the slow and the ultra-slow modes were recalculated so that $A_{s,1} = A_{s,2} + A_{us,2}$. The equations used to calculate the relative amplitudes of the fast (A_f), slow (A_s) and ultra-slow (A_{us}) modes are provided by Eqs AI-5, AI-6 and AI-7 respectively, and verify the condition $A_f + A_s + A_{us} = 1$.

$$A_f = A_{f,1} \tag{AI-5}$$

$$A_s = \frac{A_{s,2}}{A_{s,2}+A_{us,2}} A_{s,1} \tag{AI-6}$$

$$A_{us} = \frac{A_{us,2}}{A_{s,2}+A_{us,2}} A_{s,1} \tag{AI-7}$$

Figure AI-10 shows the quotient $\Delta R_s/\Delta R_f$, which is the ratio between the contributions of the fast and the slow modes to the total excess Rayleigh ratio ΔR, as a function of the scattering vector q. For comparison with data from the literature, it is worth noting that $\Delta R_s/\Delta R_f = A_s/A_f$.

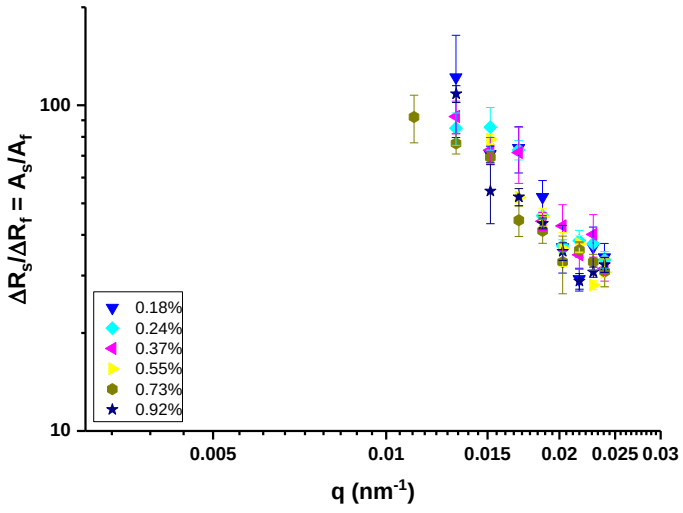

Figure AI-10: q- and $c_{Na\ CMC}$-dependences of the ratio of the excess Rayleigh contributions of the slow and the fast modes $\Delta R_s/\Delta R_f$. *N.B:* In the literature, the ratio $\Delta R_s/\Delta R_f$ is often reported as the ratio of the amplitudes of both modes A_s/A_f.

AI-3.5.2.Fast mode

The contribution of the fast mode to the total excess Rayleigh ratio was calculated using Eq. AI-4 applied to the fast mode. Its variation as a function of the scattering vector q and the Na CMC concentration is shown in Figures AI-11.A and C, while the concentration-dependence of ΔR_f at 60°, 90° and 130° is shown in Figure AI-11.B.

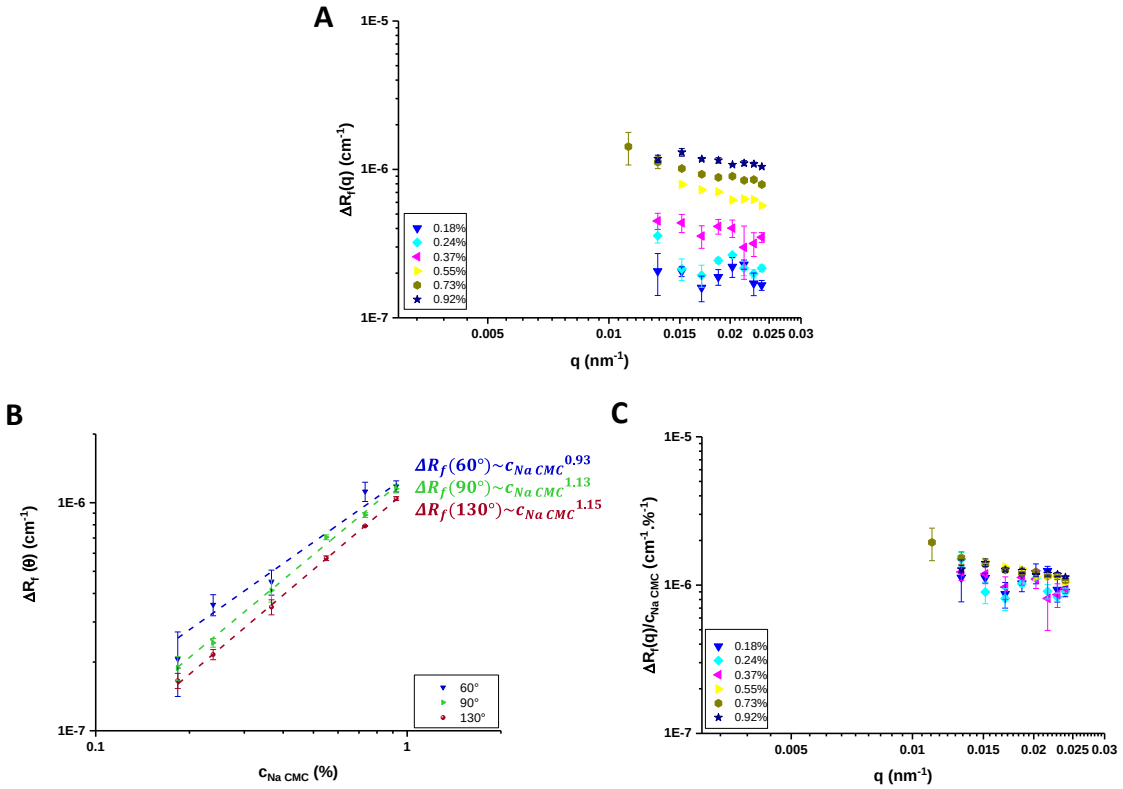

Figure AI-11: q- and $c_{Na\ CMC}$-dependences of the fast mode contribution to the excess Rayleigh ratio scattering. **A.** Fast mode contribution to the excess Rayleigh ratio scattering ΔR_f as a function of the scattering vector q for all studied concentrations. The dashed lines are power law fits of the curves. **B.** Concentration dependence of ΔR_f at different angles. **C.** q-dependence of ΔR_f normalised by Na CMC concentration.

Figure AI-12 illustrates the different methods used to calculate the diffusion coefficient of the fast mode. Details about the calculations are provided in the paragraph about the fast mode in Section 3-3.5.

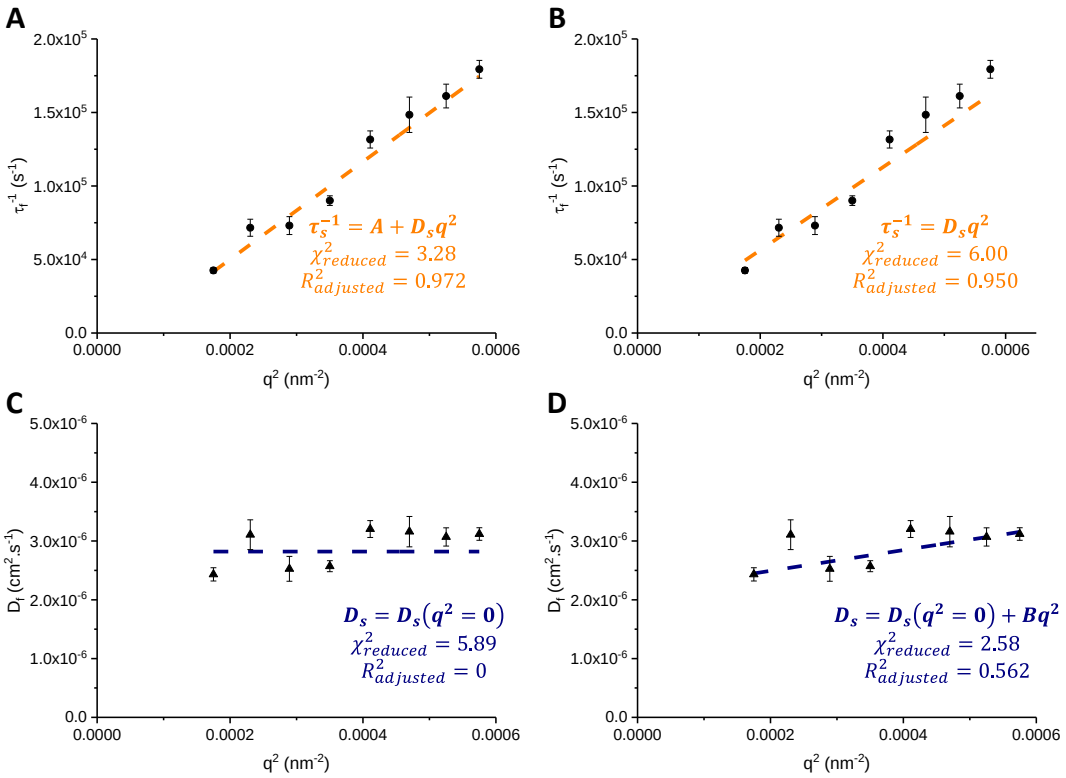

Figure AI-12: Illustration of the calculation of the fast mode diffusion coefficient D_f with the 0.92% Na CMC solution. **A. B.** Graphs of $\tau_f^{-1} = f(q^2)$. The data shown on both graphs are identical, but fits (dashed lines; equations displayed on the graphs) are different. **C. D.** Graphs of $D_f = f(q^2)$. D_s values were calculated with $D_f = \tau_f^{-1} q^{-2}$. The data shown on both graphs are identical, but fits (dashed lines; equations displayed on the graphs) are different.

AI-3.5.3.Slow mode

The contribution of the slow mode to the total excess Rayleigh ratio was calculated using Eq. AI-4 applied to the slow mode. Its variation as a function of the scattering vector q and the Na CMC concentration is shown in Figures AI-12.A and D, while the concentration-dependence of ΔR_s at 60°, 90° and 130° is shown in Figure A-13.C. Figure A-13.B shows the power law exponents of the fits shown in Figure A-13.A. It is worth noting that the behaviour of ΔR_s is very similar to the one of ΔR (see Figure 3-7); which suggests that the behaviour of ΔR is mainly driven by the slow mode.

To determine the values of the apparent radius of gyration $R_{g,app}$ related to the slow mode and shown in Figure 3-15, Zimm, Berry and Guinier graphs (see Section AI-3.4 where similar plots are shown for ΔR) were plotted for ΔR_s. As for the plots obtained for the total excess Rayleigh ratio ΔR, the intercepts of the Zimm plots had small negative values for most of the studied solutions, and the Berry plots had a broader linear region than the Guinier ones. Hence, $R_{g,app}$ was determined from the Berry plots using Eq. AI-8,[40] where

a and *b* are the intercept and the slope of the first order polynomial model describing the linear region of the Berry plots, respectively.

$$R_{g,app} = \sqrt{6\frac{b}{a}} \tag{S8}$$

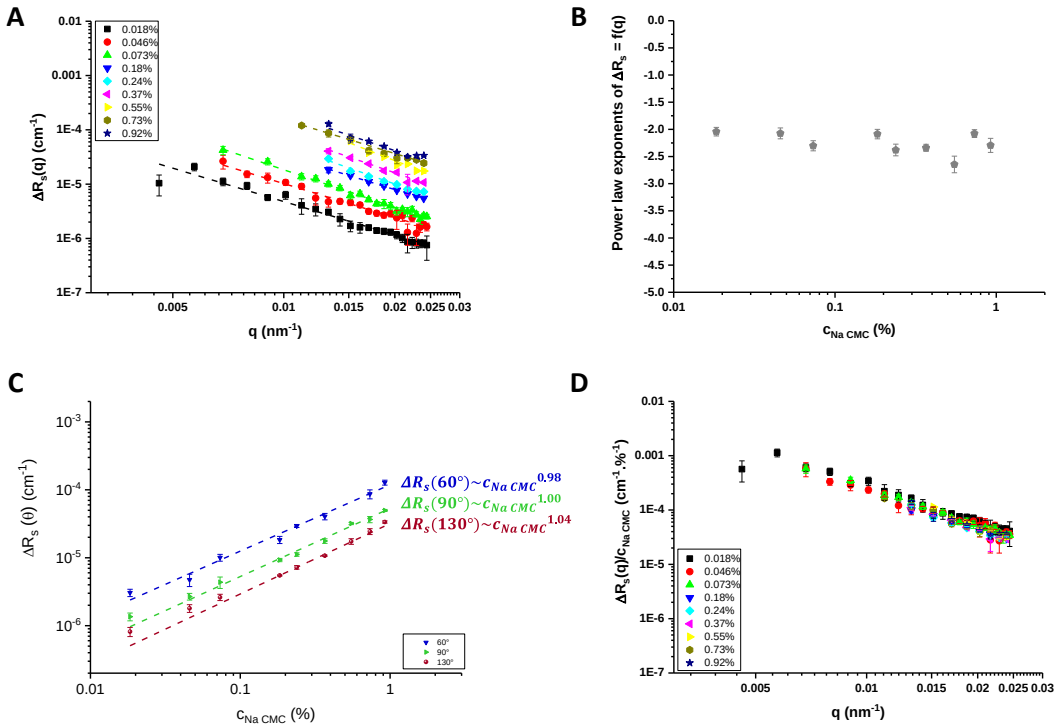

Figure AI-13: q- and $c_{Na\ CMC}$-dependences of the slow mode contribution to the excess Rayleigh ratio scattering. **A.** Slow mode contribution to the excess Rayleigh ratio scattering ΔR_s as a function of the scattering vector q for all studied concentrations. The dashed lines are power law fits of the curves. For the 0.92% Na CMC solution, the τ_s value obtained at the highest q value was not included in the fit. **B.** Exponents of the power law fits represented in A. **C.** Concentration dependence of ΔR_s at different angles. **D.** q-dependence of ΔR_s normalised by Na CMC concentration.

Figure AI-14 shows the power law exponents of the power law fits of $\tau_s = f(q)$ shown in Figure 3-13. Their values are close to 2; suggesting that the slow mode is related to a diffusive process. An average value of -2.4 ± 0.2 can be calculated across the studied concentration range.

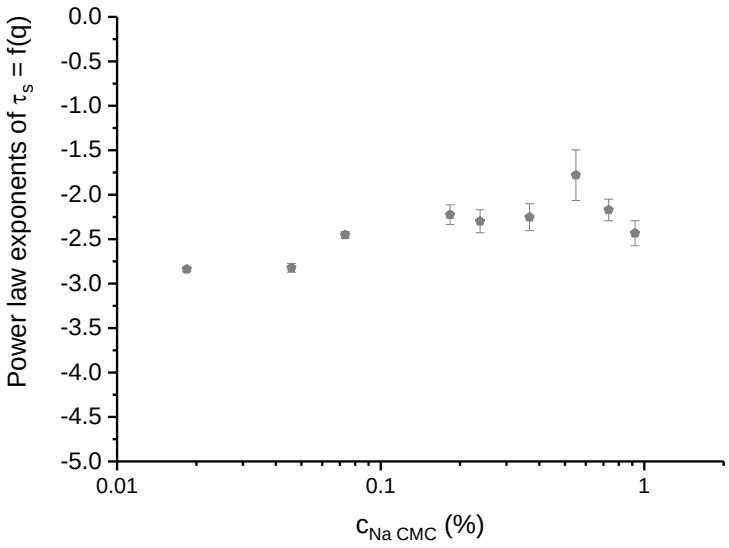

Figure AI-14: Concentration-dependence of the power law exponents of τ_s = f(q). The data and their fits are shown in Figure 3-13.

Figure AI-15 shows the concentration dependence of the slow relaxation time τ_s for three different scattering angles. The data at 90° scattering angle is already shown in Figure 3-14.A where it is compared to the specific viscosity. τ_s exhibits a similar behaviour at the three scattering angles.

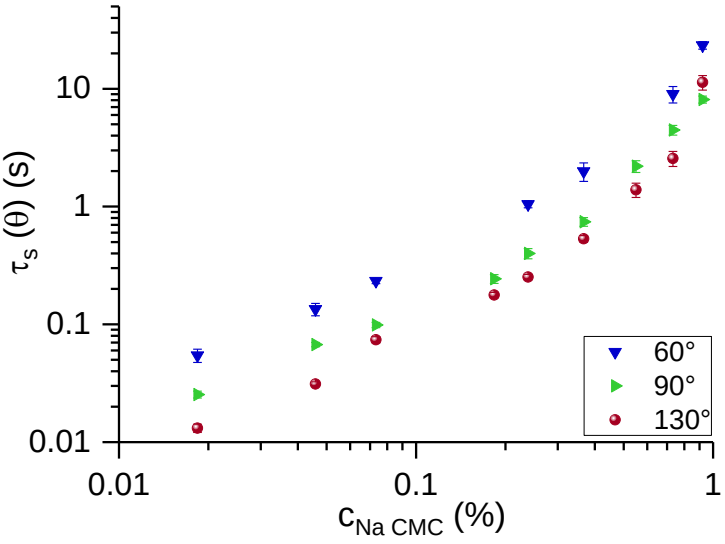

Figure AI-15: Concentration and angle dependence of the slow mode relaxation time τ_s.

Figures AI-16 and AI-17 illustrate the different methods used to calculate the diffusion coefficient of the slow mode for a low Na CMC concentration and a high Na CMC

concentration, respectively. Details about the calculations are provided in the paragraphs about the fast and the slow modes in Section 3-3.5.

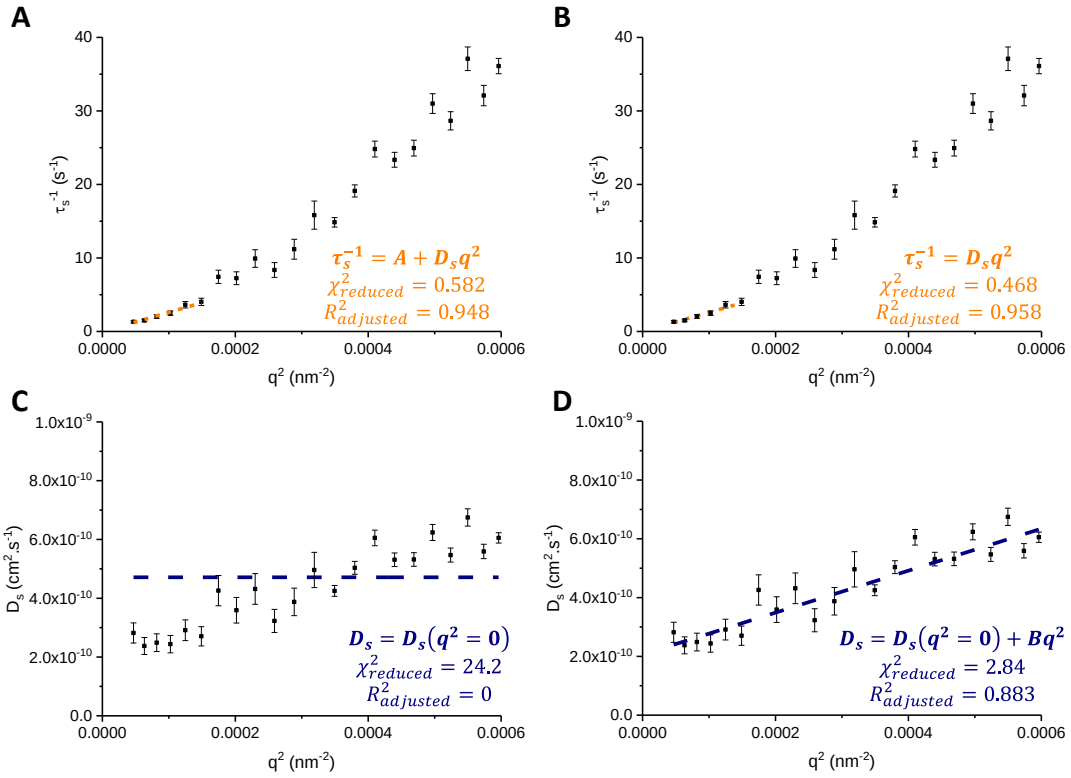

Figure AI-16: Illustration of the calculation of the slow mode diffusion coefficient D_s with the 0.046% Na CMC solution. **A. B.** Graphs of τ_s^{-1} = f(q^2). The data shown on both graphs are identical, but fits (dashed lines; equations displayed on the graphs) are different. **C. D.** Graphs of D_s = f(q^2). D_s values were calculated with $D_s = \tau_s^{-1} q^{-2}$. The data shown on both graphs are identical, but fits (dashed lines; equations displayed on the graphs) are different.

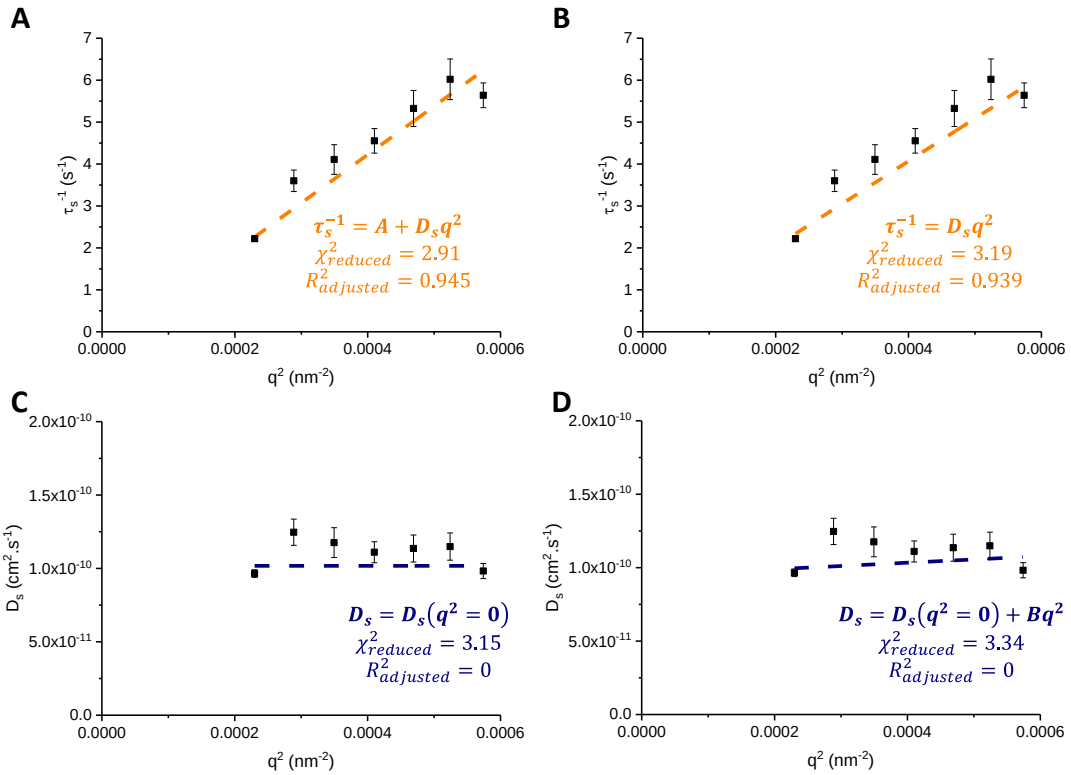

Figure AI-17: Illustration of the calculation of the slow mode diffusion coefficient D_s with the 0.18% Na CMC solution. **A. B.** Graphs of τ_s^{-1} = f(q^2). The data shown on both graphs are identical, but fits (dashed lines; equations displayed on the graphs) are different. **C. D.** Graphs of D_s = f(q^2). D_s values were calculated with $D_s = \tau_s^{-1} q^{-2}$. The data shown on both graphs are identical, but fits (dashed lines; equations displayed on the graphs) are different.

The values of the slow mode diffusion coefficient D_s calculated using the four methods illustrated in Figures AI-16 and AI-17 are shown in Figure AI-18 as a function of Na CMC concentration. The four plots, shown together in Figure 3-14, look similar to each other: a change in behaviour occurs in the intermediate concentration range, while the low and high concentration ranges can each be described by a power law. The fitting parameters of the power laws as well as the crossover concentrations are shown in Table AI-2.

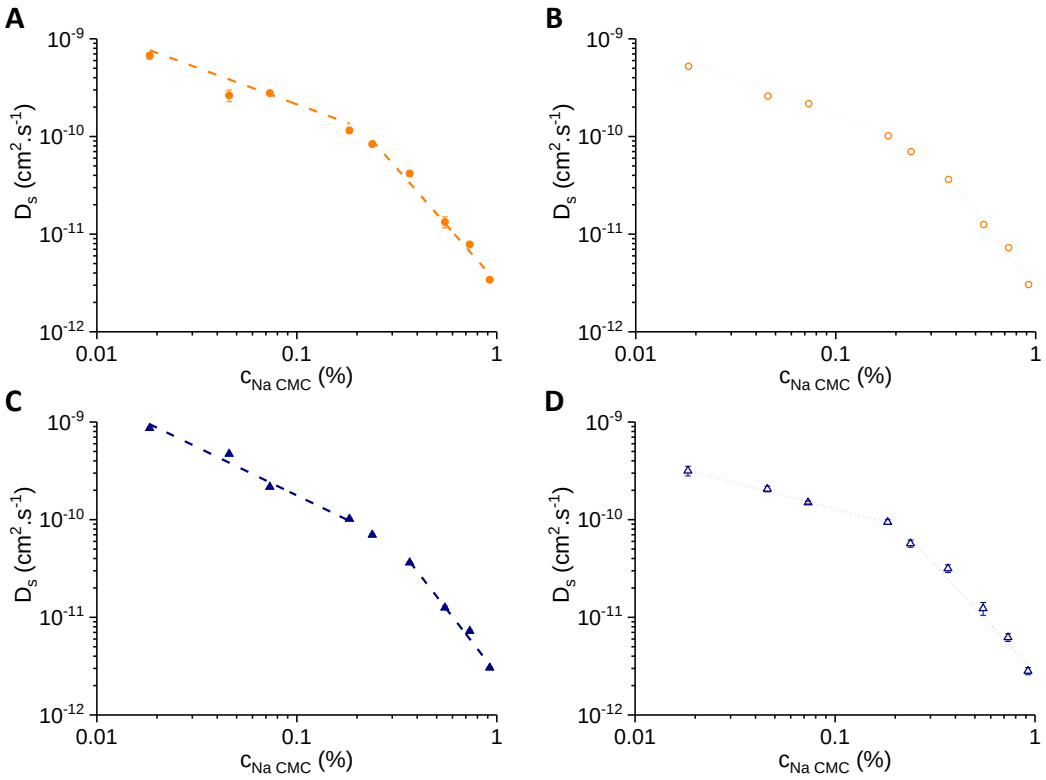

Figure AI-18: Concentration dependence of the slow mode diffusion coefficient D_s calculated using four different methods. The methods used to determine the values of D_s in A, B, C and D are the ones illustrated in Figures AI-16 and AI-17.A, B, C and D, respectively. The dashed and dotted lines represent power law fits. The values of the fitting parameters are provided in Table AI-2.

Table AI-2: Fitting parameters of the power laws describing the behaviour of $D_s = f(c_{Na\ CMC})$ at low and high $c_{Na\ CMC}$ and shown in the plots A, B, C and D of Figure AI-18. *a* is the slope and *b* the power law exponent. $c_{e,LS}$ is the crossover concentration corresponding to the concentration at the intersection between the two power law fits.

Plot	$c_{Na\ CMC}$ range	*a*	*b*	χ_{red}^2	R_{adj}^2	$c_{e,LS}$ (%)
A	Low	$(3 \pm 1) \times 10^{-11}$	$-(0.8 \pm 0.2)$	14.0	0.917	0.21
	High	$(3.2 \pm 0.5) \times 10^{-12}$	$-(2.3 \pm 0.2)$	12.5	0.938	
B	Low	$(3.0 \pm 0.05) \times 10^{-11}$	$-(0.73 \pm 0.07)$	13.0	0.974	0.28
	High	$(2.6 \pm 0.3) \times 10^{-12}$	$-(2.6 \pm 0.2)$	30.0	0.966	
C	Low	$(1.8 \pm 0.8) \times 10^{-11}$	$-(1.0 \pm 0.2)$	164	0.910	0.31
	High	$(2.6 \pm 0.3) \times 10^{-12}$	$-(2.6 \pm 0.2)$	29.5	0.966	
D	Low	$(3.8 \pm 0.4) \times 10^{-11}$	$-(0.53 \pm 0.04)$	0.47	0.988	0.21
	High	$(2.7 \pm 0.4) \times 10^{-12}$	$-(2.2 \pm 0.2)$	4.94	0.928	

Appendix II: Supplementary information to Chapter 4

Table AII-1: Fitting parameters of the power law fits shown in Figure 4-1.

Data	$c_{Na\ CMC}$ range (%)	Slope	Exponent	χ_{red}^2	R_{adj}^2
$\Delta R_f(90°)$	0.0009-0.009	$(4 \pm 4) \times 10^{-4}$	1.1 ± 0.3	5.34×10^{-14}	0.931
$\Delta R(90°)$	0.0009-0.009	$(5 \pm 7) \times 10^{-3}$	1.4 ± 0.3	4.15×10^{-13}	0.942
$\Delta R_f\ (30°)$	0.0045-0.18	$(3 \pm 1) \times 10^{-6}$	0.4 ± 0.2	2.73×10^{-12}	0.729
$\Delta R_f(90°)$	0.0045-0.18	$(1.3 \pm 0.3) \times 10^{-6}$	0.2 ± 0.1	6.37×10^{-13}	0.543
$\Delta R(30°)$	0.0045-0.18	$(1.8 \pm 0.8) \times 10^{-5}$	0.6 ± 0.2	4.78×10^{-11}	0.851
$\Delta R(90°)$	0.0045-0.18	$(4.53 \pm 0.05) \times 10^{-5}$	0.366 ± 0.005	5.67×10^{-15}	1.00

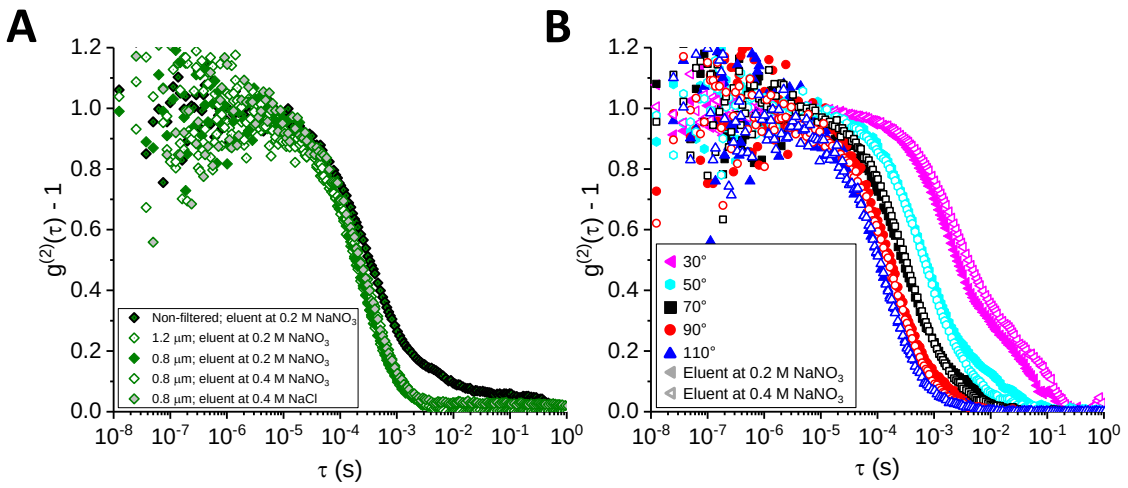

Figure AII-1: Influence of filtration and/or eluent characteristics on the intensity auto-correlation data for a 0.0045% (**A**) and a 0.09% (**B**) Na CMC solutions.

Gaussian model (Gauss in Origin software)[203]

$$f(x) = y_0 + \frac{A}{w\sqrt{\pi/2}} e^{-2\frac{(x-x_c)^2}{w^2}} \quad \text{(AII-1)}$$

where y_0 corresponds to the peak baseline, A is the peak area, x_c is the centre of the peak and w is the width.

Exponential Modified Gaussian (EMG; GaussMod in Origin software)[204]

$$f(x) = y_0 + \frac{A}{t_0} e^{\frac{1}{2}(\frac{w}{t_0})^2 - \frac{x-x_c}{t_0}} \int_{-\infty}^{z} \frac{1}{\sqrt{2\pi}} e^{-\frac{y^2}{2}} dy \quad \text{(AII-2)}$$

where $z = \frac{x-x_c}{w} - \frac{w}{t_0}$, y_0 corresponds to the peak baseline, A is the peak area, x_c is the centre of the peak, w is the width and t_0 the relaxation parameter of the exponential decay.

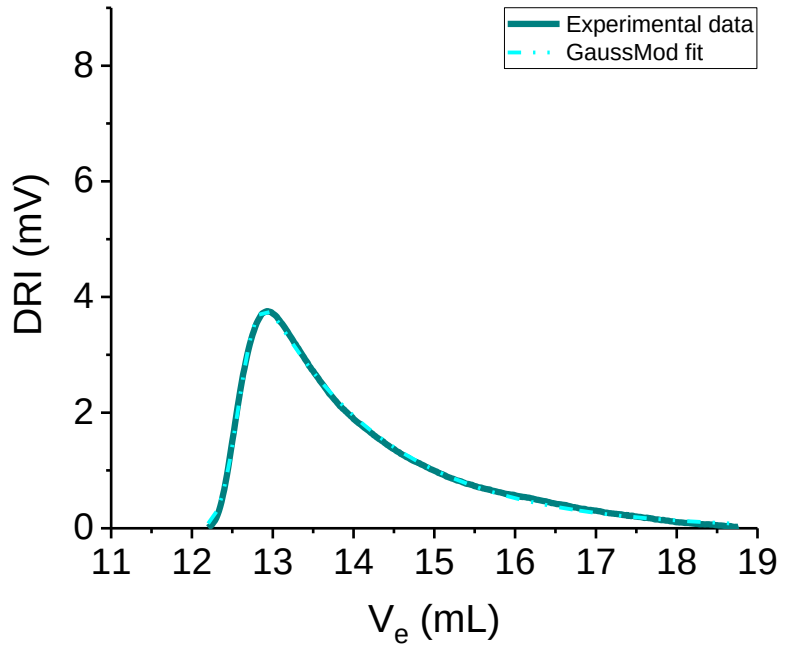

Figure AII-2: Chromatogram obtained for the high molecular weight *co*-ATBS-PAM used to determine the void volume of the column. The fit of the experimental data to the EMG model is also shown.

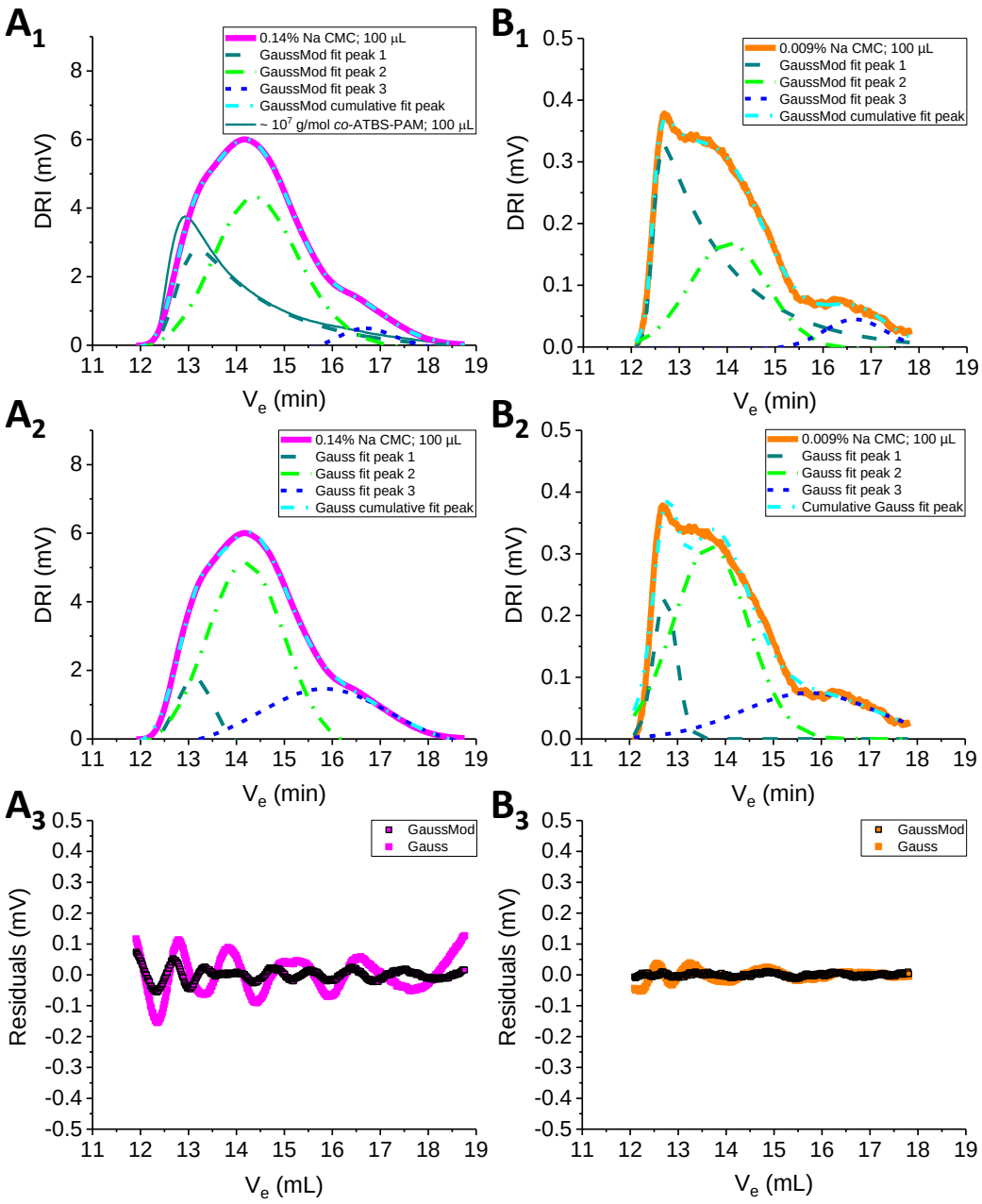

Figure AII-3: Peak deconvolution applied to the data of the 0.14% ($\mathbf{A_i}$) and 0.009% ($\mathbf{B_i}$) Na CMC solutions. Both EMG (GaussMod; $\mathbf{X_1}$) and Gaussian (Gauss; $\mathbf{X_2}$) models are compared. The residuals, calculated as $RI_{experimental} - RI_{model}$, are shown in $\mathbf{X_3}$.

Table AII-2: Fitting parameters of the fits shown in Figure 4-4.

Peak	Model	a (mV.mL.µg^{-1})	b (mV.mL)	χ_{red}^2	R_{adj}^2
1	$A = a\, m_{Na\ CMC} + b$	0.052 ± 0.007	0.0 ± 0.3	38.2	0.896
2	$A = a\, m_{Na\ CMC} + b$	0.060 ± 0.005	0.0 ± 0.3	50.4	0.959
3	$A = b$	*n/a*	1.10 ± 0.09	41.4	1.21×10^{-14}

Estimation of the shear-rate in a SEC column. After Barth and Carlin.[197]

$$\dot{\gamma} = \frac{4Q}{\varepsilon A R_h} \quad \text{(AII-3)}$$

where Q is the flow rate, ε equals 1 for an open tube, A is the cross-sectional area of the tube, and R_h is the hydraulic radius defined as $R_h = \frac{D_p \varepsilon}{3(1-\varepsilon)}$ with D_p the packing diameter and ε the porosity (ε = 0.36 for a packed column).

Estimation of the shear-rate in a SEC column. After Cave *et al.*[179]

$$\dot{\gamma} = \frac{74.6Q}{Ad} \quad \text{(AII-4)}$$

where Q is the flow rate, A is the cross-sectional area of the tube, and d is the average sphere diameter and can be approximated as $d \approx 10 \times$ average void size.

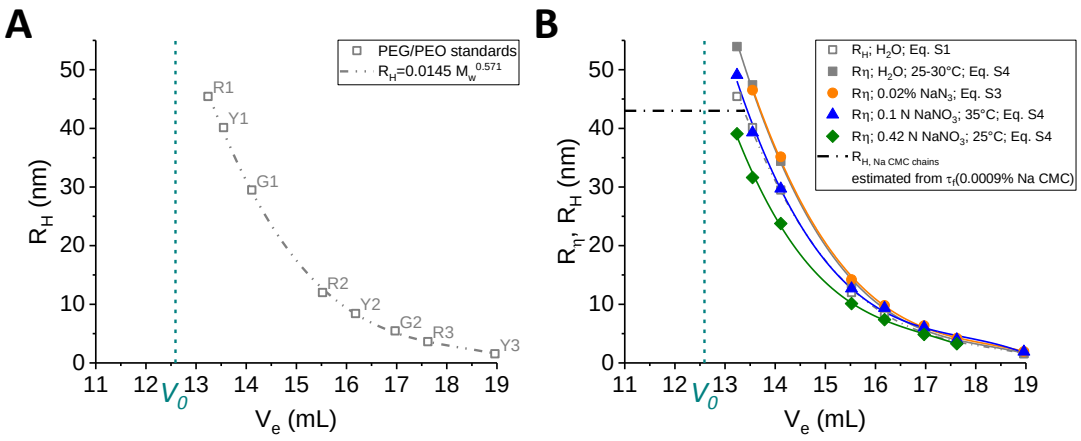

Figure AII-4: Calibration curves based on the size of PEG/PEO standards. The calibration curves are third order polynomial models and their equations are given in Table AII-4. The shor dashed turquoise line represents the void volume V_0. **A.** Calibration curve $R_H = f(V_e)$ with R_H the hydrodynamic radii of the PEO/PEG standards calculated with Eq. AII-5 from the M_w values measured by DLS and provided by the supplier, and V_e the elution volume of the PEO/PEG standards. X_i refers to the polymer standard the data point corresponds to (see Table AII-3). **B.** Calibration curves R_H or $R_\eta = f(V_e)$ with R_H the hydrodynamic radii and R_η the viscometric radii of the PEO/PEG standards in different aqueous solvents calculated with Eqs AII-5, AII-6 and AII-8 from the M_w values measured by DLS and provided by the supplier, and V_e the elution volume of the PEO/PEG standards. The black dashed-dotted line represent the hydrodynamic radius estimated from the fast relaxation time determined at 90° scattering angle for the 0.0009% Na CMC solution (see Figure 4-1).

Table AII-3: Manufacturer information about the PEG/PEO polymer calibration standards and details about the methods used to estimate the PEG/PEO hydrodynamic and viscometric radii (R_H and R_η respectively) in different aqueous media and shown in Figure AII-4.

Provided by/ calculated with	Manufacturer							Eq. AII - 5	Eq. AII - 6	Eq. AII - 8	Eq. AII - 8	Eq. AII - 8
Solvent	0.02% NaN_3							H_2O	0.02% NaN_3	H_2O 25-30°C	0.1 N $NaNO_3$ 35°C	0.42 N NaOH 25°C
$K_{PEO} \times 10^2$ (mL/g)	*n/a*							*n/a*	*n/a*	1.25	3.47	2.5
α_{PEO}	*n/a*							*n/a*	*n/a*	0.78	0.7	0.66
$K_{PEG} \times 10^2$ (mL/g)	*n/a*							*n/a*	*n/a*	1.25	10.1	
α_{PEG}	*n/a*							*n/a*	*n/a*	0.78	0.58	
ID in Figure AII-4	[η] (dL/g)	M_w(LS) (g/mol)	M_n (g/mol)	M_w (g/mol)	PDI	M_p (g/mol)	Polymer	R_H (nm)	R_η (nm)	R_η (nm)	R_η (nm)	R_η (nm)
R1		1327000	1197000	1352000	1.13	1378000	PEO	45		54	49	39
R2	1.4059	129000	110000	117700	1.07	122200	PEO	12	14	14	13	10
R3	0.2947	15870	14330	15260	1.06	16100	PEG	3.6	4.2	3.9	4.0	3.3
R4	0.0447	640	585	625	1.07	615	PEG	0.58	0.77	0.58	0.72	
Y1	5.9465	1067000	807500	922500	1.14	942000	PEO	40	47	47	39	32
Y2	0.8552	69400	64300	66450	1.03	67600	PEO	8.4	9.8	9.4	9.4	7.4
Y3	0.131	3580	3730	3830	1.03	3870	PEG	1.6	2.0	1.6	1.9	
Y4					1	194	PEG					
G1	4.4063	622000	493500	550500	1.12	552000	PEO	29	35	34	30	24
G2	0.4978	32480	29760	31150	1.05	31630	PEG/PEO?	5.5	6.4	6.0	6.1	4.9
G3	0.0687	1570	1420	1470	1.03	1450	PEG	0.97	1.20	0.99	1.15	
G4					1	106	PEG					

The Mark-Houwink parameters K and α are from Barth and Mori.[177] The first letter of the polymer ID refers to the colour of the vial containing the polymer. The polymer nature has been identified by comparing the molecular weight values from the certificate of analysis to the information available on the manufacturer website for such calibration kits.[188] PDI: polydispersity index.

Equations to estimate the size of the polymer chains

$$R_H = 0.0145 {M_w}^{0.571} \quad \text{(AII-5)}$$

$$R_\eta = \left(\frac{3[\eta]M_w}{10N_A\pi}\right)^{1/3} \quad \text{(AII-6)}$$

$$[\eta] = K{M_w}^{\alpha} \quad \text{(AII-7)}$$

$$R_\eta = \left(\frac{3K{M_w}^{\alpha+1}}{10N_A\pi}\right)^{1/3} \quad \text{(AII-8)}$$

Table AII-4: Fitting parameters of the calibration curves shown in Figure 4-5 and Figure AII-4.

Eq	Solvent	*A*	*B*	*C*	*D*	χ_{red}^2	R_{adj}^2
AII-5	H_2O	$(1.7 \pm 0.3) \times 10^3$	$-(2.7 \pm 0.4) \times 10^2$	14 ± 3	$-(0.27 \pm 0.05)$	0.371	1.00
AII-6	0.02% NaN_3	$(2.1 \pm 0.3) \times 10^3$	$-(3.5 \pm 0.5) \times 10^2$	18 ± 3	$-(0.34 \pm 0.06)$	0.508	0.999
AII-8	H_2O 25-30°C	$(2.1 \pm 0.3) \times 10^3$	$-(3.4 \pm 0.5) \times 10^2$	18 ± 3	$-(0.34 \pm 0.06)$	0.293	0.999
AII-8	0.1 N $NaNO_3$ 35°C	$(2.2 \pm 0.4) \times 10^3$	$-(3.6 \pm 0.7) \times 10^2$	20 ± 4	$-(0.38 \pm 0.09)$	0.978	0.997
AII-8	0.42 N NaOH 25°C	$(2.2 \pm 0.5) \times 10^3$	$-(3.8 \pm 0.9) \times 10^2$	22 ± 5	$-(0.4 \pm 0.2)$	0.346	0.998

A 3rd-order polynomial model defined as $R_H \text{ or } R_\eta = A + BV_e + CV_e^2 + DV_e^3$ was used to fit the data. The errors are the standard errors provided by Origin when fitting the data. The equations refer to the method used to calculate R_H or R_η as in Table AII-3.

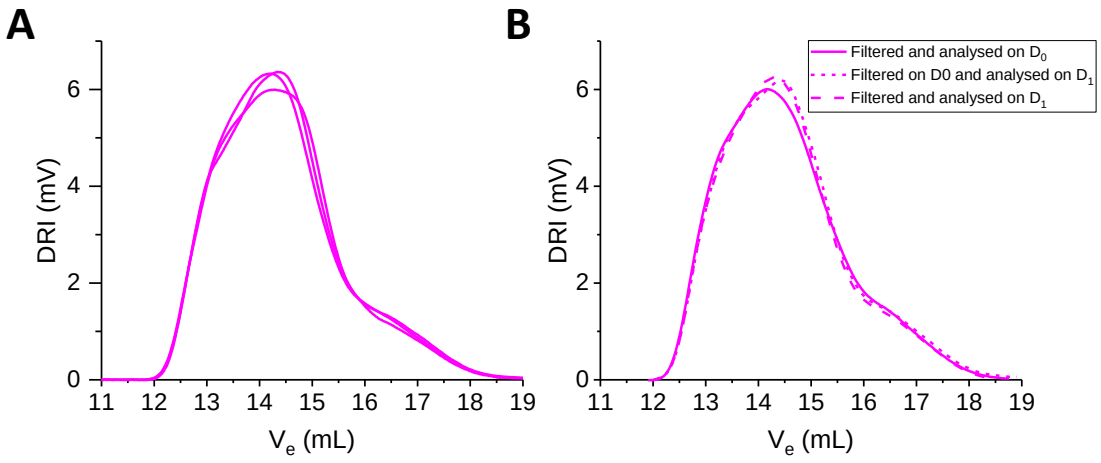

Figure AII-5: Evaluation of the reproducibility of the SEC measurements. **A.** Chromatogram of three different 0.14% Na CMC solutions. **B.** Chromatogram of the same 0.14% Na CMC solution (i) filtered and injected on the day it was prepared (D_0), re-injected on the next day (D_1), and filtered and injected on the next day. The elution volume and the area under the three peaks obtained from deconvolution are shown in Figure AII-6.

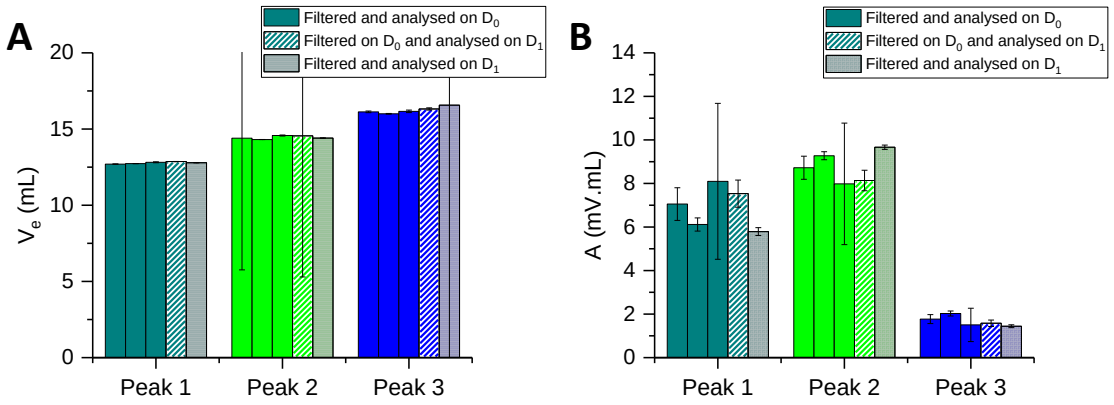

Figure AII-6: Elution volume V_e (**A**) and area A (**B**) of the three peaks obtained from the deconvolution of the overall peaks shown in Figure AII-5 with the EMG model. Error bars represent the standard errors provided by Origin when deconvoluting the peaks.

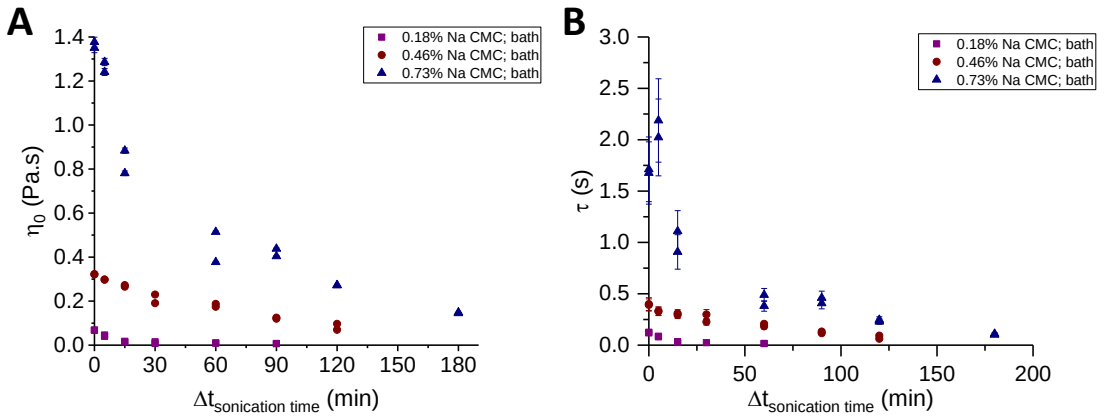

Figure AII-7: Lin-lin representations of the zero-shear viscosity η_0 and parameter τ obtained from the fits of the viscosity curves to the Carreau model or constants as a function of the sonication time. The data are similar to the ones shown in Figure 4-7, except that the data collected for the 0.18% Na CMC solutions sonicated with the probe are not shown.

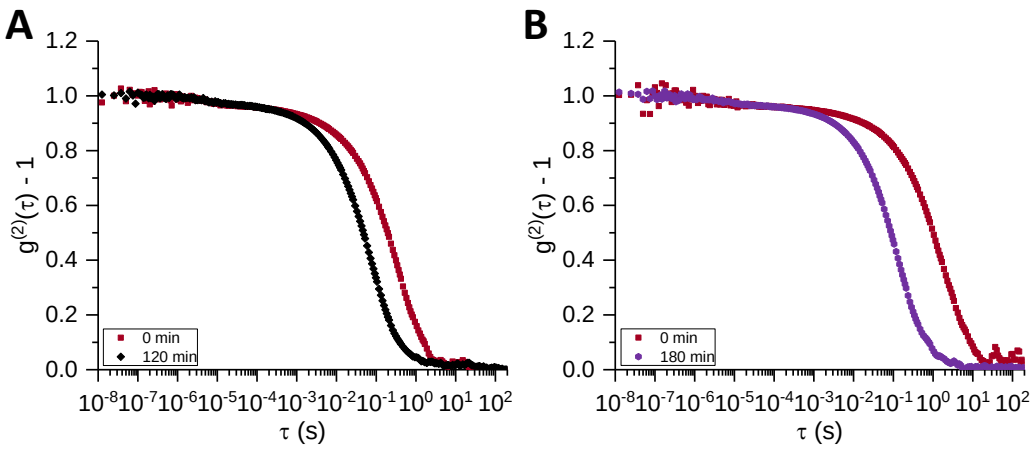

Figure AII-8: Examples of intensity auto-correlation data of sonicated and non-sonicated 0.46% (**A**) and 0.73% (**B**) Na CMC solutions.

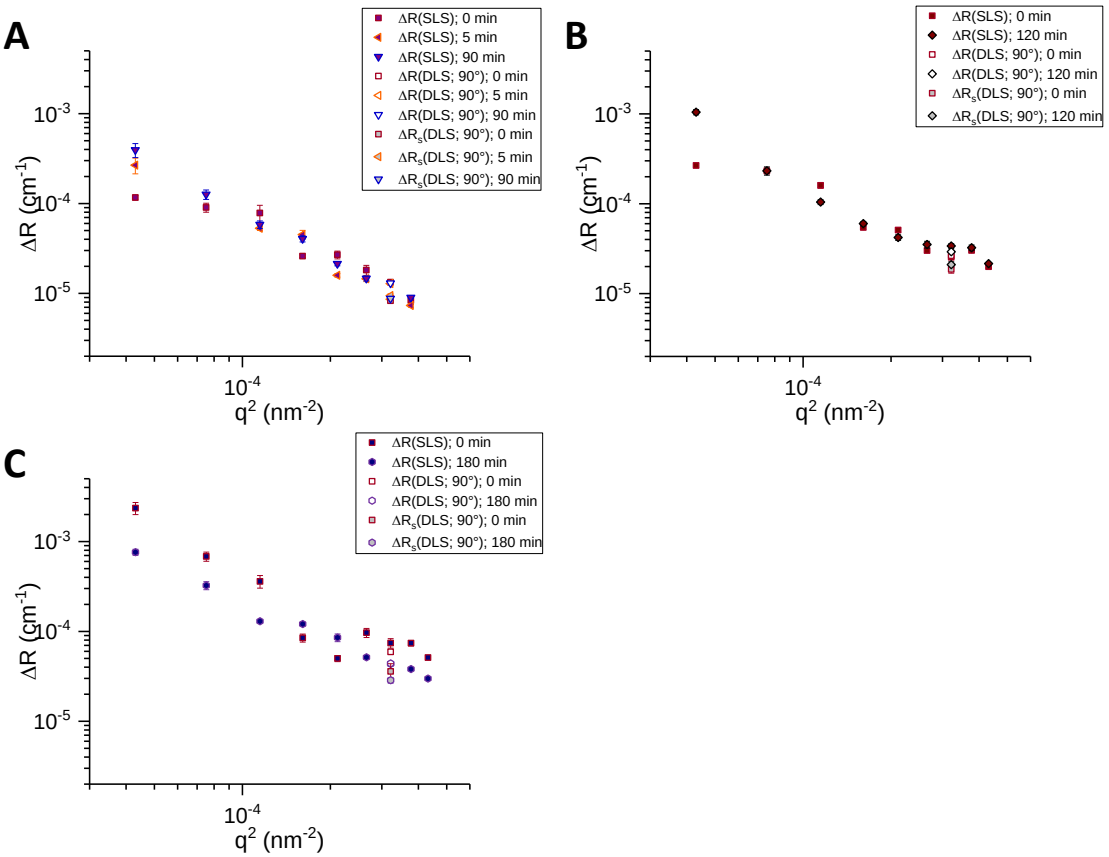

Figure AII-9: SLS data from non- and bath-sonicated 0.18% (**A**), 0.46% (**B**) and 0.73% (**C**) solutions. The total excess Rayleigh ratio ΔR obtained from SLS measurements is plotted against the squared scattering vector q^2. The excess Rayleigh ratio obtained from the SLS data collected during the long DLS measurements at 90° scattering angle as well as the contribution of the slow mode to the excess Rayleigh ratio determined from these DLS measurements are also shown.

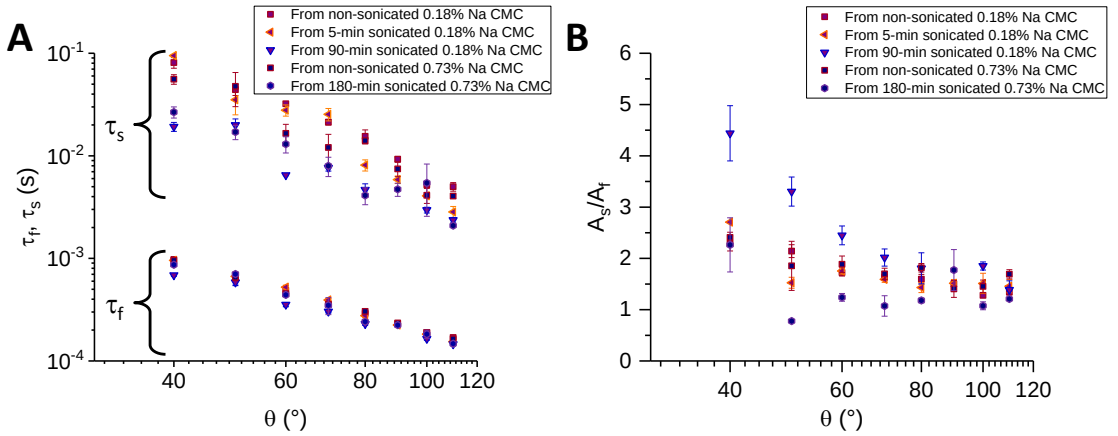

Figure AII-10: DLS of SEC samples (*i.e.* 0.14% Na CMC solutions in the eluent). **A.** Fast and slow relaxation times τ_f and τ_s of SEC samples made from non- and bath-sonicated 0.18% and 0.73% Na CMC solutions. **B.** Quotient of the amplitudes of the slow and the fast relaxation modes for the same solutions as the ones shown in A. It is worth noting that $A_s/A_f = \Delta R_s/\Delta R_f$, with ΔR_i the contribution of the mode *i* to the total excess Rayleigh ratio ΔR.

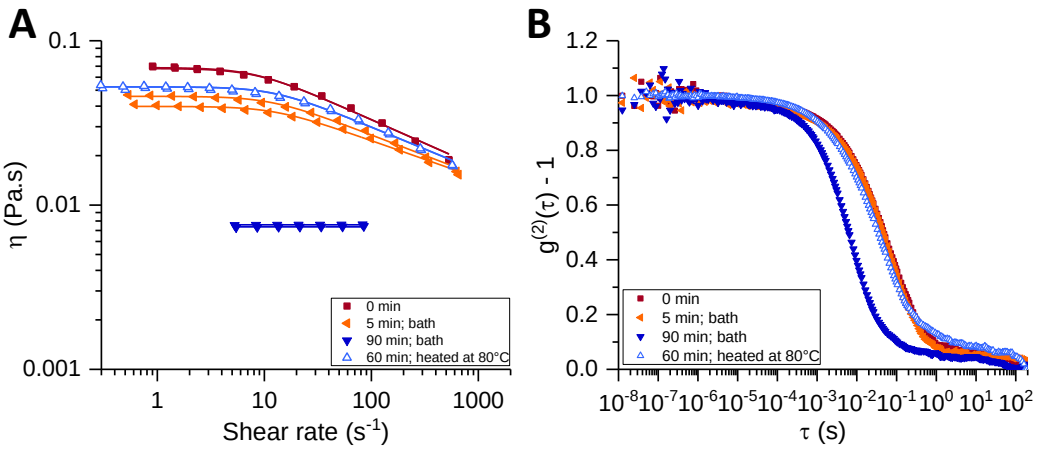

Figure AII-11: Behaviour of 60-min heated, 0-min, 5-min and 90-min sonicated 0.18% Na CMC solutions using rheology (**A**) and DLS (**B**). The lines in A are fits of the experimental data to the Carreau model or constants for solutions exhibiting a shear-thinning and a Newtonian behaviour respectively.

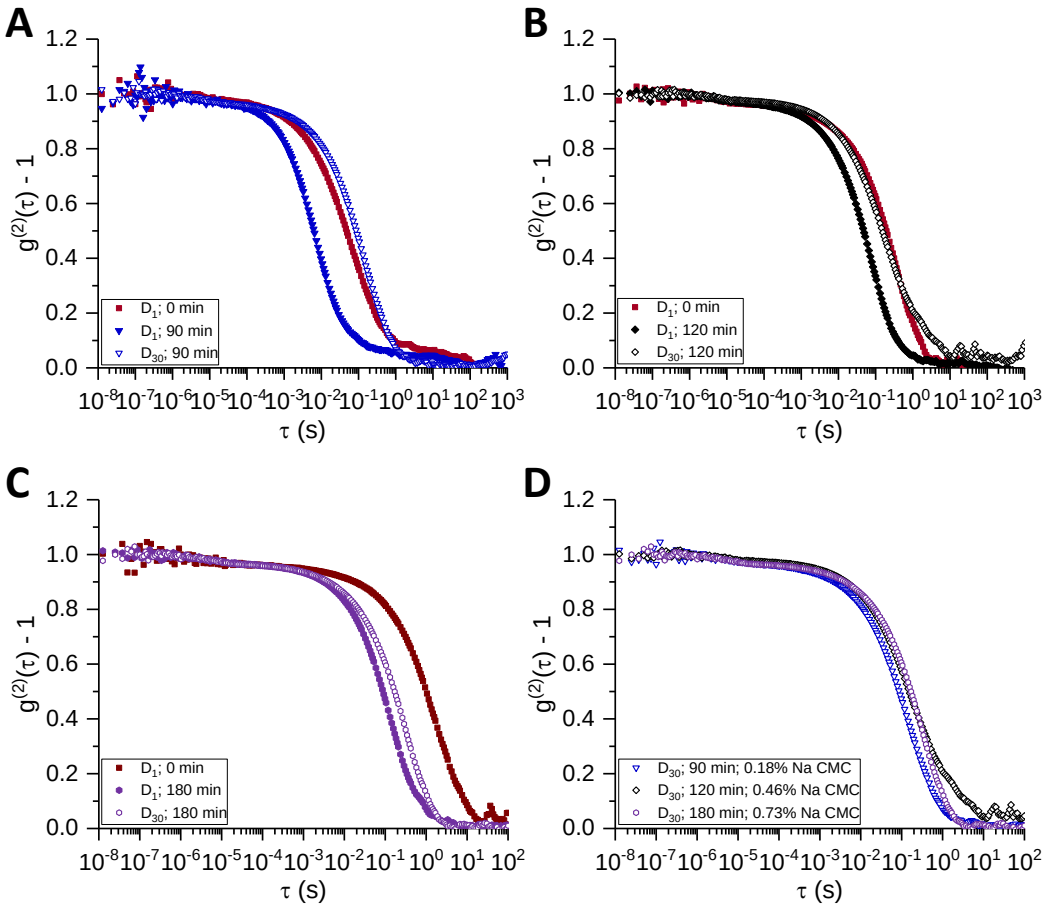

Figure AII-12: Intensity auto-correlation data collected on the sonication day (D_1) and a month later (D_{30}) for the 0.18% (**A**), 0.46% (**B**) and 0.73% (**C**) Na CMC solutions for the solutions sonicated for the longest durations (*i.e.* 90 min, 120 min and 180 min respectively). The data of the non-sonicated solutions are shown for comparison. **D** displays the data of the sonicated solutions after a month ageing.